Functionalised Metal Nanoparticles as Novel Reagents for Biomedical Analysis

Yon Kyeong Ju Nam

A thesis submitted in partial fulfilment of the requirements of Sheffield Hallam University for the degree of Doctor of Philosophy

December 2007

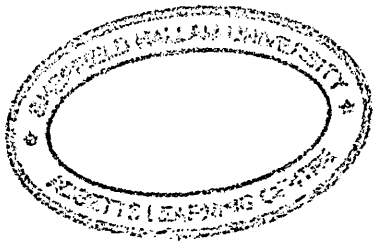

DECLARATION

The work presented in this thesis was carried out by Yon Kyeong JuNam at the Biomedical Research Centre, Faculty of Health and Wellbeing, between July 2004 and September 2007. The author declares that this work has not been submitted for any other degree. The work is original except where acknowledged by reference.

Yon Kyeong Ju Nam

ABSTRACT

This thesis describes a study of the synthesis and characterisation of a new family of cationic alkane-thiolate and -selenolate compounds bearing a phosphonium (or phosphine oxide) head group, and the applications as ligands for the stabilisation of gold nanoparticles. The ability of these cationic phosphonium gold nanoparticles as substrates for the detection of negatively charged biomolecules has also been explored.

In chapter 1, topics concerning the synthesis of functionalised gold nanoparticles, their biorecognition properties, the application of these nanoparticles in the biomedical field and gold nanoparticles stabilised with phosphorus-containing ligands, are outlined in a literature review.

Instrument details of the analytical methods employed to characterise all the compounds and nanoparticles obtained in the study are outlined in Chapter 2. The syntheses and structural characterisation by NMR, ESMS and X-ray crystallography of cationic phosphonium-containing ligands are described in Chapters 3 to 5. Chapter 3 contains the description of the synthesis of phosphonioalkylthiosulfate zwitterions. The synthesis of related phosphonioalkylselenide compounds is presented in Chapter 4, and Chapter 5 is concerned with the synthesis of phosphonioalkylthioacetate and related phosphine oxide ligands.

In Chapter 6, the preparation of the cationic phosphonium-functionalised gold nanoparticles using the phosphonium-containing compounds as protecting ligands, in a two-phase liquid-liquid (DCM-H_2O) and one phase (ethanol) systems, is described. This chapter also contains details of characterisation of these nanoparticles by NMR, XPS and TEM. The ability of the cationic phosphonium gold nanoparticles to interact with RNA and cDNA, and the potential of using these nanoparticles as biorecognition systems was investigated by the Biacore Surface Plasmon Resonance technique and this work is described in Chapter 7. Finally, a summary of conclusions and some suggestions for future work are presented in Chapter 8.

ACKNOWLEDGMENTS

Firstly, I would like to thank my academic supervisors Dr. Neil Bricklebank, Dr. Philip Gardiner and Prof. David Allen for their invaluable guidance and advice throughout this work and their unconditional support over the past three years. I also wish to thank the Biomedical Research Centre (BMRC), Sheffield Hallam University (SHU), for their financial support.

I would like to extend my thanks to the following people for their help and contribution to this research project:

- Leon Bowen and Stuart Creasy of the Materials Research Institute, Sheffield Hallam University, for obtaining the TEM micrographs.
- Kevin Osbourne and Joan Hague of the BMRC, for the NMR and MS analysis.
- Gautam Mishra of the University of Sheffield, for obtaining the XPS spectra.
- Antoine Fouillet and Bahare Vahabi of the BMRC, for providing me the cDNA and RNA samples.
- Dr Robert Smith of the BMRC, for the training in the Biacore Surface Plasmon Resonance technique.

I also wish to mention my friends who have provided me the best moments during the last three years in Sheffield, these include Maria Elena Romero, Mahera Moin, Adrien Destribats, Vanessa Diaz, Cesar Pichardo, and Clare Williamson.

I would like to express my gratitude to my family (my mother, Sun Hee Nam, my father, Ju Chang Sok, my brother, Hyo Jun Ju Nam) for their love and support all the time.

Finally, I would like to thank my husband, Jesus Javier Ojeda Ledo, who has tirelessly supported and helped me throughout my studies, I couldn't have done it without you, I will never find enough words to express all my gratitude to you.

CONTENTS

CHAPTER 1

Literature review

CHAPTER 2

Experimental-General Methods

CHAPTER 3

Synthesis of Phosphonioalkylthiosulfate Zwitterions

CHAPTER 4

Synthesis of Phosphonioalkylselenide Ligands

CHAPTER 5

Phosphonioalkylthioacetate and Related Phosphine Oxide Ligands

CHAPTER 6

Phosphonium Monolayer-Protected gold Nanoparticles

CHAPTER 7

Studies of Cationic Phosphonium-Gold Nanoparticles as Substrates for Biorecognition using the Surface Plasmon Resonance Technique

CHAPTER 8

Conclusions and Future Work

TABLE OF ABBREVIATIONS

AFM	Atomic force microscopy
ATP	Adenosine triphosphate
AuNPs	Gold nanoparticles
CM5	Biacore sensor chip with a carboxymethylated dextran matrix covalently attached to a gold surface
DCM	Dichloromethane
DMSO	Dimethyl sulfoxide
DNA	Deoxyribonucleic acid
ESMS	Electrospray mass spectrometry
FC1	Flow cell channel 1
FC2	Flow cell channel 2
FTIR	Fourier transform infrared
HEPES	(2-Hydroxyethyl)-1-piperazineethanesulfonic acid
HRTEM	High resolution transmission electron microscopy
IFC	Integrated fluidic cartridge
MALDI-TOFMS	Matrix assisted laser desorption ionisation-time of flight mass spectrometry
MeOH	Methanol
MMPCs	Mixed monolayer-protected clusters
MPCs	Monolayer-protected clusters
MS	Mass spectrometry
mt-DNA	Mitochondrial- deoxyribonucleic acid
NMR	Nuclear magnetic resonance
RNA	Ribonucleic acid
RT	Room temperature
RT-PCR	Real time- polymerase chain reaction
RU	Response unit
SA	Biacore sensor chip with a carboxymethylated dextran-streptavidin matrix
SAMs	Self-assembled monolayers
SAXS	Small-angle X-ray scattering
SMAD	Solvated metal atom dispersion
SPB	Surface plasmon band
SPR	Surface plasmon resonance
STM	Scanning tunnelling microscopy
TEM	Transmission electron microscopy
TGA	Thermogravimetric analysis
THF	Tetrahydrofuran
TLC	Thin-layer chromatography
TOAB	Tetra-octyl ammonium bromide
TOPO	Tri-*n*-octyl phosphine oxide
TOPSe	Tri-*n*-octyl phosphine selenide
UV-Vis	Ultraviolet-visible
XPS	X-ray photoelectron spectroscopy

1.1 Introduction

Nanobiotechnology is an interdisciplinary field based on fundamental chemistry, biotechnology and materials science which has evolved over the past few decades. Nanobiotechnology is a convergence of nanotechnology and biomedical sciences which has opened a wide variety of biological research topics and medical uses at the molecular and cellular level (Figure 1).[1]

The main purpose of developments in nanobiotechnology is the integration of biological and non-biological materials and structures in order to generate new biocompatible devices of nanoscale dimensions, potentially useful for sensing, catalysis, transport, and other applications in biological and medical sciences.[2,3,4] Learning how to control the formation of two- and three-dimensional assemblies of molecular scale building blocks into well-defined nanostructures, and understanding the interface between biological and non-biological materials on the molecular scale are the principal challenges in this area.[5,6]

The utilisation of nanoparticles of a variety of shapes, sizes and compositions has made possible the fabrication of the biocompatible and functional devices, and has also changed the analytical measurement landscape for biomolecules.[7,8] It is clear that nanoparticles will be able to overcome many of the significant chemical and spectral limitations of molecular fluorophores. Nanoparticles are being used as tags in biological assays to eliminate the use of either organic fluorophores or radioactive labeling.[9] For this reason, methods for the preparation and handling of nanoparticle-biomolecule

conjugates and organic ligand-stabilized nanoparticles have been developed. These functionalised nanoparticles have already had an impact in the designing of biosensors, in drug and gene delivery, and tissue engineering technologies.[10-13]

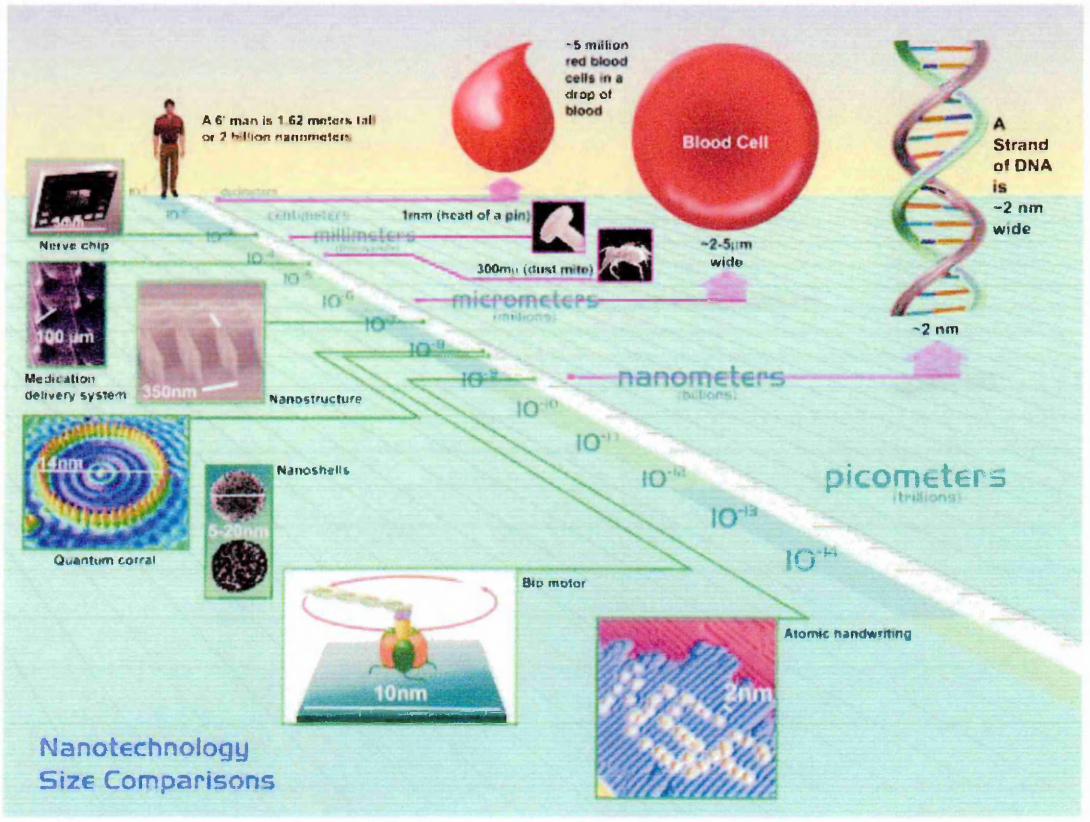

Figure 1. Size comparisons between several human made nanodevices and biological species. (Figure taken from: http://www.nsf.gov/news)

Metal nanoparticles are generally considered to be a number of atoms or molecules bonded together with a radius of < 100 nm. These particles differ from the bulk materials in the number of atoms (Figure 2) and their physical properties are also different from those of the bulk.[14] These differences arise through the small size and

large surface area of the particles: for a 10 nm particle, 15% of atoms occupy surface positions, compared with 0.0015% for a 1 μm (1000nm) particle.[15]

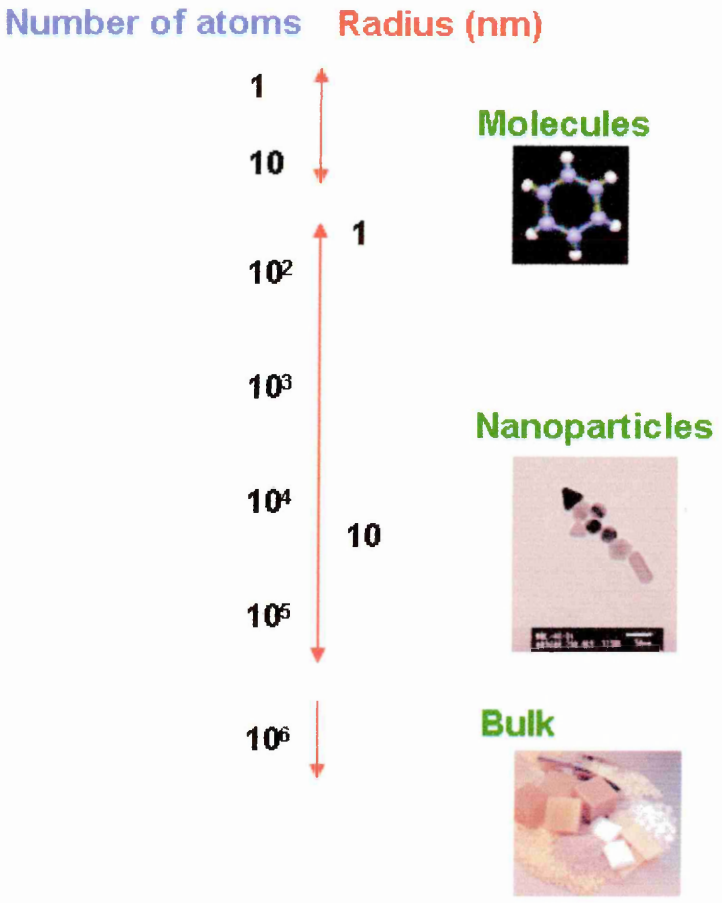

Figure 2. Distinction between molecules, nanoparticles, and bulk materials according to the number of atoms.

Nanoparticles that act as signal transducers show the most promise in diagnostic assays, due to the elimination of the need to tag a biological sample. With the sample preparation steps reduced or eliminated, the diagnostic test will become more robust and less expensive.[16] The eventual goal for any diagnostic assay is detection from whole

blood. This goal has been achieved by Hirsch and co-workers,[17] who developed an aggregation assay to detect immunoglobins in whole blood using gold nanoshells, which are spherical nanoparticles made up of a dielectric core (often silica) and surrounded by a thin metal shell.

One of the most exciting areas of nanobiotechnology is the use of nanomaterials to carry out particle-specific functions. In other words, intrinsic physical or chemical properties of the particles effect analytically relevant transformations. Recently, Tkachenko and co-workers[18] published their initial findings on multi-functional gold nanoparticle-peptide complexes for nuclear targeting. For this function, the particles must be small enough to penetrate cells and nuclear membranes, rugged enough to survive harsh endosomal/lysosomal processes, and must be able to carry targeting peptides for nuclear localization. These functions were met by 20 nm diameter gold nanoparticles coated with bovine serum albumin and derivatised with well-defined quantities of combinations of targeting peptides.

Despite the considerable variety of contributions, this literature review will focus on the synthesis and stabilization of gold nanoparticles (AuNPs), and various types of assemblies, their physical and chemical properties, and finally their applications in biochemistry, biomedicine and catalysis.

1.2 Gold nanoparticles (AuNPs)

There is a current interest in the development of receptor-functionalised metal and semiconductor nanoparticles which are able to recognise and interact with specific biomolecules. Such systems are expected to form the basis of new diagnostic biosensor technologies and novel therapeutic agents, and the most widely studied systems are based on gold.[19,20] Gold nanoparticles present interesting aspects such as their stability, inertness, behaviour as individual particles, and size-related electronic, magnetic and optical properties. Furthermore, gold nanoparticles (AuNPs) have the advantages of easy preparation and the possibility of chemical modification of the surface.[21,22]

The beginning of the chemistry of gold colloids dates from the middle of nineteenth century, when Michael Faraday performed his famous experiments to generate gold colloids. Faraday reduced tetrachloroaurate using white phosphorus to yield deep-red solutions.[19,21] At the beginning of 20th century, Wilhelm Ostwald contributed decisively to the further development of colloid science. He was the first to establish that the properties of metal particles in the nanometre range are predominantly determined by surface atoms and he concluded that those nanoparticles, called colloids, should exhibit novel properties with respect to bulk particles. The term "colloid" has meanwhile been mostly substituted by "nanoparticle", or "cluster".[19]

1.3 Synthesis of gold nanoparticles

The number of procedures for generating gold nanoparticles is almost indeterminable. There are two main approaches to synthesize gold nanoparticles: a physical and a chemical one. Physical methods are defined as those by which gold nanoparticles are directly generated from bulk gold *via* the generation of isolated atoms by various distribution techniques, whereas chemical routes use gold compounds as a starting material, linked with reduction steps.

An important aspect of both approaches is the stabilization of the particles to avoid coalescence between them. This stabilization can occur in many different ways, for instance by electrostatic repulsion, steric hindrance, or using organic ligand molecules to functionalise the gold nanoparticles.

1.3.1 Synthesis of AuNPs based on physical methods

The simplest way to obtain nanoparticles is the generation of metal atoms in the gas phase followed by their controlled condensation to nanoparticles through a process known as metal-vapour synthesis. In special cases the colloidal metals can be studied in the gas phase; however, in order to obtain them as solid matter, the vapours have to be condensed into a dispersing medium.

Recently, laser ablation has been used for the production of nanoparticles but the range of dimensions of the nanoparticles obtained was very large. A further improvement in the laser technique is laser-induced size reduction. Laser irradiation of metal sheets in diluted sodium dodecyl sulfate at 532 nm yields nanoparticles in the range of 1.7 and 3.2 nm.[21] Another recent method described is the solvated metal atom dispersion (SMAD) method. In this technique, metal atoms are generated from bulk metal and frozen at 77K in acetone vapour and then warmed to give colloid metal stabilized in acetone. The colloids can be further stabilized by dodecanethiol and can then be dispersed in toluene.[23] These methods allow for the easy handling of colloids in common organic solvents.

Stable gold nanoparticles can be generated in the presence of an ultrasonic field (200 kHz), which allows the control of the rate of $AuCl_4^-$ reduction in an aqueous solution containing only a small amount of 2-propanol, and also of the sizes of the formed AuNPs, by using parameters such as the temperature of the solution and the intensity of the ultrasound.[24,25] AuNPs have also been fabricated *via* decomposition of $[AuCl(PPh_3)]$ by reduction in a monolayer at the gas/liquid interface.[26] The thermolysis of $[C_{14}H_{29}\text{-}Me_3N][Au(SC_{12}H_{25})_2]$ at 180 °C for 5 hours under N_2 produced alkyl-group-passivated AuNPs of 26 nm.[27]

1.3.2 Synthesis of AuNPs based on chemical methods

The basic concept of chemical synthesis of gold nanoparticles is that a salt of the metal is dissolved in an appropriate solvent and then reduced to the zero valence state (Figure 3). The problem is that the lifetime of the atoms in the solution is short, and they tend to coalesce into large aggregates. The crucial step in the process is then to determine when to stop the growth and thus prevent the formation of large aggregates- "bulk formation". In many cases the use of ligand molecules has been found to be effective in stopping bulk formation. These ligands coordinate strongly with the surface atoms of the growing nanoparticle.[28-30]

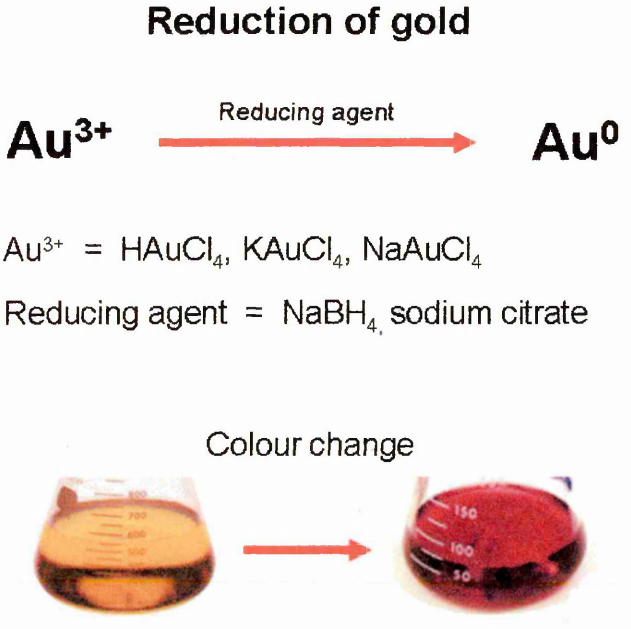

Figure 3. Reduction of Au^{III} using a reducing agent.

1.3.2.1 Citrate reduction: synthesis of gold nanoparticles stabilised by sodium citrate

Among the so-called salt reduction methods, the Turkevitch[31] route is still one of the most commonly applied procedures. Sodium citrate reduces $[AuCl_4]^-$ in hot aqueous solution to give colloid particles of 15-20nm. Citrate itself and its oxidation products (e.g. acetone dicarboxylate) can act as protecting agents, if no other stabiliser is used. Frens[32] reported a method to obtain AuNPs of chosen size between 16-147 nm. The method was based on the variation of the ratio between the reducing/stabilising agents (the tri-sodium citrate-to-gold ratio) in order to control the size of the AuNPs. Many variations and improvements of this method have been reported.[33-35]

1.3.2.2 The Brust method: synthesis of gold nanoparticles in a two-phase solvent system and stabilisation by thiols

The use of ligands with greater affinity for the gold than citrate was a major improvement for the synthesis and handling of gold solutions. Ligand-capped gold clusters have been known for many years; however, the practical formation of stable, isolable monolayer-protected clusters (MPCs) has only recently been demonstrated.[36] Phosphines and thiols are excellent stabilisers due to rather strong Au-P bonds and even stronger Au-S bonds.[37] These molecules allow the isolation of gold nanoparticles as solid materials that can be re-dispersed in appropriate solvents. This is not possible with weakly binding stabilisers such as citrate.[38]

Thiols are the most important type of stabilizing molecule for gold nanoparticles of any size. The stabilisation of AuNPs with alkanethiols was first reported in 1993 by Mulvaney and co-workers.[39] It is commonly accepted that the use of thiols leads to the formation of RS^- thiolates that form strong covalent Au-S bonds.[36,39,40]

One of the most popular modern methods for preparing gold nanoparticles of various sizes was published by Brust and co-workers.[41] The strategy consists of growing the metallic clusters with the simultaneous attachment of self-assembled thiol monolayers on the growing nanoparticles. In order to allow the surface reaction to take place during metal nucleation and growth, and also due to the solubility of the thiol compounds, the particles are grown in a two phase system (water-toluene). Brust used tetraoctylammonium bromide as a phase transfer reagent, to transfer $AuCl_4^-$ from aqueous solution to the organic phase (toluene) in the presence of dodecanethiol ($C_{12}H_{25}SH$). The method uses $NaBH_4$ to reduce gold salts in the presence of alkanethiols to yield 1-3 nm gold particles (Figure 4).

By varying the thiol concentration, the particle size can be controlled between 2 and 5 nm.[42] Recently, thiol-stabilised gold nanoparticles have become available following a seeding growth approach starting with 3.5 nm particles. The particle size can be varied by changing the seed-particle to metal-salt ratio.[43]

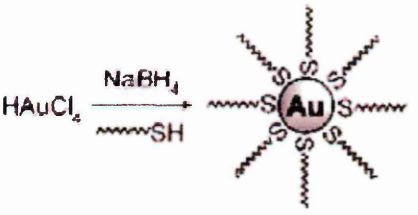

$$AuCl_4^-(aq) + N(C_8H_{17})_4^+(C_6H_5Me) \longrightarrow N(C_8H_{17})_4^+ AuCl_4^-(C_6H_5Me)$$

$$mAuCl_4^-(C_6H_5Me) + nC_{12}H_{25}SH(C_6H_5Me) + 3me^- \longrightarrow 4mCl^-(aq) + [Au_m(C_{12}H_{25}SH)_n](C_6H_5Me)$$

Figure 4. Formation of AuNPs coated with organic shells by reduction of Au^{III} with $NaBH_4$ in the presence of thiols in a two-phase liquid-liquid system using tetraoctylamonium bromide as the phase-transfer reagent.[41]

Other thiol ligands containing reactive end groups have been used in the synthesis of functionalised gold nanoparticles in order to design new biomolecular surface recognition systems.[43] Among thiol ligands reported in the literature for the fabrication of stable gold nanoparticles with the ability to interact with biomolecules, the ones containing trimethylammonium- and fluorophore-end groups are the most widely studied.[44-46]

1.3.2.3 Other sulfur- and selenium-containing ligands

It has been shown that organic thiosulfates (Bunte salts) with either aliphatic or aromatic groups as part of their chemical structure, constitute a novel family of surface-active compounds containing sulfur, making possible the synthesis of stable self-

assembled monolayers (SAMs) and gold nanoparticles.[47,48] Lukkari[47] has described the generation of alkanethiolate-protected gold surfaces, whereas Murray and co-workers[48] have prepared clusters from sodium S-dodecylthiosulfates (Bunte salts), which are identical to those obtained directly from the use of the free thiol ligands, the sulfur-sulfur bond undergoing cleavage with loss of sulfite ion as a result of the interaction with the gold surface (Figure 5).

Selenium-containing ligands have been shown to offer interesting, and alternative chemical characteristics than the widely used alkanethiols for the formation of self-assembled monolayers on metal surfaces. Yee and co-workers[49] developed a one-phase preparation of alkaneselenol-protected gold nanoparticles using alkaneselenols and dialkyldiselenides as protecting ligands. More recently, Tong and co-workers[50] used octaneselenols as the protecting ligands to form stable monolayer-protected metal nanoparticles, and studied the gold-selenium bonding interaction by NMR making use of ^{77}Se nuclear magnetic resonance.[50]

Gold nanoparticles in a size range of about 10 and 30 nm or more have been synthesized by the $NaBH_4$ method using mercaptosuccinic acid for stabilisation. By varying the succinic acid to $HAuCl_4$ ratio from 2.5 to 0.5, particles of 10.2, 10.8, 12.8, 19.4, and 33.6 nm were isolated as water-redispersable powders.[51] 11-Mercaptoundecanoic acid was also used to cover gold nanoparticles generated by the Brust method. The carboxylic functions were then treated with trifluoroacetic anhydride

to give the corresponding carboxylic anhydrides which are highly reactive and can, for instance, be used to anchor the nanoparticles to silica supports.[52]

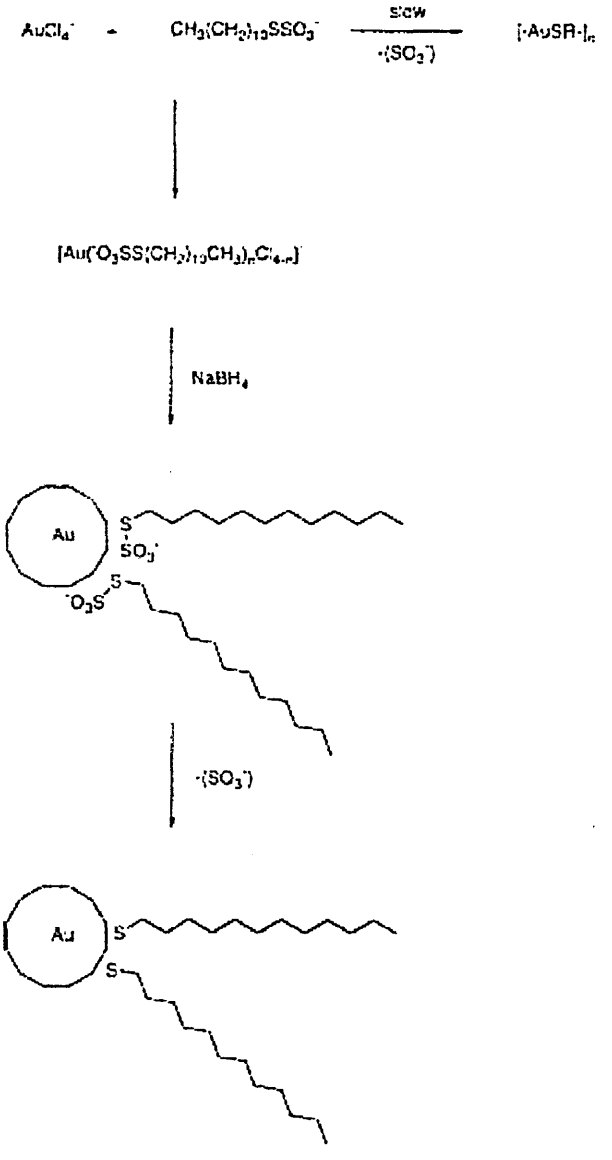

Figure 5. Synthesis of alkanthiolate-functionalised gold nanoparticles using S-dodecylthiosulfate as protecting ligand.[48]

1.3.3 Characterisation techniques

The most common characterization technique is high-resolution transmission electron microscopy (HRTEM),[39,53] from which an electron micrograph of the gold core of the AuNPs can be obtained. However the core dimensions can also be determined using scanning tunnelling microscopy (STM),[54] atomic force microscopy (AFM),[55,56] small-angle X-ray scattering (SAXS),[57] and X-ray diffraction.[58]

The histogram providing the size distribution of these cores gives relevant information on the dispersity of the nanoparticles can be obtained from TEM micrographs.[39] From the elemental analysis, giving the Au/S ratio, allows calculation of the average number of S ligands at the surface.[22,41,42] This number can also be deduced from X-ray photoelectron spectroscopy (XPS)[59] or thermogravimetric analysis (TGA).[36] Brust and co-workers also examined the oxidation state of the gold atoms of the core using X-ray photoelectron spectroscopy showed that the binding energies of the doublet for Au $4f_{7/2}$ (83.8 eV) and Au $4f_{5/2}$ (87.5eV) are characteristic of Au^0. No peak corresponding to Au^I (84.9 eV) was found in the spectrum, although one-third of the gold atoms are located at the surface and bonded to thiols, in the 2.0-2.5 nm sized particle cores,[22] and it is commonly assumed that at the surface of such assemblies, the unit $Au^I \cdots {}^-SR$ is present.

IR provides an identification of the ligands surrounding the nanoparticle core that can also be confirmed by NMR spectroscopy, except that the ligand atoms close to the core give broad signals. This latter experimental observation is due to (i) spin-spin

relaxational (T_2) broadening (main factor), (ii) variations among the gold-sulfur bonding sites around the particle, and (iii) a gradient in the packing density of the thiolate ligands from the core region to the ligand terminus at the periphery.[60-62] The NMR spectra can be very useful, as for all molecular compounds, for the part of the ligand remote from the core.

Kenndler and co-workers[63] demonstrated, by capillary zone electrophoresis in acetate buffer, that the mobility of AuNPs with a given core diameter decreased with ionic strength. They observed, at the highest ionic strength (6 mmol/L), a good linear dependence of the mobility on the reciprocal of the core radius allowing them to characterise the size of the AuNPs.

1.4 Physical properties of AuNPs

The dark-red colour of AuNP colloids dispersed in water reflects the surface plasmon band (SPB), which is a broad absorption band in the visible region around 520 nm (Figure 6).[64] The SPB is due to the collective oscillations of the electron gas at the surface of nanoparticles (6s electrons of the conduction band for AuNPs) that is correlated with the electromagnetic field of the incoming light.[65] The SPB provides a considerable amount of information on the development of the band structure in metals and has been the subject of extensive study of optical spectroscopic properties of AuNPs.

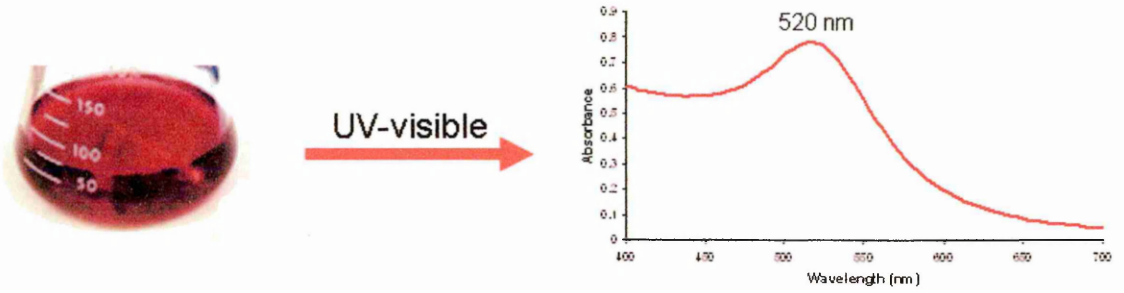

Figure 6. The deep-red colour of gold nanoparticle colloids in water reflects the surface plasmon resonance (SPR), a broad band absorption band in the visible region around 520 nm.

The main characteristics of the SPB are:

(i) Its position around 520 nm.

(ii) Its sharp decrease in wavelength with decreasing core size for AuNPs with 1.4-3.2 nm core diameters due to the onset of quantum size effects that become important for particles with core sizes < 3 nm in diameter and also cause a slight blue shift (the damping of the SP mode follows a 1/radius dependence due essentially to surface scattering of the conduction electrons;[66,67] this decrease of wavelength of the surface plasmon band (SPB) as particle size decreases is accompanied by broadening of the plasmon bandwidth.

(iii) Step like spectral structures indicating transitions to the discrete unoccupied levels of the conduction band with monodispersed AuNPs with core diameters between 1.1 and 1.9 nm.[68,69]

The SPB is absent for AuNPs with core diameter less than 2 nm, as well as for bulk gold. For AuNPs of mean diameter of 9, 15, 22, 48, and 99 nm, the SPB maximum

λ_{max} was observed at 517, 520, 521, 533, and 575 nm, respectively, in aqueous media.[19,70] The maximum and bandwidth are also influenced by the particle size, dielectric constant of the medium and temperature.[70-73]

The refractive index of the solvent has been shown to induce a shift of the SPB. Mulvaney and co-workers[74] studied solutions of dodecanethiolate-stabilised AuNPs with an average diameter of 5.2 nm, and observed an 8 nm shift in SPB as the solvent (toluene) refractive index is varied from n_d^{20} = 1.33 to 1.55. The ligand shell alters the refractive index and causes either a red or blue shift. This shift is especially significant with thiolate ligands, which are responsible for a strong ligand field interacting with surface electron cloud. With elliptical particles, the SPB is shifted to higher wavelength as the spacing between particles is reduced, and this shift is well described as an exponential function of the gap between the two particles.[71]

Fluorescence studies of AuNPs have been carried out under various conditions, including femtosecond emission[75] and steady-state investigation[76] of the interaction between thiolate ligands and the gold core. Capping fluorescent groups such as pyrenyl, polyoctylthiophenyl, fluorenyl, and other probes have been used.[77-80] Resonant energy transfer has been observed in fluorescent ligand-capped AuNPs that is due to the size and the shape of the AuNPs, and the distance between the dye molecules and the orientation of the dipole with the nanoparticles axis. These studies have contributed to developments in biophotonics and materials science.[81,82]

1.5 Chemical and recognition properties of AuNPs

1.5.1 Chemical Properties: reactions of thiolate-stabilised AuNPs

Alkanethiolate-stabilised AuNPs possess a unique property in that some of the thiolate ligands attached onto the core can be substituted by reaction with other thiols. This reaction, so-called ligand place-exchange, depends on the chain length and steric bulk of the leaving thiolates and incoming thiols and on the charge of the AuNPs.[36,83,84] The oxidation of the functionalised gold nanoparticles increases the chance of larger numbers of fresh new thiolate ligands being incorporated onto the gold surface.[85] Ligand place-exchange is a key step in monolayer protected cluster (MPC) functionalisation to obtain the mixed monolayer protected clusters (MMPCs). For instance, MPCs with alkanethiolate monolayers (RS) can be functionalised with R'S groups by the reaction:

$$x(\text{R'SH}) + (\text{RS})_m\text{MPC} \longrightarrow x(\text{RSH}) + (\text{R'S})_x(\text{RS})_{m-x}\text{MPC}$$

where x and m are the numbers of the new and original ligands, respectively. The rate and equilibrium stoichiometry (x) of the reaction are controlled by factors that include the mole ratio of R'SH to RS units, their relative steric bulk, and R versus R' chain lengths.[21,36]

The study of ligand place-exchange dynamics and mechanism shows that the exchange reaction (i) has a 1:1 stoichiometry, (ii) it is an associative (as opposed to dissociative) reaction, (iii) it yields the displaced ligand in solution as a thiol, and (iv) it does not involve disulfides or oxidized sulfur species.[83]

Various functional thiols could be partially incorporated into AuNPs using this reaction. Rotello and co-workers could incorporate 11-mercaptoundecanoic acid into thiolate-stabilized AuNPs giving amphiphilic AuNPs that were soluble in basic aqueous media but which aggregated in acidic media due to hydrogen-bonding. This property was controlled by adjusting the pH.[86]

Complexation of pyridine-functionalised thiol AuNPs also led to solid substrate assembly, and such bifunctional ligands were used to link AuNPs, which led to electron-hopping studies and applications as sensors.[87] Other electroactive and photoactive groups, and catalysts, as well as simple groups such as halides, nitriles, alkenes, and sulfonates, have similarly been introduced using the ligand-exchange reaction.[88-91]

1.5.2 Recognition properties: molecular recognition AuNPs systems

Many biomolecule-gold nanoparticle hybrids, and positively charged- and negatively charged-gold nanoparticle systems have been reported in the literature. There

is a great interest in these systems and they have been widely studied over the past 15 years due to their unique recognition property for biomolecules (Figure 7).[44,92,93]

The use of well-controlled functionalised gold nanoparticles in solution, based on non-covalent bonding, is a general strategy for biomolecule recognition.[94] Approaches using hydrogen-bonding,[95] π-π,[96] host-guest,[97] van der Waals,[98] electrostatic,[99] and antigen-antibody[100] interactions have also been reported.

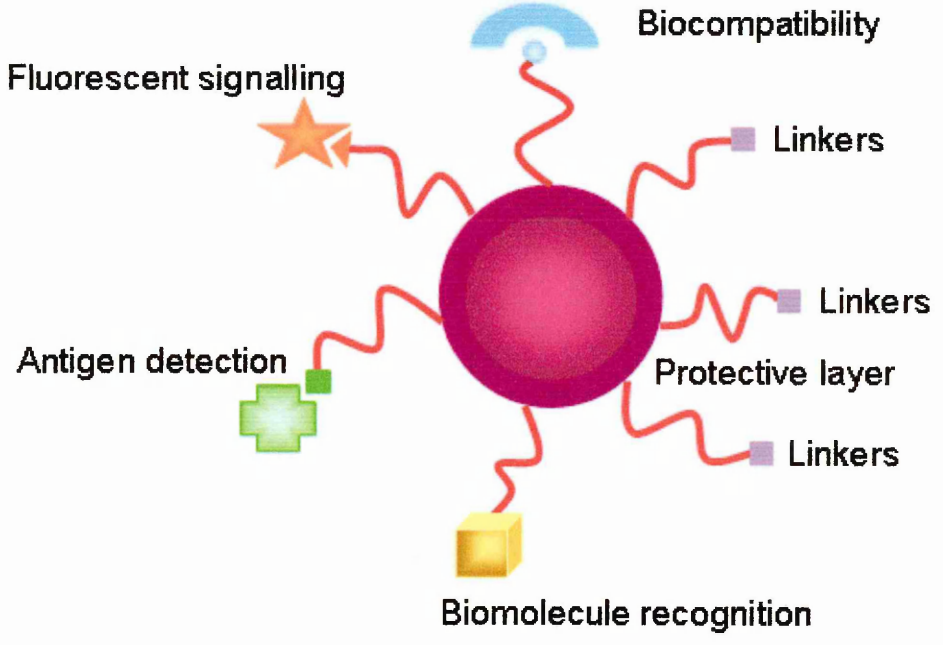

Figure 7. Features of the metal nanoparticles for biorecognition

Amide-functionalised AuNPs have been synthesised and used as optical sensors for anions,[101] and heavy metals have also been recognised using AuNPs-based

sensors.[102] The sensitivity of the plasmon band with the core environment is a source of sensing, and the optical response (SPB) has been studied,[103] in particular the colour sensitivity of the AuNP-DNA assemblies.

1.6 Applications of gold nanoparticles in biology and medicine

The use of gold colloids in biological applications began in 1971, when Faulk and Taylor invented the immunogold staining procedure. Since that time, the labelling of targeting molecules, especially proteins, with gold nanoparticles has achieved the visualisation of cellular or tissue components by electron microscopic techniques.[104]

There are two basic strategies in the development of receptor functionalised gold nanoparticles: the utilisation of (i) organic dyes and (ii) biological coatings that possess the ability to recognise and interact with specific biomolecules. Such systems are expected to form the basis of new diagnostic biosensor technologies and novel therapeutic agents. The most widely studied systems, reported in the literature, are based on gold due to their unique physical and chemical properties, previously mentioned. The main purpose of the construction of these biocompatible materials in most investigations is the detection of precise DNA sequences.[105]

1.6.1 Biomolecule-AuNP hybrid systems: conjugates for recognition of biomolecules

Many conjugation protocols have been reported in the literature for the labelling of a broad range of biomolecules with gold colloid, e.g., involving protein A, avidin, streptavidin, glucose oxidase and DNA (single and doubled-stranded).

Mirkin's group has pioneered strategies that rely on the use of biomolecules, such as DNA, to organise nanometer-sized and functional structures and materials. There are three categories: the use of

(i) Oligonucleotides (single stranded DNA) to prepare meso- and macroscopic organic structures.

(ii) Duplex DNA as a physical template for growing inorganic wires and organising nonbiological building blocks into extended hybrid materials.

(iii) Oligonucleotide functionalised gold nanoparticles and sequence-specific hybridisation reactions for organising such particles into functional structures.[5] Some of their strategies have already been shown to be useful in generating novel nanostructured materials,[106-108] and in developing a promising new detection technology for DNA.[109,110]

Gold nanoparticle conjugation was applied to polynucleotide detection in a manner that exploited the change in optical properties resulting from plasmon-plasmon interactions between locally adjacent gold nanoparticles. The characteristic red colour of gold colloid is known to change to a bluish-purple colour upon colloid aggregation.[93]

Storhoff and co-workers[109] developed a one-pot selective colourimetric polynucleotide detection method based on AuNP probes which align in a "tail-to-tail" manner onto a target polynucleotide. AuNPs (~ 13 nm diameter), which were capped with 3'- and 5'-(alkanethiol)oligonucleotides, were used to complex a 24 base polynucleotide target. They observed that after the hybridisation of the target with the probes, a change in colour of the solution from red to purple occurred, indicating the formation of an extended polymeric AuNP/polynucleotide aggregate. This change in colour was monitored by UV-visible techniques and a dramatic shift of the surface plasmon band of the AuNPs was observed (red shift of the SPB from 520 to 600 nm). Because of the extremely strong optical absorption of gold colloid, Storhoff and Mirkin[110] also suggested that this colourimetric method can be used to detect ~ 10 fmol of an oligonucleotide, which is 50 times more sensitive than sandwich hybridisation detection methods based on fluorescence detection.

Brust and co-workers[111] developed a highly sensitive and simple microarray method for protein detection and for assaying enzyme functionality. The identification and characterisation of substrates and inhibitors of kinases is of interest for the biomedical sciences since the phosphorylation of proteins by kinases plays a key role in regulating cellular processes and is believed to be involved in many diseases such as cancer, diabetes, and inflammation.[112,113] The method reported by Brust is based on labelling specific recognition or phosphorylation events on a microarray with gold nanoparticles using avidin-biotin chemistry followed by silver deposition for enhancement and resonance light scattering detection. This approach overcame the need

to use the radioactive labelling required for traditional assaying of kinase activities. Also, with this method, the screening of many different protein-protein or peptide-kinase interactions could be carried out simultaneously on the same microarray.

More recently, Wang and Brust[114] showed the use of specifically designed, peptide-stabilised gold nanoparticles as artificial substrates for kinases, and developed a very simple colorimetric method for the evaluation of kinase activity and inhibition, suggesting that this may have important implications for the future use of nanoparticle-based technologies in drug discovery.

1.6.2 Organic ligand coated-AuNPs: biocompatible nanomaterials for biomolecule recognition

Biomolecules are often coupled through non-covalent electrostatic interactions. Ligands carrying a positive group can interact with the polyanionic DNA molecule. The repulsive charges of these biomolecules should, in theory, prevent flocculation. As noted by Kumar and co-workers,[115] the attractive Coulombic interactions between the positively charged gold nanoparticle and the negatively charged DNA form linear, closely packed assemblies of varying lengths depending on the size of the DNA molecule. Petty and co-workers[116] also agree that the interaction of DNA with nanoparticles by electrostatic interaction depends on the nucleotide length.

The recognition of biomolecular surfaces relies on the fundamental interactions involved in small molecule host-guest systems and core-shell nanoparticle systems such

as monolayer protected clusters (MPCs) and mixed monolayer protected clusters (MMPCs). These possess four important attributes that make them promising scaffolds for the creation of receptors targeted to biomolecular surfaces:

(i) The size of the nanoparticle core can be controlled from 1.5 to 8 nm with overall diameters of 2.5 to 11 nm.[117] This control of core size allows particles to be made on comparable size scales to their biomolecular targets (Figure 8).

(ii) Nanoparticles can be fabricated with a wide range of surface functionality, providing a flexible route to the creation of surface-specific receptors.

(iii) MMPCs can be generated with a range of metal and semiconductor cores featuring useful electronic, fluorescence, and magnetic properties.[44] This versatility makes these systems excellent materials for probes and diagnostic agents.

(iv) MMPCs can self-template to complementary surfaces, which allows an increase in the affinity and selectivity of the recognition process on incubation with the guest.[118,119]

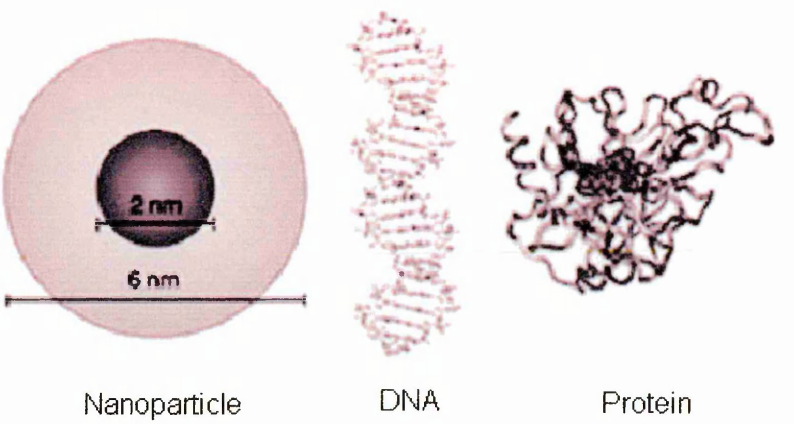

Figure 8. Fabrication of functionalised gold nanoparticles on comparable size scale of their biomolecular targeting, controlling their core size.[117]

To test the ability of MMPCs in modulation of DNA activity through non-covalent interactions, Rotello and co-workers[119] used gold nanoparticles (2nm) functionalised with octanethiol and 11-trimethylammoium-undecanethiol units, as MMPCs, to bind to DNA. The trimethylammonium end-groups on the MMPC surface could bind to the negatively charged phosphate backbone of 37mer duplex DNA through electrostatic complementarity (Figure 9). The binding of the DNA to the positively charged nanoparticles was monitored through a UV centrifugation assay, which relies on the change of the DNA conformation on the binding to this MMPC surface and its subsequent precipitation from the solution. The stoichiometry of association was found to be 4:1 nanoparticles to DNA duplex.

In solid phase studies, extended aggregates of this MMPC have been assembled using DNA templates.[120] The strength of the binding was further tested by the ability of the nanoparticles to inhibit DNA transcription in vitro. The authors demonstrated that on incubation with DNA, the MMPC effectively inhibited DNA transcription by T7 RNA polymerase.[121] The experimental results indicated that the MMPC with trimethylammonium end-groups binds with higher affinity than the T7 RNA polymerase or that the altered conformation of the nanoparticle-bound DNA interrupts the recognition process.

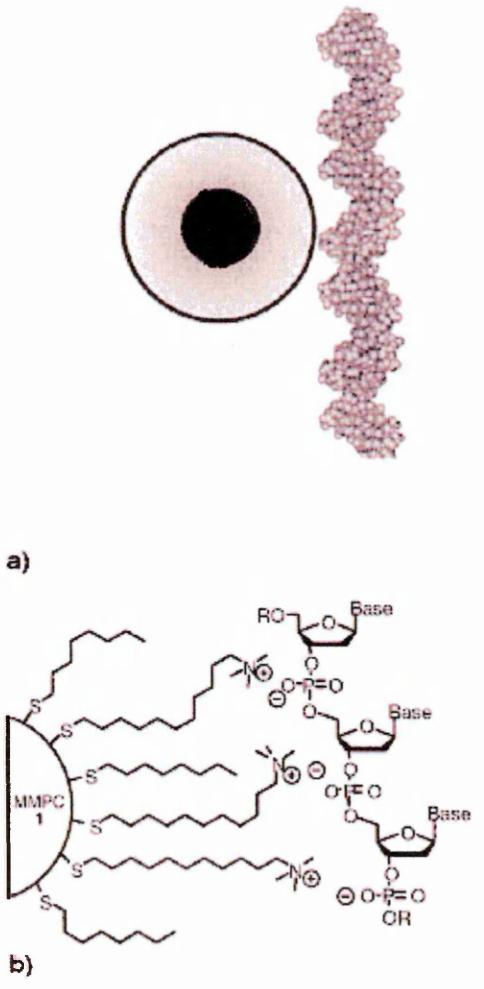

Figure 9. a) MMPC with C_8 and trimethylammonium end-group and 37-mer DNA counterpart (to scale), **b)** specific interactions formed between the cationic trimethylammonium side chains of MMPC and the anionic DNA[119]

Recently, the use of inorganic nanoparticles such as cationic gold nanoparticles as functional gene carriers was reported. The special character of the gold nanoparticles differs from that of organic gene carrier molecules and their use in nonviral gene delivery into cells promises to overcome the major obstacles of the application of nonviral systems to gene therapy.[122] Sandhu and co-workers[123] demonstrated that gold nanoparticles modified with *N,N,N*-trimethyl(11-mercaptoundecyl)ammonium chloride

and alkylthiols of several chain lengths (MMPCs) showed DNA-binding and transfection ability in cultivated mammalian cells. More recently, Niidome and co-workers[122] developed an easy method for the preparation of cationic gold nanoparticles modified with 2-aminoethanethiol, which have a shorter alkyl chain than the MMPCs, and examined the DNA-binding ability and transfection efficiency of these nanoparticles into cultivated cells (Figure 10).

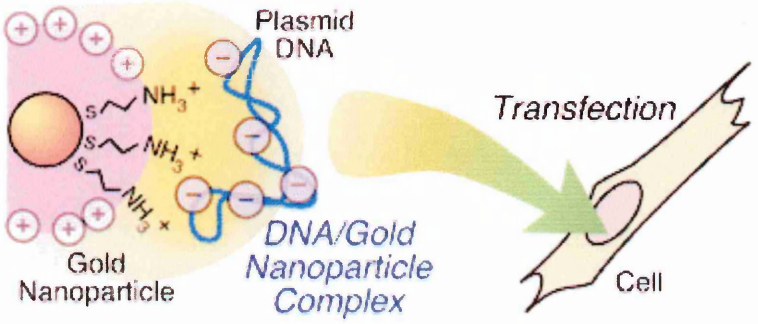

Figure 10. Preparation of primary amine-modified AuNPs and their transfection ability into cultivated cells.[122]

Wang and co-workers[124] have studied the possibility of ethidium intercalation as a means of inducing binding of AuNPs to DNA (Figure 11). These workers referred to their AuNPs as monolayer protected Au clusters (MPCs) because of the protective virtue of the ligand covering the gold. Ethidium cation was incorporated onto the surface of the cationic nanoparticle (AuNPs functionalised with *N,N,N*-trimethyl(11-mercaptoundecyl)ammonium chloride) only at a few places, restricting the reaction

sites. An increase in the ethidium fluorescence in the DNA-MPC solution was observed, indicating that the ethidium binding to DNA released some of the excitation energy.

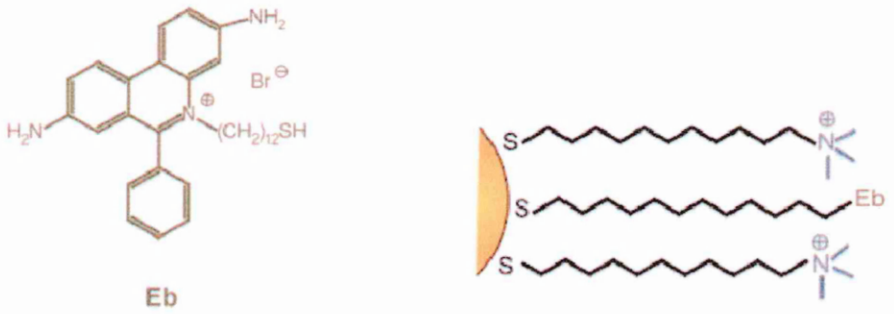

Figure 11. Structure of ethidium bromide (Eb) and structure of mixed monolayers protected cluster of trimethylammonium and ethidium thiolate.[124]

Cationic-functionalised nanoparticles have demonstrated versatility as transfection and recognition agents in a number of biomedical applications. However, all cationic-functionalising ligands currently reported in the literature contain various ammonium species. Based on the physical and chemical properties and the previous work on cationic monolayer protected gold colloids, this thesis describes the synthesis and characterisation of a family of novel cationic functionalised nanoparticles of gold modified with a new series of phosphonium thiolate ligands, as new alternative systems. The phosphonium moiety offers a number of advantages including biocompatibility and the relative ease of preparing a wide range of derivatives using a variety of substitution patterns. Lipophilic cations, such as methyltriphenylphosphonium (TPMP), have been shown to have a remarkable ability to cross phospholipid bilayers of mitochondrial membranes and accumulate inside the mitochondrion, with consequent influence on the chemistry of the host cell.[125-127] This ability to pass through biological membranes is due to the distribution of charge over a large, hydrophobic surface area.[128]

The more recent discovery of mitochondrial DNA (mtDNA)-associated diseases and the proposed role of mtDNA mutations in aging have led to renewed interest in these organelles and the genome they carry.[129] Few important proteins are encoded on mtDNA and expressed exclusively in the mitochondrial matrix. Long recognised as the site of ATP production in the animal cell, these organelles (Figure 12) are also key players in the apoptosis pathway for programmed cell death in addition to being involved in thermogenesis and calcium homeostasis.[129] Mitochondrial dysfunction may be due to mutations/deletions in either the nuclear genes encoding mitochondrial proteins or due to mutations/deletions in mtDNA.[125, 129]

Any mutation in mtDNA affects the normal function of the respiratory chain and causes defects in the final common pathway of oxidative metabolism. Therefore, the correction of these disorders by the administration of alternative metabolic carriers of energy does not seem to be possible.[130] However, strategies can be designed to repair mutations in the existing mtDNA or prevent the mutated mtDNA copies from replicating. For a permanent cure of mtDNA diseases, it is considered that the balance between mutated and healthy mtDNA needs to be shifted below the threshold level required for the phenotypic expression of the disease for the complete eradication of the mutated portion of the mitochondrial genome.[129, 130]

Due to the widely advanced development of nucleus targeting viral and non-viral vectors, many efforts to correct mitochondrial DNA defects have relied on the delivery of the therapeutic DNA to the nucleus. The viral approach to correct the

mtDNA mutations is based on the delivery of a construct of the wild type mitochondrial gene fused to a sequence encoding a mitochondrial targeting sequence into the nucleus, followed by nuclear cytosolic expression and subsequent import of the gene product into the mitochondria.[131,132] In contrast to the viral strategy, non-viral gene delivery systems have had a promising start in mitochondrial gene therapy.[133,134,135] Weissig and co-workers[129,134] have designed two non-viral mitochondria specific delivery vectors. The best characterised system is based on the use of vesicles prepared from mitochondriopic quinolinium compounds. These vesicles called DQAsomes have been developed for the purpose of transporting DNA specifically to the immediate vicinity of the mitochondrion of a live cell.[133,136,137]

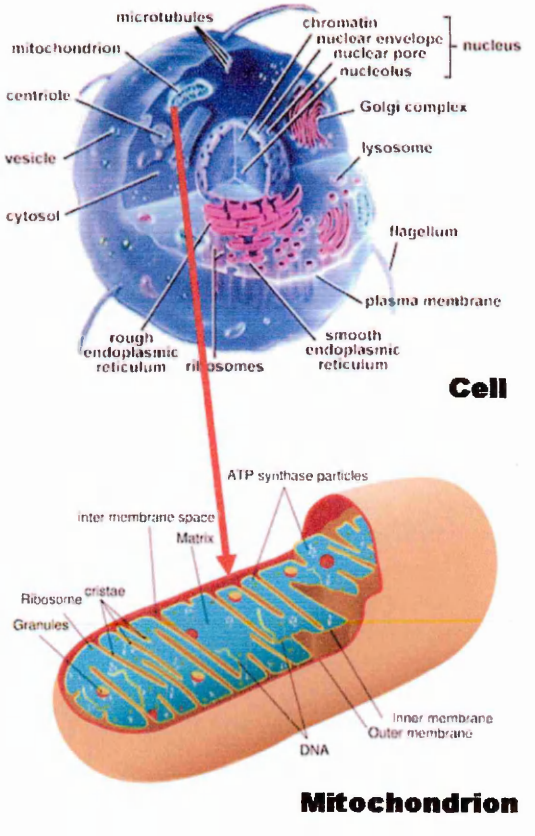

Figure 12. Mitochondrial organelle (Figure taken from: http://www.search.com/reference/Mitochondrion)

Given the relative ease with which liposome formulations can be modified with various targeting ligands, mitochondriotropic moieties synthesised with suitable linker motifs could be used to produce mitochondriotropic liposomes. Boddapati and co-workers[138] have described in their work the preparation of liposomes with a novel lipid consisting of a mitochondriotropic triphenylphosphonium cation conjugated to a stearyl anchor. These liposomes have been shown to be mitochondria specific in their subcellular distribution and preliminary data showed that these liposomes can be formulated to bind DNA and hence putatively serve as mitochondria-specific DNA delivery systems.[129] Following similar approaches, the phosphonioalkanethiol-capped gold nanoparticles in this thesis might be suitable for mitochondrial gene therapy using them as non viral gene delivery vectors (Figure 13).

The versatility of the triphenylphosphonium cation has been shown in several studies reported in the literature. Murphy and co-workers[139,140,141] have conjugated triphenylphosphonium cations with antioxidants and other probes to direct them selectively to mitochondria within cells and *in vivo*, and one such compound is now in phase II trials for Parkinson's disease. They have also improved the extent and selectivity of mitochondrial delivery by using lipophilic dications, and they have shown that these dications are dramatically more effective at delivering antioxidants to mitochondria *in vivo*.[125] Rideout and co-workers[142] have shown that cationic lipophilic compounds containing a triphenylphosphium group selectively accumulate in the mitochondria of carcinoma cells compared to normal cells, due to the characteristically elevated plasma membrane potentials of neoplastic cells.

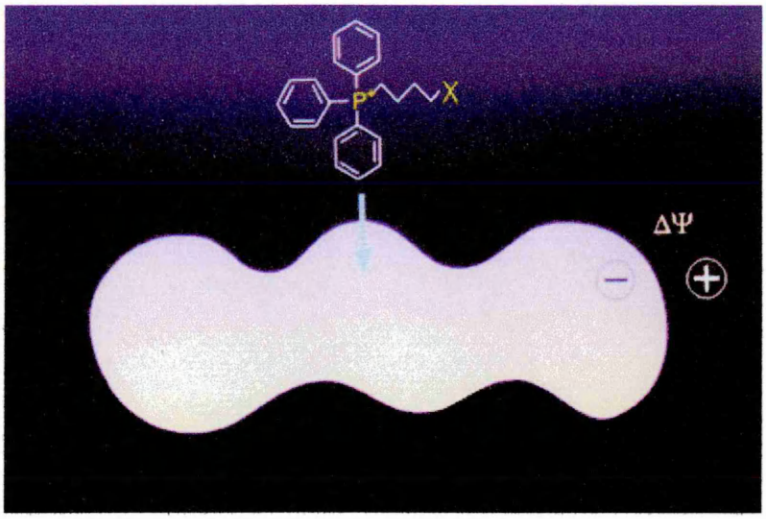

Figure 13. Utilisation of triphenylphosphonium cations as non-viral DNA delivery vectors in gene therapy.[128]

Thiobutyltriphenylphosphonium bromide has been used successfully by Murphy and co-workers[128] to identify changes in the redox state of mitochondrial thiol compounds during oxidative stress. They demonstrated that the lipophilic triphenylphosphonium cation interacts with the negatively charged mitochondrial matrix causing its accumulation inside the isolated mitochondria and in mitochondria from living cells.[143] These workers also detected the formation of disulfide bonds due to the reaction of the thiol groups in the matrix with the mitochondrial protein and low molecular weight thiols during the oxidative stress. This showed that such salts containing lipophilic cations can be used to determine mitochondrial dysfunction.[128,143,144]

Based on the importance of the mitochondriotropic triphenylphosphonium cations in mitochondrial gene therapy, gold nanoparticles functionalised with phosphonium cation-containing ligands have been fabricated as new potential delivery

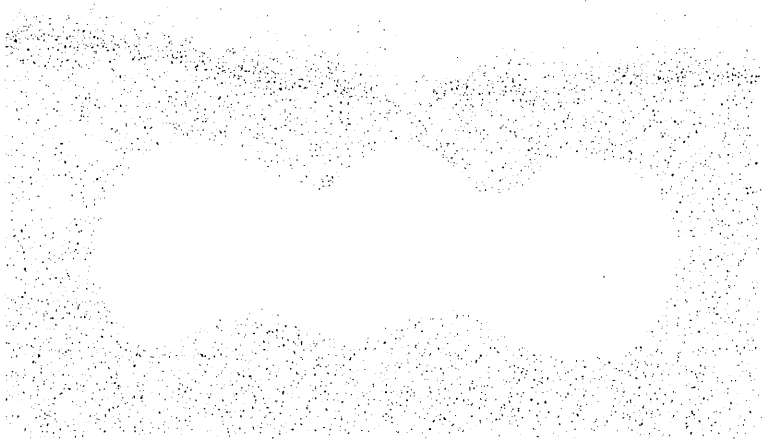

systems. This thesis describes the synthesis a new series of phosphonium thiolate compounds which behave as masked thiol ligands, and the fabrication and characterisation of a family of novel cationic functionalised gold nanoparticles using these ligands. The potential of these phosphonioalkylthiolate-functionalised gold nanoparticles as biorecognition systems for DNA detection through electrostatic interactions, using the Surface Plasmon Resonance technique, has also been explored.

1.7 Monolayer-protected metal clusters stabilised with phosphorus-containing ligands

Phosphorus has perhaps been one of the most studied elements and this has been translated into a considerable number of applications based on these discoveries expanding in different areas. According to Walker, one of the most prominent contributors in organophosphorus chemistry, phosphorus can be considered as dynamic element which can mimic carbon depending on its coordinated state.[145,146]

Organophosphorus chemistry can be classified into two broad categories. First, the reactions of the phosphorus atom itself, and second the modification of the reactions of the organic substituents by the presence of the phosphorus atom. Phosphorus, as carbon, occupies a fairly central position in the periodic table and can easily form bonds with either electronegative or electropositive elements. These bonds are generally strong (e.g. P—O, P—F, P—C), and therefore a wide variety of phosphorus compounds are known.[146]

In the trivalent state, phosphorus possesses a lone pair of electrons and is readily polarisable, which enables it to act as a nucleophile towards a wide range of species. However, phosphorus is relatively electropositive and so can also act as electrophile. This behaviour is assisted by the ready oxidation of phosphorus (III) to phosphorus (V), which further increases the range of compounds obtainable.[146]

The main objective of this section is to emphasize the most recent work based on the utilisation of phosphorus-containing compounds as protecting ligands in the synthesis of monolayer-protected metal clusters. The interest in these systems has been growing for several reasons during the past few years. Among these are the relevance to biological systems, the application to supramolecular chemistry, and electronics. Moreover, it has been shown that ^{31}P NMR spectroscopy is a convenient method to monitor monolayer-protected metal clusters synthesis and to characterise the phosphorus-containing ligands surrounding the metal nanoparticle surface.[147]

One of the most widely studied systems is the tertiary phosphine-stabilised gold nanoparticle, originally formulated as $Au_{55}(PPh_3)_{12}Cl_6$ by Schmid and co-workers in 1981.[37] These nanoparticles have been investigated as models for metallic catalysts and as building blocks for nanoscale electronic devices. The synthesis of the phosphine-stabilised gold nanoparticles reported by Schmid and co-workers[37] involved rigorous anaerobic conditions and diborane gas as reducing agent. However, Hutchinson and co-workers[148] reported a safer and more convenient synthesis of phosphine-stabilised nanoparticle analogous to those originally reported by Schmid.[37] The synthesis

eliminates the use of diborane or borane, and can be carried out quickly under ambient conditions. It allows the utilisation of a wide range of phosphines as passivating ligands, and provides control over particle core size.[148]

Hyeon and co-workers[149] have reported the synthesis of monodisperse palladium nanoparticles stabilised with several phosphine compounds. This has become possible through an understanding of the coordination chemistry of phosphine ligands on the palladium particles achieved using ^{31}P NMR spectroscopy. These palladium systems have also been investigated by El-Sayed and co-workers.[150] They investigated the effect of reagents and surfactants on the stability of palladium nanoparticles during Suzuki coupling reactions. The synthesis of phosphine fuctionalised nanoparticles has become very important due to the most recent work reported in the literature.[151] They discovered asymmetric catalytic applications of chiral phosphine-stabilised palladium nanoparticles.[149]

Glueck and co-workers[152] have described the synthesis of monolayer-protected gold cluster coated with phosphido (PR_2^-) groups. They prepared these nanoparticles in order to extend the investigations of the surface chemistry of gold, and they showed that in comparison to the Au-thiolate MPCs, fewer larger phosphido groups were required to cover the surface, and that the Au-P bond is not cleaved in reactions with small molecules as is its Au-S counterpart.[152]

Le Floch and co-workers[153] were the first to report the synthesis of gold nanoparticles coated by a substoichiometric amount of phosphinine ligands, and their immobilisation on mesostructured silica and titania hosts. They have shown that the phosphinines possess a pronounced π-accepting capacity and therefore are attractive ligands for the stabilisation of zerovalent metal nanoparticles.[153]

The synthesis of phospholipid-capped gold nanoparticles has been reported in the literature by Zhu and co-workers.[154] They have provided a method to fabricate biocompatible metal quantum dots based on liposomes as a template. Phospholipids are traditionally considered as a model system to study the biological membrane and its interaction with proteins due to their well-defined structure and property. The combination of biomolecules, especially lipids, with metal particles has been extensively applied as biosensors or for the drug delivery.[154,155] It has been shown that quantum dots of encapsulated CdS or CdSe semiconductor nanocrystals by phospholipid worked as *in vitro* fluorescent probes to hybridise to specific complementary sequences when conjugated to DNA.[156]

Organometallic-based pathways to obtain high quality cadmium selenide (CdSe) nanoparticles have been improved since their first synthesis in early 90's. A wide range of precursors of passivating ligands has been used to prepare nanoparticles of the desired size and shape. The most common surfactant, tri-*n*-octylphosphine oxide (TOPO) has been used as a passivating agent and as solvent for a wide range of materials, from semiconductors, to metals and metal oxides. In the synthesis of CdSe

nanoparticles, the selenium is often delivered in the form of a tri-*n*-octylphosphine selenide (TOPSe) solution, which has also been identified as a passivating agent as well as the selenium precursor. Green and co-workers[157] have investigated a phosphonium ionic liquid as a replacement for TOPO due to its potential to bind to both anionic (selenium) and cationic (cadmium) surface sites maintaining the solubility in organic solvents. The ionic liquid used by Green's group was trihexyl(tetradecyl)phosphonium bis(2,4,4-trimethylpentylphosphinate) and it was selected due to its thermal stability at temperatures associated with the nanoparticle synthesis, low bioactivity and potential for recycling.[157]

In Chapter 2, a brief description of the analytical methods employed to characterise all the compounds obtained in the project is outlined. In the three following chapters, the syntheses of phosphonium cation-containing ligands are described. Chapters 3, 4 and 5 describe the synthesis and structural characterisation by NMR, ESMS and X-ray crystallography of a new family of stable phosphonioalkylthiosulfate zwitterions, triphenyl- and thioacetyl-alkylphosphonium bromide and phosphonioalkyl selenolate zwitterions, respectively. In Chapter 6, the synthesis and characterisation by NMR, XPS and TEM of the cationic functionalised-gold nanoparticles using the previously synthesised compounds as protecting ligands are described. In Chapter 7, the immobilisation of the gold nanoparticles onto dextran sensor chips and studies of their potential as biorecognition systems using Surface Plasmon Resonance technique are described. Finally, Chapter 8 contains a summary of conclusions and some suggestions for future work.

CHAPTER 2

Experimental-General Methods

This chapter describes the general analytical methods used to characterise all the compounds and nanoparticles obtained during this project.

2.1 Melting point

Determination of the melting points of the solid state compounds were carried out using Electrothermal melting point apparatus, with a temperature gradient from room temperature (temp. ramp: 0.5°C).

2.2 Elemental analysis

All the samples submitted for elemental analysis were dried in an oven at 60°C. Carbon and Hydrogen analysis was carried out by MEDAC Ltd. (analytical and chemical consultancy service), Brunel Science Centre, Coopers Hill Lane, Englefield Green, Egham, Surrey, UK.

2.3 Thin layer chromatography (TLC)

Analytical thin layer chromatography (TLC) was performed on Merck silica gel 60F254 plates using mixtures of dichloromethane : methanol as eluent system.

2.4 Fourier transform infrared spectroscopy (FTIR)

KBr discs were prepared for solid samples (previously dried in an oven at 60°C) for the analysis by FTIR. Spectra were obtained on an ATI Mattson Instruments

Genesis Series FTIR spectrometer. The data were recorded using Winfirst software version 3.57.

2.5 Nuclear magnetic resonance spectroscopy (NMR)

Samples were dissolved in an appropriate deuterated solvent to a concentration of 10 to 15 mg mL^{-1} for proton and phosphorus-31 experiments. Spectra were obtained using a Brucker DMX 250 (250 MHz) nuclear magnetic resonance spectrometer with data recording and handling carried out using a Brucker mass spec 3000 computer running ADAKOS version 890201.0 software.

2.6 Mass spectrometry (MS)

Samples were dissolved in an appropriate solvent (methanol or acetonitrile) to a concentration of ~ 2 mg mL^{-1} for molecular ion determination. Electrospray mass spectra were recorded using an Applied Biosystems "QStar-Pulsar-i" hybrid quadrupole time of flight LCMSMS instrument.

2.7 Ultraviolet-visible absorption spectroscopy (UV-Vis)

Samples were analysed in quartz cuvettes with a 2 cm pathlength. UV-visible spectra were obtained on an ATI UNICAM UV2 spectrometer with data recording using Unicam Vision software version 3.42.

2.8 X-ray crystallography

Crystalline samples were submitted to the EPSRC National Crystallography Service at the Department of Chemistry, University of Southampton, Highfield, Southampton, UK. Detailed crystallographic reports, that give experimental details for each of the structures presented in this thesis, are contained in the appropriate experimental details in the respective chapters.

2.9 Transmission electron microscopy (TEM)

TEM analysis of the phosphonium gold nanoparticles was performed on a FEG-NOVA Nano-SEM (MERI, Sheffield Hallam University) and ZEISS STEM (Cambridge) instruments operating at 15 kV and 30 kV accelerating voltages, respectively.

2.10 X-ray photoelectron spectroscopy (XPS)

XPS measurements of the freeze-dried cationic phosphonium-AuNP samples were made on a KRATOS AXIS 165 Ultra Photoelectron Spectrometer operated at 10KV and 20mA using the Al K X-ray source (1486.6 eV). The takeoff angle was fixed at 90°.

CHAPTER 3

Synthesis of Phosphonioalkylthiosulfate Zwitterions

3.1 Introduction

Sulfur-Au bonding has been extensively investigated in many papers reported in the literature based on the synthesis of gold nanoparticles and self-assembled monolayers (SAMs). Among the reported sulfur-containing ligands that have been used for the generation of self-assembled monolayers on gold surfaces and nanoparticles, the most commonly used are thiols and disulfides.[19,21,48] In general, the synthetic strategies for the preparation of thiol- or disulfide-containing organic compounds consist of the addition of hydrogen sulfide to alkenes, or the substitution of alkyl halides and haloaromatic compounds carrying a strong electron-withdrawing substituent with RS^-. It is well-known that these reactions are accompanied by a significant amount of side products, mostly sulfur-containing compounds, in the synthesis of the thiol-containing ligands. In order to avoid the formation of these side products during the reaction, several synthetic methods have been developed including additional hydrolysis, reduction and bond cleavage steps. One disadvantage of thiol compounds is their strong and unpleasant smell,[47] and so their generation *in-situ* is a desirable goal.

Lukkari[47] and Murray[48] were the first to report the use of thiosulfate-containing ligands in the preparation of SAMs and functionalised gold nanoparticles, respectively, as novel alternatives to the thiol compounds already reported in the literature. Organic thiosulfates have the formula $RSSO_3M$, where R is an aliphatic or aryl group and M a monovalent cation. They also can be considered as *S*-alkyl or *S*-aryl esters of thiosulfuric acid, and are known as Bunte salts after the German chemist Hans Bunte, who was the first to study them, as long ago as the 1870s.[48]

Bunte salts have been shown to possess biological activity. For instance, sodium ethylthiosulfate exhibits a striking synergic effect when used with bacteriostatic 2-mercaptobenzothiazole against *Staphylococcus aureus*[158] and *tubercle bacillus*.[159] This antibacterial activity can be explained by the interaction of Bunte salts with cell membranes or by their influence on oxidation and reduction processes inside a bacterial cell. Czerwinski and co-workers[161] studied the electrochemical behaviour of the Bunte salts, and described the influence of the organic thiosulfate adsorption on their oxidation processes at the surfaces of two different electrodes, gold and platinum.

The principal advantage of using thiosulfates is their easy preparation compared to that of the corresponding thiols. Bunte salts can be obtained by the reaction of sodium thiosulfate and the corresponding alkyl halide in aqueous phase or in a mixture of organic and aqueous solvents (equation 1), and in many cases, the synthesis of a surface-active Bunte salt can be carried out in a one-step procedure.

$$R\text{-}X + Na_2S_2O_3 \longrightarrow R\text{–}SSO_3Na \qquad (1)$$

The crystalline odourless salts, which form as the final products, can be easily separated from the reaction mixture. Additionally, Bunte salts can be converted into the corresponding thiols in good yields without previous isolation. Lukkari[47] and Murray[48], using X-ray photoelectron spectroscopy (XPS), demonstrated the ability of the sulfur-sulfur bond to undergo cleavage with loss of sulfite ion as a result of the interaction with gold surfaces.

The interest in the chemistry of phosphonium systems has led to the design and synthesis of a family of novel phosphonioalkylthiosulfate ligands which can be used to functionalise the surface of gold nanoparticles. In this chapter, the synthesis and characterisation of a family of phosphonioalkylthiosulfate zwitterions is described.

3.2 Experimental

3.2.1 Synthesis of the series of triphenyl- and tributyl-phosphonioalkylthiosulfate zwitterions

The synthesis of the series of triphenyl- and tributyl-phosphonioalkylthiosulfate zwitterions has been carried out based on the work of Lukkari[47] and Murray.[48] Adapting these approaches, ω-bromoalkylphosphonium salts (**4**) have been converted into a series of phosphonioalkylthiosulfate zwitterions (**5a-5e**, R = phenyl, n = 3, 4, 6, 8, 10; **5f-5g**, R = butyl, n = 3, 6), which act as cationic masked thiols, being sources of the phosphonioalkanethiolates for the synthesis of the functionalised gold nanoparticles.

The pathway used in the synthesis of triphenyl- and tributyl-phosphonioalkylthiosulfate zwitterions is shown in Scheme 1. All the compounds were generated by the reaction of triphenylphosphine or tributylphosphine (3.8 mmol) with the appropriate bromo-alcohol (15 mmol) in acetonitrile under reflux for four hours, to obtain the corresponding hydroxyalkylphosphonium salts (**3**). The salts (**3**) were dissolved in HBr (48%) and heated under reflux for five hours to obtain the bromoalkylphosphonium salts (**4**). Finally, a series of phosphonioalkylthiosulfate zwitterions (**5**) was prepared by treatment of the salts (**4**) (1 mol) with sodium thiosulfate (1.5 mol) in aqueous ethanol under reflux for five hours. Progress of the reactions was monitored by TLC, using 20% methanol : 80% dichloromethane as mobile phase. Compounds (**4**) and (**5**) were obtained by dichloromethane extraction of

the reaction mixtures and initially purified by trituration with dry diethyl ether. Only the reaction of tributylphosphine with the corresponding bromo-alcohols was performed under nitrogen. The 4-triphenylphosphoniobutylthiosulfate (**5b**) was prepared from the commercially-available (4-bromobutyl)triphenylphosphonium bromide.

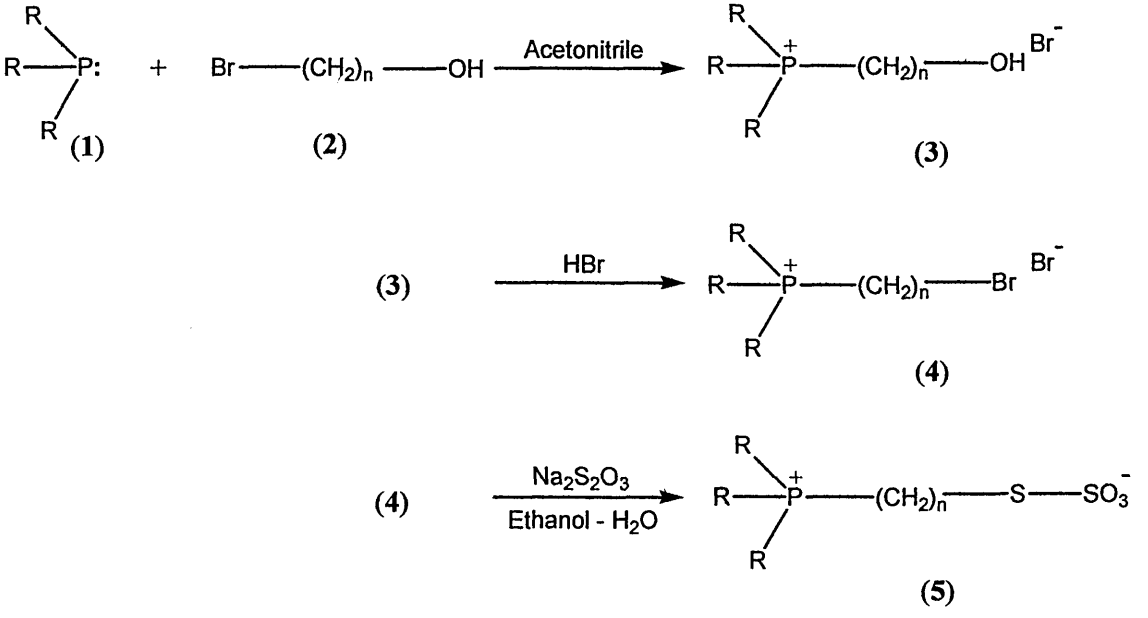

5a - 5e, R = Ph, n = 3, 4, 6, 8, 10
5f - 5g, R = Bu, n = 3, 6

Scheme 1

3.2.2 Synthesis of diphenyl-1-pyrenylphosphoniopropyl thiosulfate zwitterion

In order to investigate the use of fluorescent phosphoniumalkanethiosulfate zwitterions as protecting ligands for AuNPs, their interactions with DNA, and their use in fluorescence detection methods, the synthesis of the diphenyl-1-pyrenylphosphoniopropyl thiosulfate zwitterion (**11**) was carried out.

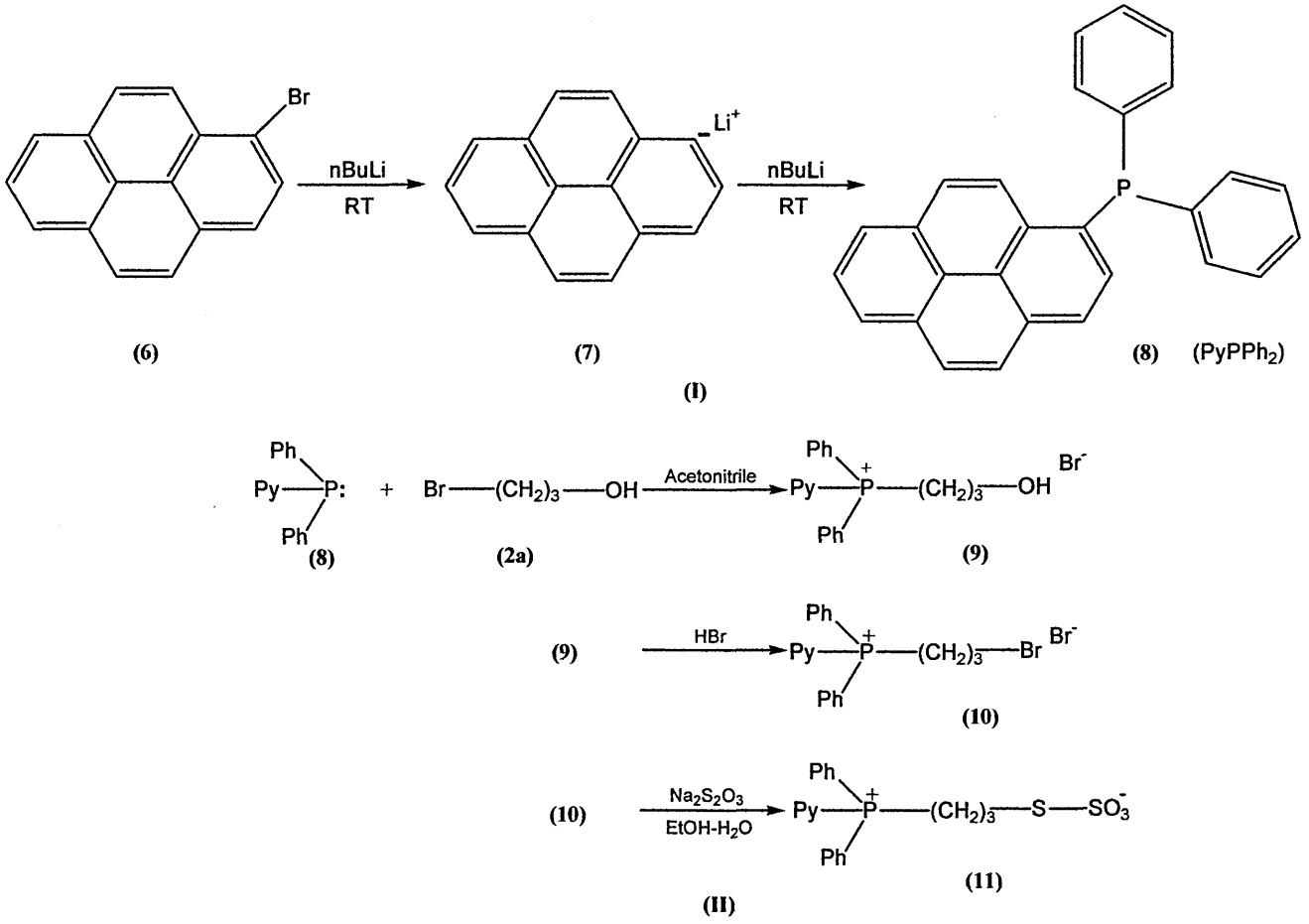

Scheme 2. Synthesis of diphenyl-1-pyrenylphosphine (**I**) and synthesis of diphenyl-1-pyrenylphosphoniopropyl thiosulfate zwitterion (**II**)

As a first step in the synthesis of diphenyl-1-pyrenylphosphoniopropyl thiosulfate zwitterion (**11**), the preparation of diphenyl-1-pyrenylphosphine (**8**), using the method of Craft[161] was carried out in order to use it as a starting material. This method involves the reaction of methyl diphenylphosphinite with 1-pyrenyllithium at -70°C. However, using this route, a lower yield of product was obtained than claimed by Craft. Furthermore, the ^{31}P NMR spectrum of the crude product displayed, in addition to the diphenyl-1-pyrenylphosphine signal at δ -13.1 ppm, peaks at δ -15.3, +22.2 and +33.4 corresponding to Ph_2PBu, Ph_2POMe and diphenyl-1-pyrenylphosphine oxide[161] in significant amounts. Consequently, in the present study, the synthesis of diphenyl-1-pyrenylphosphine was carried out at room temperature, using chlorodiphenylphosphine instead of methyl diphenylphosphinite as a starting material for the nucleophilic substitution reaction (Scheme 2. I).

The compound was formed by the reaction of bromopyrene (**6**) (1 mol) with n-butyllithium (1.2 mol) in dry THF at room temperature to give pyrenyllithium (**7**). After 1 hour, chlorodiphenylphosphine (0.9 mol) dissolved in dry THF, was added to the reaction mixture to obtain the diphenyl-1-pyrenylphosphine (**8**) after 3 hours stirring.

The diphenyl-1-pyrenylphosphoniopropyl thiosulfate zwitterion was obtained following the same procedure for the synthesis of triphenylphosphoniopropyl thiosulfate zwitterion (**5a**), using the previously synthesized diphenyl-1-pyrenylphosphine (**8**) instead of triphenylphosphine (**1**) (Scheme 2. II).

3.3 Characterisation of the series of triphenyl- and tributyl-phosphonioalkylthiosulfate zwitterions

3.3.1 3-Triphenylphosphoniopropylthiosulfate (5a)

The chemical structure of the compound **5a** is shown in Figure 14. This compound was isolated as colourless crystals which were suitable for X-ray crystallographic analysis. These crystals are soluble in polar organic solvents such as methanol, dichloromethane and acetonitrile.

Analytical and electrospray mass spectrometry (ESMS) data, ^{1}H and ^{31}P NMR spectroscopy support the formulation of this compound as **5a**. When studied by ESMS in positive mode, ions corresponding to [M+H], [M+Na] and [2M+Na] were observed.

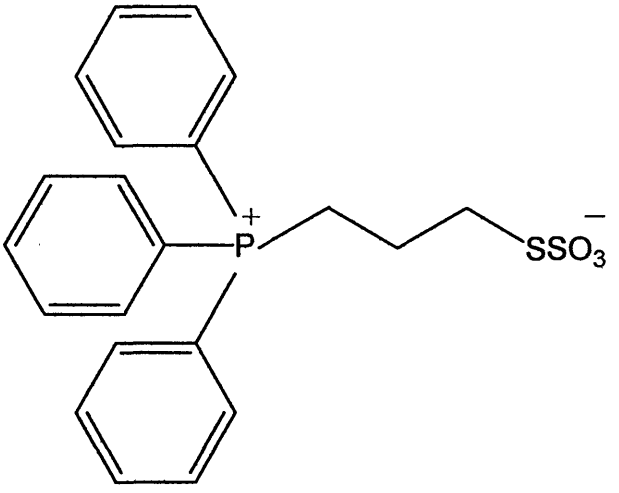

Figure 14. 3-Triphenylphosphoniopropylthiosulfate (**5a**)

Formula: $C_{21}H_{21}O_3PS_2$, Formula weight: 416.5

Melting Point: 240-243°C

Elemental Analysis:

Element	Carbon (%)	Hydrogen (%)
Theory	60.56	5.08
Found	60.53	5.11

ESMS: 417 [$M+H^+$], 439 [$M+Na^+$], 855 [$2M+Na^+$]

NMR: $\delta^{31}P$ NMR ($CDCl_3$/DMSO) = 23.2 ppm; δ^1H NMR ($CDCl_3$/DMSO) = 1.6 (2H,m), 2.6 (2H,m), 3.1 (2H,m), 7.2-7.3 (15H,m) ppm

3.3.2 4-Triphenylphosphoniobutylthiosulfate (5b)

The chemical structure of the compound **5b** is shown in Figure 15. This compound was isolated as a crystalline solid. The obtained crystals are soluble in polar organic solvents such as methanol and dichloromethane and fairly soluble in acetonitrile.

Analytical and electrospray mass spectrometry (ESMS) data, and ^1H and ^{31}P NMR spectroscopy support the formulation of this compound as **5b**. When studied by ESMS in positive mode, ions corresponding to [M+H], [M+Na] and [2M+Na] were observed.

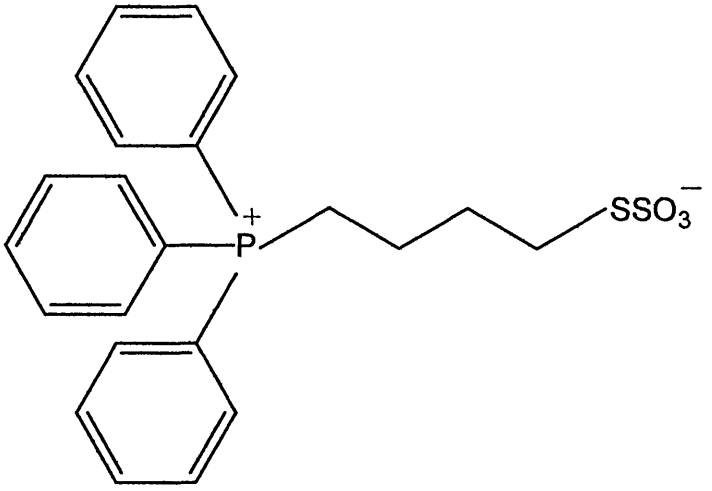

Figure 15. 4-Triphenylphosphoniobutylthiosulfate (**5b**)

Formula: $C_{22}H_{23}O_3PS_2$, Formula weight: 430.52

Melting Point: 256-260°C

Elemental Analysis:

Element	Carbon (%)	Hydrogen (%)
Theory	61.38	5.38
Found	61.24	5.55

ESMS: 431 [$M+H^+$], 453 [$M+Na^+$], 883 [$2M+Na^+$]

NMR: $\delta^{31}P$ NMR ($CDCl_3$/DMSO) = 23.6 ppm; δ^1H NMR ($CDCl_3$/DMSO) = 1.6 (2H,m), 2.2 (2H,m), 2.7 (2H,t), 3.5 (2H,m), 7.3-7.5 (15H,m) ppm

3.3.3 6-Triphenylphosphoniohexylthiosulfate (5c)

The structure of compound **5C** is shown in Figure 16. It was isolated as light crystalline flakes; however this solid proved to be unsuitable for X-ray crystallographic analysis. Analytical and electrospray mass spectrometry (ESMS) data, ^{1}H and ^{31}P NMR spectroscopy, support the formulation of this compound as 6-triphenylphosphoniohexylthiosulfate.

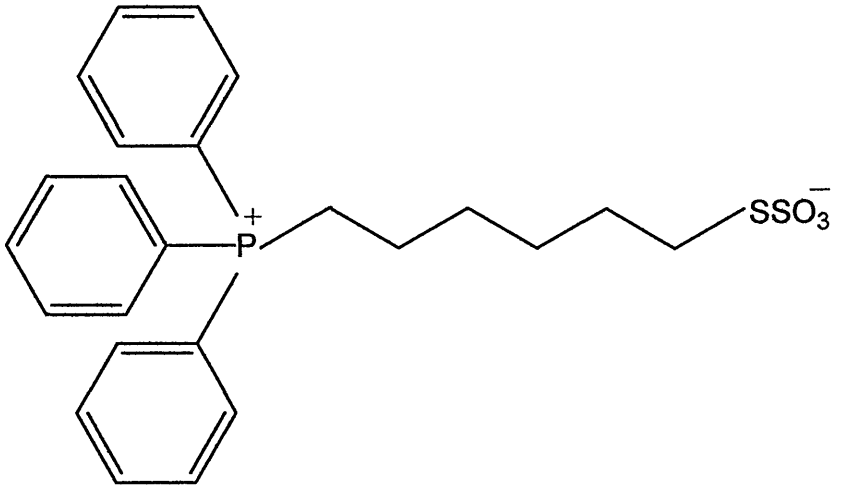

Figure 16. 6-Triphenylphosphoniohexylthiosulfate (**5c**)

Formula: $C_{24}H_{27}O_3PS_2$, Formula weight: 458.58

Melting Point: 63-65°C

Elemental Analysis:

Element	Carbon (%)	Hydrogen (%)
Theory	62.86	5.93
Found	62.12	5.95

ESMS: 459 [$M+H^+$], 481 [$M+Na^+$], 939 [$2M+Na^+$]

NMR: δ^{31}P NMR ($CDCl_3$) = 24.06 ppm; δ^1H NMR ($CDCl_3$) = 1.5 (2H,m), 1.6 (4H,m), 1.7 (2H,m), 3.05 (2H,t), 3.4 (2H,m), 7.6-7.8 (15H,m) ppm.

3.3.4 8-Triphenylphosphoniooctylthiosulfate (5d)

The structure of compound **5d** is shown in Figure 17. It was isolated as a pale cream powder. Attempts to isolate this compound as a crystalline solid were unsuccessful and it was therefore unsuitable for X-ray analysis. Analytical and electrospray mass spectrometry (ESMS) data, ^{1}H and ^{31}PNMR spectroscopy support the formulation of this compound as 8-triphenylphosphoniooctylthiosulfate.

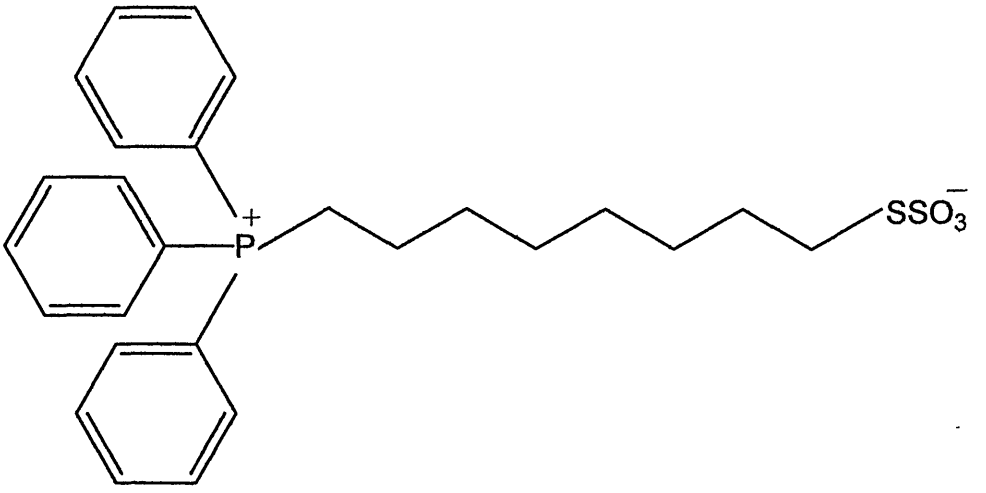

Figure 17. 8-Triphenylphosphoniooctylthiosulfate (**5d**)

Formula: $C_{26}H_{31}O_3PS_2$, Formula weight: 486.63

Melting Point: 40-45°C

Elemental Analysis:

Element	Carbon (%)	Hydrogen (%)
Theory	61.88	6.59
Found	62.14	6.37

ESMS: 485 [M^+], 510 [$M+Na^+$]

NMR: δ^{31}P NMR ($CDCl_3$) = 23.8 ppm; δ^1H NMR ($CDCl_3$) = 1.2 (5H,m), 1.5 (7H,m), 2.4 (1H,m), 2.9 (1H, t, J = 6.2 Hz), 3.3 (2H,m), 7.6-7.7 (15H,m) ppm.

3.3.5 10-Triphenylphosphoniodecylthiosulfate (5e)

The structure of compound **5e** is shown in Figure 18, and it was isolated as pale yellow solid. Attempts to isolate this compound as a crystalline solid were unsuccessful and it was therefore proved to be unsuitable for X-ray analysis. Analytical and electrospray mass spectrometry (ESMS) data, ^{1}H and ^{31}P NMR spectroscopy supported the formulation of this compound as 10-triphenylphosphoniodecylthiosulfate.

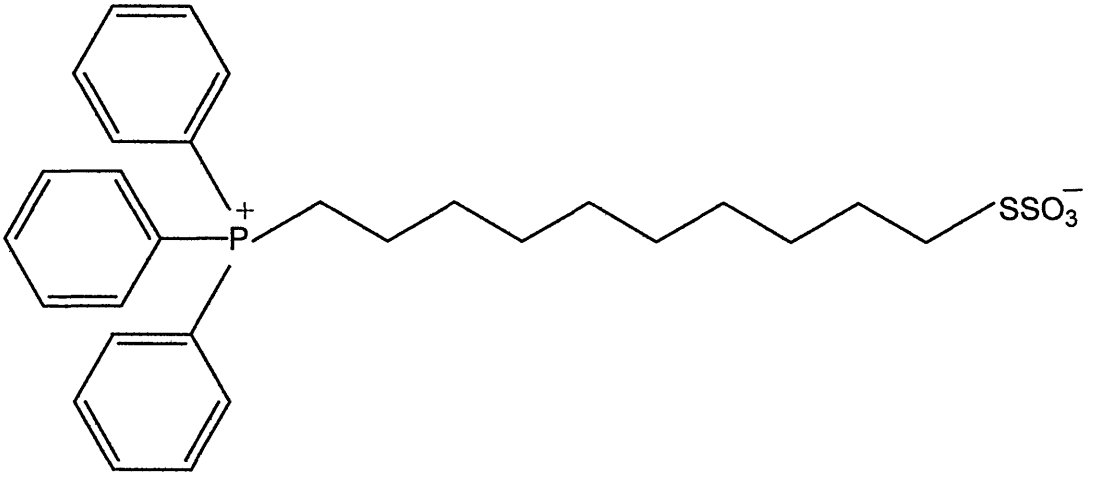

Figure 18. 10-Triphenylphosphoniodecylthiosulfate (**5e**)

Formula: $C_{28}H_{35}O_3PS_2$, Formula weight: 514.68

Melting Point: 60-65°C

Elemental Analysis:

Element	Carbon (%)	Hydrogen (%)
Theory	63.13	7.00
Found	63.69	6.75

ESMS: 513 [M^+], 538 [$M+Na^+$]

NMR: δ^{31}P NMR ($CDCl_3$) = 23.6 ppm; δ^1H NMR ($CDCl_3$) = 1.0 (8H,m), 1.4 (6H,m), 3.2 (2H,m), 3.9 (4H,m), 7.5-7.7 (15H,m) ppm.

3.3.6 3-Tributylphosphoniopropylthiosulfate (5f)

The structure of compound **5f** is shown in Figure 19. **5f** was isolated as colourless crystals. They proved to be suitable for X-ray analysis. Analytical and electrospray mass spectrometry (ESMS) data, ^{1}H and ^{31}PNMR spectroscopy supported the formulation of this compound as 3-tributylphosphoniopropylthiosulfate.

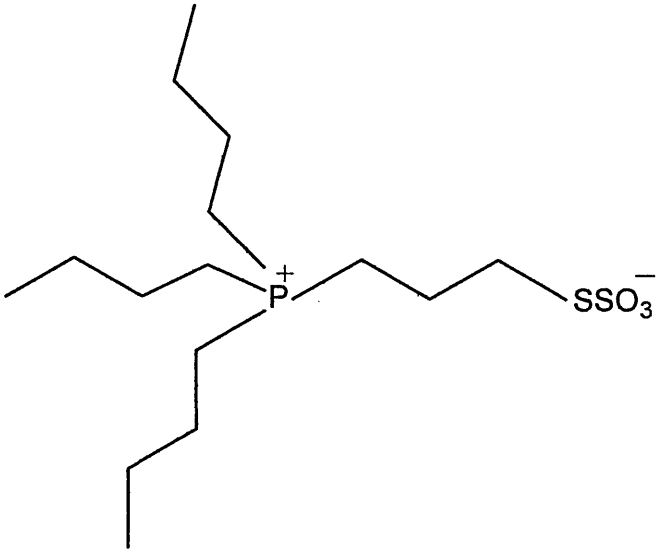

Figure 19. 3-Triphenylphosphoniopropylthiosulfate (**5f**)

Formula: $C_{15}H_{33}O_3PS_2$, Formula weight: 356.53

Melting Point: 133-136°C

Elemental Analysis:

Element	Carbon (%)	Hydrogen (%)
Theory	50.53	9.33
Found	50.27	9.69

ESMS: 357 [$M+H^+$], 379 [$M+Na^+$], 735 [$2M+Na^+$], 1091 [$3M+Na^+$]

NMR: $\delta^{31}P$ NMR ($CDCl_3$) = 33.7 ppm; δ^1H NMR ($CDCl_3$) = 0.9 (9H,t), 1.5 (12H,m), 2.1 (8H,m), 2.5 (2H,m), 3.1 (2H, t, J = 6.7 Hz) ppm.

3.3.7 6-Tributylphosphoniohexylthiosulfate (5g)

The structure of compound **5g** is shown in Figure 20. **5g** was isolated as a colourless oil. Attempts to isolate **5g** as a crystalline solid for X-ray analysis were unsuccessful. Matrix-assisted laser desorption ionization (MALDI) time-of-flight mass spectrometry (TOFMS) positive ion mode (accurate analysis), ^1H and ^{31}P NMR spectroscopic data supported the formulation of this compound as 6-tributylphosphoniobutylthiosulfate.

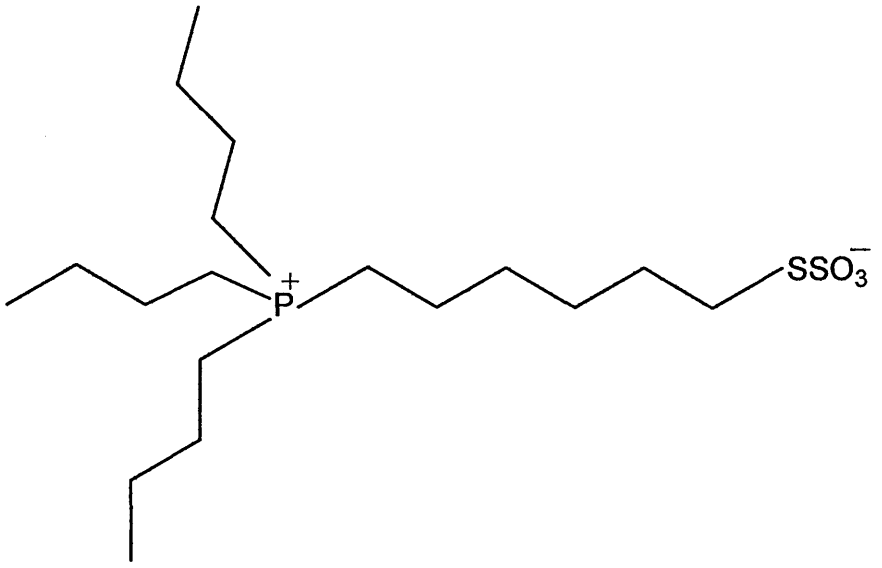

Figure 20. 6-Tributylphosphoniohexylthiosulfate (**5g**)

Formula: $C_{18}H_{39}O_3PS_2$, Formula weight: 398.61

MALDI-TOFMS:

Elemental	**[M+H$^+$]**
Theory	399.6103
Found	399.6099

NMR: δ^{31}P NMR ($CDCl_3$) = 24.06 ppm, δ^1H NMR ($CDCl_3$) = 1.5 (2H,m), 1.6 (4H,m), 1.7 (2H,m), 3.05 (2H, t, J = 6.6 Hz), 3.4 (2H,m), 7.6-7.8 (15H,m) ppm.

3.3.8 Diphenyl-1-pyrenylphosphoniopropyl thiosulfate zwitterion

3.3.8.1 Diphenyl-1-pyrenylphosphine (8)

The structure of compound **8** is shown in Figure 21. Compound **8** was isolated as a yellow powder. Attempts to isolate **8** as a crystalline solid for X-ray analysis were unsuccessful. Electrospray mass spectrometry (ESMS), MALDI-TOFMS positive ion mode (accurate analysis), ^{1}H and ^{31}P NMR spectroscopic data supported the identification of this compound as diphenyl-1-pyrenylphosphine.

The yield of the product from the reaction with the new conditions was 76%. The ^{31}P NMR spectrum of the final product showed a major signal at -13.3 ppm due to the phosphine, and traces of the corresponding oxide at 32.8 ppm. The ESMS spectrum in positive mode showed a well-defined molecular ion $[M+H^{+}]$ 383.

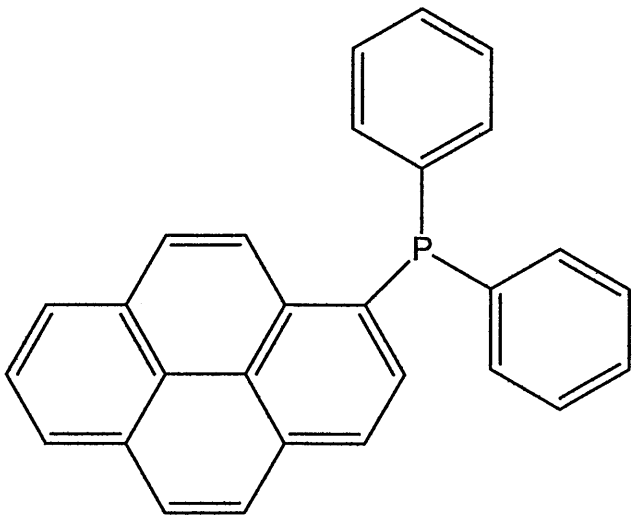

Figure 21. Diphenyl-1-pyrenylphosphine (**8**)

Formula: $C_{28}H_{19}P$, Formula weight: 386.12

Melting Point: 183 °C

ESMS: 387 [$M+H^+$]

MALDI-TOFMS:

Elemental	[M]
Theory	386.1224
Found	386.1233

NMR: $\delta^{31}P$ NMR ($CDCl_3$) = -13.3 ppm, $\delta^{1}H$ NMR ($CDCl_3$)=7.6-7.9 (10H,m), 8.1-8.5 (9H,m).

3.3.8.2 Diphenyl-1-pyrenylphosphoniopropylthiosulfate (11)

The chemical structure of compound **11** is shown in Figure 22. Compound **11** was isolated as a tanned yellow powder. Attempts to isolate **11** as a crystalline solid for X-ray analysis were unsuccessful. Electrospray mass spectrometry (ESMS), MALDI-TOFMS positive ion mode (accurate analysis), ^{1}H and ^{31}P NMR spectroscopic data supported the identification of this compound as diphenyl-1-pyrenylphosphoniopropylthiosulfate.

The ^{1}H NMR and ^{31}P NMR and electrospray mass spectrometry (ESMS) data supported the identification of the synthesized compound. This compound is soluble in ethanol, acetonitrile and dichloromethane.

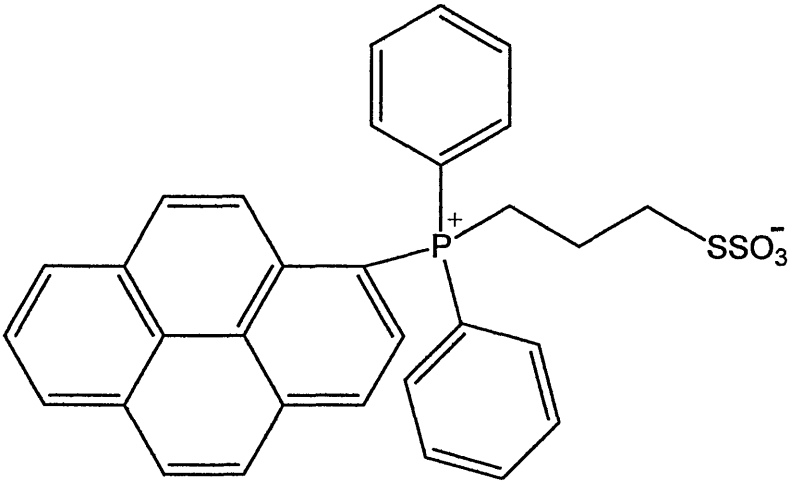

Figure 22. Diphenyl-1-pyrenylphosphoniopropylthiosulfate (**11**)

Formula: $C_{31}H_{25}O_3S_2P$, Formula weight: 540.63

Melting Point: 255 °C

ESMS: 541 [M+H$^+$]

MALDI-TOFMS:

Elemental	**[M+H$^+$]**
Theory	541.1262
Found	541.1259

NMR: $\delta^{31}P$ NMR ($CDCl_3$)=23.5ppm, $\delta^{1}H$ NMR ($CDCl_3$)=2.3 (2H,m), 3.3 (2H,m), 3.9 (2H,m), 7.2-7.9 (10H,m), 8.1-8.5 (9H,m) ppm.

3.4 X-ray crystallography

3.4.1 3-Triphenylphosphoniopropylthiosulfate zwitterion (5a)

An X-ray structural study of the triphenylphosphoniopropylthiosulfate (**5a**, R = Ph, n = 3) was carried out which confirms the expected structure (Figure 23). Crystal data and structure refinement details are presented in Table 1. Selected bond lengths and bond angles are presented in Table 2. There are no intramolecular interactions between the cationic head group and the thiosulfato group which could lead to the formation of a quasi-7-membered cyclic structure from the electrostatic attraction of P^+ with O^-.

Similarly, intermolecular electrostatic effects do not appear to dominate the way in which the dipolar units pack in the crystal, which is rather unusual. Along the [101] direction the individual units pack in a head-to-head manner in which 'supramolecular edge to face' interactions between the triphenylphosphonio units[162], and possible weak C-H · · · O hydrogen bonds (*ca.* 2.5Å) seem to dominate. Along the [10-1] direction an intermolecular 'head-to-tail' arrangement is found, whereas along the [010] direction, the individual units associate as 'head-to-tail' dimers.

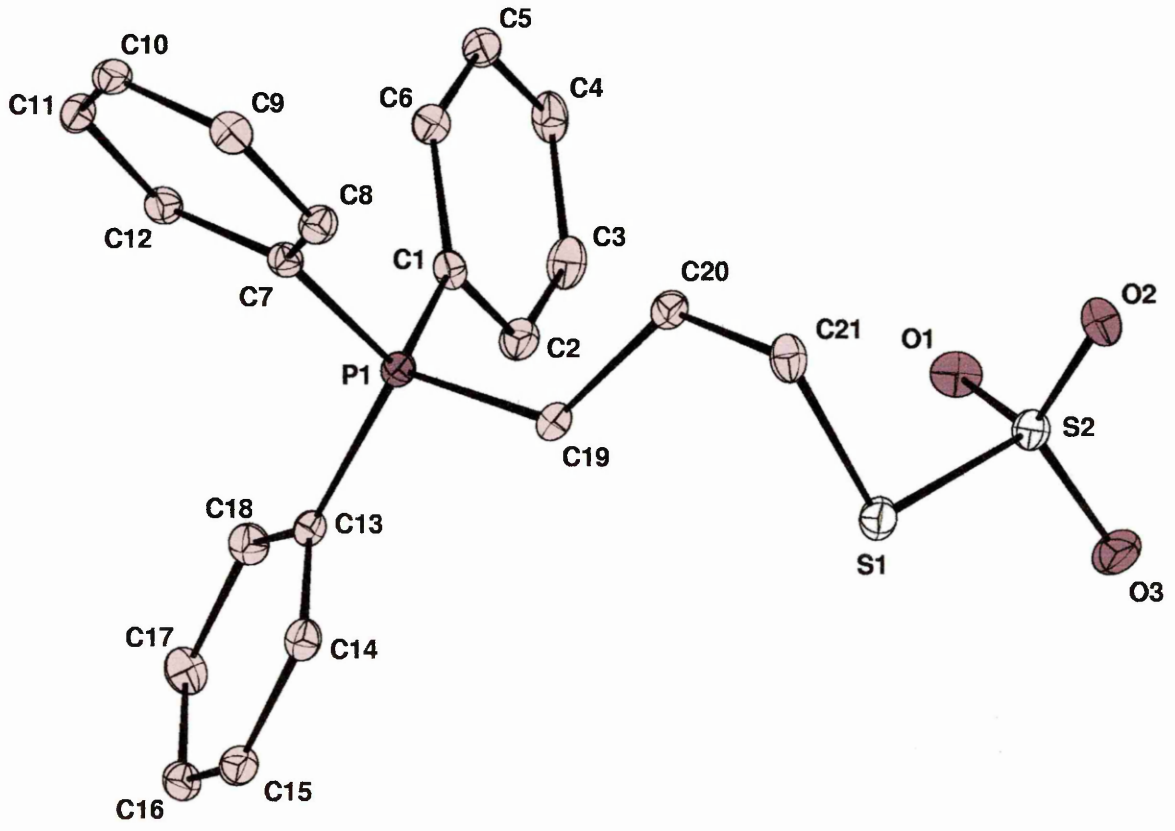

Figure 23. Molecular structure of 3-triphenylphosphoniopropylthiosulfate (**5a**)-an ORTEP drawing with 30% probability ellipsoids.

Table 1. Crystal data and structure refinement for 3-triphenylphosphoniopropylthiosulfate (**5a**)

Compound	**5a**
Empirical formula	$C_{21}H_{21}O_3PS_2$
Formula weight	416.47
Crystal system	Monoclinic
Space group	$P2_1/n$
a (Å)	11.6475(3)
b (Å)	14.2692(3)
c (Å)	12.0730(3)
β (°)	β = 106.561(1)
Volume (Å^3)	1923.30(8)
Z (	4
D_{calc} (Mg / m^3)	1.438
Absorption coefficient (mm^{-1})	0.380
F(000)	872
Crystal	Colourless Block
Crystal size (mm^3)	0.15 × 0.08 × 0.08
θ range for data collection (°)	3.39 – 25.02
Reflections collected	6267
Independent reflections	3381 [R_{int} = 0.0434]
Completeness to θ = 25.02°	99.7 %
Max. and min. transmission	0.9924 and 0.9630
Data / restraints / parameters	3381 / 0 / 244
Goodness-of-fit on F^2	1.043
Final R indices [$F^2 > 2\sigma(F^2)$]	*R1* = 0.0416, *wR2* = 0.0994
R indices (all data)	*R1* = 0.0565, *wR2* = 0.1068
Largest diff. peak and hole	0.311 and –0.444 e Å^{-3}

Table 2. Selected bond lengths [Å] and angles [°] in 3-triphenylphosphoniopropylthiosulfate zwitterion (**5a**).

C1–P1	1.795(2)	O1–S2	1.4507(19)
C7–P1	1.792(2)	O2–S2	1.4442(18)
C13–P1	1.794(2)	O3–S2	1.4484(19)
C19–P1	1.805(2)	S1–S2	2.1117(9)
C21–S1	1.820(3)		
C20–C19–P1	115.39(17)	C21–S1–S2	99.77(9)
C20–C21–S1	114.77(18)	O2–S2–O3	115.11(12)
C7–P1–C1	107.97(11)	O2–S2–O1	113.38(11)
C7–P1–C13	111.12(11)	O3–S2–O1	113.15(12)
C1–P1–C13	110.13(11)	O2–S2–S1	105.60(7)
C7–P1–C19	111.92(11)	O3–S2–S1	101.20(8)
C1–P1–C19	108.79(11)	O1–S2–S1	106.97(8)
C13–P1–C19	106.90(11)		

3.4.2 3-Tributylphosphoniopropylthiosulfate zwitterion (5f)

An X-ray structural study of the 3-tributylphosphoniopropylthiosulfate (**5f**, R = Bu, n = 3) confirmed the expected structure (Figure 24). Crystal data and structure refinement details are presented in Table 3. Selected bond lengths and bond angles are presented in Table 4. Figure 25 shows possible hydrogen bonding between C–H bonds α to the phosphonium centre and the thiosulfato oxygen atoms which influence the packing of the molecules in the unit cell. The structural parameters for these hydrogen bond interactions are presented in Table 5.

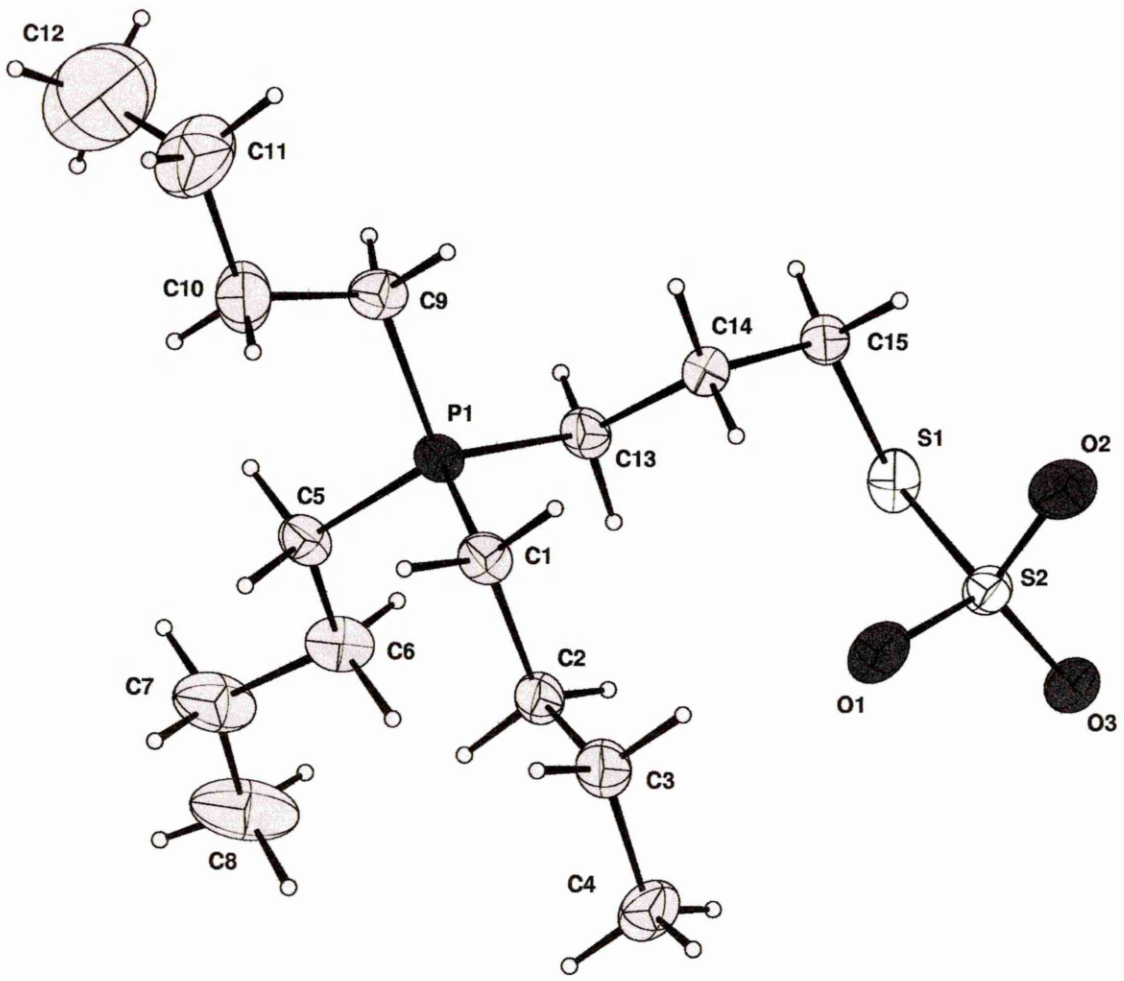

Figure 24. Molecular structure of 3-tributylphosphoniopropylthiosulfate (**5f**)

Table 3. Crystal data and structure refinement for 3-tributylphosphoniopropylthiosulfate zwitterion (**5f**)

Compound	**5f**
Empirical formula	$C_{15}H_{33}O_3PS_2$
Formula weight	356.50
Crystal system	Monoclinic
Space group	$P2_1/n$
a (Å)	9.0500(3)
b (Å)	14.3012(4)
c (Å)	15.0732(6)
β (°)	96.326(2)
Volume (Å^3)	1938.98(11)
Z (	4
D_{calc} (Mg / m^3)	1.221
Absorption coefficient (mm^{-1})	0.364
F(000)	776
Crystal	Colourless Block
Crystal size (mm^3)	0.10 × 0.10 × 0.03
θ range for data collection (°)	3.07 – 25.02
Reflections collected	23499
Independent reflections	3406 [R_{int} = 0.0797]
Completeness to θ = 25.02°	99.7 %
Max. and min. transmission	0.9892 and 0.9645
Data / restraints / parameters	3406 / 39 / 194
Goodness-of-fit on F^2	1.042
Final R indices [$F^2 > 2\sigma(F^2)$]	$R1$ = 0.0594, $wR2$ = 0.1487
R indices (all data)	$R1$ = 0.0775, $wR2$ = 0.1589
Largest diff. peak and hole	1.078 and –0.633 e Å^{-3}

Table 4. Selected bond lengths [Å] and angles [°] in 3-tributylphosphoniopropylthiosulfate zwitterion (**5f**).

P1–C9	1.796(4)	S1–S2	2.1030(14)
P1–C5	1.798(3)	S2–O2	1.439(3)
P1–C13	1.799(4)	S2–O3	1.440(3)
P1–C1	1.805(3)	S2–O1	1.441(3)
S1–C15	1.805(4)		
C9–P1–C5	107.56(17)	O3–S2–O1	113.90(18)
C9–P1–C13	108.13(18)	O2–S2–S1	104.75(14)
C5–P1–C13	110.89(17)	O3–S2–S1	102.34(13)
C9–P1–C1	110.16(16)	O1–S2–S1	106.67(14)
C5–P1–C1	110.32(18)		
C13–P1–C1	109.73(18)		
C15–S1–S2	99.78(14)		
O2–S2–O3	114.45(18)		
O2–S2–O1	113.3(2)		

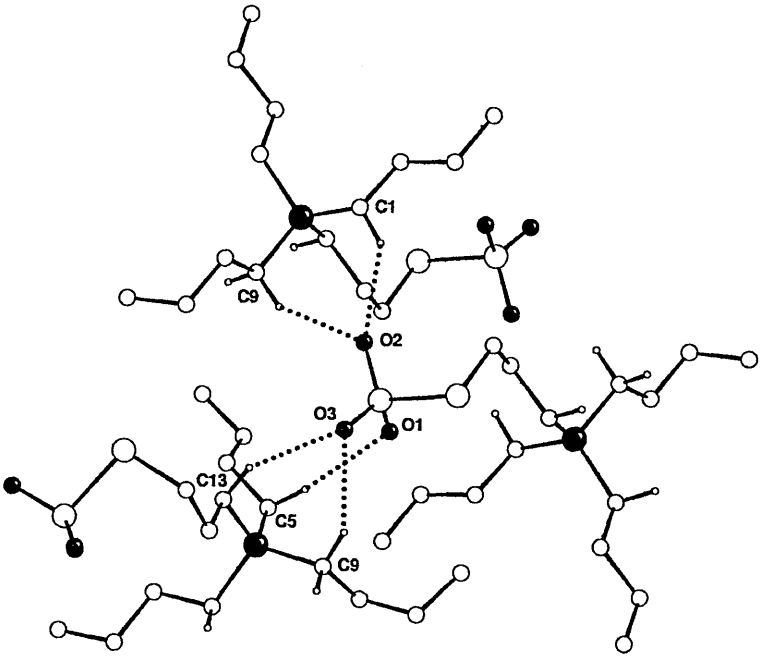

Figure 25. Intermolecular contacts showing possible hydrogen bonding between C–H bonds α to the phosphonium centre and thiosulfato oxygen atoms in 3-tributylphosphoniopropylthiosulfate.

Table 5. Intermolecular contacts for hydrogen bonding between C–H bonds α to the phosphonium centre and thiosulfato oxygen atoms in 3-tributylphosphoniopropylthiosulfate **5f**

Donor	H	Acceptor	Symm	D - H	H...A	D...A	D - H...A
C(1)	H(1A)	O(2)	$1	0.99	2.44	3.2657	140
C(5)	H(5B)	O(1)	$2	0.99	2.44	3.4173	171
C(9)	H(9A)	O(2)	$1	0.99	2.39	3.2529	146
C(9)	H(9B)	O(3)	$2	0.99	2.45	3.2929	142
C(13)	H(13B	O(3)	$2	0.99	2.54	3.3672	141

$1 = 1-x,-y,1-z,
$2 = -1/2+x,1/2-y,-1/2+z

P1...O2 = 3.744(13) $1
P1...O3 = 3.541(12) $2
P1...O1 = 4.730(16)

A successfully synthetic strategy has been developed for the preparation of a novel family of compounds containing cationic phosphonium functional groups. The use of these compounds for the formation of functionalised gold nanoparticles is presented in Chapter 6.

CHAPTER 4

Synthesis of Phosphonioalkylselenide Ligands

4.1 Introduction

Most of the compounds used as protecting ligands in the synthesis of functionalised gold nanoparticles reported in the literature are those containing thiol groups. Selenoate anions offer an alternative to thiolates as capping agents for gold surfaces as a result of the similarity of the sulfur and selenium atoms in terms of chemical properties. Despite this similarity, organo-selenols and diselenides have not received the same attention as the sulfur analogues in this regard and there are only a few examples of organoselenium-stabilised MPCs, although organoselenium species, including dialkyl diselenides and dialkyl selenides are known to form self-assembled monolayers (SAMs) on planar noble metal surfaces.[163]

Kim and co-workers investigated the adsorption behaviour of benzeneselenol (BSe) and diphenyl diselenide (DPDSe) on a gold substrate by Surface Enhanced Raman Spectroscopy (SERS). They demonstrated that the selenol chemisorbs on gold as the selenolate, and in the case of diselenides, the Se-Se bond is cleaved when the diselenide is in contact with the gold surface, resulting in the formation of a stable monolayer.[164] Zharnikov and co-workers[165] confirmed Se-Se bond cleavage in bis(biphenyl)diselenide on gold and silver substrates by High Resolution X-Ray Photoelectron Spectroscopy (HRXPS).[165] Selenoate-stabilised MPCs have been reported by Yee and co-workers,[49] who investigated the use of the alkaneselenols and dialkyldiselenides to protect the nanoparticle surface. They developed a one-phase preparation of alkaneselenol-protected gold nanoparticles and also provided a detailed study of the gold nanoparticle morphology, structure and bonding preference as

compared to their alkanethiolate analogues. As is well-known, when the S/Au mole ratio decreases from 2:1 to 1:1 to 1:2 to 1:3 in the synthesis of alkanethiol-protected gold nanoparticles, the average particle size increases.[49] However, in the case of the dialkyldiselenide/Au ratio, no such tendency and no significant dependence were observed.[49] Tong and co-workers[50] synthesized octaneselenol-protected gold nanoparticles using the method developed by Brust and Schiffrin, with dioctyldiselenide as the precursor of the protecting ligand. They were the first to report the observation of ^{77}Se NMR signals from the octaneselenoate-protected gold nanoparticles, showing the potential of NMR as a powerful tool to investigate the interactions of the ligand with the nanoparticle surface.[50]

Thus, selenium capping agents would appear to be an attractive alternative to sulfur-based compounds for the stabilisation of gold monolayer-protected clusters. In this chapter, the synthesis and characterisation of a series of masked phosphonioalkyl selenoate ligands is described.

4.2 Experimental

4.2.1 Synthesis of the series of triphenyl-phosphonioalkylselenide ligands

The synthetic strategy is outlined in scheme 3 and is based on the protocol described previously for the preparation of phosphonioalkyl 'masked' thiolate ligands (Section 3.2.2, Chapter 3). The syntheses of **15a** and **13b** were performed by the reaction of the corresponding (bromoalkyl)triphenylphosphonium bromide (**4**, 1mol) with potassium selenocyanate (**12**, 4 mol) in aqueous ethanol under nitrogen and heated under reflux for 6 hours. Progress of the reaction was monitored by TLC, using 10% methanol : 90% dichloromethane as a mobile phase. The resulting compound was obtained by dichloromethane extractions of the reaction mixture and initially purified by trituration with dry diethyl ether.

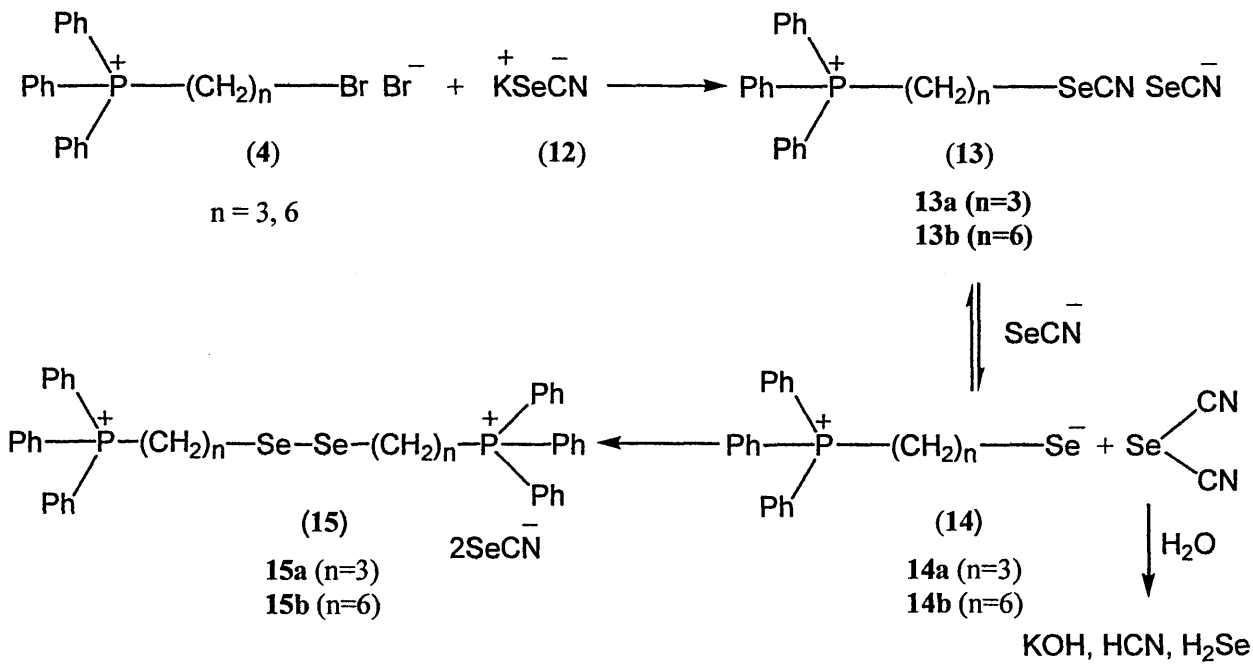

Scheme 3

4.3 Characterisation of the series of triphenylphosphonioalkylselenide ligands

4.3.1 Bis(3-triphenylphosphoniopropyl)diselenide–di(selenocyanate) (15a)

Initially the synthesis of the selenocyanopropyl phosphonium salt (**13a**, n = 3) was planned as a possible source of the phosphonioalkylselenide zwitterion (**14**) after the reduction of (**13**) with $NaBH_4$ or Au^0 during gold nanoparticle functionalisation. However, spectroscopic data indicated that the bis(3-triphenylphosphoniopropyl)diselenide–di(selenocyanate) salt (**15a**, n = 3), rather than **13a**, was obtained by treatment of the bromopropylphosphonium salt (**4a**, n =3) with an excess of potassium selenocyanate in aqueous ethanol. It is likely that the diselenide (**15a**) is formed by *in-situ* oxidation of the phosphonioselenoate (**14a**, n = 3), which may arise as shown.

Microanalytical data supported the formulation of **15a** (Figure 26) but indicated the presence of one mole of KOH per mole of diselenide salt. Electrospray mass spectrometry also supported the formulation of this compound as containing the bis(3-phosphoniopropyl)diselenide cation. When studied by ESMS in positive ion mode, ions corresponding to 1/2M+H, 1/2M+Na, 1/2M+Se and M+K were observed.

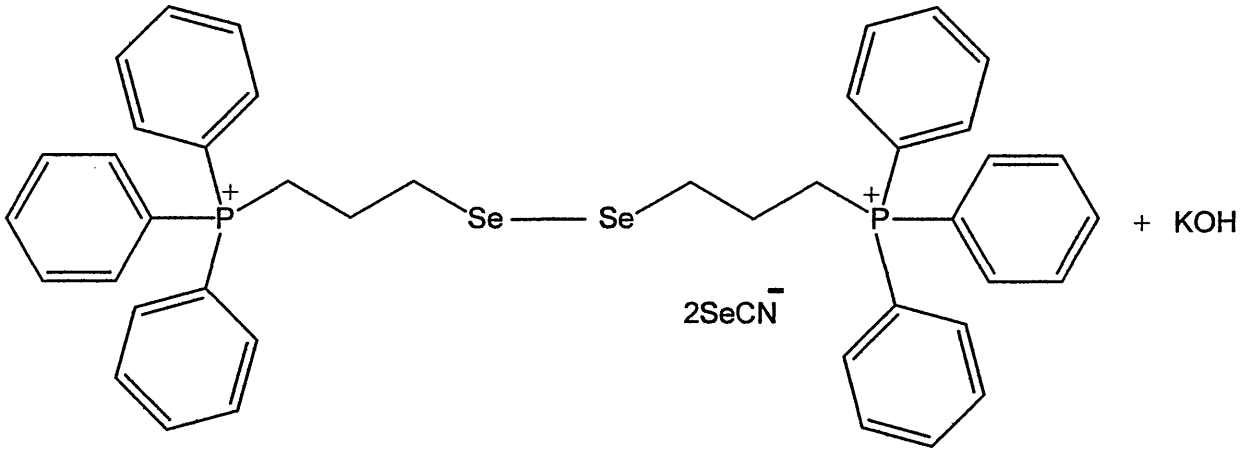

Figure 26. Bis(3-triphenylphosphoniopropyl)diselenide–di(selenocyanate) (**15a**)

Formula: $C_{44}H_{42}N_2P_2Se_4.KOH$, Formula Weight: 1032.71

Melting Point: 106 °C

Elemental Analysis:

Elemental	Carbon (%)	Hydrogen (%)	Nitrogen (%)
Theory	51.17	4.20	2.71
Found	51.47	4.56	2.55

ESMS: 383 [1/2M+H^+], 410 [1/2M+Na^+], 460 [1/2M+Se], 804 [M+K^+]NMR: $\delta^{31}P(CDCl_3)$ = 23.4 and 23.5 ppm, $\delta^1H(CDCl_3)$ = 2.2 (2H,m), 3.2 (2H, t, J = 6.2 Hz), 3.7 (2H,m), 7.7-7.8 (15H,m) ppm

4.3.2 6-(selenocyano)hexyl-triphenylphosphonium selenocyanate (13b)

Since the synthesis of the propyl analogue did not follow the expected pathway the synthesis of the six carbon chain analogue of **15a** was attempted by following the same synthetic route. However, 6-(selenocyano)hexyl-triphenylphosphonium selenocyanate (**13b**, n = 6, Figure 27), rather than **15b** (**15**, n = 6, Scheme 3), was obtained. NMR spectroscopy supported the proposed structure of this compound. Compound **13b** forms as a yellow oil, the longer chain 3-triphenylphosphonioalkylthiosulfates also tend to form as oils. When studied by MALDI TOFMS positive ion mode (accurate analysis), an ion corresponding to M + H was observed. It may be that the longer carbon chain suppresses the inductive effect of the phosphonium group on the cyano group of the alkyl selenocyanato group, such that nucleophilic attack by excess of selenocyanate anions is not favoured.

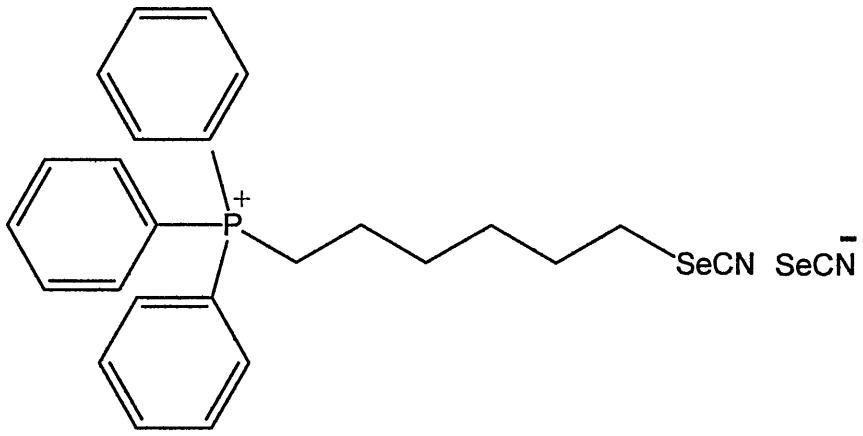

Figure 27. 6-(selenocyano)hexyl-triphenylphosphonium selenocyanate (**13b**)

Formula: $C_{26}H_{27}N_2PSe_2$, Formula Weight: 556.40

MALDI TOFMS:

Elemental	**$[M^+ + H^+]$**
Theory	452.1040
Found	452.1045

$\delta^{31}P(CDCl_3)$ = 23.6 ppm, $\delta^{1}H(CDCl_3)$ = 1.5-1.8 (6H,m), 1.9 (2H,m), 3.1 (2H, t, J = 6.2 Hz), 3.5 (2H,m), 7.6-7.8 (15H,m) ppm.

4.4 X-ray crystallography

4.4.1 Bis(3-triphenylphosphoniopropyl)diselenide–di(selenocyanate) (15a)

Salt **15a** was re-crystallised from DCM-ether as a yellow crystalline solid suitable for single crystal X-ray diffraction. X-ray analysis confirmed the formulation of **15a** as a diselenide rather than as the selenocyanate (**13a**) originally anticipated. Crystal data and structure refinement details are presented in Table 6. Selected bond lengths [Å] and bond angles [°] in **15a** are presented in Table 7.

The molecular structure of **15a** (Figure 28) contains Se-Se and C-Se-Se bonds which indicate the presence of a dialkyldiselenide group in the molecular structure. The Se-Se bond length in **15a** [2.318(10)Å] is similar to those found in other diorganodiselenides (R-Se-Se-R); although the molecular structures of a number of diorgandiselenides have been reported the majority contain aryl groups or sterically demanding alkyl groups as substituents.[166] Previous studies of diorganodiselenides have shown that the Se-Se and Se-C bond lengths are largely independent of the organic substituents and steric strain is relieved by increasing the C-Se-Se-C dihedral angle.[166,167] The phosphonioalkyl groups in **15a** are not particularly sterically demanding and the dihedral angle C(22)-Se(2)-Se(1)-C(21) [62.80(4)°] is significantly lower than those with bulkier groups, which typically lie in the range 73 - 104°.[166] The bond lengths and angles around the triphenylphosponium moieties are similar to those in the comparable 3-triphenylphosphoniopropylthiosulfate zwitterion (Section 3.4.1,

Chapter 3) The crystal structure of **15a** shows two N-C-Se bond systems, indicating the presence of two selenocyanates as counter ions (two anions per molecule for neutrality), and confirms the presence of K^+ and OH^- ions in the unit cell.

The overall structure consists of bis(3-triphenylphosphoniopropylselenium) diselenocyanate units arranged in pairs around an inversion centre. The potassium ion is disordered over several positions but its main component forms a near linear [172.99(7)°] K...Se contact of 3.459(6)Å to the diselenide group, which is similar to the K...Se distances found in other compounds;[168] *e.g.* potassium 2-methoxybenzenecarboselonate has K-Se bond lengths in the range 3.309(1) - 3.625(2)Å. One of the two independent selenocyanate anions forms a slightly bent hydrogen bond (O1W-H1W...N2 = 166°) to the OH anion; the other is involved in Se...K interactions to the disordered potassium (the exact nature of these interactions is hard to assess due to the disorder). Figure 29 shows interactions between the K and the Se atoms corresponding to the diselenide group of the molecule and Se atom of the counterion. These K...Se interactions, (and the O-H···N hydrogen bonds (Table 8), influence the packing of the cations and anions in the unit cell.

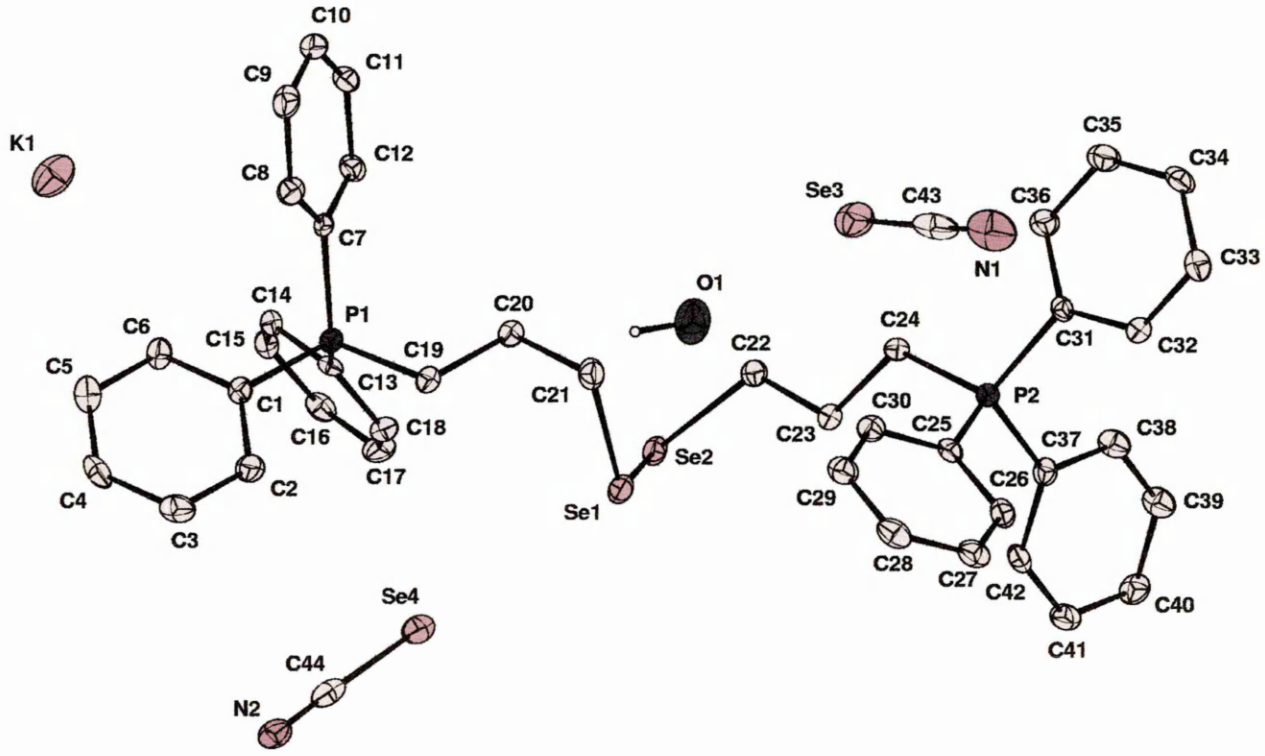

Figure 28. Molecular structure of bis(3-triphenylphosphoniopropyl)diselenide–di(selenocyanate) (**15a**)

Table 6. Crystal data and structure refinement for bis(3-triphenylphosphoniopropyl)diselenide–di(selenocyanate) (**15a**)

Compound	**15a**
Empirical formula	$C_{44}H_{43}KN_2OP_2Se_4$ $C_{42}H_{42}P_2Se_2^{2+} . (SeCN^-)_2 . K^+OH^-$
Formula weight	1032.68
Crystal system	Monoclinic
Space group	$P2_1/n$
a (Å)	12.4500(2)
b (Å)	18.3601(2)
c (Å)	19.4363(3)
β (°)	β = 103.0690(10)
Volume (Å^3)	4327.74(11)
Z (	4
D_{calc} (Mg / m^3)	1.585
Absorption coefficient (mm^{-1})	3.597
F(000)	2056
Crystal	Yellow Sharp
Crystal size (mm^3)	0.40 × 0.25 × 0.15
θ range for data collection (°)	3.09 – 25.03
Reflections collected	50997
Independent reflections	7618 [R_{int} = 0.0890]
Completeness to θ = 25.02°	99.6 %
Absorption correction	Semi-empirical from equivalents
Max. and min. transmission	0.6145 and 0.3272
Refinement method	Full-matrix least-squares on F^2
Data / restraints / parameters	7618 / 2 / 504
Goodness-of-fit on F^2	1.035
Final R indices [$F^2 > 2\sigma(F^2)$]	$R1$ = 0.0424, $wR2$ = 0.0925
R indices (all data)	$R1$ = 0.0748, $wR2$ = 0.1029
Largest diff. peak and hole	0.694 and –1.115 e Å^{-3}

Table 7. Selected bond lengths [Å] and angles [°] in bis(3-triphenylphosphoniopropyl)diselenide–di(selenocyanate) (**15a**)

P1–C19	1.79(6)	Se1–C21	1.96(7)
P1–C7	1.79(6)	Se1–Se2	2.318(10)
P1–C1	1.79(6)	Se2–C22	1.97(6)
P1–C13	1.80(6)	Se3–C43	1.74(12)
P2–C37	1.79(6)	C43–N1	1.18(11)
P2–C24	1.79(6)	Se4–C44	1.83(9)
P2–C25	1.79(6)	C44–N2	1.12(9)
P2–C31	1.80(6)		

C19–P1–C7	111(3)	C8–C7–P1	119(5)
C19–P1–C1	109(3)	C12–C7–P1	122(5)
C7–P1–C1	109(3)	C18–C13–P1	121(5)
C19–P1–C13	110(3)	C14–C13–P1	118(5)
C7–P1–C13	108(3)	C20–C19–P1	114(4)
C1–P1–C13	110(3)	C20–C21–Se1	114(5)
C37–P2–C24	112(3)	C23–C22–Se2	114(4)
C37–P2–C25	108(3)	C23–C24–P2	114(4)
C24–P2–C25	109(3)	C30–C25–P2	120(5)
C37–P2–C31	108(3)	C26–C25–P2	120(5)
C24–P2–C31	109(3)	C32–C31–P2	118(5)
C25–P2–C31	110(3)	C36–C31–P2	121(5)
C21–Se1–Se2	100(2)	C38–C37–P2	120(5)
C22–Se2–Se1	100.4(19)	C42–C37–P2	121(5)
C6–C1–P1	120(5)	N1–C43–Se3	179(8)
C2–C1–P1	120(5)	N2–C44–Se4	178(7)

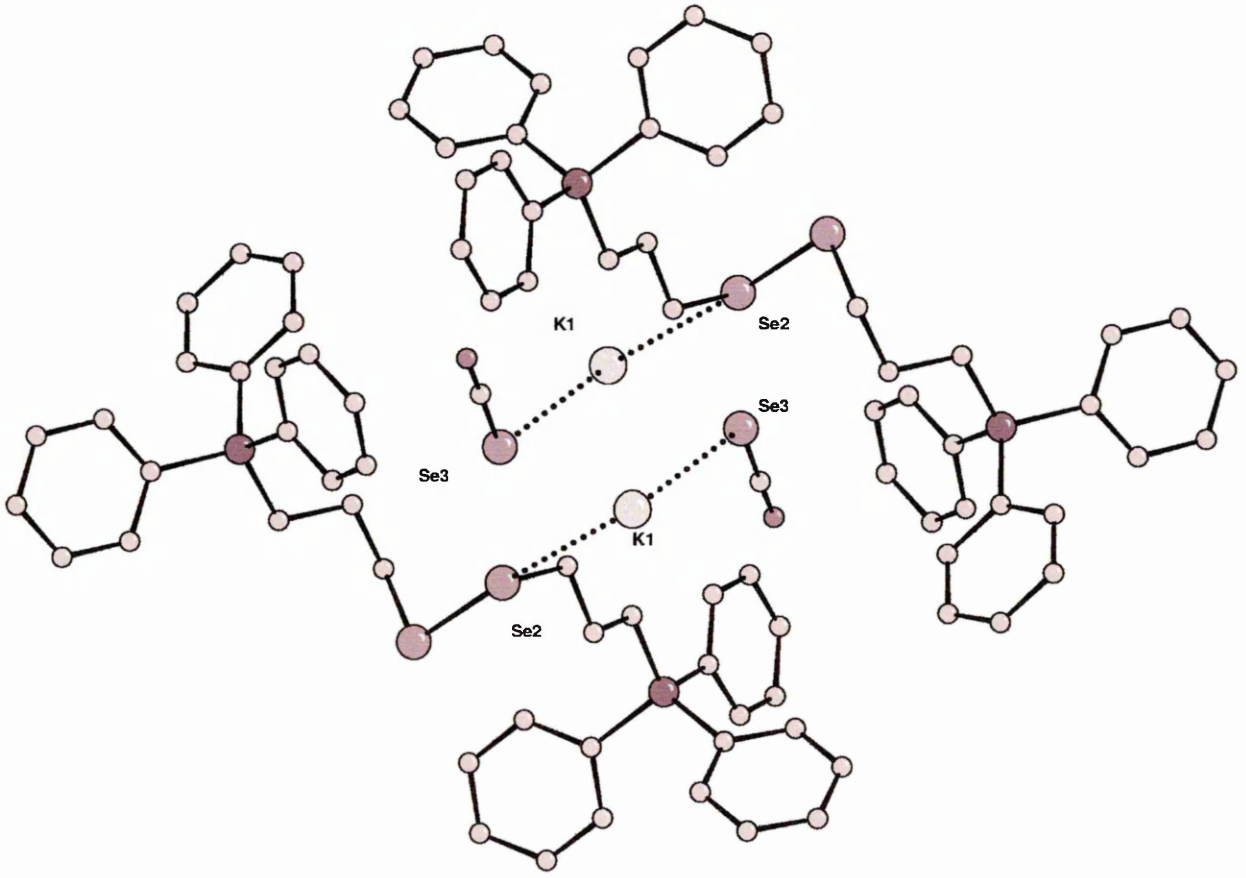

Figure 29. Intramolecular contacts showing possible K...Se interactions between the K cations and the Se atoms corresponding to the diselenide groups and the selenocyanate counterions in bis(3-triphenylphosphoniopropyl)diselenide–di(selenocyanate) (**15a**).

Table 8. Intramolecular contacts for hydrogen bonding between O-H of the KOH moiety and nitrogen atom of the selenocyanate counterion in bis(3-triphenylphosphoniopropyl)diselenide–di(selenocyanate) (**15a**)

D–H···*A*	*d*(*D*–H)	*d*(H···*A*)	*d*(*D*···*A*)	∠(*DHA*)
O1W–H1W···N2^{i}	0.900(16)	2.1(3)	3.03(9)	166(100)

Symmetry transformations used to generate equivalent atoms:
(i) –x+2,–y+2,–z+1

A successfully synthetic procedure has been developed for the preparation of a series of masked phosphonioalkylselenoate ligands. The use of these selenium containing compounds for the stabilisation of gold nanoparticles is shown in Chapter 6.

CHAPTER 5

Phosphonioalkylthioacetate and Related Phosphine Oxide Ligands

5.1 Introduction

Other sulfur-containing organic ligands have been reported in the literature and used as precursors of the corresponding thiolates in the gold nanoparticle stabilisation. The organic thiols can undergo air-oxidation, to form the related disulfides, therefore, various easily removable thiol-derivatives, e.g. S-acetyl, S-cyano and S-(N-ethylcarbamoyl), have been prepared. These protecting groups have been shown to undergo cleavage *in situ* in the presence of a gold electrode.[169]

Molecules terminated in thioacetate groups have been used for the preparation of self assembled monolayers (SAMs).[170,171] Aromatic thiols or thiolates, which are the typical molecules used for the synthesis of SAMs, have been reported to be more susceptible to air oxidation, forming disulfides and other oxidised products.[171] For this reason, thioacetate derivatives have been shown to be a more stable alternative to thiols and to be deprotected *in situ* to corresponding thiolate by reacting with a small amount of base (e.g. aqueous ammonium solution), and form a SAM on the Au substrates.[170]

Ashwell and co-workers[172] have reported the synthesis of self-assembled monolayers on gold using zwitterionic dyes containing-thioacetate tail-groups, such as CH_3COS-$(CH_2)_n$-**A**-CH=CH-**D**, where **A** is a quinolinium acceptor and **D** a phenolate donor. The ligands were synthesised through the reaction of the dihalogenated precursor and potassium thioacetate under reflux for 24 hours. The zwitterionic dyes

were left in contact with a gold substrate in an ethanolic solution with ammonium hydroxide which was used to remove the acetyl group.[172]

Plenio and co-workers[173] have synthesised cavitands with thioacetate terminal groups. They showed that the thioacetate protective group in these cavitand compounds can undergo cleavage with a reducing agent such as $LiAlH_4$, leading to the formation of the corresponding hemicarcerands with SH groups.[173]

However, Tour and co-workers[171] suggested that thioacetate tail-groups can be linked to gold substrates without prior conversion to the corresponding thiolates for monolayer assembly. They showed that a similar coverage of the surface relative to that achieved by Ashwell and co-workers[171,172] can be achieved using a higher concentration of thioacetate ligands and a longer adsorption time without the use of ammonium hydroxide.

Knowing the important role of the hydrogen bonding interactions between biomolecules in biological processes, it has been decided to synthesise phosphine oxide related ligands and explore the potential of these ligands to interact with biomolecules. Due to the strong hydrogen-bonding properties of phosphonic acids, $R\text{-}P(O)(OH)_2$ are of general interest, as they exhibit a wide range of biological activity as potent antibiotics and enzyme inhibitors.[174] Phosphonic acids are also used as corrosion inhibitors and adhesion promoters. The phosphonic acid group can act both as a hydrogen-bond donor through the two P—OH groups and as an acceptor via the P=O oxygen. Reven and co-workers[174] have recently reported the synthesis of gold

nanoparticles capped with sodium 10-mercaptodecanesulfonic acid (MDS) and 11-mercaptoundecanylphosphonic acid (MUP). They have investigated the effect of the acid terminal groups (PO_3H_2 tail groups) on the monolayer properties by NMR chemical shift and relaxation measurements.[174] The synthesis of the phosphine oxide related ligands was carried out in this project in order to use them as protecting ligands in the gold nanoparticle stabilisation and promote interactions with biomolecules through hydrogen bonds.

Thioacetate-containing molecules appear to be an alternative to thiols and have the potential to act as 'masked thiolate' ligands for the preparation of gold MPCs. In this chapter, the synthesis and characterisation of phosphonioalkylthioacetate ligands are outlined. Chapter 5 also describes the synthesis of phosphine oxide related ligands.

5.2 Experimental

5.2.1 Synthesis of the triphenyl-phosphonioalkylthioacetate ligands

The synthesis of triphenyl(3-thioacetylalkyl)phosphonium bromide is shown in Scheme 4. The compound was generated by the reaction of the (3-bromoalkyl)triphenylphosphonium bromide (**4**, 2 mmol) with potassium thioacetate (**16**, 3 mmol) in a mixture of ethanol and water at room temperature. The reaction mixture was left stirring overnight under nitrogen. Progress of the reaction was monitored by TLC, using 10% methanol : 90% dichloromethane as mobile phase. The triphenyl (3-thioacetylalkyl) phosphonium bromide (**17**) was obtained by dichloromethane extractions of the reaction mixture and initially purified by triturations with dry diethyl ether.

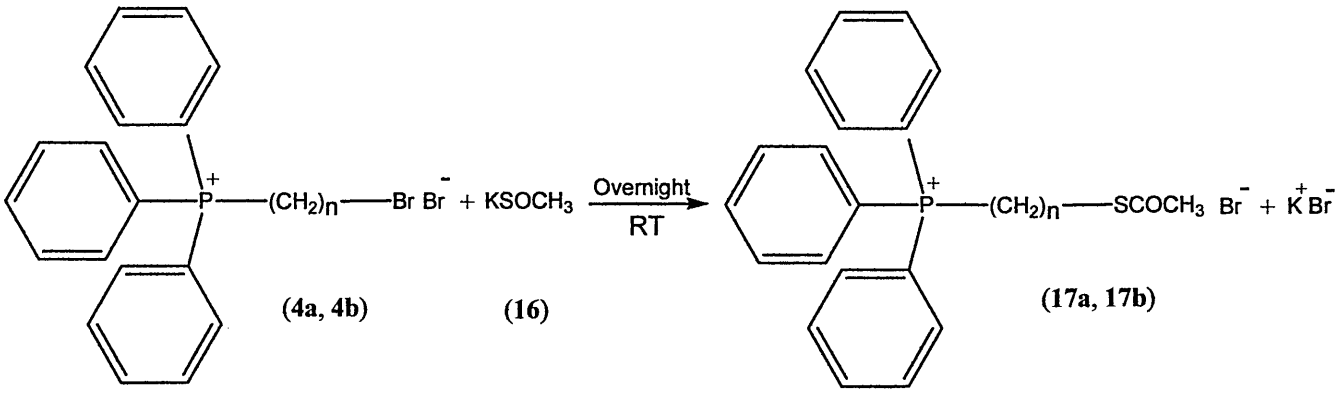

(4a, 4b) **(16)** **(17a, 17b)**

n = 3 (**a**), 6 (**b**)

Scheme 4

5.2.2 Synthesis of (3-thioacetylpropyl)diphenylphosphine oxide

The synthesis of (3-thioacetylpropyl)diphenylphosphine oxide is shown in Scheme 5. The compound was generated by an alkaline hydrolysis of hydroxypropylphosphonium salt (**3a**) as a first step to obtain the (hydroxypropyl)diphenylphosphine oxide, following the Okuma and co-workers method.[175] Hydroxypropylphosphonium salt (**3a**, 1 mmol) was dissolved in 1.5 mL of ethanol and then heated with 2mL of 20% aqueous NaOH solution. The (hydroxypropyl)diphenylphosphine oxide (**18**) was then dissolved in HBr (48%, 5mL) and heated under reflux for five hours to obtain the corresponding bromopropylphosphine oxide (**19**). The (3-thioacetylpropyl)diphenylphosphine oxide (**20**) was then obtained by the reaction of the latter (**19**, 2 mmol) with potassium thioacetate (3 mmol) in a mixture of ethanol and water (4mL) at room temperature. The reaction mixture was left stirring overnight under nitrogen.

Progress of the reaction was monitored by TLC, using 10% methanol : 90% dichloromethane as mobile phase. The (3-thioacetylpropyl)diphenylphosphine oxide (**20**) was obtained by dichloromethane extractions of the reaction mixture, and then all the extracts were combined and dried with $MgSO_4$ and rotary evaporated. Initially, the product was purified by triturations with dry diethyl ether to yield a yellow oil.

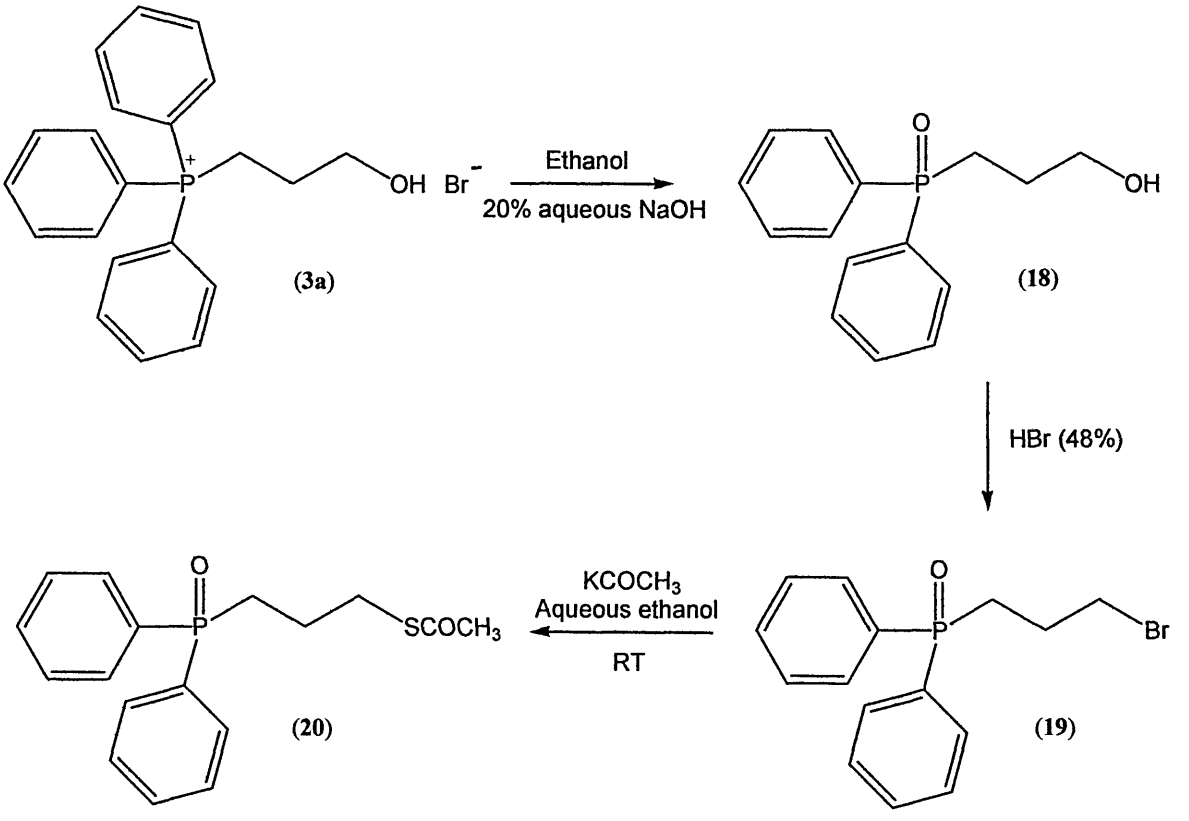

Scheme 5

5.2.3 Synthesis of 3,3'-bis(diphenylphosphinylpropyl)disulfide

In order to show the capacity of the (3-thioacetylpropyl)diphenylphosphine oxide (**20**) ligand to form its corresponding thiolate species under reductive conditions and explore the air-oxidation of the corresponding thiolate, an oxidation reaction using **20** as starting material was carried out under the reductive condition and O_2 to yield the corresponding disulfide compound. The synthesis of 3,3'-bis(diphenylphosphinylpropyl)disulfide (**21**) is shown in Scheme 6. The synthesis

of this ligand was carried out by the reaction of (3-thioacetylpropyl)diphenylphosphine oxide (**20**, 0.25 mmol) with ammonium hydroxide (20% solution) in aqueous ethanol stirring the mixture at room temperature overnight. The reaction mixture was then extracted with DCM (3×10mL), and then all the extracts were combined and dried with $MgSO_4$ and rotary evaporated to yield a yellow oil. As a further purification step for the oily sample was performed. Several triturations with dry diethyl ether were done to give a fine pale powder.

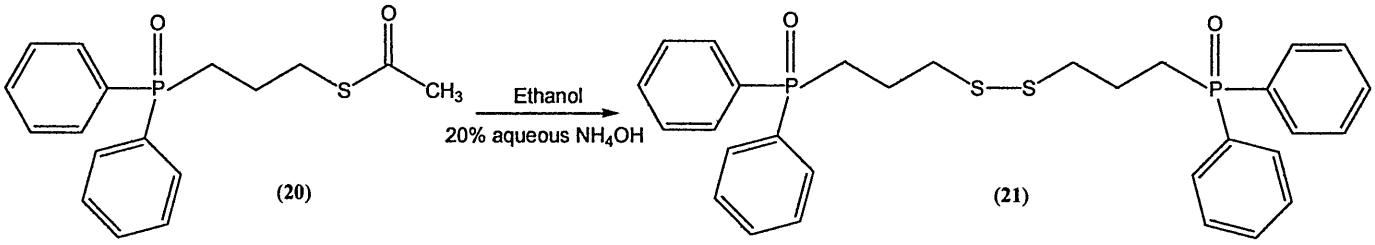

Scheme 6

5.3 Characterisation of the series of phosphonioalkylthioacetate and related phosphine oxide ligands

5.3.1 Triphenyl (3-thioacetylpropyl) phosphonium bromide (17a)

The structure of **17a** is shown in Figure 30. **17a** was isolated as pale cream powder. Attempts to grow crystals of **17a** suitable for single crystal X-Ray analysis were unsuccessful. Compound **17a** is air stable and soluble in methanol, ethanol, acetonitrile, and dichloromethane. NMR data, MALDI-TOFMS positive ion mode (accurate analysis) and electrospray mass spectral results supported the structure of this compound as triphenyl(3-thioacetylpropyl)phosphonium bromide. When studied by ESMS in positive ion mode, an ion corresponding to M^+ was observed. The structure of triphenyl(3-thioacetylpropyl)phosphonium bromide (**17a**) was also supported by IR. A significant absorption band at $\nu_{C=O}$ 1680 cm^{-1} due to the presence of the carbonyl group was observed in the spectrum, as well as absorption bands corresponding to Ar-H stretching, C-H stretching of methylene groups, symmetric and asymmetric C-H stretching vibrations of the methyl group, and Ar-H bending. This compound could potentially be used as a protecting ligand in the formation of monolayer-protected gold nanoparticles, assuming that S-$COCH_3$ cleavage occurs in presence of Au^0 and a reducing agent ($NaBH_4$).

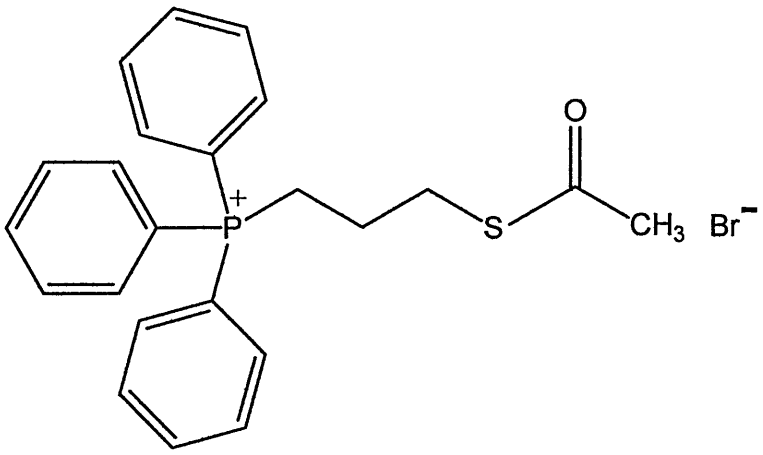

Figure 30. Triphenyl(3-thioacetylpropyl)phosphonium bromide (**17a**)

Formula: $C_{23}H_{24}OPSBr$, Formula Weight: 459.38

Melting Point: 85-89 °C.

ESMS: 380 [$M+H^+$]

MALDI TOFMS:

Elemental	**[M^+]**	**[$M+H^+$]**
Theory	379.1285	380.1366
Found	379.1307	380.1323

$\delta^{31}P$ NMR ($CDCl_3$)=23.8 ppm; δ^1H NMR ($CDCl_3$)=1.9 (2H,m), 2.2 (3H,s), 3.2 (2H,m), 3.8 (2H,m), 7.6-7.8 (15H,m) ppm.

FT-IR: ν_{Ar-H} 3010, ν_{C-H} 2800-2880 (methylene and methyl groups), $\nu_{C=O}$ 1680, $\nu_{C=C}$ 1600, vibrations of Ar ring 1450, δ_{C-H} 900-1000, δ_{Ar-H} 700-750 cm^{-1}.

5.3.2 Triphenyl (6-thioacetylhexyl) phosphonium bromide (17b)

The structure of compound **17b** is shown in Figure 31. **17b** was isolated as a pale yellow oil. Attempts to isolate **17b** as a crystalline solid for X-ray analysis were unsuccessful. MALDI-TOFMS positive ion mode (accurate analysis), ^{1}H and $^{31}PNMR$ spectroscopic data supported the formulation of this compound as 6-tributylphosphoniohexylthiosulfate.

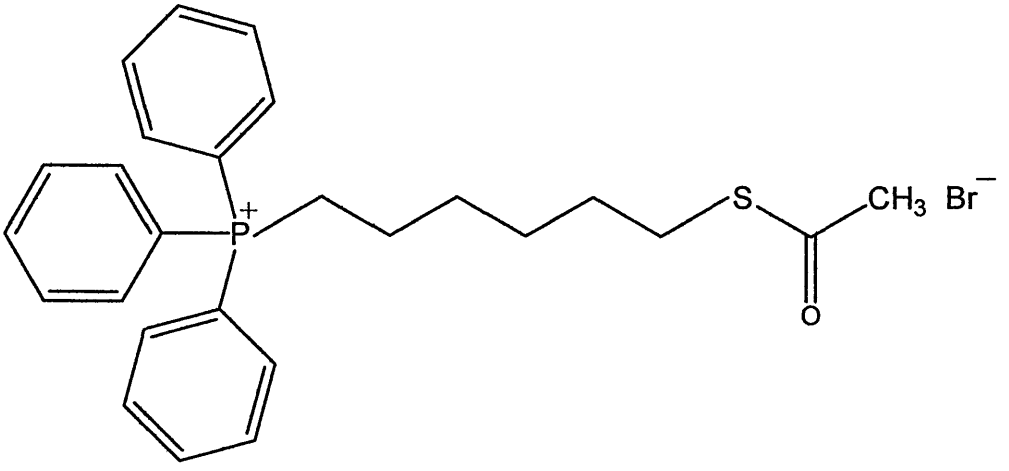

Figure 31. Triphenyl (6-thioacetylhexyl) phosphonium bromide (**17b**)

Formula: $C_{26}H_{30}OPSBr$, Formula weight: 501.46

MALDI TOFMS:

Elemental	[M]	[M+H$^+$]
Theory	421.1755	422.1835
Found	421.1742	422.1824

NMR: δ^{31}P NMR ($CDCl_3$) = 23.91 ppm, δ^{1}H NMR ($CDCl_3$) = 1.14-1.59 (8H,m), 2.19 (3H,s), 2.72 (2H, t, J = 6.1 Hz), 3.68 (2H,m), 7.6-7.8 (15H,m) ppm.

5.3.3 (3-Thioacetylpropyl)diphenylphosphine oxide (20)

The structure of compound **20** is shown in Figure 32. Compound **20** was isolated as a yellow oil. Attempts to isolate **20** as a crystalline solid for X-ray analysis were unsuccessful. MALDI-TOFMS positive ion mode (accurate analysis), ESMS, ^{1}H and ^{31}P NMR spectroscopic data supported the formulation of this compound as (3-thioacetylpropyl)diphenylphosphine oxide.

It was also observed that there is a significant difference in terms of the ^{31}P chemical shift between this compound (**20**) and the triphenyl(3-thioacetylpropyl)phosphonium bromide (**17a**). The δ^{31}P corresponding to the phosphine oxide compound (**20**) is 31.42 ppm, whereas the δ of the phosphorus atom contained in the triphenyl(3-thioacetylpropyl)phosphonium bromide (**17a**) is 23.8 ppm. This difference might be due to the oxygen atom double bonded to the phosphorus atom of **20**, which is more electronegative than the carbon atoms corresponding to the phenyl groups bound to the phosphorus atom in the chemical structure of **17a**.

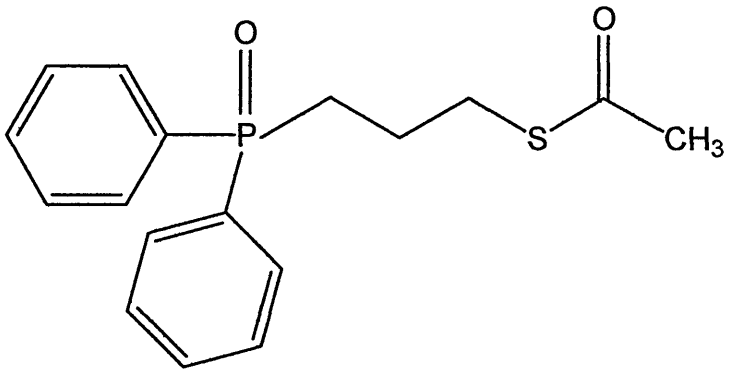

Figure 32. (3-Thioacetylpropyl)diphenylphosphine oxide (**20**)

Formula: $C_{17}H_{19}O_2PS$, Formula weight: 318.37

ESMS: 244 [M-$SCOCH_3$], 319 [M+H^+], 341 [M+Na^+]

MALDI TOFMS:

Elemental	**[M+H^+]**
Theory	319.1143
Found	319.1136

NMR: δ^{31}P NMR ($CDCl_3$) = 31.42 ppm, δ^1H NMR ($CDCl_3$) = 1.76-1.92 (2H,m), 2.22 (3H,s), 2.24-2.33 (2H,m), 2.90 (2H, t, J = 7.2 Hz), 7.35-7.50 (5H,m) ppm, 7.63-7.71 (5H,m).

5.3.4 3,3'-Bis(diphenylphosphinylpropyl)disulfide (21)

The structure of compound **21** is shown in Figure 33. Compound **21** was isolated as a fine pale powder. Attempts to isolate **21** as a crystalline solid suitable for X-ray analysis were unsuccessful.

The synthesis of this compound involved the utilisation of ammonium hydroxide (20% aqueous solution) in order to remove the acetyl group of the starting compound (**20**), as reported by Ashwell and co-workers,[172] and an *in situ* oxidation reaction. The synthesis of **21** took almost 24 hours to be completed. The reaction was monitored by TLC. At the beginning of the reaction, only one spot was observed on the TLC plate (Rf 0.33) when the reaction mixture was run using 90:10 of DCM:MeOH. During the first 2 hours, the formation of a clear pale yellow spot (Rf 0.25) on the plate was observed. However, even after 15 hours, the reaction was not completed. A small amount of the starting material could still be observed on the TLC plate. At the time of 24 hours, the spot with Rf 0.33 completely disappeared indicating that the oxidation reaction was completed. MALDI-TOFMS positive ion mode (accurate mass analysis), ^{1}H and ^{31}P NMR spectroscopic data supported the formulation of this compound as 3,3'-bis(diphenylphosphinylpropyl)disulfide.

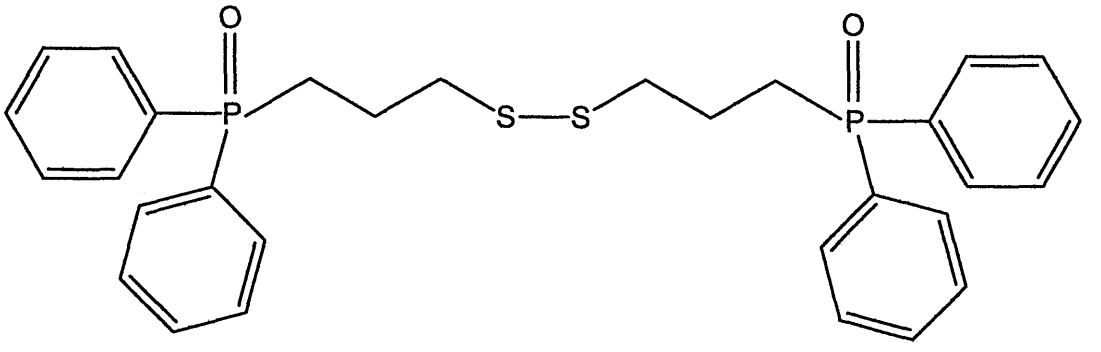

Figure 33. 3,3'-Bis(diphenylphosphinylpropyl)disulfide (**21**)

Formula: $C_{30}H_{32}O_2P_2S_2$, Formula weight: 550.65

MALDI TOFMS:

Elemental	**[M+H$^+$]**	**[M+Na$^+$]**
Theory	551.13973	573.12167
Found	551.13746	573.12151

NMR: δ^{31}P NMR ($CDCl_3$) = 31.93 ppm, δ^1H NMR ($CDCl_3$) = 1.86-2.09 (4H,m), 2.28-2.40 (4H,m), 2.66 (4H, t, J = 6.9 Hz), 7.40-7.50 (10H,m) ppm, 7.67-7.75 (10H,m).

Synthetic strategies have been successfully developed for the preparation of a novel family of phosphonioalkylthioacetate and the related phosphine oxide ligands. The use of these compounds for the formation of functionalised gold nanoparticles is presented in Chapter 6.

CHAPTER 6

Phosphonium Monolayer-Protected gold Nanoparticles

6.1 Introduction

The preparation of the monolayer-protected gold clusters using the compounds previously synthesised (described in Chapters 3-5) as protecting ligands was carried out following the chemical methods developed by Brust[41] and Murray[48] (methods cited in the main Introduction, Chapter 1).

The Brust strategy[41] involves synthesis of the metallic nanoparticles with the simultaneous attachment of self-assembled thiol monolayers on the surface of the growing nanoparticles. In order to allow the surface reaction to take place during metal nucleation and growth, and also due to the solubility of the thiol compounds, the particles are grown in a two phase system (water-toluene). Brust[41] used tetraoctylammonium bromide (TOAB) as the phase transfer reagent to transfer $AuCl_4^-$ from aqueous solution to an organic phase (toluene) in the presence of dodecanethiol ($C_{12}H_{25}SH$). Murray and co-workers[48] carried out a similar approach using sodium S-dodecylthiosulfates (Bunte salts) instead of alkanethiol type compounds.

In this project, the cationic phosphonioalkanethiolate-capped gold nanoparticles were synthesised in a two phase liquid-liquid system, following the methods developed by Brust[41] and Murray[48], via reduction of potassium tetrachloroaurate in biphasic media with an excess of sodium borohydride, with two variations based on the use of dichloromethane: water instead of toluene: water as the biphasic system, and without the use of tetraoctylammonium bromide to aid transfer of the $AuCl_4^-$ ions to the organic solvent, as it was felt that this role would be fulfilled by the phosphoniothiosulfate

zwitterion. The dichloromethane-water system was used due to the solubility of the already synthesized cationic masked thiol ligands in DCM. No TOAB transfer agent was used due to the affinity of the phosphonium-gold nanoparticles to the aqueous phase. It would appear that the tetrachloroaurate anions ($AuCl_4^-$) play the transfer agent role in this case, and help to transfer the phosphonium containing ligands to the aqueous phase.

This chapter outlines the fabrication of the phosphonium-gold nanoparticles in three major sections. In section 6.2, the stabilisation of the gold nanoparticles using phosphonioalkyl-thiosulfate and –thioacetate ligands is described. In sections 6.3 and 6.4, the stabilisation attempts of the gold nanoparticles using phosphioalkylselenide and the pyrenyl containing ligands are outlined, respectively. Each of these sections includes the experimental description, results and discussion of the related functionalised gold nanoparticle synthesis.

6.2 Stabilisation of gold nanoparticles using phosphonioalkyl-thiosulfate and -thioacetate ligands

6.2.1 Experimental

6.2.1.1 Studies of the potential of the phosphonium containing compounds as protecting ligand precursors - Synthesis of 3-(methylthio)propyl-triphenylphosphonium iodide (24)

Before the synthesis of the cationic phosphonium monolayer-protected gold nanoparticles using the phosphonium -zwitterions and -thioacetates, studies of the potential of these compounds as protecting ligands precursors were carried out.

In order to show the capacity of the phosphonioalkyl-thiosulfate and -thioacetate ligands to form the corresponding thiols during the synthesis of the functionalised gold nanoparticles, an alkylation reaction using triphenylphosphoniopropylthiosulfate zwitterion and iodomethane as starting materials was carried out under the same reductive conditions used for the preparation of the capped nanoparticles.

The alkylation of (**5a**) was carried out using the synthetic route shown in Scheme 7. Triphenylphosphoniopropylthiosulfate (**5a**, 0.5 mmol) was dissolved in 3 mL of methanol. A freshly prepared aqueous solution of sodium borohydride (5 mmol) was then added dropwise to the reaction flask, in order to allow formation of the zwitterion $Ph_3P^+(CH_2)_3S^-$ (**22**). The mixture was stirred for 3 hour at room

temperature, and then, iodomethane (**23**, 5mmol) was added. The resulting mixture was then stirred overnight. Progress of the reaction was monitored by TLC, using 10% methanol : 90% dichloromethane as a mobile phase. The resulting mixture was extracted with dichloromethane, the organic phase was collected and after removing the solvent, the resulting compound (**24**) was initially purified by trituration with dry diethyl ether.

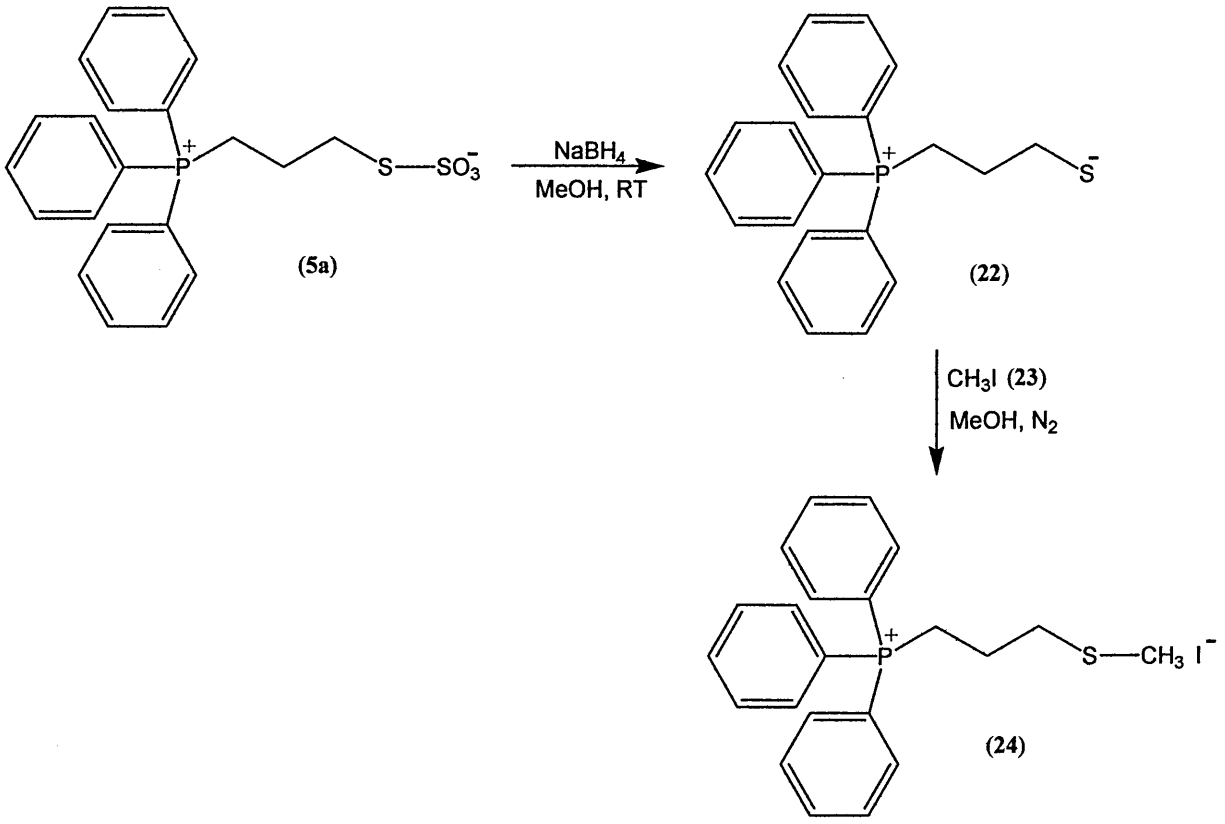

Scheme 7

6.2.1.2 Synthesis of phosphonium-monolayer protected gold clusters using phosphonioalkyl-thiosulfate and -thioacetate compounds as protecting ligands in a two phase liquid-liquid system (dichloromethane : water)

For the syntheses of gold nanoparticles modified with a coating containing phosphonium cationic head groups, so called phosphonium monolayer protected clusters (phosphonium-MPCs), the triphenyl- and tributyl-phosphonioalkylthiosulfate zwitterions and triphenyl(3-thioacetylalkyl)phosphonium bromide and (3-thioacetylpropyl)diphenylphosphine oxide were used as protecting ligands. The preparation technique (Scheme 8) was the same for all cases, as described below.

A solution of the phosphonium-containing compound corresponding to the protecting ligand was prepared in DCM (0.25 mmol, 14 mmol L^{-1}) and potassium tetrachloroaurate (0.12 mmol, 7 mmol L^{-1}) was then added to the solution. This was vigorously stirred for 10 minutes until the gold salt was totally dissolved. The reduction was carried out by adding dropwise a freshly prepared aqueous solution of sodium borohydride (3mL, 400 mmol L^{-1}) with vigorous stirring. Immediately after the addition of the reducing agent, 15 mL of deionised water was added to the mixture, and the stirring was continued for a further 24 hours. DCM extractions (3×10 mL) were then carried out for the purification of the aqueous phase. Part of the original solutions was kept to carry out stability studies and the rest was freeze-dried to aid resuspension the gold nanoparticles in a suitable solvent for further applications.

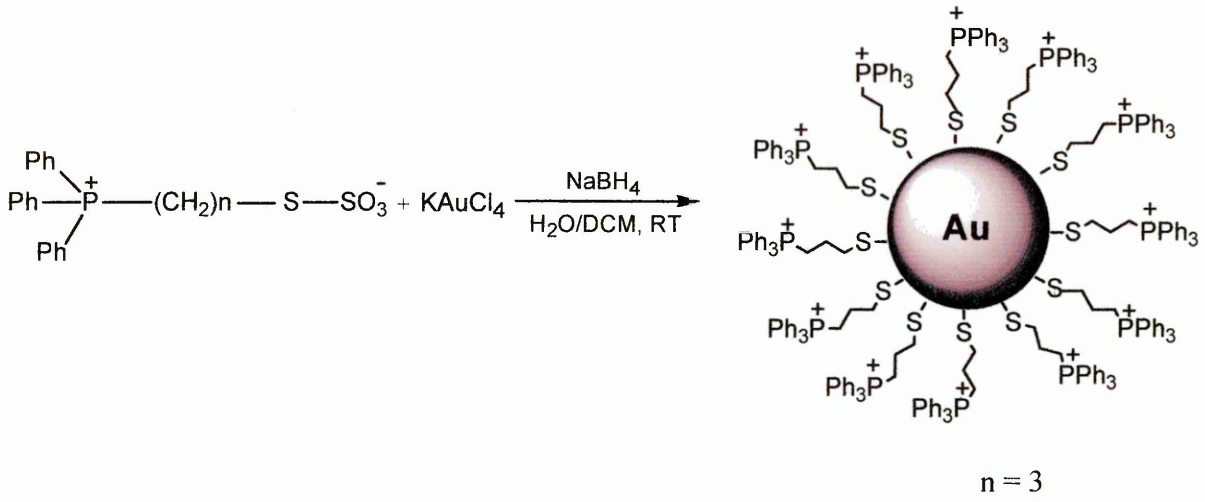

n = 3

Scheme 8

6.2.1.3 Characterisation of the colloidal solutions of the phosphonio-monolayer protected gold nanoparticles

The samples of functionalised AuNPs with phosphonioalkyl-thiosulfate and -thioacetate ligands were analysed by UV-visible, transmission electron microscopy (TEM), nuclear magnetic resonance (NMR) and X-ray photoelectron spectroscopy (XPS). The samples to be analysed by UV-visible spectroscopy were kept in their original form (nanoparticles dispersed in water). The samples to be analysed by the other techniques, were freeze-dried in order to remove the water and facilitate re-dispersal in suitable solvents for the various investigations.

6.2.2 Results and Discussion

6.2.2.1 Studies of the potential of the phosphonium compounds as protecting ligand precursors - 3-(methylthio)propyl-triphenylphosphonium iodide (24)

Following the study of the gold nanoparticle-binding properties of the cationic thiols involving a phosphonium head group, the synthesis of 3-(methylthio)propyl-triphenylphosphonium iodide (**24**) was carried out, in order to prove the formation of $Ph_3P^+(CH_2)_3S^-$ (**22**) in solution, which could bind to the gold nanoparticle surface. This synthesis involved, first the formation of **22** by the reaction of the corresponding phosphonioalkylthiosulfate zwitterion (**5a**) and sodium borohydride ($NaBH_4$), and then alkylation of this zwitterion intermediate (**22**) using methyl iodide to give **24**.

The structure of **24** is shown in Figure 34. **24** was isolated as pale cream solid and the attempts to isolate **24** as a crystalline solid for X-ray analysis were unsuccessful. The NMR spectroscopy and MALDI-TOFMS positive ion mode (accurate analysis) supported the formulation of this compound as 3-(methylthio)propyl-triphenylphosphonium iodide. When studied by MALDI TOFMS in positive ion mode, a well-defined molecular ion corresponding to the 3-methylthiopropylphosphonium cation was observed.

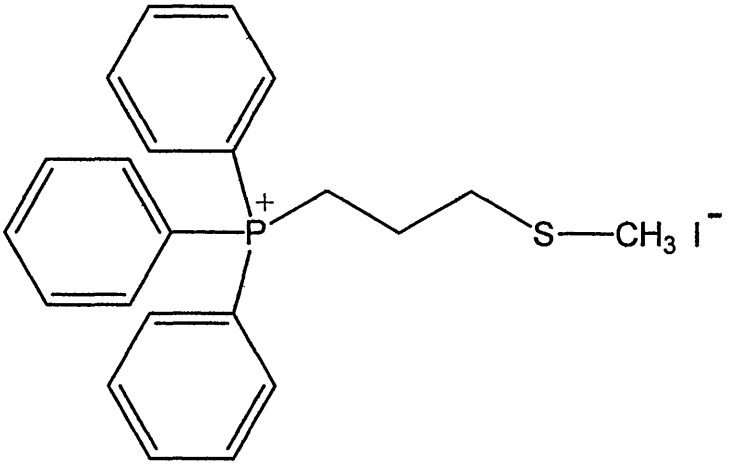

Figure 34. 3-(Methylthio)propyl-triphenylphosphonium iodide (**24**)

Formula: $C_{22}H_{24}PSI$, Formula Weight: 478.37

Melting Point: 136-138 °C.

MALDI TOFMS:

Elemental	**[M^+]**
Theory	351.1336
Found	351.1307

$\delta^{31}P$ NMR ($CDCl_3$)=24.3 ppm; δ^1H NMR ($CDCl_3$)=1.9 (3H,s), 2.8 (2H, t, J = 6.2 Hz), 3.3 (2H,m), 3.8 (2H,m), 7.6-7.8 (15H,m) ppm.

The same results were obtained when the synthesis of 3-(methylthio)propyl-triphenylphosphonium iodide (**24**) was carried out using the

phosphoniopropylthioacetate ligand as the starting material. The synthesis was carried out under the same conditions used as above which involved the generation of the phosphonioalkylthiosulfate zwitterion. According to the results obtained by NMR (δ^{31}P NMR ($CDCl_3$) = 24.3 ppm; δ^1H NMR ($CDCl_3$) =1.9 (3H,s), 2.8 (2H,t), 3.3 (2H,m), 3.8 (2H,m), 7.6-7.8 (15H,m) ppm) and MALDI TOFMS positive ion mode accurate analysis (found: 351.1342 [M^+], required: 351.1312 [M^+]), it could be assumed that the acetyl group is removed from the original structure of the ligand under the reductive conditions and, therefore, the thiolate $Ph_3P^+(CH_2)_3S^-$ was formed in solution and then bound to the gold nanoparticle surface.

6.2.2.2 Synthesis of phosphonium-monolayer protected gold clusters using phosphonioalkyl-thiosulfate and -thioacetate compounds as protecting ligands in a two phase liquid-liquid system (dichloromethane : water)

Previous studies have indicated that gold nanoparticles and colloidal gold solutions have the ability to cleave the S–S bonds present in organic disulfides and alkylthiosulfates, yielding organic thiolates which then bind to the surface of the particle.[19,47,48] Consequently, it was assumed that the S–S bond of the phosphonioalkylthiosulfate zwitterions would be cleaved under the reductive conditions used for the synthesis of the capped nanoparticles, to form the related phosphonioalkylthiolates, e.g., **22** (Scheme 7). This was confirmed by sodium borohydride reduction of the salt (**5a**), the resulting phosphonioalkylthiolate being trapped with iodomethane to form the salt (**24**). The preparation technique was the same

for each of the phosphonioalkylthiosulfate zwitterions (**5a-g**, syntheses described in Chapter 3), and was as follows.

A solution of ligand was prepared in dichloromethane (DCM) and solid potassium tetrachloroaurate (0.5 mol equiv.) was then added to the solution. This was vigorously stirred for 4-6 hours until the gold salt was totally dissolved. The reduction was carried out by adding dropwise a freshly prepared aqueous solution of sodium borohydride with vigorous stirring. When the tetrachloroaurate was added to the solution of the ligand in DCM, the stirring organic solution turned yellow, and then became dark purple/blue after the $NaBH_4$ addition, indicating that the reduction had taken place. In the case of the triphenylphosphonioalkylthiosulfate (**5a-d**, n = 3, 4, 6, and 8), tributylphosphoniohexylthiosulfate (**5g**) zwitterions, and triphenyl(3-thioacetylpropyl)phosphonium (**17a**) and triphenyl(6-thioacetylhexyl)phosphonium bromides (**17b**) , when the stirring was stopped after 24 hours, the DCM layer was colourless and the aqueous phase was dark purple/blue, indicating that phosphonioalkylthiolate-capped nanoparticles were present in the aqueous phase (Figure 35).

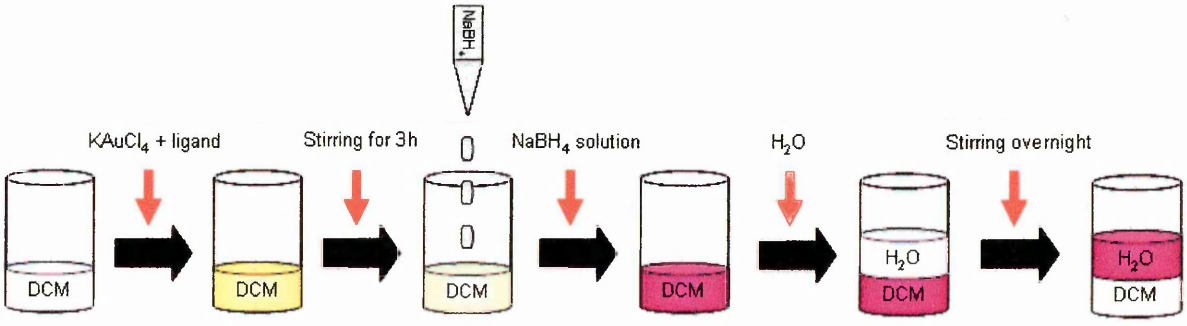

Figure 35. Illustration of phase colour changes in each of the steps in the synthesis of the phosphonium gold nanoparticles

After 24 hours, the stirring was stopped, and due to the affinity of the phosphonium-MPCs for the aqueous phase, DCM extractions were carried out in order to remove the excess of the organic matter. Three DCM extractions were done, and all the extracts were monitored by TLC, using 10% methanol : 90% dichloromethane as mobile phase. In Figure 36, a total removal of the organic compound excess can be observed in the TLC plate, with the third DCM extraction.

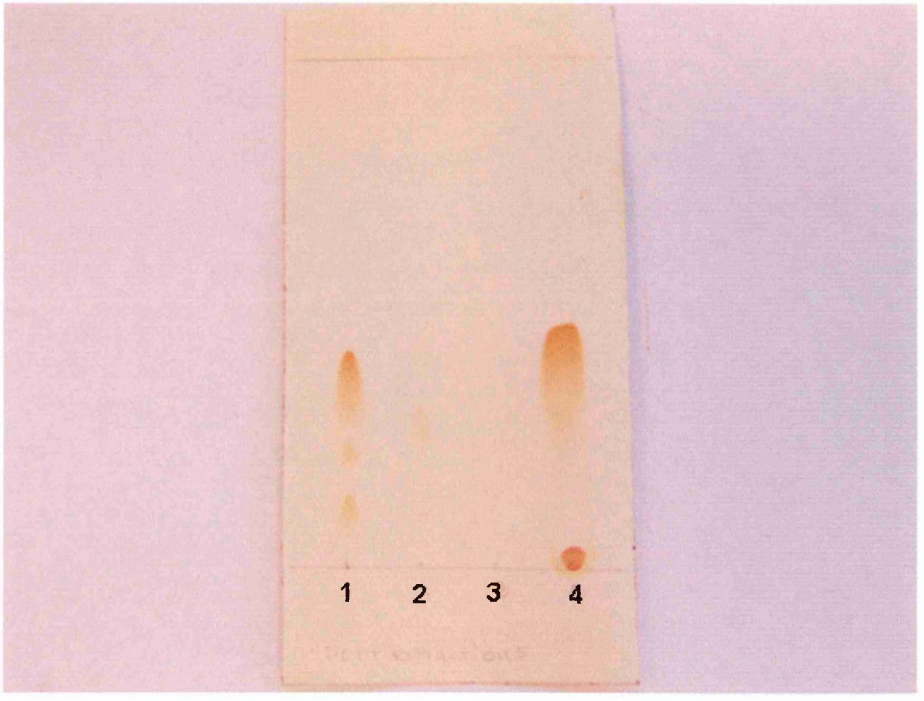

Figure 36. TLC plate of the DCM extracts obtain after the synthesis of the phosphonium-MPCs solution in presence of triphenyl(3-thioacetylpropyl)phosphonium bromide. **1**: DCM extraction No. 1, **2**: DCM extraction No. 2, **3**: DCM extraction No. 3, **4**: triphenyl(3-thioacetylpropyl)phosphonium bromide solution

Essentially, the reduction and functionalised gold nanoparticle formation occur in DCM. However, when the water is added to the solution, an affinity of the phosphonium-MPCs for the aqueous phase was observed. For this reason, the excess of organic reagents could be removed with the DCM extractions. All the DCM extracts were collected and water extractions were carried out. The organic phase was dried using $MgSO_4$, and the DCM was then removed in order to weigh the remaining organic matter. 88% (W/W) of the phosphonium ligand was consumed during the functionalised gold nanoparticle formation.

The reaction time between thiosulfate ligands $[Ph_3P^+(CH_2)_nS_2O_3^-]$ and the tetrachloroaurate anion ($AuCl_4^-$) was set to 4 hours, due to the aggregations observed when the sodium borohydride solution was added immediately after the gold salt dissolution (10 minutes). Coalescence of the particles occurred almost immediately, and the same observations were made in all the reactions involving phosphonioalkylthiosulfate zwitterions. Therefore, the reaction time was increased and the optimum was found to be 6 hours. In every case, during this time the colour of the solution changed from yellow to cloudy white.

According to Murray and co-workers[48], who prepared gold nanoparticles functionalised with alkanethiosulfate, this yellow to colourless change is due to the formation of $[\text{-Au(I)-SR-}]_n$ polymers prior to the sodium borohydride addition. Brust[41] and Murray[48] suggested that the ligand and the gold salt is allowed to react for 3 hours because at this stage of the reaction, a reduction of Au(III) to Au(I) occurs prior to the

formation of the polymer. Indeed, Murray and co-workers have been able to isolate and characterise the Au(I) polymer from one their reactions.

Murray and co-workers[48] reported the possibility of different relative reactivities in the case of S-alkylthiosulfates with the gold salt, in comparison to the corresponding alkanethiols. No colour changes were observed in the reactions between $RS_2O_3^-$ and $AuCl_4^-$, regardless of the reaction time. Consequently, they suggested that the reduction from Au(III) to Au(I) by the thiosulfate ligand that they used is either very slow or does not occur.[48] Contrary to the observations of Murray and co-workers[47], in the case of the reactions between phosphonioalkylthiosulfate zwitterions and the gold salt, colour changes from yellow to cloudy white were observed during the reaction time (6 hours). This experimental observation concurs with the suggestions made by Murray and Brust, and may indicate the formation of polymer species in solution at this stage of the reaction.

When 10-triphenylphosphoniodecylthiosulfate (**5e**) and 3-tributylphosphoniopropylthiosulfate (**5f**) were used, in the first instance a dark blue solution was observed. However, after 2 hours dark particles of aggregated colloidal gold were observed at the interface between the aqueous and organic phases, showing no affinity for either the dichloromethane or water. It would appear that as the carbon chain length increases to more than 8 in the triphenylphosphonium ligands, the formation of phosphonium monolayer-protected gold colloids that are stable in an aqueous medium becomes more difficult. Replacing the triphenylphosphonium cationic

group by tributylphosphonium group also appears to destabilise the nanoparticles and this might be due to the head group packing. In the case of the triphenylphosphonium-containing gold nanoparticles, the inductive effect of the phenyl groups on the positive charge of the phosphonium head group and the inter- and intra-molecular pi-pi interactions may stabilise the packing of the ligands surrounding the gold nanoparticle surface. In the case of 3-tributylphosphoniopropylthiosulfate (**5f**), it would appear that the cationic phosphonium head groups repel each other and, therefore, there is no stable gold nanoparticle formation. However, in the case of 6-tributylphosphoniohexylthiosulfate (**5g**), there is formation of stable nanoparticles and it might be due to the flexibility of the longer carbon chain of the ligand which might avoid the repulsion between the ligands attached to the gold nanoparticle core.

In contrast to the thiosulfate reactions described above, reactions of the thioacetates, triphenyl(3-thioacetylpropyl)phosphonium (**17a**) and triphenyl(6-thioacetylhexyl)phosphonium bromides (**17b**) and tetrachloroaurate, no such observations were obtained. In these cases, there were no colour changes in the reaction mixtures after 6 hours of stirring. Therefore, the addition of the sodium borohydride solution was done immediately after dissolving the gold salt in the organic phase. After the addition of the reducing agent and the water to the reaction flask, the mixture was left stirring overnight. When the stirring was stopped after 24 hours, burgundy solutions of colloidal gold were obtained, with no evidence of aggregation of the particles.

In the case of the synthesis of functionalised gold nanoparticles using (3-thioacetylpropyl)diphenylphosphine oxide (**20**) as protecting ligand, after the addition of sodium borohydride, a dark blue organic phase and a transparent aqueous phase were observed. It would appear that the gold nanoparticles functionalised with this phosphine oxide containing ligand have more affinity to the DCM, which is opposite to the other cases previously described. However, after 2 hours, complete aggregation and visible particles were observed at the bottom of the flask, making it impossible to use the solutions for further analysis and applications

6.2.2.3 Characterisation of the colloidal solutions of the phosphonio- monolayer protected gold nanoparticles

UV-visible spectroscopy

Evidence for the formation of gold nanoparticles was provided by UV-visible spectroscopy. A broad band centred at 524 nm was observed in the aqueous phase in the dark purple/blue solutions containing gold nanoparticles functionalised with **5a**, **5c-d**, **5g** and **17a-b** (Figure 37), indicating that the particle sizes were between 5-10 nm in diameter, according to the values for other thiolate-capped gold nanoparticles reported in the literature.[19]

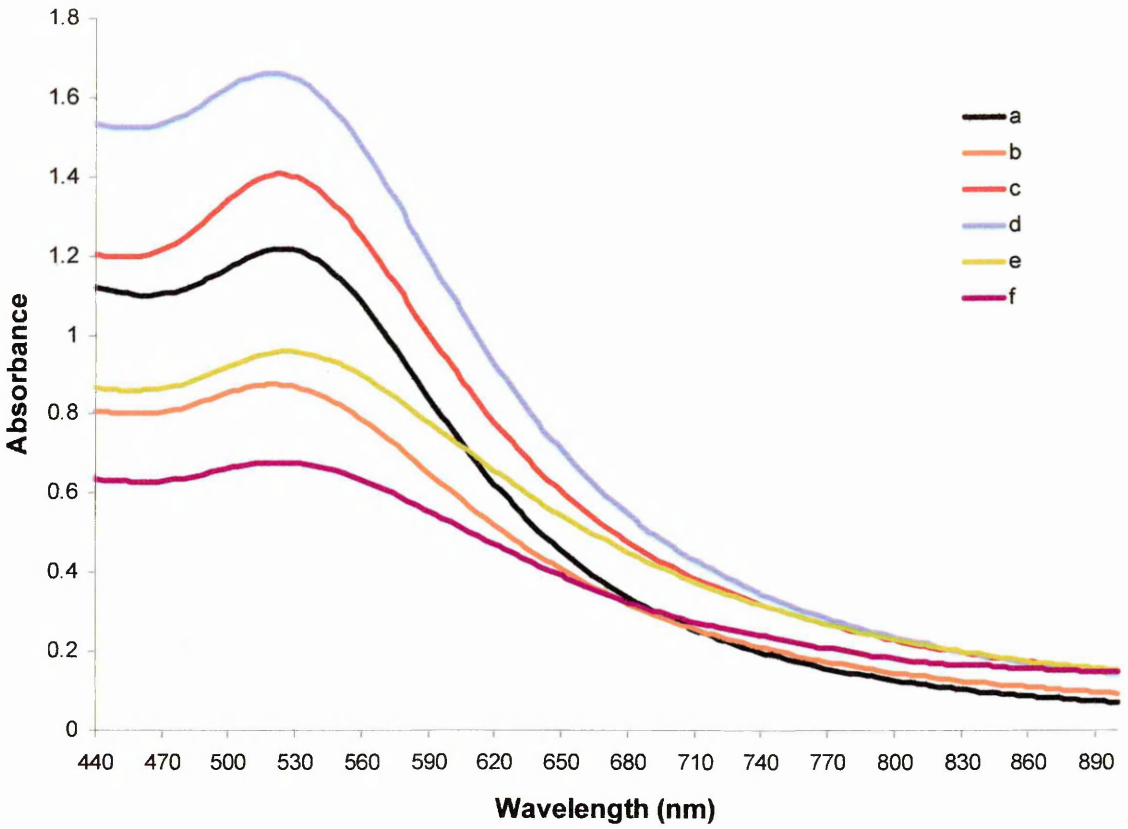

Figure 37. UV-visible spectra of the functionalised gold nanoparticles solutions (different dilution factors) with 3-triphenylphosphoniopropylthiosulfate (**5a**, a), tributylphosphoniohexylthiosulfate (**5g**, b), 6-triphenylphosphoniohexylthiosulfate (**5c**, c) and 8-triphenylphosphoniooctylthiosulfate (**5d**, d) zwitterions, triphenyl(3-thioacetylpropyl)phosphonium (**17a**, e), and with triphenyl(6-thioacetylhexyl)phosphonium bromides (**17b**, f)

These experimental results show that the same particle sizes were obtained in all the solutions and this might be due to the same molar ratio ligand:$KAuCl_4$:$NaBH_4$ being used in the preparation of all the functionalised gold nanoparticles, regardless of the nature of the protecting ligand. This particle size distribution was confirmed by TEM.

All the samples of colloidal gold were freeze-dried in order to remove water and keep them stable for longer periods of time, and to enable their re-dispersal in suitable solvents for analyses using other analytical techniques.

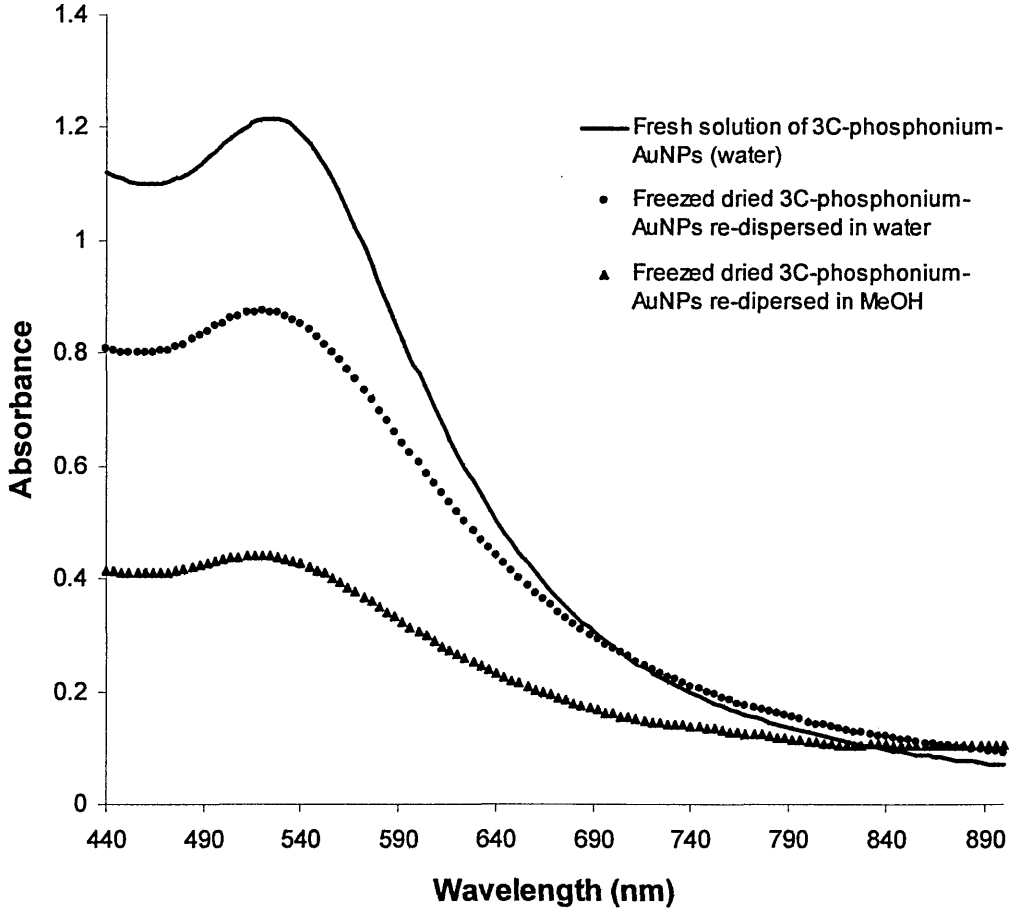

Figure 38. UV-visible spectra of the fresh solution of AuNPs functionalised with 3-triphenylphosphoniopropyl thiosulfate zwitterion (**5a-AuNPs**, —) and freeze dried **5a-AuNPs** re-suspended in water (•) and methanol (▲)

All the solutions of phosphonium-gold nanoparticles obtained using phosphonium containing ligands were freeze-dried. They could be re-suspended in solvents such as DMSO, water, methanol, and ethanol. Attempts at re-suspending the freeze-dried particles in iso-propanol, were unsuccessful. The UV-visible spectra of the solutions (different concentrations) corresponding to the freeze-dried gold nanoparticles functionalised with 3-triphenylphosphoniopropyl thiosulfate zwitterion (**5a-AuNPs**) re-suspended in water and methanol are shown in Figure 38. No changes in the surface plasmon bands of the solutions obtained from the freeze-dried particles were observed when their spectra were compared to that of a freshly prepared solution. These results indicate that even after the freeze drying process, the **5a-AuNPs** do not change their particle size. Similar results were obtained with the other phosphonium-gold nanoparticles.

Additionally, stability studies of the colloidal solution of gold nanoparticles functionalised with the 6-triphenylphosphoniohexylthiosulfate zwitterion (**5c-AuNPs**) was carried out in order to monitor possible changes in the surface plasmon band and therefore the particle size, in order to study the aging process of the phosphonium-gold nanoparticles and to determine the shelf-life of this colloidal solution. This experiment was carried out taking an aliquot of 2 mL of the **5c-AuNP** solution every month for 6 months and analysing it by UV-visible spectroscopy.

Figure 39 shows the UV-visible spectra corresponding to the fresh solution and the same colloidal solution after 1, 2, 3, 4, 5 and 6 months. No changes in the position

of the surface plasmon bands were observed indicating that the particle size was the same over this period of time. However, after 6 months, particle aggregations were observed in the **5c-AuNP** solution. Similar results were obtained for phosphonium-AuNPs prepared from thiacetate ligands (See Appendix A).

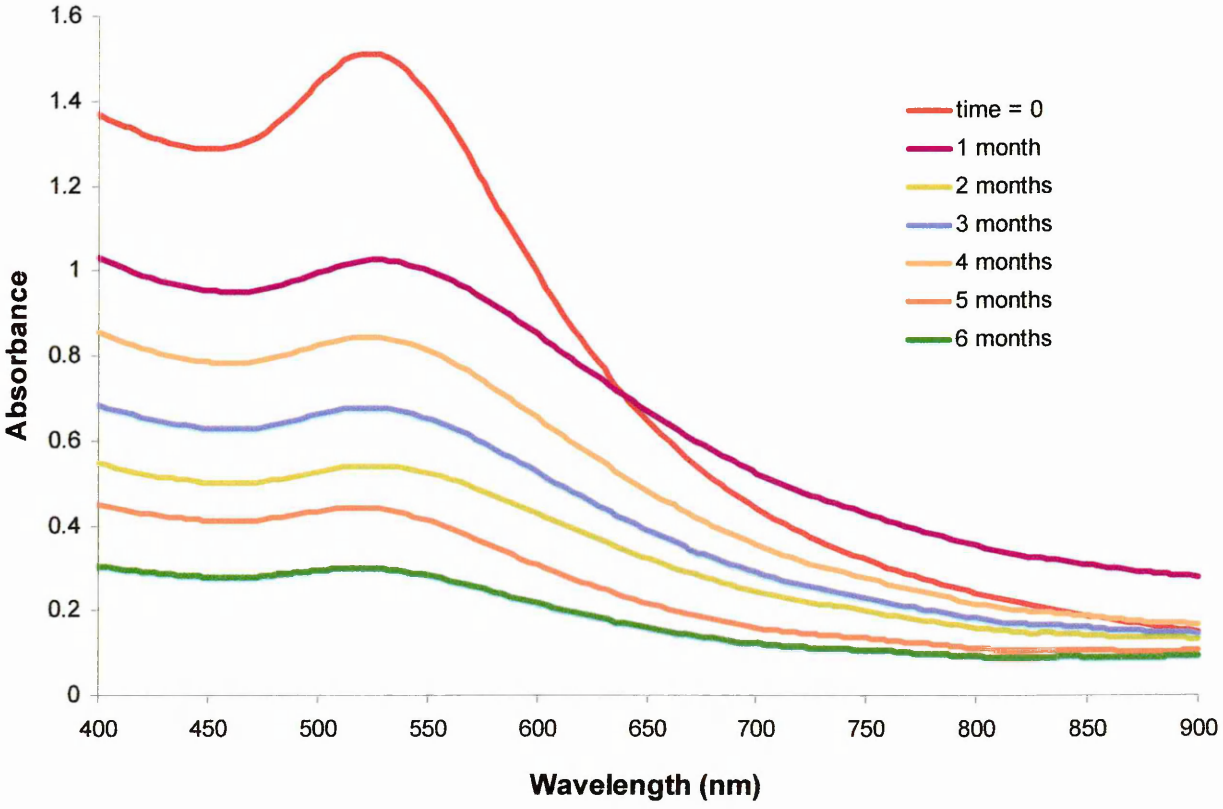

Figure 39. UV-visible spectra of a solution of AuNPs functionalised with 6-triphenylphosphoniohexyl thiosulfate zwitterion (**5c-AuNPs**), after 1, 2, 3, 4, 5, and 6 months (solutions made using different dilution factors)

Several attempts to synthesise functionalised gold nanoparticle using 10-triphenylphosphoniodecylthiosulfate zwitterion were unsuccessful, as was in the case of the tributylphosphoniopropylthiosulfate zwitterion. After the addition of the

sodium borohydride solution to the reaction mixture containing the gold salt and the ligand, a dark blue solution with a homogeneous appearance was observed in the organic phase (DCM). However, after the first hour the particles started to coalesce and after 2 hours of stirring, aggregation was complete, the aggregates remained at the interface between the aqueous and organic phases, and showed no affinity for either dichloromethane or water. An aliquot of the dark blue solution from the organic phase corresponding to the synthesis of functionalised gold nanoparticles using 10-triphenylphosphoniodecylthiosulfate zwitterion (**5e**) was taken and analysed by UV-visible spectroscopy.

Evidence of the formation for nanoparticles in DCM during the first hour of reaction is shown in Figure 40. The surface plasmon band of the spectrum of this solution occurs at 592 nm indicating that the formation of gold nanoparticles was taking place in the organic phase. According to the literature,[19,70] for AuNPs stabilised with sodium citrate with a mean diameter of 9, 15, 22, 48, and 99 nm, the SPB (maximum wavelength, λ_{max}) was observed at 517, 520, 521, 533, and 575 nm, respectively, in aqueous media. The formation of a band at 592 may suggest that the size of the prepared gold nanoparticles is greater than 100 nm, and these could act as a seed for the formation of larger particles.

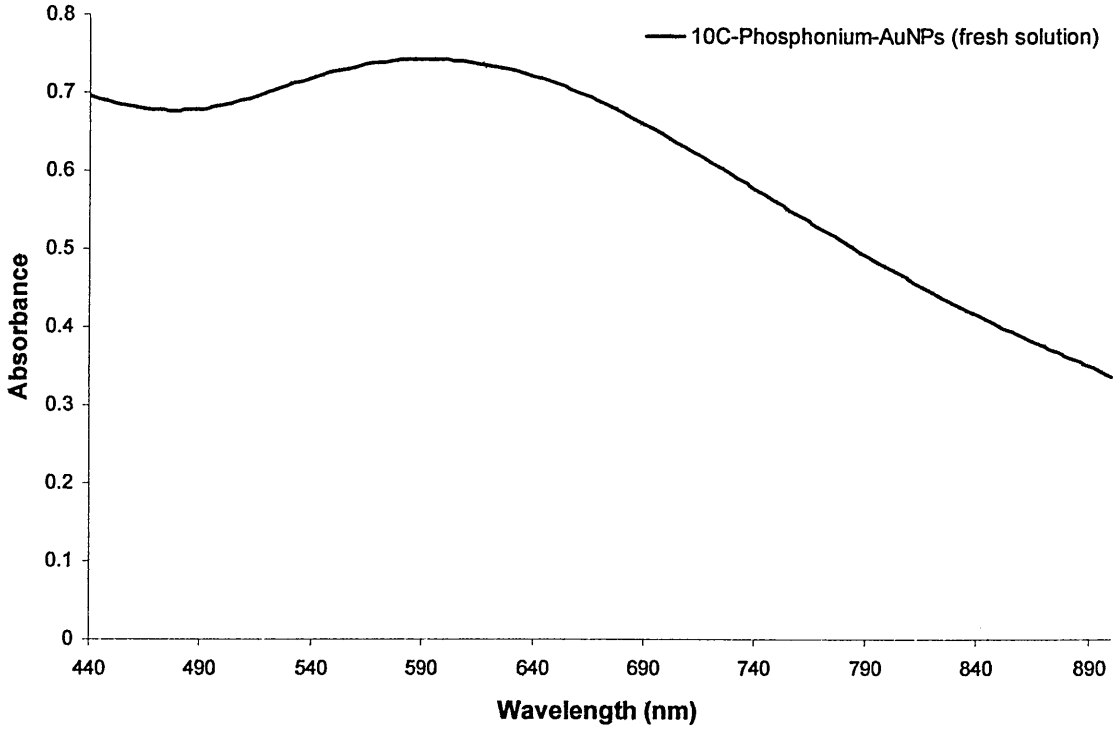

Figure 40. UV-visible spectrum of the dark blue solution (organic phase) corresponding to the attempts to prepare gold nanoparticle using 10-triphenylphosphoniodecylthiosulfate zwitterion as the precursor of the protecting ligand (Sample analysed during the first 10 minutes of the reaction)

Particle size obtained by the UV-visible technique was confirmed using a Transmission Electron Microscopic (TEM) technique.

Transmission Electron Microscopy (TEM)

The solutions of the gold nanoparticles functionalised with triphenylphosphoniopropylthiosulfate (**5a**) and triphenylphosphoniohexylthiosulfate (**5c**) zwitterions and triphenyl(3-thioacetylpropyl)phosphonium bromide (**17a**) were investigated by transmission electron microscopy (TEM). These gold nanoparticles were partially characterised using TEM (Zeiss, Cambridge University and Nano STEM, Sheffield Hallam University).

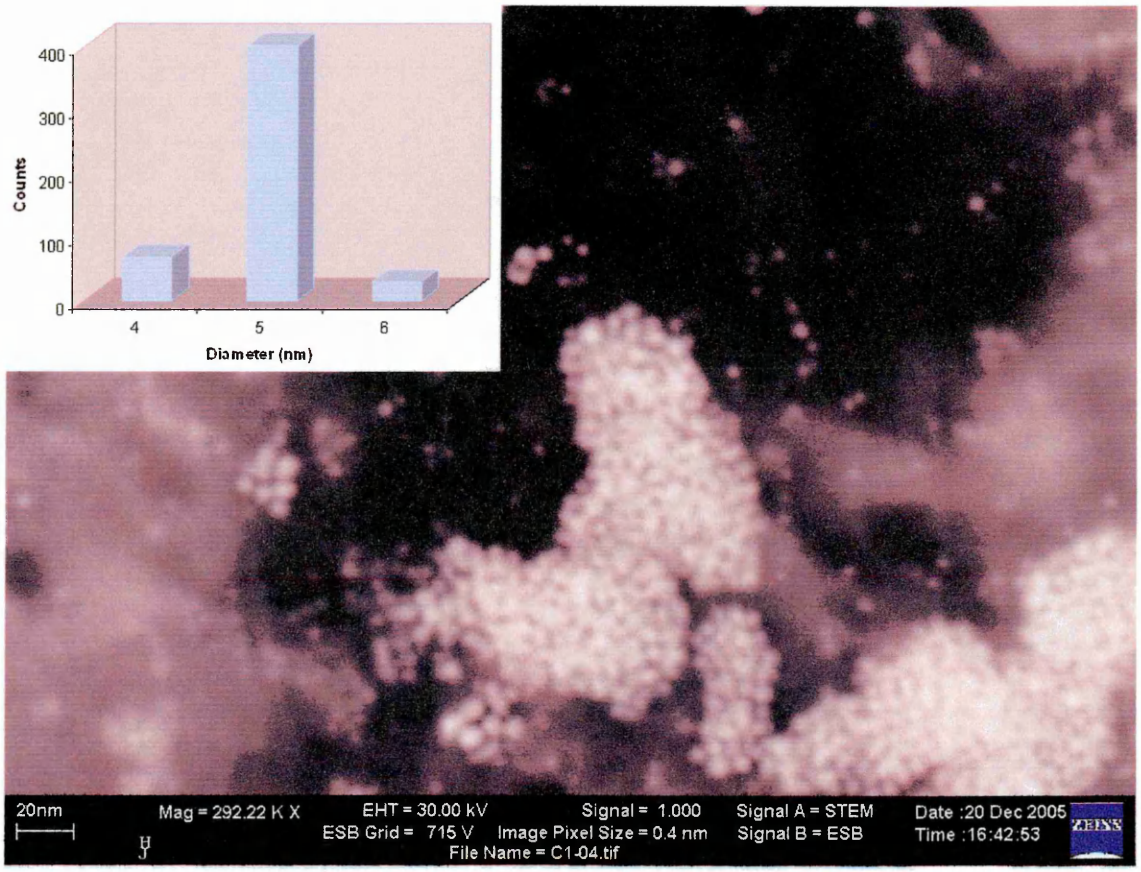

Figure 41. TEM micrograph and the core-size histogram of the gold nanoparticles functionalised with triphenylphosphoniopropylthiosulfate zwitterion (**5a**)

The TEM images were obtained by dropping a solution of AuNPs dispersed in water onto a carbon-coated copper grid. A small piece of tissue was used to remove the

excess of water and then the samples were left to stand overnight allowing the remaining solvent to evaporate. The copper grids used in this study were 1000 mesh. Highly uniform spherical nanoparticles of *ca* 5 nm can be observed in the TEM images and core-size histograms (Figures 41, 42 and 43) corresponding to the AuNPs functionalised with the triphenylphosphoniopropylthiosulfate (**5a**) and triphenylphosphoniohexylthiosulfate (**5c**) zwitterions and triphenyl(3-thioacetylpropyl)phosphonium bromide (**17a**), supporting the results obtained by the UV-visible spectroscopy. The colloidal solutions presented good stability over 6 months at room temperature. The solutions were monitored by UV-visible spectroscopy and no changes were observed in their spectra during this period.

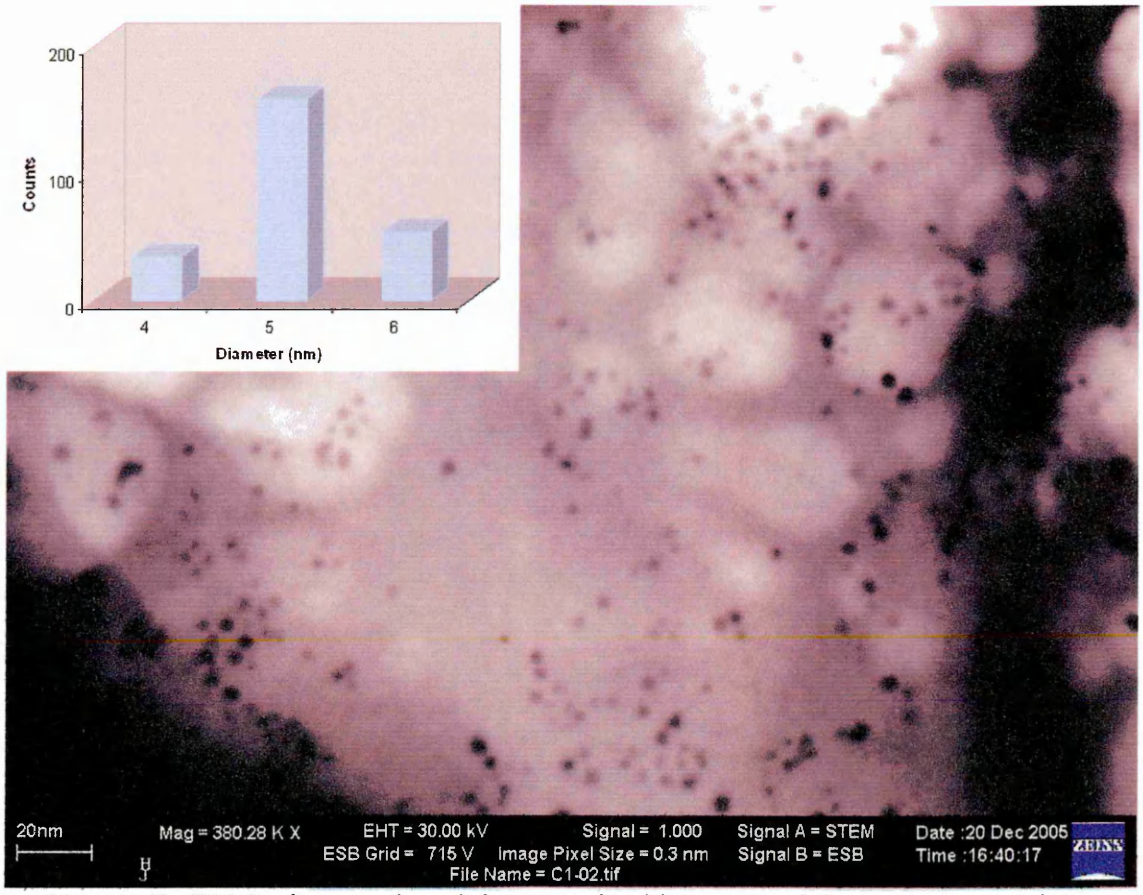

Figure 42. TEM micrograph and the core-size histogram of the gold nanoparticles functionalised with triphenylphosphoniohexylthiosulfate zwitterion (**5c**)

All the TEM micrographs were obtained using low voltage (low kV values), between 12 and 30 kV, so as to minimise decomposition of the organic matter.

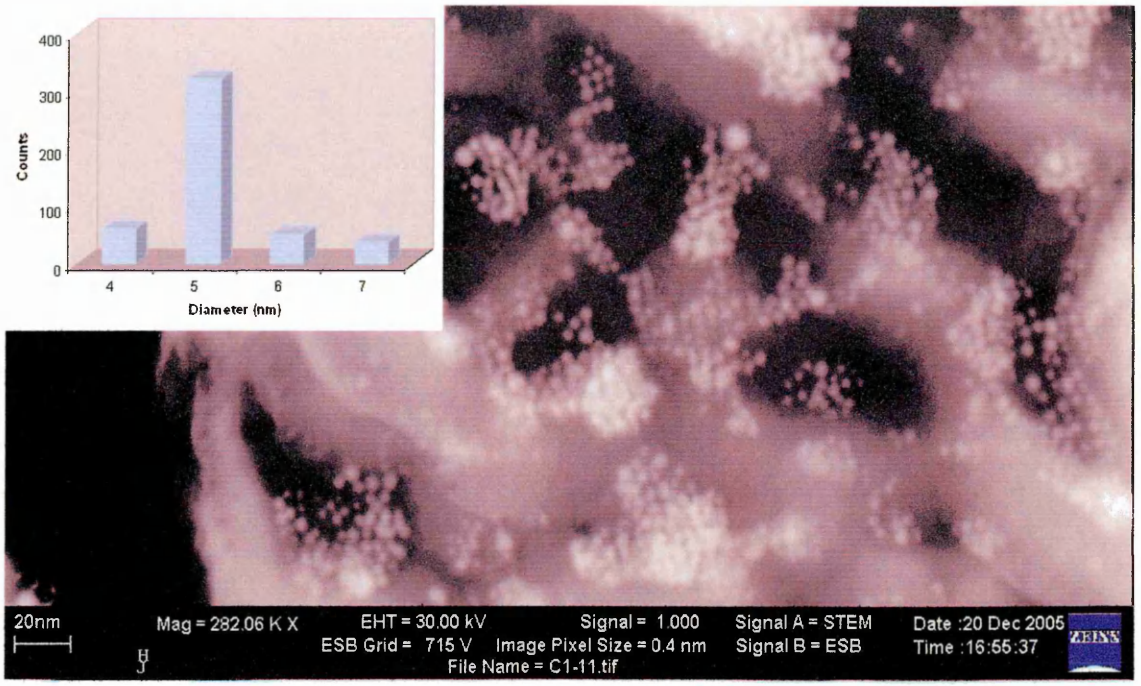

Figure 43. TEM micrograph and the core-size histogram of the gold nanoparticles functionalised with triphenyl(3-thioacetylpropyl)phosphonium bromide (**17a**)

Following the stability study of the **5c-AuNP** solution by UV-visible spectroscopy, in which no changes in the position of the surface plasmon bands were observed over 6 months, the aged sample was analysed by TEM in order to confirm the UV results. After 6 months, particle aggregation was observed in the **5c-AuNP** solution. Evidence of this can be seen in Figure 44. In the UV-visible spectrum corresponding to the aged solution, a shoulder between 700 and 800 nm can be observed indicating the possible formation of particles much bigger than 5 nm.

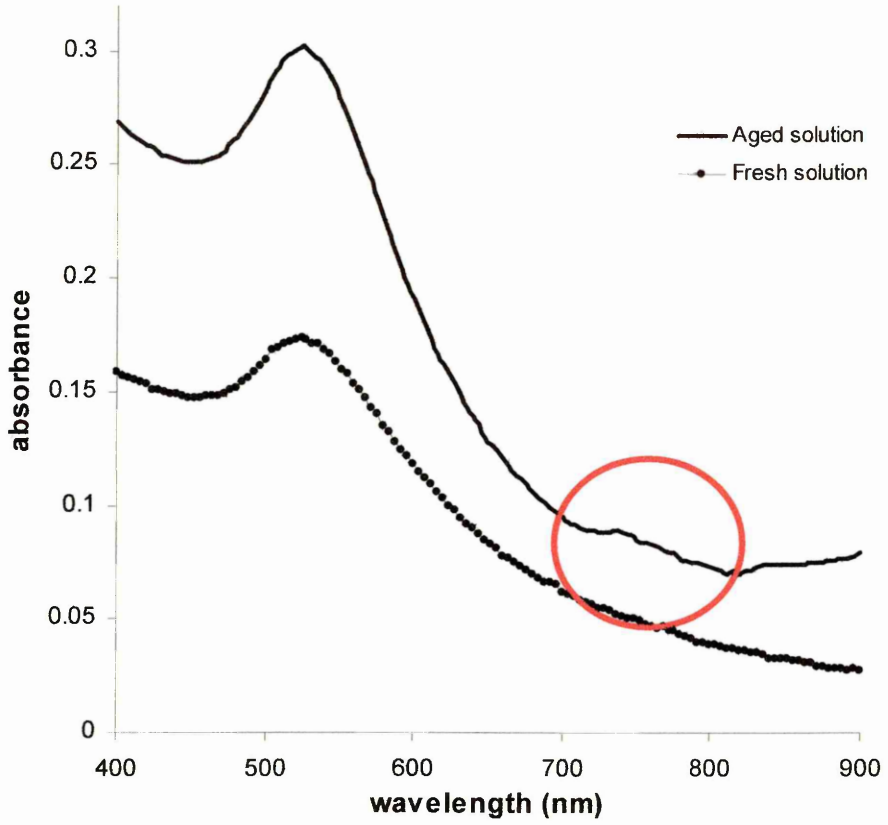

Figure 44. UV-visible spectra of a fresh solution of functionalised AuNPs with 6-triphenylphosphoniohexyl thiosulfate zwitterion (**5c-AuNPs**, •) and after 7 months (—). Solutions prepared using different dilution factors.

This result was confirmed by TEM analysis. In the corresponding micrograph and core-size histogram (Figure 45), a mixture of different particles in terms of size is observed. Particle size of around 5-20 nm and larger are present in the sample. In size, the larger particles vary between 35 and 65 nm. The aggregations observed in this solution after 6 months could be attributed to the presence of these bigger particles which act as the seeds for the growth of larger, observable particles during the aging

process of the gold colloidal solution. The air-oxidation of thiolate ligands causes a de-protection of the gold nanoparticle surface. The latter can promote aggregation due to the plasmon-plasmon interactions between the gold nanoparticles and cause a shift in the surface plasmon absorption band to longer wavelengths.[176,177]

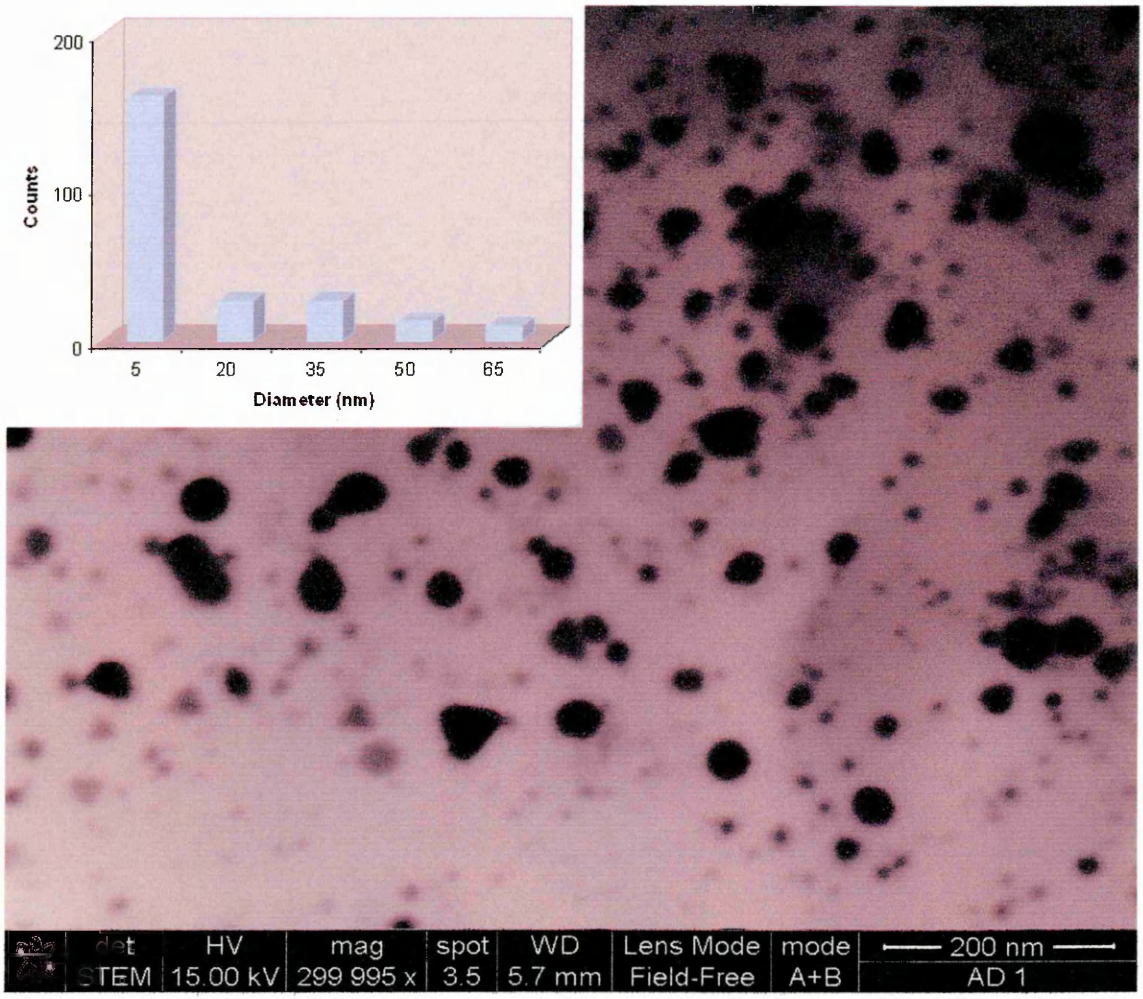

Figure 45. TEM micrograph and the core-size histogram of the gold nanoparticles functionalised with 6-triphenylphosphoniohexyl thiosulfate zwitterion (**5c-AuNPs**) corresponding to a solution aged for 7 months

^{31}P Nuclear Magnetic Resonance (^{31}P NMR) spectroscopy of phosphonium-functionalised gold nanoparticles

In order to characterise the ligands surrounding and protecting the gold nanoparticle surface, a ^{31}P NMR analysis of the phosphonium-containing gold nanoparticles was carried out. A freeze-dried sample (8 mg) of gold nanoparticles functionalised with triphenyl(3-thioacetylpropyl)phosphonium bromide (**17a-AuNPs**) was taken and dissolved in 4 mL of DMSO. The sample was then placed in the NMR instrument to collect the signals corresponding to ^{31}P. After overnight scanning, a significant signal corresponding to a chemical shift corresponding to the phosphorus atom of the surface-bound triphenylphosphonioalkyl thiolate was observed, as it is shown in Figure 46.

No significant change could be seen in the ^{31}P NMR spectrum, between the chemical shift of the ligand as itself (spectrum obtained in DMSO) and that corresponding to the ligand coating the gold nanoparticle core. Only a difference of 0.1 ppm in the chemical shifts is observed. This indicates that the phosphonium head group is in a similar chemical environment in both cases. However, the very slight difference in chemical shift could be due to the influence of the metal core on the chemical environment of the phosphonium containing ligand.

There is no interference of the excess of triphenyl(3-thioacetylpropyl)phosphonium bromide (**17a**) ligand, used in the synthesis of the corresponding gold nanoparticles, in this experiment, and the chemical shift of the ^{31}P

corresponding to the phosphoniopropylthioacetate ligand coating the gold nanoparticle surface is only due to the phosphorus of the ligand attached to the metal core. The excess of ligand was removed from the original gold colloidal solution (aqueous phase) with DCM extractions in order to avoid the interference of the signals corresponding to the free ligand in solution. Finally, it can be concluded from the evidence obtained in this ^{31}P NMR experiment, that the chemical structure of the ligand stabilising the metal core is the same of the structure of ligand as itself and that at least the phosphonium head group is intact.

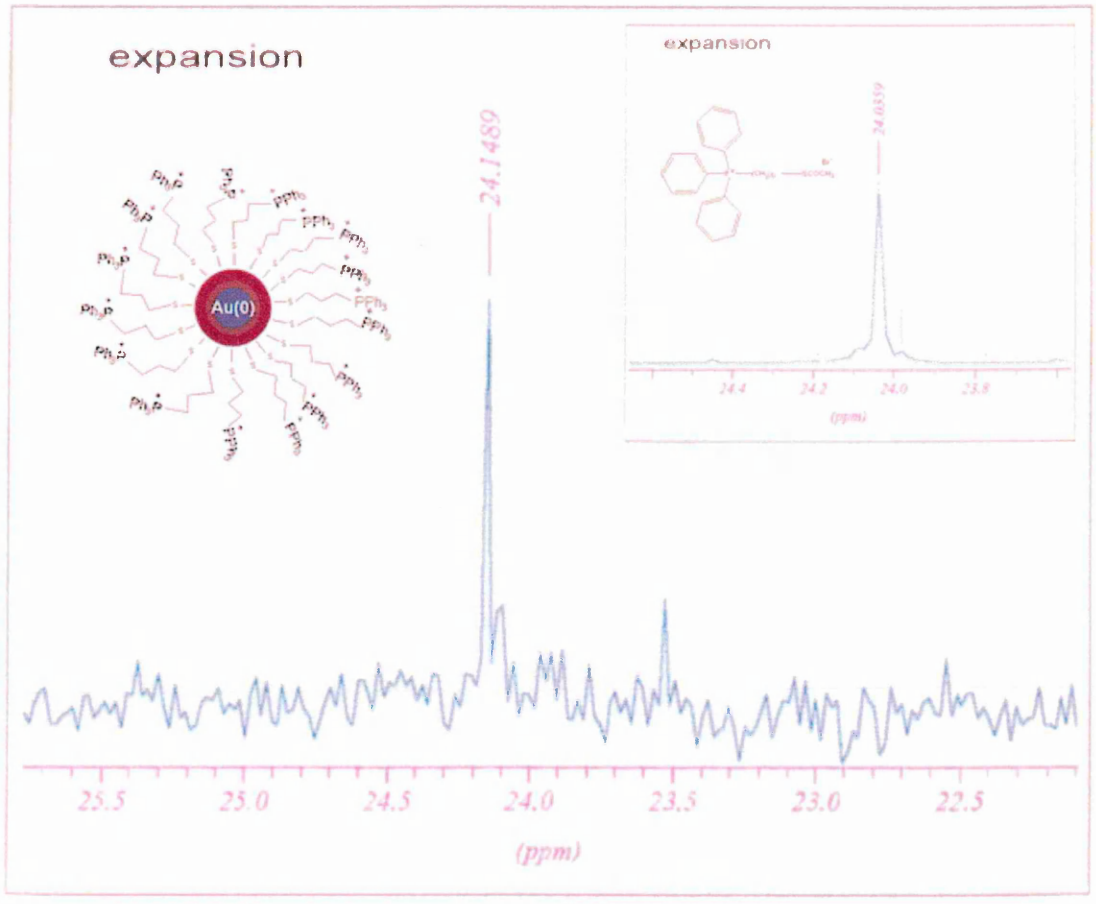

Figure 46. ^{31}P NMR spectra of the **17a-AuNPs** and triphenyl(3-thioacetylpropyl)phosphonium bromide (**17a**)

X-ray Photoelectron Spectroscopy (XPS)

X-ray photoelectron spectroscopy has been employed in this project to determine the ligand-substrate bond characteristics, such as S-Au linkage, for the gold nanoparticles functionalised with phosphonioalkylthiolate ligands. X-ray photoelectron spectroscopy (XPS) has been widely used to study numerous monolayer-protected metal cluster and self-assembled monolayer systems.[48,49,59]

XPS offers a direct chemical description of the surface layer (2-5 nm depth) of the sample. The binding energy measured by this technique is influenced by the electron density due to the chemical shift of a component peak, and the chemical state of individual elements can be deduced. Indeed, chemical bonding information or evidence of the oxidation states of individual elements can be obtained.[178]

XPS has been used to investigate the nature of the S-Au linkage in phosphonium-AuNP samples. The functionalised gold nanoparticle samples obtained using the 3-triphenylphosphonioproylthiosulfate zwitterion (**5a-AuNPs**) and triphenyl(3-thioacetylpropyl)phosphonium bromide (**17a-AuNPs**) as the source of the protecting ligands were used for the XPS analysis in this project. The freeze-dried samples were placed on a standard sample stud employing double sided adhesive tape and the takeoff angle was fixed at 90°. XPS peaks corresponding to Au and S were analysed at high resolution and deconvoluted to measure the contributions from each component.

Figure 47 shows the XPS wide scan corresponding to the phosphonium-gold nanoparticles prepared using the 3-triphenylphosphoniopropylthiosulfate zwitterion (**5a-AuNPs**). In this spectrum, signals of gold (4p, 4d and 4f), sulfur (2s and 2p), phosphorus (2p), carbon (1s), sodium (KLL, 2s and 2p), boron (1s), potassium (2s, 2p and 3p), chlorine (2s and 2p) and oxygen (1s and 2s) were observed. A wide scan corresponding to the phosphonium-AuNPs obtained using triphenyl(3-thioacetylpropyl)phosphonium bromide (**17a-AuNPs**), showed that the same peaks were observed (See Appendix B).

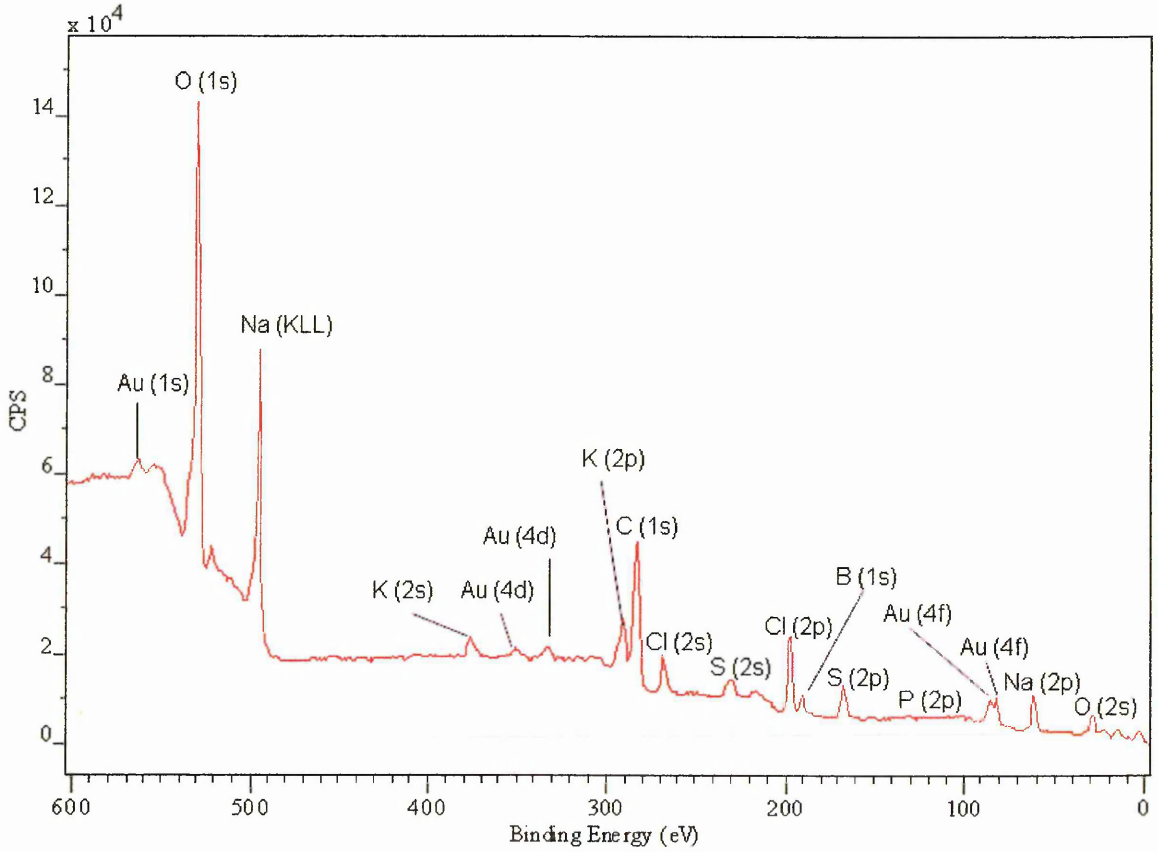

Figure 47. XPS wide scan spectrum corresponding to the freeze-dried sample of gold nanoparticles functionalised with the 3-triphenylphosphoniopropylthiosulfate zwitterion (**5a-AuNPs**)

The high resolution Au_{4f} spectra collected from the phosphonium-AuNP sample, **5a-AuNP**, is shown in Figure 48.

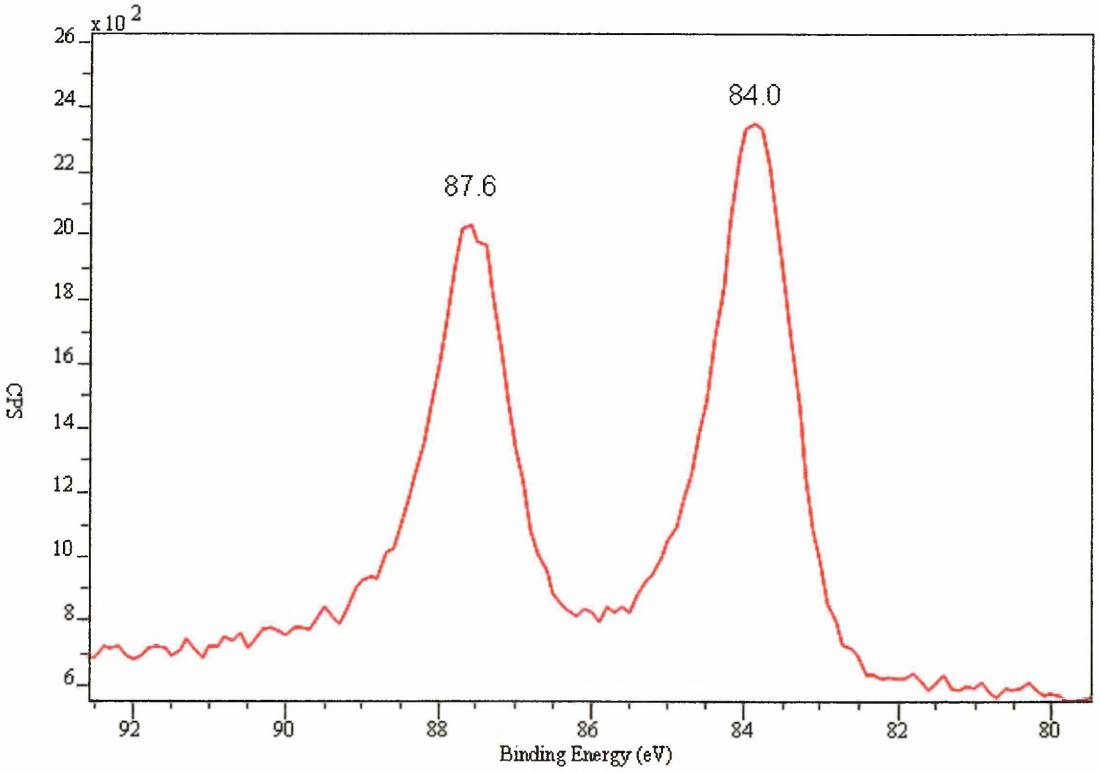

Figure 48. XPS high resolution spectrum of Au 4f collected from the freeze-dried **5a-AuNP** sample

A doublet with a peak-to-peak distance of about 3.6 eV was observed for the Au 4f level. This Au 4f doublet ($4f_{7/2}$ and $4f_{5/2}$) represents the standard measure of the gold oxidation state. The binding energies for the doublet were 84.0 and 87.6 eV. These values are similar to those reported by Yee and co-workers[49] in surface chemistry studies of gold nanoparticles coated with dodecanethiol ligands by XPS (Figure 49).

According to Heath and co-workers and their results obtained in the characterisation of hydrophobic and organically-soluble gold nanocrystals functionalised with primary amine (laurylamine) by XPS, this data is consistent with the Au^0 oxidation state, and therefore indicates the absence of Au(I).[49,179] McNeillie and co-workers[180] reported that if Au(I) is present in the sample, it would be expected to give rise to a peak, or at least a shoulder, on the Au^0 $4f_{5/2}$ peak at *ca* 84.9 eV.

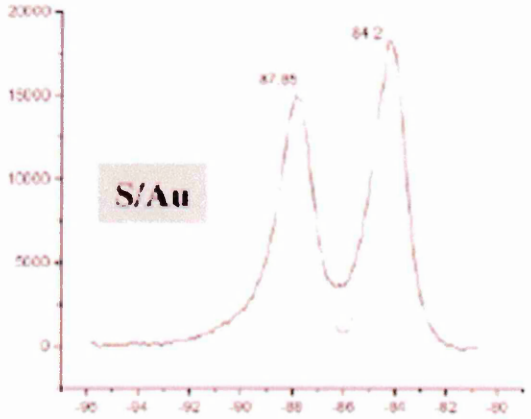

Figure 49. XPS high resolution spectrum of Au 4f collected from dodecanethiol-AuNP sample. Binding energy values of Au 4f reported by Yee and co-workers[49]

Moreover, in accordance with Heath and co-workers,[179] the absence of such a signal in the high resolution scan can allow as estimate that if charged Au atoms are present in the sample no more than 8% of the Au surface atoms are in an ionised state. They inferred that most of the ligand-Au interactions are of neutral charge and also

suggested that the 8% representing the surface charge can help to increase the solubility of the particles in polar solvents such as water, methanol, or acetone.[179]

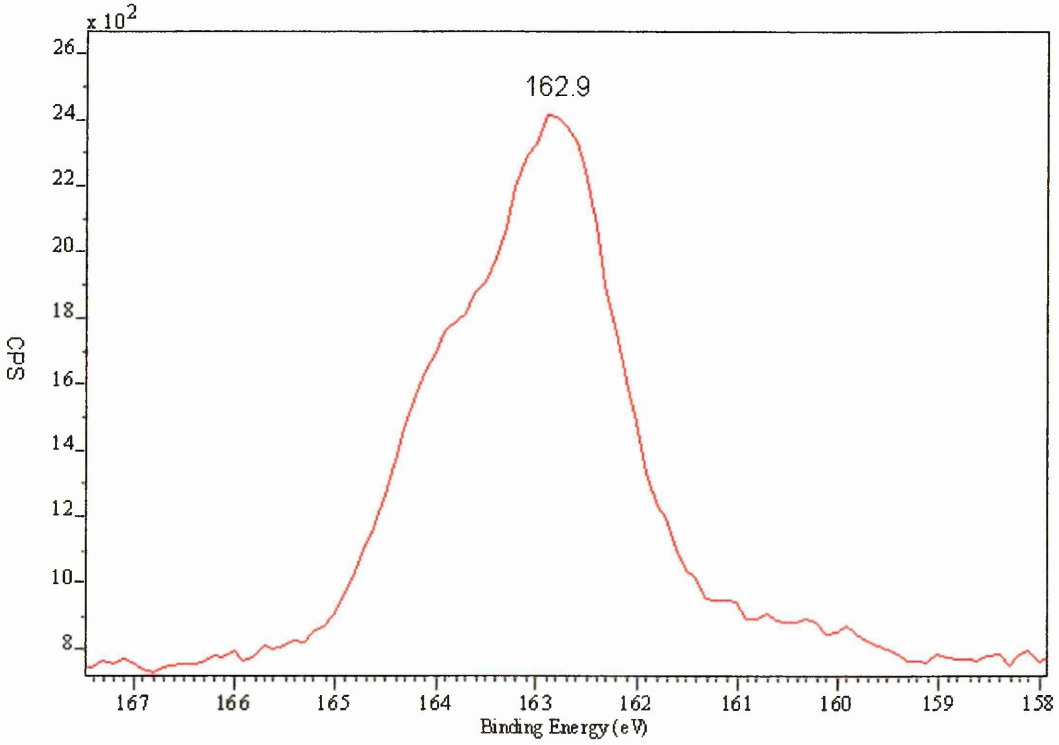

Figure 50. XPS high resolution scan spectrum of S_{2p} corresponding to **5a-AuNP**

In the high resolution scan spectrum of S_{2p} corresponding to **5a-AuNP** shown in Figure 50, a binding energy corresponding to S $2p_{3/2}$ appeared at 162.9 eV. This wide scan of the sulfur atom is different when is compared to the sulfur wide scan corresponding to the thiosulfate ligand itself (3-triphenylphosphoniopropylthiosulfate zwiterion, **5a**, Figure 51).

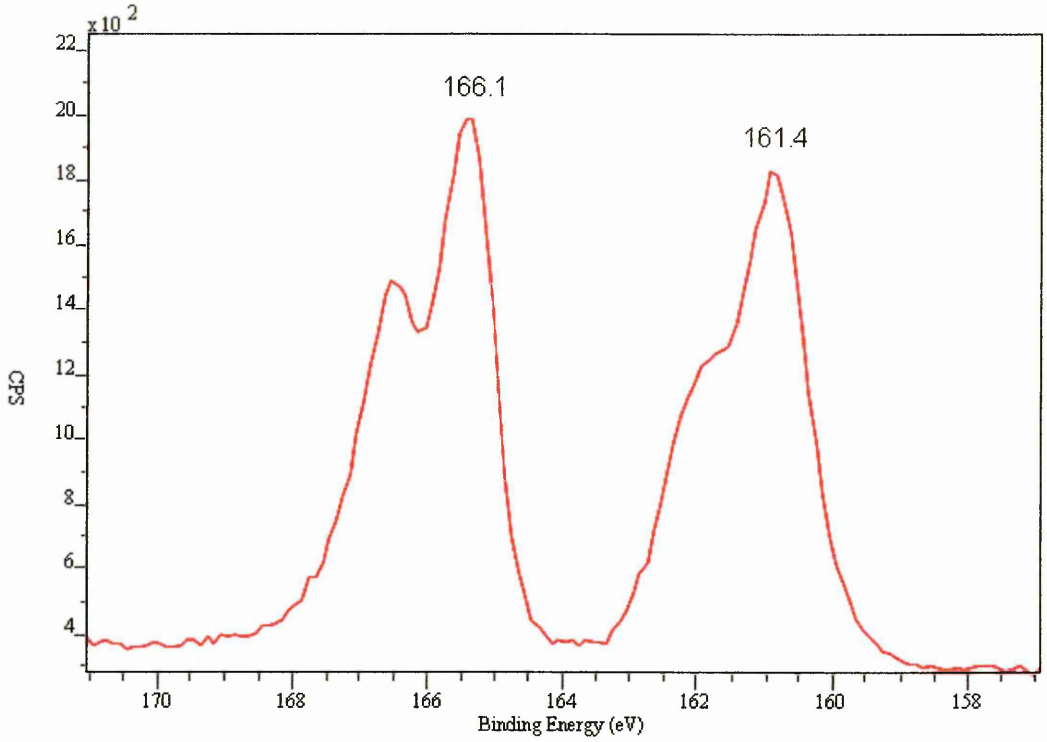

Figure 51 XPS high resolution scan spectrum of S_{2p} corresponding to the 3-triphenylphosphoniopropylthiosulfate zwiterion **(5a)**

In Figure 51, two binding energy signals at 161.4 and 166.1 eV can be observed. The thiosulfate containing compounds (Bunte salts) possess sulfur in two different environments in terms of chemical structure and, consequently, with the 3-triphenylphosphoniopropylthiosulfate zwitterion, two oxidation states of sulfur with different binding energies and equal intensities (or counts per seconds, CPS) were observed in the S 2p XPS wide scan spectrum. The lower binding energy at 161.4 eV in the doublet can be attributed to sulfur bound to a carbon atom. Fornasiero and co-workers[181] have found similar values for the sulfur atom contained in inorganic thiosulfates. They measured PbS_2O_3 and $Na_2S_2O_3$, obtaining binding energies at 162.2

and 161.7-162.5 eV, respectively. The higher binding energy at 166.1 eV in the doublet in Figure 51, can be assigned to the sulfur atom bound to the oxygen atoms of the thiosulfate group, and the binding energy of this signal is a little lower than the values reported for sulfur in inorganic thiosulfates (167.7 eV).[181]

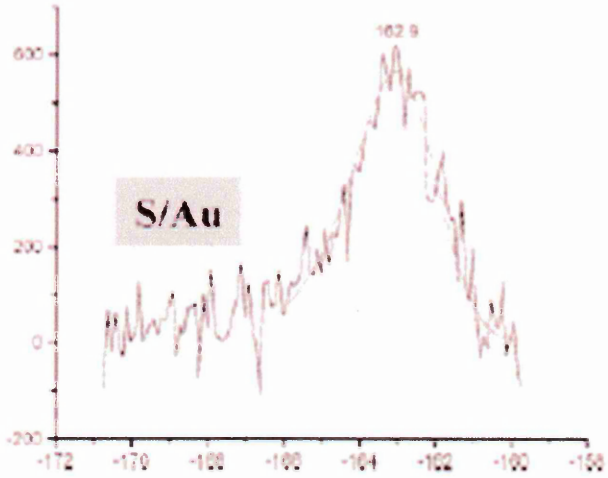

Figure 52. XPS high resolution spectrum of S_{2p} collected from dodecanethiol-AuNP sample. Binding energy values of S_{2p} reported by Yee and co-workers[49]

The value of the binding energy of S $2p_{3/2}$ at 162.9 eV corresponding to **5a-AuNP** (Figure 50) is similar to the binding energy of S $2p_{3/2}$ found reported in the literature and typical for organic thiolates binding to gold (162.0-162.9 eV) (Figure 52).[182,183] No signal due to the oxygen-containing sulfur species in the wide scan of S 2p corresponding to **5a-AuNP** (Figure 50) was observed, indicating that the S-S bond of

the 3-triphenylphosphoniothiosulfate zwitterion has been cleaved, leaving the phosphoniopropylthiolate species to interact with the gold nanoparticle surface.

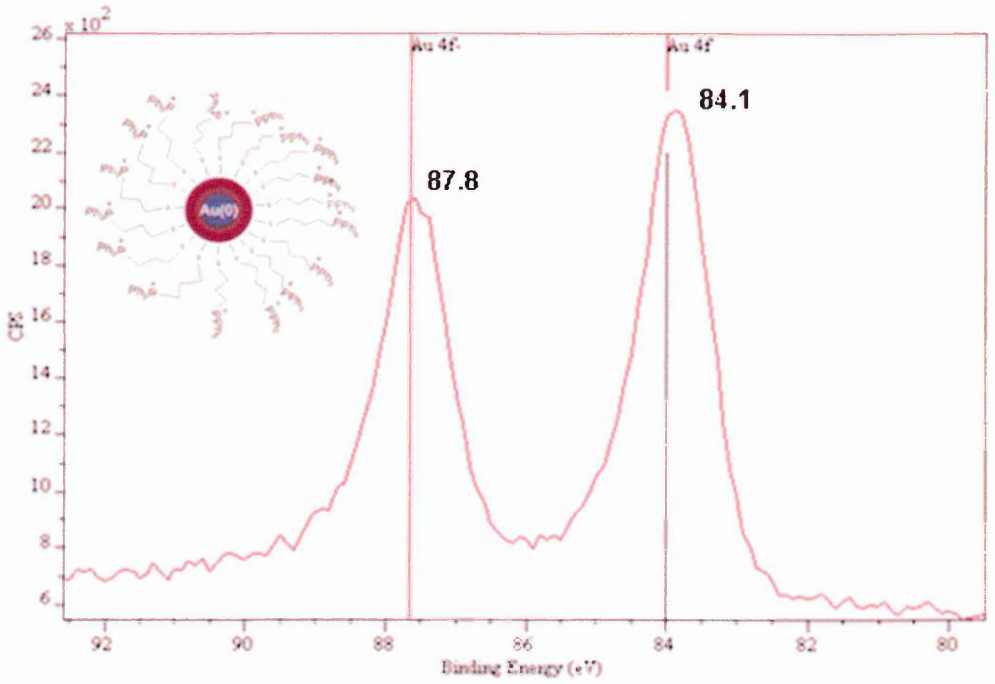

Figure 53. XPS high resolution spectrum of Au 4f collected from the freeze-dried **17a-AuNP** sample

The high resolution Au_{4f} and S_{2p} spectra collected from the phosphonium-AuNP sample obtained using triphenyl(3-thioacetylpropyl)phosphonium bromide, **17a-AuNP**, are shown in Figures 53 and 54 respectively. In Figure 53, a doublet with a peak-to-peak distance of about 3.7 eV was observed for the Au 4f level. The binding energies for the doublet were 84.1 and 87.8 eV (corresponding to $4f_{7/2}$ and $4f_{5/2}$, respectively). These values are similar to those obtained in the analyses carried out with **5a-AuNP** and

also to those reported by Yee and co-workers[49] in the surface chemistry studies of gold nanoparticles coated with dodecanethiol ligands by XPS (Figure 49).

In the high resolution scan spectrum of S_{2p} shown in Figure 54 (a), a binding energy corresponding to S $2p_{3/2}$ appeared at 162.1 eV for the phosphonium-AuNP sample. This value was slightly higher than that of the S atom value found for the free thioacetate ligand [161.1 eV, see Figure 54 (b)]. The binding energy of S $2p_{3/2}$ = 162.1 eV found in this analysis is similar to the values reported for thiolates binding to gold (162.0-162.9 eV) (Figure 52).[182,183]

Additionally, a signal at 167.0 eV was also observed in Figure 54 (a). According to the literature, this binding energy value can be attributed to the sulfur atom bonded to another sulfur atom, as a sulfur-sulfur bond, possibly due to the product of the air oxidation that such thiolate ligands can undergo in the presence of air.[49] This result was expected since the sample of gold nanoparticles used in this analysis had been aged for 4 months.

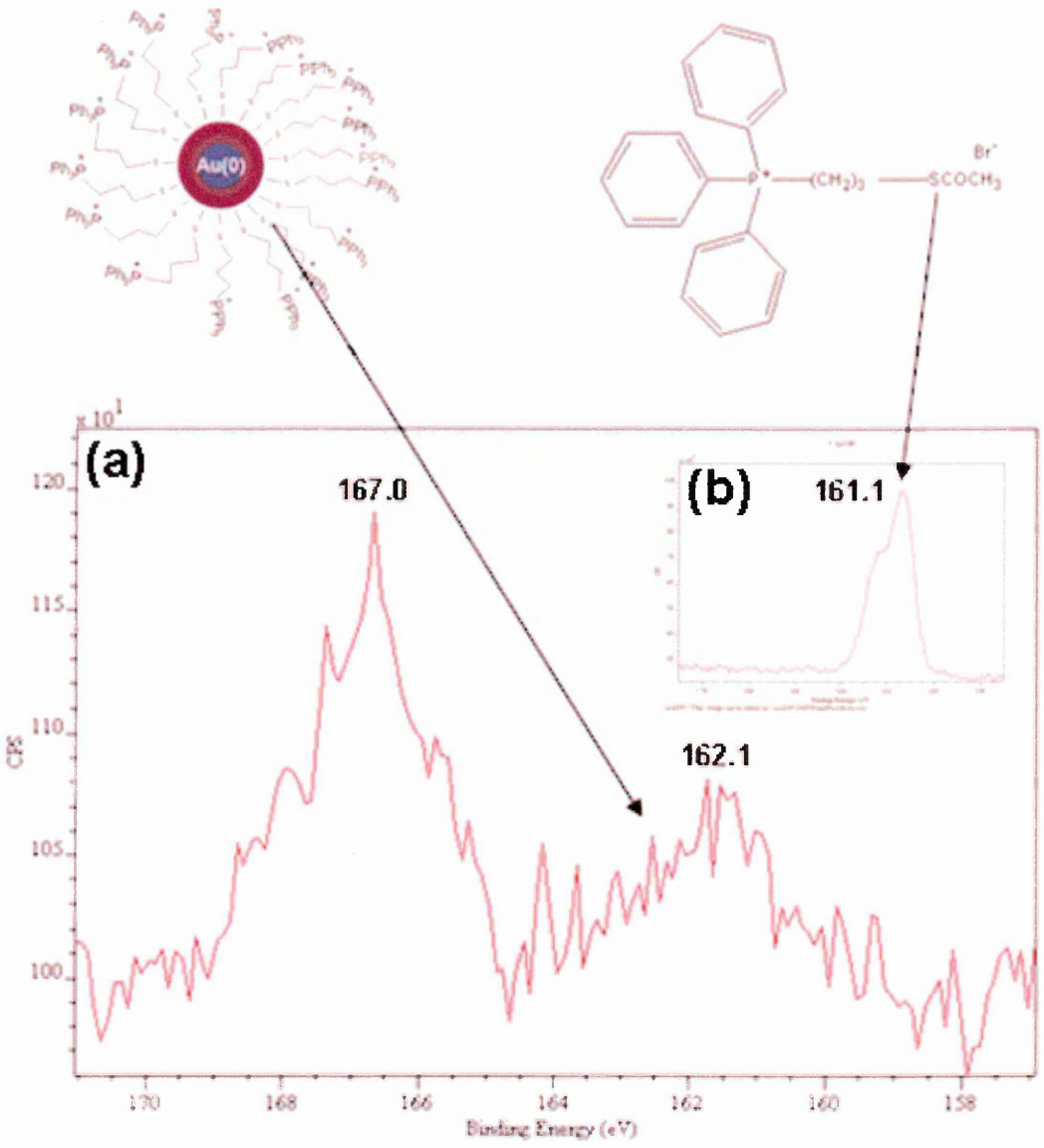

Figure 54. XPS high resolution scan spectra of S_{2p} corresponding to **17a-AuNPs** (**a**) and the triphenyl(3-thioacetylpropyl)phosphonium bromide (**b**)

6.3 Attempts to stabilise gold nanoparticles using phosphonioalkylselenide compounds as protecting ligands

6.3.1 Experimental

6.3.1.1 Studies of the potential of the phosphonioalkylselenide compounds as precursors of the protecting ligands - Synthesis of 3-(methylseleno)propyl-triphenylphosphonium iodide (25)

Before attempting to prepare cationic phosphonium monolayer-protected gold nanoparticles using bis(3-triphenylphosphoniopropyl)diselenide–di(selenocyanate) (**15a**) and 6-(selenocyano)hexyl-triphenylphosphonium selenocyanate (**13b**), studies of the potential of these compounds to act as protecting ligands precursors were carried out.

In order to show the capacity of the phosphonioalkylselenide ligands to form the corresponding selenoate species during the synthesis of the functionalised gold nanoparticles, an alkylation reaction using bis(3-triphenylphosphoniopropyl)diselenide–di(selenocyanate) (**15a**) and iodomethane as starting materials was carried out under the same reductive conditions used for the preparation of the capped nanoparticles.

The alkylation of **15a** was carried out using the following method: bis(3-triphenylphosphoniopropyl)diselenide–di(selenocyanate) (**15a**, 0.5 mmol) was dissolved in 3 mL of methanol. A freshly prepared aqueous solution of sodium borohydride (2 mL, 5 mmol) was then added drop by drop to the reaction flask, in order to allow formation of

the zwitterion $Ph_3P^+(CH_2)_3Se^-$ (**14a**). The mixture was stirred for 1 hour at room temperature. The formation of 3-(methylseleno)propyl-triphenylphosphonium iodide (**25**) was achieved by the reaction of **15a** and methyl iodide (**23**, 0.3 mL, 5mmol) under nitrogen and the mixture was stirred overnight at room temperature (Scheme 9). Progress of the reaction was monitored by TLC, using 10% methanol : 90% dichloromethane as a mobile phase. The resulting mixture was extracted with dichloromethane, the nonaqueous phase was collected and after removing the solvent, the resulting compound was initially purified by trituration with dry diethyl ether.

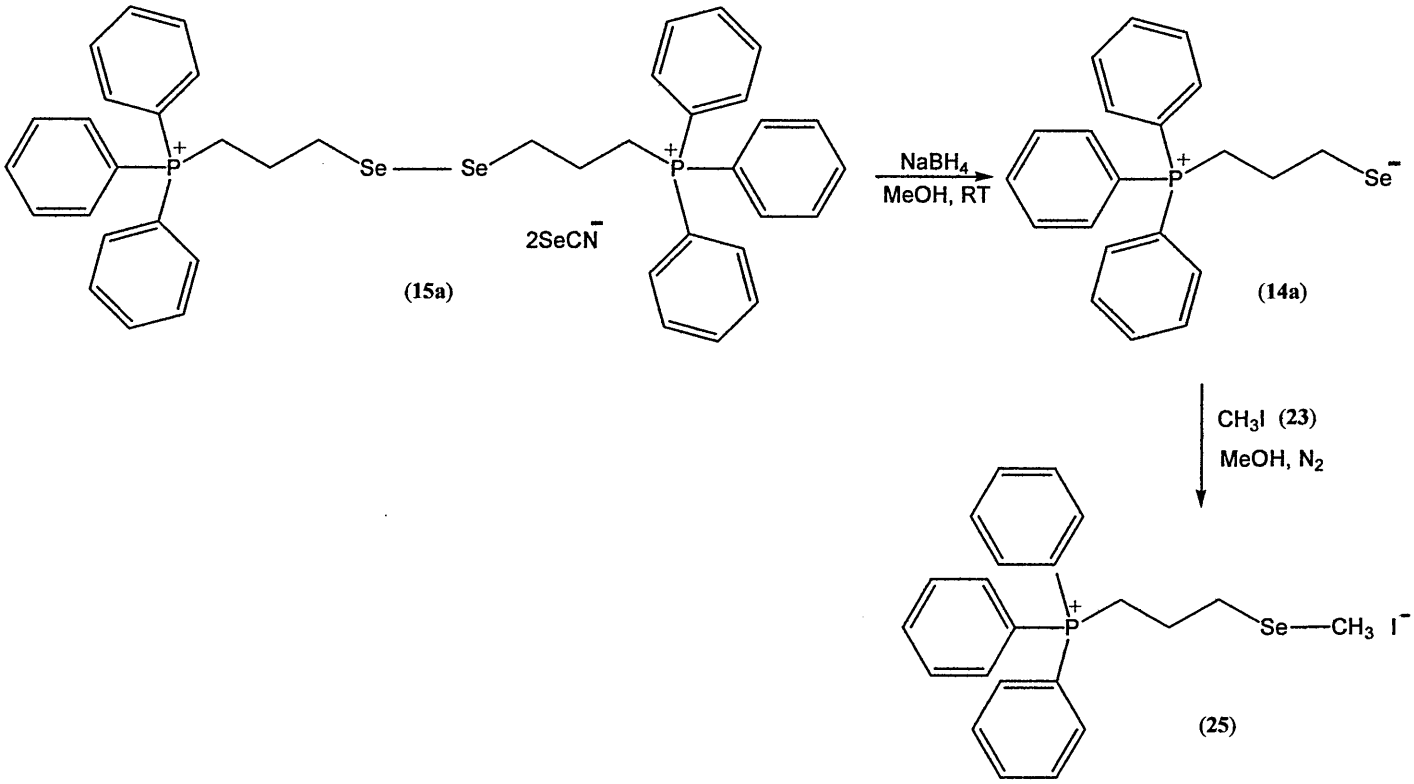

Scheme 9

6.3.1.2 Attempts to synthesize gold nanoparticles using bis(3-triphenylphosphoniopropyl)diselenide–di(selenocyanate) (15a) and 6-(selenocyano)hexyl-triphenylphosphonium selenocyanate (13b) as protecting ligands in a two phase liquid-liquid system (dichloromethane : water)

Having shown the capacity of the diselenide compound to act as potential protecting ligands, attempts to stabilise gold nanoparticles using the bis(3-triphenylphosphoniopropyl)diselenide–di(selenocyanate) (**15a**) and 6-(selenocyano)hexyl-triphenylphosphonium selenocyanate (**13b**) were carried out. The preparation technique was the same for both cases and was as follows.

A solution of ligand was prepared in DCM (0.12 mmol, 7 mmol L^{-1}; and 0.25 mmol, 14 mmol L^{-1}) and potassium tetrachloroaurate (0.12 mmol, 7 mmol L^{-1}) was then added to the solution. This was vigorously stirred until the gold salt was totally dissolved. The reduction was carried out by adding dropwise a freshly prepared aqueous solution of sodium borohydride (3mL, 400 mmol L^{-1}) with vigorous stirring, and 15 mL of deionised water was then added to the mixture.

6.3.2 Results and Discussion

6.3.2.1 Synthesis of 3-(methylseleno)propyl-triphenylphosphonium iodide

Previous studies have shown that the Se-Se and Se-OH bonds present in organic diselenides and alkylselenols can be cleaved in the presence of a metal surface and gold nanoparticles, enabling the formation of self assembled-monolayers (SAMs) and functionalised nanoparticles, respectively.

In order to study the capacity of compound **15a** as a protecting ligand and to prove the formation of the zwitterion $Ph_3P^+(CH_2)_3Se^-$ in solution, it was attempted to trap the latter by alkylation, to give 3-(methylseleno)propyl-triphenylphosphonium iodide (**25**). This was achieved by sodium borohydride reduction of the salt (**15a**), and alkylation of the resulting phosphonioalkylselenolate zwitterion with iodomethane to form **25** (Scheme 9). Other workers have shown that alkyl selenocyanates also undergo reduction on treatment with sodium borohydride to form the related alkyl selenols.[184]

The structure of **25** is shown in Figure 55. Compound **25** was isolated as pale cream solid but attempts to isolate **25** as a crystalline solid suitable for X-Ray analysis were unsuccessful. However, NMR spectroscopy and electrospray mass spectrometry supported the formulation of this compound. When studied by MALDI TOFMS in positive ion mode (accurate mass analysis), an ion corresponding to the methylselenopropylphosphonium cation was observed.

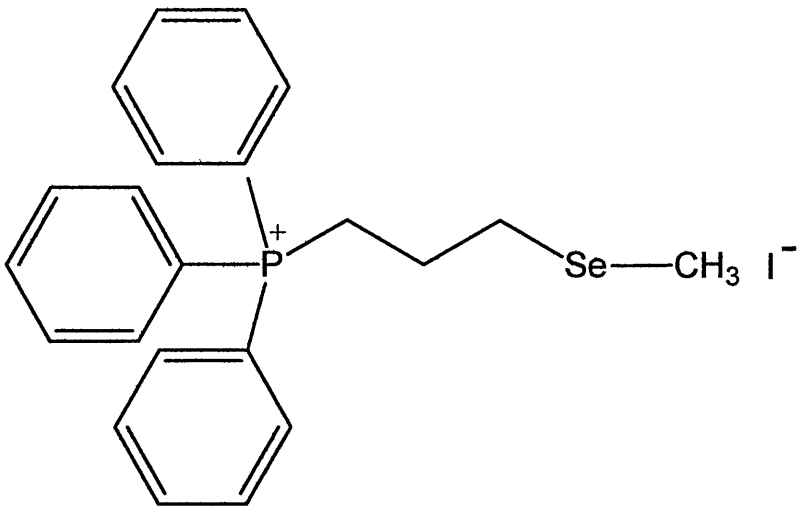

Figure 55. 3-(Methylseleno)propyl-triphenylphosphonium iodide (**25**)

Formula: $C_{22}H_{24}PSeI$, Formula Weight: 525.26

Melting Point: 140 °C.

MALDI TOFMS:

Elemental	**[M^+]**
Theory	399.0780
Found	399.0761

$\delta^{31}P$ NMR ($CDCl_3$) = 24.06 ppm, $\delta^{1}H$ NMR ($CDCl_3$) = 1.8 (3H,s), 2.8 (2H, t, J = 6.2 Hz), 3.2 (2H,m), 3.9 (2H,m), 7.6-7.8 (15H,m) ppm.

According to the results obtained by NMR and MALDI TOFMS, it could be assumed that the Se-Se bond is cleaved under the reductive conditions, to form the selenoate $Ph_3P^+(CH_2)_3Se^-$ in solution, which might then bind to the gold nanoparticle surface.

6.3.2.2 Attempts to synthesize gold nanoparticles using 15a and 13b as protecting ligands in a two phase liquid-liquid system (dichloromethane : water)

Having demonstrated the potential of the diselenide compound to act as a precursor of the protecting ligand in the synthesis of monolayer-protected cationic phosphonium-gold nanoparticles, the first attempts to stabilise gold nanoparticles using the bis(3-triphenylphosphoniopropyl)diselenide–di(selenocyanate) (**15a**) and 6-(selenocyano)hexyl-triphenylphosphonium selenocyanate (**13b**) were carried out.

The synthesis of the gold nanoparticles was carried out following the method previously described in section 6.2.1.2 of this chapter, *via* reduction of potassium tetrachloroaurate in a biphasic medium (dichloromethane:water) with an excess of sodium borohydride.[41,48] A solution of the ligand was prepared in dichloromethane (DCM) and solid potassium tetrachloroaurate (Se/Au molar ratio, 1:1) was then added to the solution. This was vigorously stirred until the gold salt was totally dissolved. The reduction was carried out by adding dropwise a freshly prepared aqueous solution of sodium borohydride with vigorous stirring, under a nitrogen atmosphere. After 1 hour, the stirring was stopped and dark blue particles of aggregated colloidal gold were

observed at the bottom of the flask. No evidence of stable gold nanoparticle formation was observed in both cases (**15a** and **13b**).

Following this result, the molar quantity of the ligand was increased and a Se/Au molar ratio of 2:1 was used in order to assure the complete stabilisation of all the gold nanoparticles in solution. However, after the reduction and 2 hours of vigorous stirring, particles of aggregated colloidal gold were again observed at the bottom of the reaction vessel. Even with a further increase in the quantity of ligand, the formation of functionalised gold nanoparticles was not achieved. If stirring is continued overnight then the blue aggregates slowly re-dissolved, giving a pale yellow coloured solution.

The observation that neither **15a** nor **13b** facilitates the formation of stabilised gold nanoparticles is obviously disappointing. It can be assumed that the selenocyanate ions present in both **15a** and **13b** may be a complicating factor and it is well known that the cyanide ion, and other pseudo halides, have very high affinities for gold and are widely used for the dissolution, recovery and recycling of gold metal.[185]

Furthermore, it has been reported that treatment of gold(I) captopril (captopril = 1-[(2S)-3-mercapto-3-methylpropionyl]-L-proline) with KSeCN or selenourea in aqueous solution produces unstable species that readily undergo disproportionation and decomposition.[185] Selenocyanate complexes of gold(I) are comparatively rare and complexes of the type $[(R_3P)Au(SeCN)]$, formed through the reaction of $[(R_3P)AuCl]$

with KSeCN in a biphasic water/dichloromethane system were found to be less stable thermally, and to air and moisture, than their thiocyanate analogues.[186]

6.4 Stabilisation of gold nanoparticles using the diphenyl-1-pyrenylphosphoniopropylthiosulfate zwitterion

In order to investigate the use of fluorescent phosphonioalkylthiosulfate zwitterions as protecting ligands for AuNPs, their interactions with DNA, and their potential use in fluorescence detection methods for biomolecule recognition, the synthesis of functionalised gold nanoparticles using diphenyl-1-pyrenylphosphoniopropyl thiosulfate zwitterion (**11**, section 3.2.2, Chapter 3) as precursor of the protecting ligand was carried out. Details of the preparation of the gold nanoparticles coated with this fluorescent dye (experimental part) and discussion of the subsequent results are presented in this section.

6.4.1 Experimental

6.4.1.1 Synthesis of phosphonium-monolayer protected gold clusters using diphenyl-1-pyrenylphosphoniopropyl thiosulfate zwitterion as protecting ligand

In the case of the diphenyl-1-pyrenylphosphoniopropyl thiosulfate zwitterion (**11**), solubility problems were observed when this ligand was used during the functionalisation of gold nanoparticles. Due to its solubility in ethanol, the synthesis of pyrenylphosphonium-gold nanoparticles was carried out as follows.

A solution of the diphenyl-1-pyrenylphosphoniopropyl thiosulfate zwitterion was prepared in ethanol (0.25 mmol, 3 mmol L^{-1}) and potassium tetrachloroaurate (0.12

mmol, 1.5 mmol L^{-1}) was then added to the solution. This was vigorously stirred for 10 minutes until the gold salt was totally dissolved and then, this was left stirring for an additional 4 hours. The reduction was carried out by adding dropwise a freshly prepared aqueous solution of sodium borohydride (3mL, 400 mmol L^{-1}) with vigorous stirring, and 15 mL of deionised water was then added to the mixture. After 24 hours, the stirring was stopped and a burgundy/blue solution was obtained.

6.4.1.2 Characterisation of the colloidal solutions of the pyrenylphosphonio-monolayer protected gold nanoparticles

The colloidal solution of AuNPs functionalised with diphenyl-1-pyrenylphosphoniopropyl thiosulfate zwitterion was analysed by UV-visible spectroscopy. Additionally, fluorescence measurements were carried out using a Hitachi (model F-4500) spectrophotometer, and collected for the pyrenylphosphonium-gold nanoparticles and the ligand on its own. The samples to be analysed by UV-visible spectroscopy and fluorimetry were kept in their original state (nanoparticles dispersed in ethanol). All the fluorescence measurements were carried out at room temperature, and during the interval of time selected to investigate possible changes in fluorescence emission in the aged solutions of pyrenylphosphonium-gold nanoparticles, these samples were kept sealed and protected from the light.

6.4.2 Results and Discussion

In this case, pyrenylphosphonium-gold nanoparticles were prepared in ethanol, due to the solubility properties of the diphenyl-1-pyrenylphosphoniopropyl thiosulfate zwitterion, the latter being insoluble in water. Several attempts to synthesise these gold nanoparticles in a two phase liquid-liquid system (DCM : water), following the method previously used to synthesise the phosphonium-gold nanoparticles, were carried out. The attempts were unsuccessful including those in which the concentration of ligand was varied. However, aggregations were observed immediately after the addition of sodium borohydride to the reaction mixture. The coalesced particles remained at the interface between the aqueous and organic phases, showing no affinity for either dichloromethane or water. These aggregations could be due to the hydrophobicity of the diphenyl-1-pyrenylphosphoniopropyl thiosulfate ligand.

Hence, the preparation of the pyrenylphosphonium-gold nanoparticles was attempted in ethanol. However, with this synthetic method, the excess of the organic matter of the ethanolic solution could not be removed by extraction with suitable solvents (DCM, toluene and acetone), in which the ligand can be dissolved, due to the miscibility between these solvents and ethanol. In a further attempt, ethanol was removed from the solutions and a dark blue paste was obtained. This was rinsed with DCM, toluene and acetone. However, the paste started to clump and appear as a bulk material, and fine visible particles could be observed suspended in the solvent. These particles were allowed to settle and then the rinsing solvent was decanted. This procedure was repeated several times. Finally, the particles were dried under nitrogen

and attempts were made to re-suspend them in ethanol, but no colloidal solution was observed.

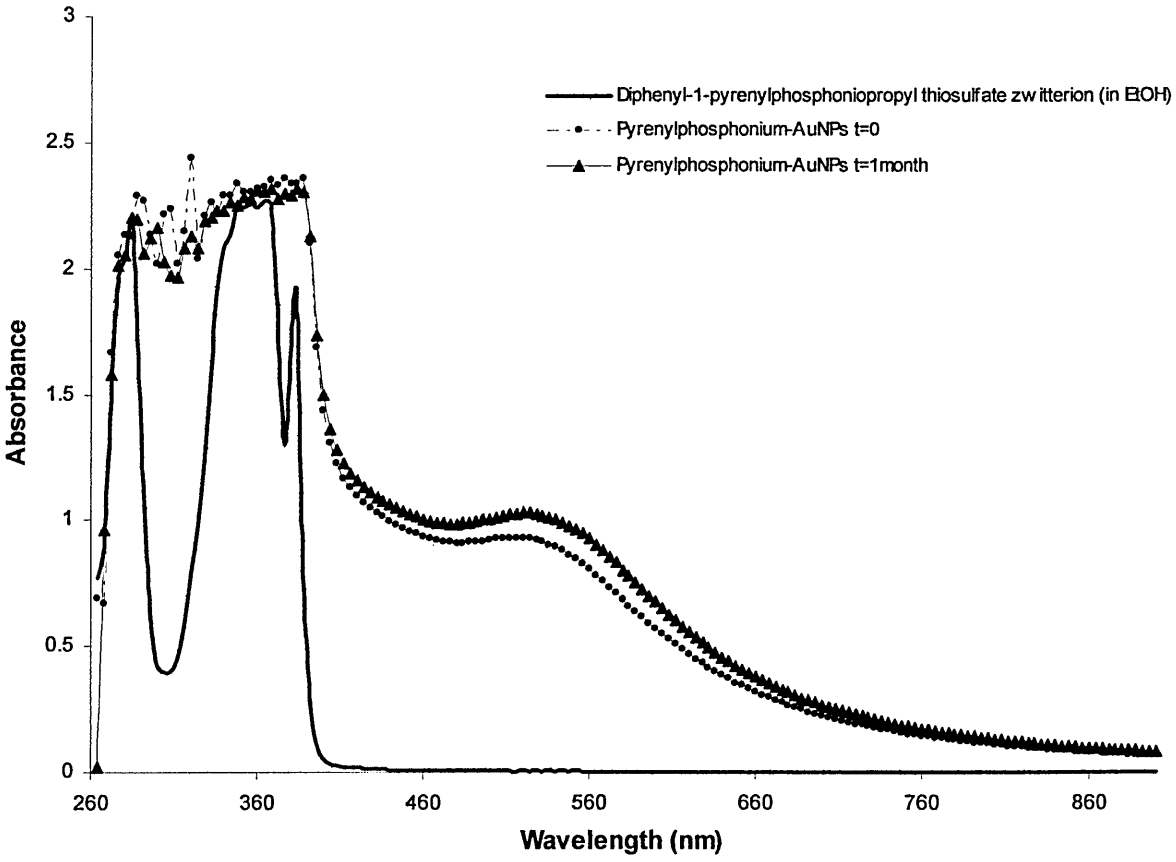

Figure 56. UV-visible spectra of diphenyl-1-pyrenylphosphoniopropyl thiosulfate zwitterion in ethanolic solution (3 mmol L^{-1}, —), pyrenylphosphonium-gold nanoparticle solution at t = 0 (•) and at t = 1 month (▲)

At the end of the synthesis of the pyrenylphosphonium-gold nanoparticles in ethanol, a dark purple solution was obtained. The original colloidal solution of pyrenylphosphonium-gold nanoparticles was analysed by UV-visible spectroscopy in

order to monitor their stability. Evidence for the formation of colloidal gold nanoparticles was observed in the UV-visible spectrum (Figure 56) of the freshly prepared solution. A broad band at 520 nm was observed, indicating that the reduction of A(III) to Au(0) took place and that the particle size is in the range 5-10 nm, according to the literature.[19] Figure 56 also shows the spectrum of the pyrenylphosphonium-gold nanoparticles at 1 month. No changes in surface plasmon band were observed during this period of time. However, within the second month, visible dark blue particles were seen in the ethanol solution, leaving the solution devoid of colloidal gold nanoparticles.

In Figure 56, the spectrum of the diphenyl-1-pyrenylphosphoniopropyl thiosulfate zwitterion in ethanolic solution (same concentration used for the synthesis of the functionalised gold nanoparticles, 3 mmol L^{-1}) can also be seen. Absorption bands of the ligand do not interfere with the gold nanoparticle broad band at 520 nm. It can also be assumed that the absorption bands in the range of 260-380 nm present in the colloidal gold solution spectra are due to the pyrene units of the ligands coating the metallic surface.[187]

The fluorescence spectrum of the diphenyl-1-pyrenylphosphoniopropyl thiosulfate zwitterion is displayed in Figure 57. All the fluorescence measurements of the nanoparticles and the ligand were carried out with an excitation wavelength fixed at 390 nm. One strong emission band located at 410 nm is observed in Figure 57.

The fluorescence spectrum of a fresh prepared pyrenylphosphonium-gold nanoparticle solution is shown in Figure 58. One emission band positioned at 410 nm is observed, which is the same as that of the diphenyl-1-pyrenylphosphoniopropyl thiosulfate zwitterion.

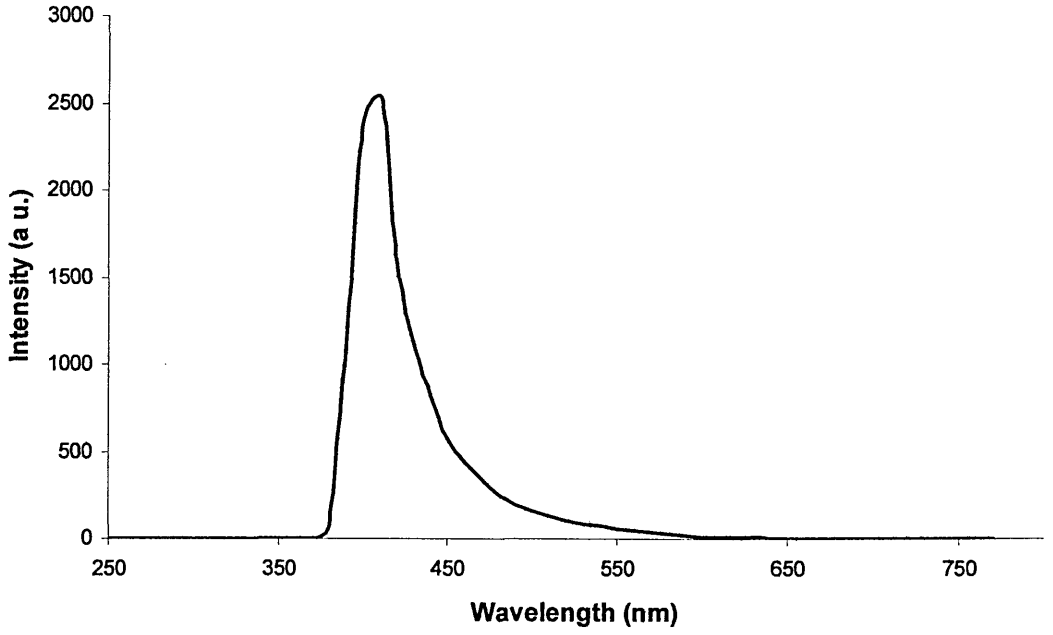

Figure 57. Fluorescence spectrum (excitation wavelength fixed at 390 nm) of the diphenyl-1-pyrenylphosphoniopropyl thiosulfate zwitterion (**11**)

Moreover, a weak broad emission band ranging from 500 to 650 nm is observed in the spectrum of the gold nanoparticle solution (Figure 58). However, even the solutions having the same concentration of ligand, the intensities of the bands in this spectrum are much lower when compared to those corresponding to the ligand (Figure 57), indicating that the fluorescence of the ligand is quenched after the functionalisation

of the gold nanoparticle. According to Wang and co-workers[187] and the results obtained in their photophysical property studies of alkanethiols with pyrene unit-capped gold nanoparticles, this can be due to weak excimer emmision of the pyrene units. It is well known that face-to-face arrangements of pyrene groups help the formation of excimers.[187] As a consequence, this weak excimer emission can indicate that most of the pyrenyl groups on one gold nanoparticle surface and between their neighbours (other particles in the same solution) are not orientated in a face-to-face way for the freshly prepared colloidal solution.

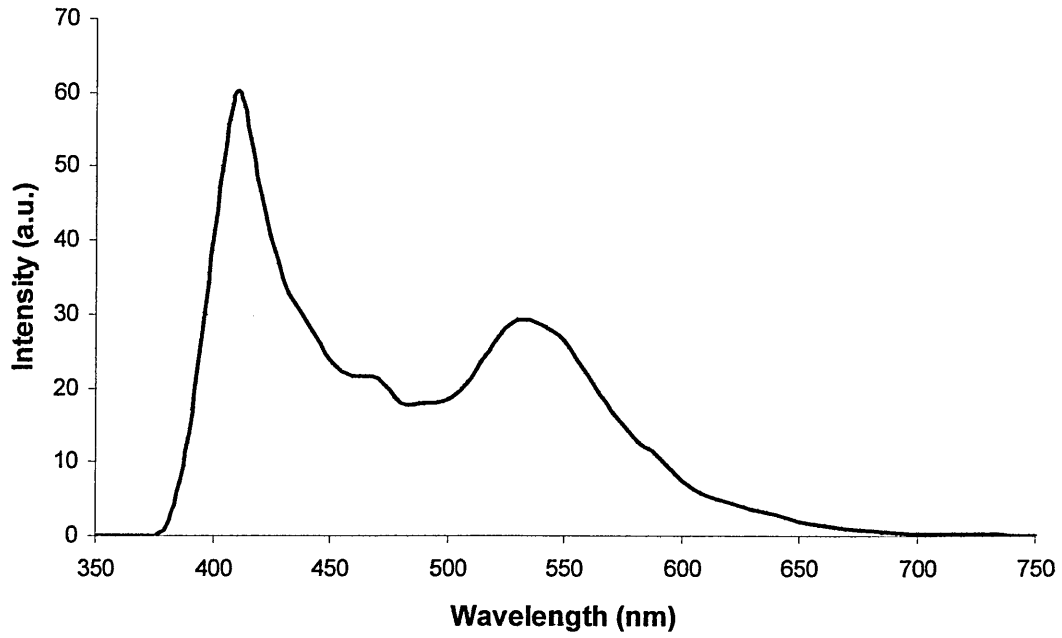

Figure 58. Fluorescence spectrum (excitation wavelength fixed at 390 nm) of the pyrenylphosphonium-gold nanoparticle solution

Apparently, the gold core is also responsible for the quenching of the excited states of the pyrenyl groups due to a through-space (alkyl chain folding) energy transfer process.[188]

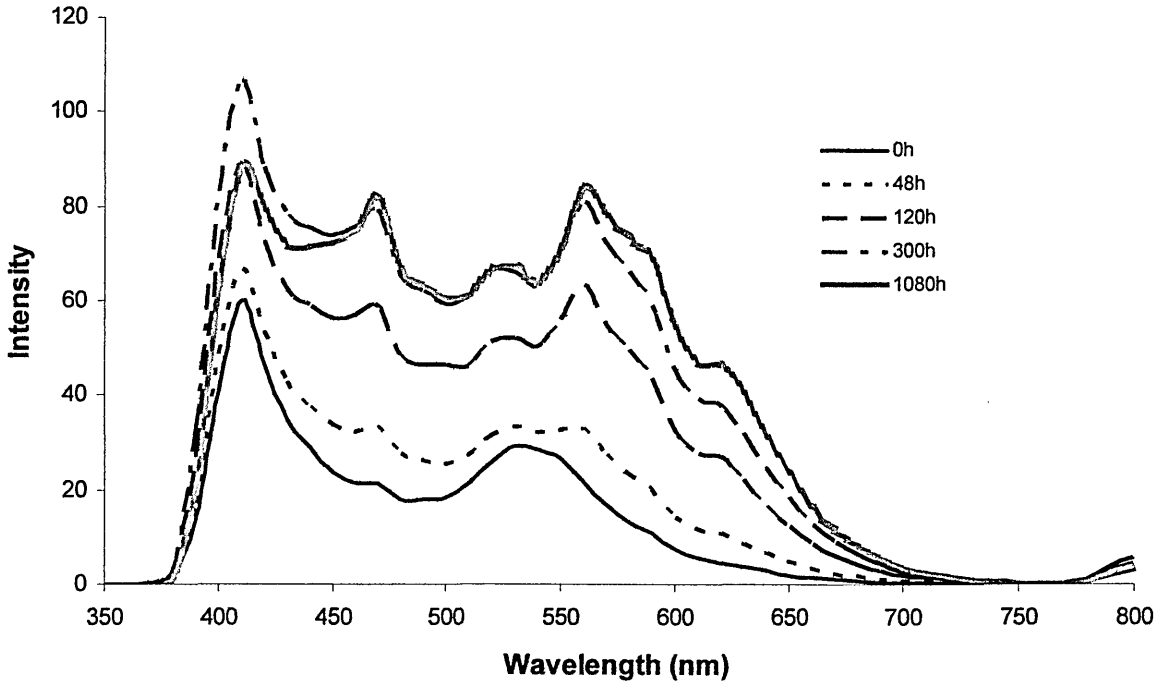

Figure 59. Fluorescence spectra (excitation wavelength fixed at 390 nm) collected from solutions of the pyrenylphosphonium-gold nanoparticle aged for 48, 120, 300 and 1080 hours

Fluorescence studies of aged solutions of pyrenylphosphonium-gold nanoparticles were also carried out. Fluorescence spectra were collected from solutions aged for 48, 120, 300 and 1080 hours and these are shown in Figure 59. Considerable enhancements in intensity of excimer emission were observed for the solutions as the

aging time increased. However, the enhancements obtained in this study are quite small in comparison to those obtained by Wang and co-workers[187] for the alkanethiols with pyrene unit-capped gold nanoparticle aged solutions (Figure 60).

In the case of the alkanethiols with pyrene unit-capped gold nanoparticles, a considerable enhancement is observed in the spectrum corresponding to the aged solution for 311 hours. It was also observed that, in this period of time, there were no changes in the shape of the emission bands corresponding to the thiols (360-440 nm) and the functionalised gold nanoparticles (450-550 nm). These investigators[187] attributed the enhancements observed during this experiment to the re-arrangement of the pyrene units, in a face-to-face orientation, of the functionalised gold nanoparticles.

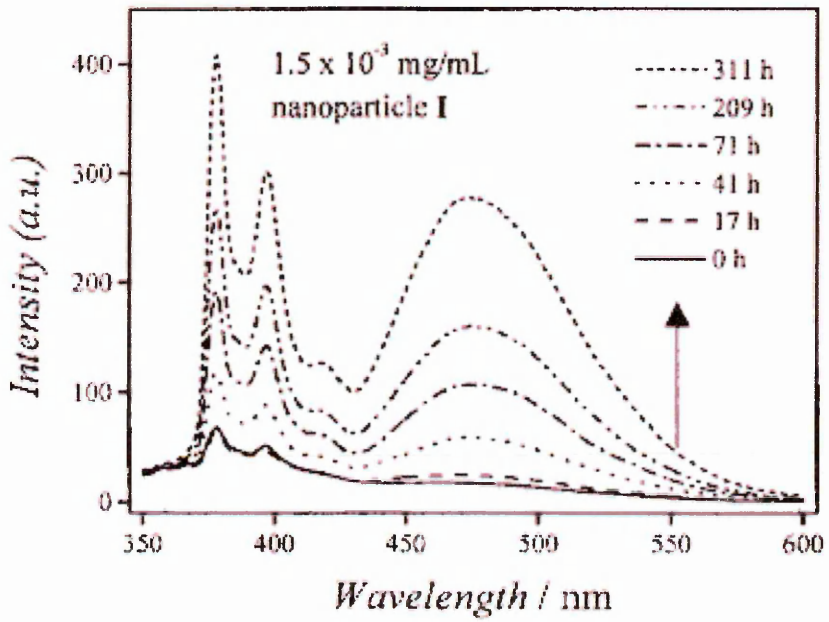

Figure 60. Fluorescence spectra of alkanethiols with pyrene unit-capped gold nanoparticle solutions aged for 0, 17, 41, 71, 209 and 311 hours[187]

However, in the case of the pyrenylphosphonium-gold nanoparticle aged solutions, changes in the shape and appearance of the new emission bands in the region between 500 and 650 nm (assigned to gold nanoparticles) were observed (Figure 59). These experimental observations might be due to changes in the nanoparticle sizes and the number of thiolate ligands on the metal core. It may be that the ligands are oxidising, de-protecting the nanoparticle surface and, therefore causing small aggregations, which could not be detected in the UV spectrum of an aged solution for 1 month (Figure 56). The re-arrangement of the pyrenyl groups in a face-to-face manner in solution may be occurring, but, in this case, it would appear not to be relevant and the changes observed in the fluorescence spectra could not be attributed solely to this effect.

In overall, it can be concluded that stabilisation strategies have been successfully developed for the synthesis of a novel family of phosphonium-functionalised gold nanoparticles, as an alternative to those cationic gold nanoparticles based on ammonium species. It has also been shown that most of the phosphonium-containing ligands synthesised in this project are able to stabilise gold nanoparticle surfaces. The resulting cationic-phosphonium gold nanoparticles are dispersable in aqueous solution (except nanoparticles protected with pyrenyl-containing ligand) which is an advantage for their biological applications. The use of these phosphonium gold nanoparticles as substrates for biomolecule recognition is presented in Chapter 7.

CHAPTER 7

Studies of Cationic Phosphonium-Gold Nanoparticles as Substrates for Biorecognition Using the Surface Plasmon Resonance Technique

7.1 Introduction

As discussed in the introduction and previous chapters, one of the principal aims of this research project has been to investigate the potential of phosphonium-functionalised gold nanoparticles to act as biorecognition systems. It was concluded that the most effective way to do this would be to use the Biacore instrument, located in the Sheffield Hallam University Biomedical Research Centre, to investigate the interaction of phosphonium-functionalised gold nanoparticles and surfaces with biological molecules, e.g. DNA. The Biacore instrument relies on the surface plasmon resonance (SPR) phenomenon to provide sensitive, label-free, analysis of the interaction between a biomolecule and substrate in real-time.

A wide range of investigations has been reported in the literature concerning to the utilisation of metallic substrates[189] and gold nanoparticles[190] as sensing devices. However, few of these have used SPR technique to investigate the interactions with biomolecules. Several reports have also focused on improving the sensitivity of conventional SPR sensors for the detection of small molecules.[191] For example, strategies that employ probe molecules with high molecular weights or high refractive index as part of the sensor chips, to bind the analytes (binding partner), have been reported,[192] and Lyon and co-workers[193] reported a more than 1000-fold enhancement in sensitivity using a gold nanoparticles-DNA conjugate as a probe molecule that binds an analyte DNA molecule captured on a sensor chip.

Specific-sequence DNA detection is an important topic in the diagnosis of pathogenic and genetic diseases. Many detection techniques have been developed that are based on target hybridisation with radioactive, fluorescent and chemiluminescent types of labelled probes. In addition, there are indirect detection methods that rely on enzymes to generate colorimetric, fluorescent or chemiluminescent signals.[106] Functionalised gold nanoparticles have been shown to be useful in biomolecular recognition,[49,109] and these provide advantages over conventional probes, such as fluorescent labels, for example, gold nanoparticles have narrower emission spectra than fluorescent probes, and obviate the need for radioactive species.

In this research project, a study has been made of the interaction between the phosphonium ligands on the gold nanoparticle surface carrying positive charges and the polyanionic DNA molecules in order to show their potential as substrates for biomolecule recognition and tagging. Recently, Rotello and co-workers[194] have developed a method based on trimethylammonium-functionalised gold nanoparticles for peptide ligation employing electrostatic interaction as the key approach, and many of the applications of such materials have been outlined in the main introduction of this thesis.

All the interaction events between the phosphonium-functionalised gold nanoparticles and biomolecules, such as, DNA and RNA, were measured and monitored in real-time using the Biacore instrument. In order to facilitate understanding of the

results obtained with these interaction study experiments, the principles of the SPR technique are described below.

7.1.1 Principles of the Surface Plasmon Resonance technique and the Biacore X instrument

A brief description of this technique is presented here. A detailed description of the technique and instrumentation can be found in reference 195. The real-time Biacore instrument monitors the association and dissociation of biomolecular complexes on a sensor surface as the interaction occurs. By covalently attaching one molecule (the *ligand*) to the surface, the interaction of another molecule in a solution (the *analyte*) with the *ligand* is followed. The measurements are carried out using conditions of continuous flow, where the sensor surface forms one wall of the flow cell. For almost all the applications, the surface can be regenerated and re-used for additional analyses. This technique is based on SPR and is an optical system that measures changes in refractive index occurring near to the surface of a sensor. The Biacore system can monitor changes in the surface concentration on a time scale of 0.1 s, which is sufficient for determination of kinetic rate constants in the range of 10^{-3}-5×10^{6} $M^{-1}s^{-1}$ for association and 10^{-1}-10^{-5} s^{-1} for dissociation for typical biomolecular interactions.

This technique can be used to study interactions of proteins, protein conjugates, nucleic acids, lipid micelles, and even larger particles such as viruses and whole cells with the sensor. This technology can support a wide range of research areas, such as

biochemistry, molecular biology, drug design, monoclonal antibody production and infectious disease research.

7.1.1.1 Biacore X instrument description

The Biacore X system consists of a processing unit with liquid and optical systems, a PC running Biacore X Control Software. Various types of sensor chips and a range of chemicals and reagents produced by Biacore, were used to carry out the real time interaction studies.

The Biacore X processing unit has the following components:

- A liquid delivery pump for maintaining a constant flow of liquid over the sensor chip surface.
- The Integrated Fluidic Cartridge (IFC) which contains liquid delivery channels, sample loops and valves.
- The detection unit, including optical and electronic components for measuring SPR response.
- Two flow cells formed by the IFC pressing against the sensor chip.

Pump

The pump is a syringe pump which provides accurate flow at rates down to 1 μL/min. The stroke capacity is 500 μL. The pump takes liquid from a buffer reservoir and pumps it into the connector block inlet (Figure 61). The connector block is directly connected to the IFC. The pump is automatically refilled at the end of the stroke. In

order to avoid refill interruptions in critical runs, the pump can be refilled at any time with a special command in the control software.

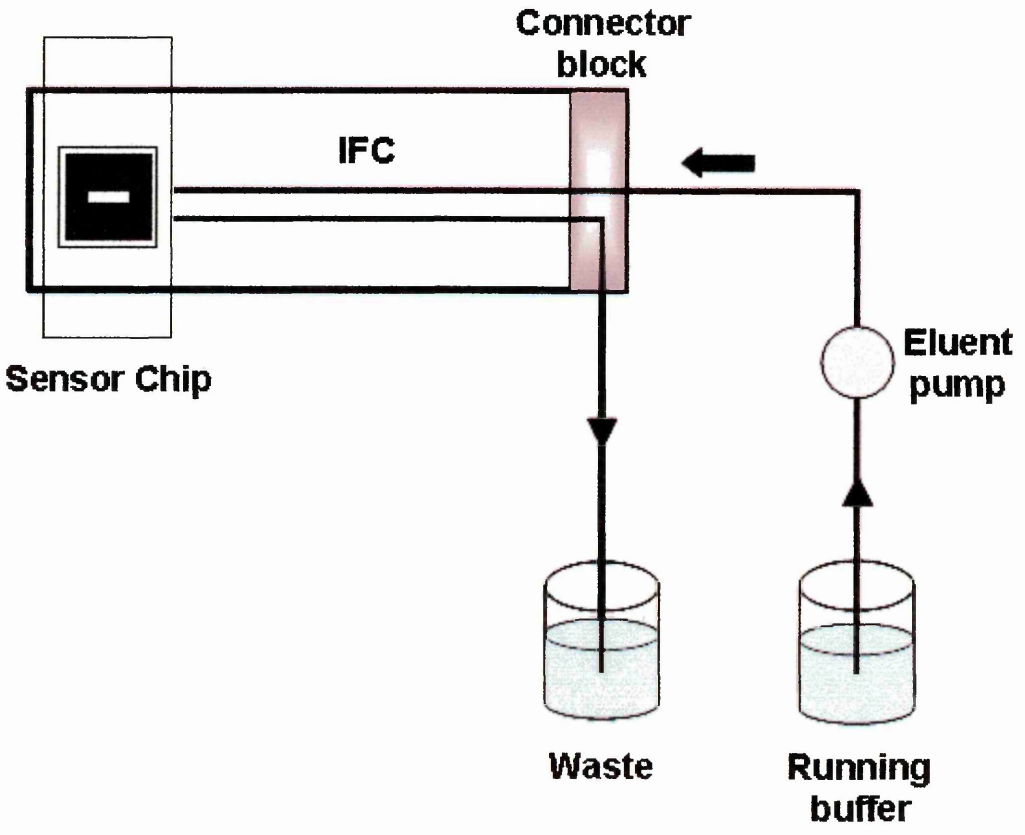

Figure 61. Schematic illustration of buffer flow in Biacore X sysntem.[195]

Connector block

The connector block has two inlet ports (Figure 62): a pump port with a screw-nipple fitting for the pump tubing (pump in), and an injection port for loading the sample loop (sample loop in). The inlets connect directly with flow channels in the IFC. There are two outlet ports on the connector block (Figure 62): sample loop out and flow

cell out. Effluent from these ports normally runs to waste and can be collected in a beaker placed under the connector block. A micropipette tip can be fitted into the outlet ports to collect excess sample injected during loop loading or the recover effluent from the flow cell. Sample is injected into the injection port using a micropipette and disposable plastic tips. The port is shaped to seal against the pipette tip.

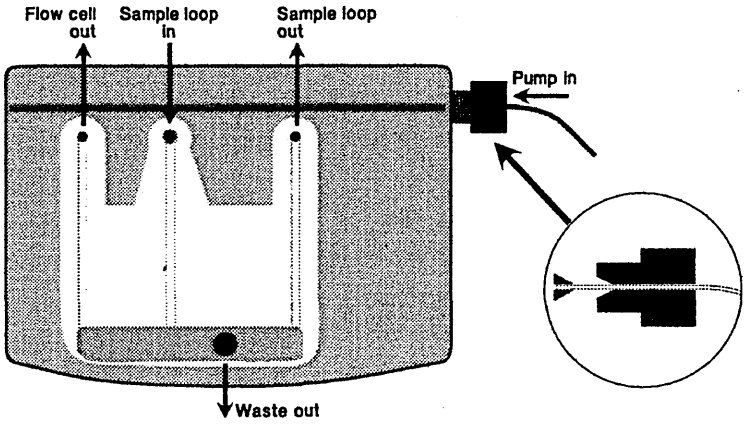

Figure 62. Connector block seen from above. The inset shows the sealing ferrule in the inlet tubing connector.

Integrated Fluidic Cartridge (IFC)

The IFC consists of a series of channels and pneumatic valves encased in a plastic compartment, and serves to control delivery of liquid to sensor chip surface. The inlet/outlet side of the IFC is in direct contact with the connector block, while the flow cell part is pressed against the sensor chip. The sensor chip and the IFC together form two flow cells which can be used independently or connected in series for multichannel analysis (Figure 63). The IFC consists essentially of a direct flow channel from pump inlet to flow cell and a sample loop for injection volumes up to 100 μL, and provides

two flow cells which can be used separately or in series. Serial flow allows simultaneous analysis of the same sample on two different surfaces, for in-line reference measurements or determination of two different analytes.

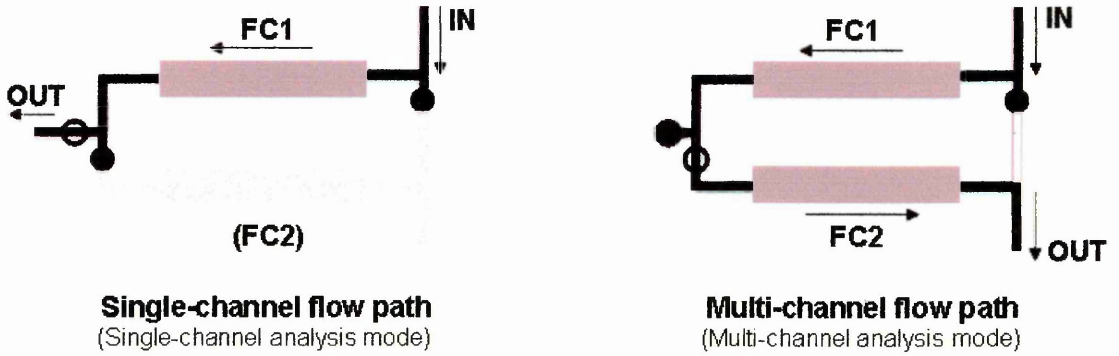

Figure 63. Diagram of single-channel flow path (flow cell 1, left), and multi-channel flow path (flow cells 1-2, right). Symbols ○ and ● represent open and closed valves, respectively.[195]

Sensor chips

Biacore has developed a range of sensor chips and the most used ones are the following:

- Sensor chip CM5 (Figure 64): general purpose chip coated with carboxy-methylated dextran to which biomolecules can be linked with a variety of established chemical methods (protocol described in Section 7.2, Chapter 7)
- Sensor chip SA: chip with streptavidin covalently immobilised on a dextran matrix for high affinity capturing of biotinylated ligands.
- Sensor chip HPA: chip with a hydrophobic surface allowing creation of lipid monolayers on the chip for study of membrane-related interactions.

The sensor chip is mounted on a plastic support frame in a protective cassette. The cassette is inserted into the sensor chip port on the side of the processing unit. Software-controlled docking presses the sensor chip in place between the glass prism and opto-interface unit on one side and the IFC flow cell block on the other.

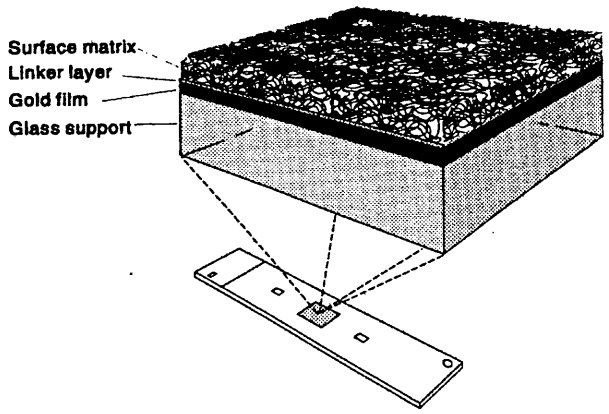

Figure 64. Sensor Chip CM5 consist in a glass slide coated with a thin gold film to which the carboxy-methylated dextran surface matrix is covalently bonded. The matrix surface forms one wall of the detector flow cell.[195]

Optical system

The glass side of the sensor chip (the outside wall of the flow cell) is pressed into contact with a glass prism in the optical unit. A silicone opto-interface between the sensor chip and the prism (Figure 65), matched in refractive index to the glass, ensures good optical coupling between the prism and the removable sensor chip.

Light from a near-infrared light-emitting diode (LED) is focused through the prism on to the sensor chip surface in a wedge-shaped beam, giving a fixed range of incident light angles. Light reflected from the sensor chip is monitored by a linear array of light-sensitive diodes covering the range of incident light angles. The diodes are spaced with a resolution corresponding to approximately 0.1°, and computer interpolation algorithms determine the angle of minimum reflection (the SPR angel) to a high accuracy. By using a wedge of incident light and a fixed array of detectors, the SPR angle is monitored accurately in real time, with no physical movement of light source, sensor chip or detector.

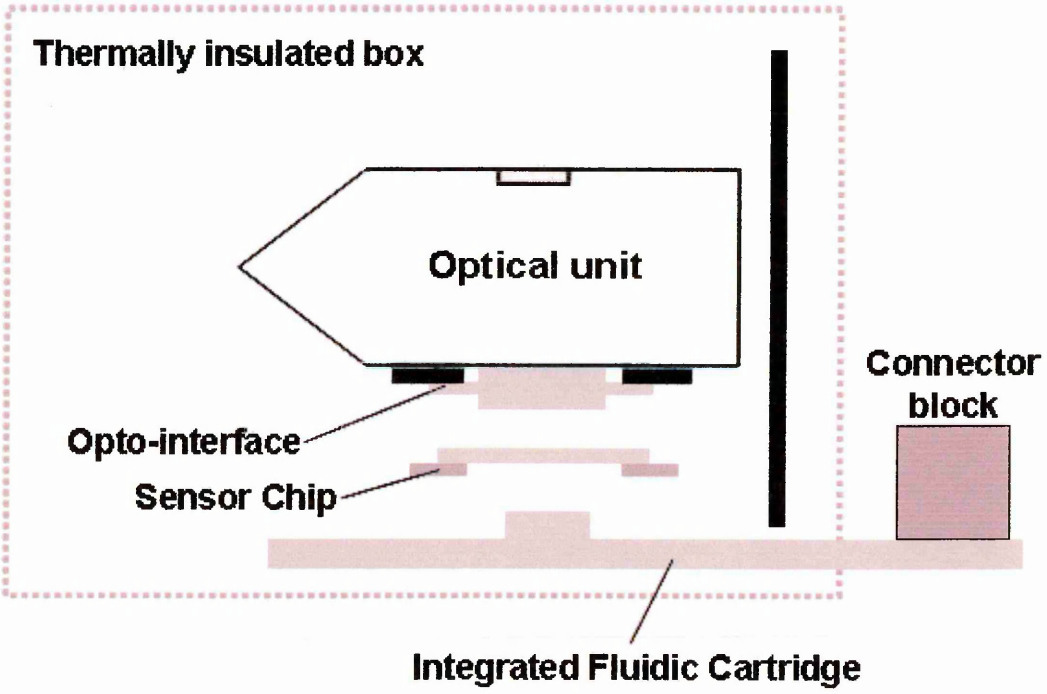

Figure 65. The detection unit contains the optical unit which includes light source and detector, the opto-interface and removable sensor chip.[195]

Temperature control

SPR measurements are sensitive to changes in temperature. It is important that a constant temperature is maintained at the sensor chip surface throughout the run. Temperature control in Biacore X uses Peltier elements to maintain a constant preset temperature at the sensor chip surface. The temperature control can keep a preset temperature in the range 4-40°C as long as the ambient temperature is not more than 10°C above the operating temperature.

7.1.1.2 Sensorgram

The binding event between the ligand and analyte, and therefore, the accumulation of the latter on the surface of the sensor chip, are translated into an increase in refractive index. The changes in refractive index occurring during the injection of the analyte are monitored in real-time and, at the end, a plot called a sensorgram is obtained. In essence, a sensorgram is the response or resonance unit (RU) plotted against time (in seconds). A schematic diagram of a sensorgram is shown in Figure 66.

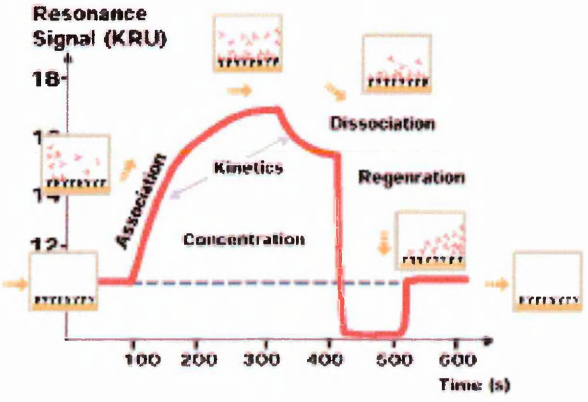

Figure 66. Sensorgram (Figure taken from: http://www.biacore.com).

7.1.2 Previous studies using surface plasmon resonance

Gold nanoparticles have been the most widely used metal for SPR detection due to their optical properties which make them suitable for sensing applications. Normally, these particles show an absorption band at ~520 nm which is caused by the excitation of plasmons by the incident light.[19] Shifts in the position of this band occur due to changes in the dielectric constant taking place in the vicinity of the particle. Therefore, perturbations in the local dielectric constant (refractive index) of the surrounding media, for example, upon contact with a ligand, results in changes in colour which is translated into an absorption band shift,[196] and provides a fundamental basis for detection analysis.

Perez-Luna and co-workers[191] have reported a sensing method based on the gold nanoparticle plasmon resonance. They have been able to monitor specific recognition events of biomolecules employing gold nanoparticles functionalised with dextran, which is a polysaccharide, in solution. They have carried out further derivatisation of the dextran matrix, with proteins such as concanavalin A, in order to investigate their potential as glucose sensing substrates. They have also derivatised the carboxyl groups of the dextran coating the gold nanoparticles with (+)-biotinyl-3,6,9-trioxaundecanediamine to obtained biotinylated dextran which can interact with streptavidin or antibiotin and promote specific biomolecular recognition.[191] The changes in absorbance at a fixed wavelength and in the absorbance spectra were monitored in order to investigate the binding events as a function of time. The results demonstrated that streptavidin and antibiotin induce particle aggregation, indicating specific biomolecular recognition. It has been shown that there was a low level of nonspecific

interactions due to unreacted carboxyl groups. However, it was suggested that this effect can be reduced further by use of a suitable buffer.[191]

Sugimoto and co workers[197] reported a polymer gel with immobilised gold nanoparticles, a so-called molecularly imprinted polymer (Au-MIP), as an SPR sensing material for detection or recognition of small molecules. Their strategy to fabricate the Au-MIP sensor chip was to immobilise gold nanoparticles functionalised with 11-mercaptoundecanoic acid on a dopamine-imprinted polymer-coated sensor chip (obtained by radical polymerisation on an allyl mercaptan-modified gold substrate). The use of gold nanoparticles was shown to enhance the signal intensity in comparison with a sensor chip without gold nanoparticles. The analyte binding process appeared to be reversible, allowing the re-use of the modified sensor chip.[197]

Chilkoti and co-workers[196] developed a colorimetric sensor also based on gold nanoparticles to investigate biomolecular interactions in real time on a surface in a commercially available UV-visible spectrophotometer and a colorimetric end-point assay using an optical scanner. This sensor chip was reported to enable high-throughput screening of bimolecular interactions in real time. The fabrication of the sensor chip involved as a first step the formation of a self-assembled monolayer of the gold nanoparticles stabilised by sodium citrate on silanized glass. Subsequently, the immobilised nanoparticles were treated with mercaptopropionic acid, functionalising them with reactive carboxyl groups which could react with biotin. The sensor chip was

used to study the specific binding of streptavidin and showed a concentration-dependent binding with a limit of detection of 16 nM.[196]

Following similar approaches, a novel strategy to use the cationic phosphonium gold nanoparticles as biorecognition substrates has been developed. These nanoparticles have been immobilised on commercially available CM5 and SA sensor chips, and then negatively charged biomolecules, such as, DNA and RNA were immobilised on these modified sensor chips. The binding events were monitored in real time by the Biacore system. Experimental details and results are outlined in the following sections.

7.2 Experimental

All the experiments were carried out on a Biacore X SPR instrument (Figure 67). The temperature of the instrument was set to 25°C and the running buffer was the commercially available HBS-EP filtered and degassed buffer, which contains 0.01 HEPES pH 7.4, 0.15 NaCl, 3 mM EDTA, 0.005% v/v surfactant P20.

Figure 67. Biacore X SPR instrument (Figure taken from: http://www.biacore.com).

The sensorgrams and data resulting from the experiments were recorded using the Biacore software. Before the Biacore instrument was used to record a sensorgram, the instrument was set to run HBS-EP buffer following the instructions displayed for the software on the PC screen. The flow rates used in the experiments were varied from 10 to 50 $\mu L \cdot min^{-1}$ in order to find the best immobilisation conditions. Sample injections must be carried out while a sensorgram is running (buffer running through the flow cell). The sample injections were also performed following the injection command instructions displayed on the PC screen which, at the same time, indicate the exact volume to be injected.

The samples were injected using the central injection port of the connector block of the instrument indicated as "sample loop in" in the figure 62. The injections were carried out using a micropipette of 100 μL capacity to deliver the amount of sample required. Once the exact amount of sample was loaded in the tip of the micropipette, 5 μL of air was introduced to the tip and an extra 5 μL of sample was loaded into the pipette, in order to form an air bubble. The latter was used to remove any trapped material within the injection loop of the instrument corresponding to the previous injected samples. The sample was then slowly introduced through the injection port to reach the injection loop by capillary mode. Immediately after the sample was placed in the injection loop, the injection was initiated, instructing the instrument to inject by using the corresponding command button displayed in the screen desktop of the PC. Finally, the instrument was programmed to run a rinse cycle with the HPB-S buffer pH 7.4 after each injection in order to remove unbound compounds. After this washing step, the sensorgram data were saved and the instrument was left idle to re-start.

Regular maintenance of the Biacore system was carried out in order to keep the instrument free from contamination such as microbial growth and absorbed biomolecules in the liquid handling system. Desorb and Sanitise procedures were performed weekly in order to clean the tubing of the flow cell channels. The Desorb procedure was carried out using two solutions contained in the BIAmaintenance Kit: Solution 1: 0.5% (w/v) SDS in water and Solution 2: 50 mM glycine-NaOH pH 9.5. The Sanitise procedure was performed using a solution of 1% of sodium hypochlorite. Both procedures were carried out following the instructions displayed for the software

on the PC screen. It was also necessary to perform a Normalise procedure in order to stabilise the resonance signal from the flow cell, to compensate small differences when a new sensor chip was docked. A solution of 70% (w/w) glycerol in deionised water was used to carry out the normalisation.

All the interaction study experiments carried out using the Biacore X SPR system are summarised in Table 9. This table contains details, such as, flow rate, injected volume, sensor chip type, biomolecule type, gold nanoparticle, regeneration, and type of analysis (single-channel or multi-channel) of each of the experiments. The results and the discussion of these experiments are presented in Section 7.3 of this chapter.

The biotinylated DNA, RNA and cDNA samples used in this project were provided by Dr. Ahslee Perry, Bahare Vahabi and Antoine Fouillet, respectively, from the Biomedical Research Centre at Sheffield Hallam University. The biotinylated DNA was prepared by the biotinylated PCR process using a mixture of biotinylated dUTPs and regular dNTPs. This method yielded a biotinylated DNA sample (32 $\mu g \cdot mL^{-1}$) of a GC rich (~70%) 750 base pair fragment of AMOC gene. The RNA-containing sample (96 $\mu g \cdot mL^{-1}$) was a purified RNA extracted from diabetic rat bladder. The cDNA was prepared by the transcription of mRNA into cDNA, as the first step, and then an amplification of this cDNA using Real Time-PCR (BIO-RAD) reaction was carried out by combining the cDNA with the corresponding primers, $MgCl_2$ and 1X absolute SybrGreen (Abgene, UK). Real time PCR products were purified using Sigmaspin™ POST reaction

Table 9. Interaction study experiments carried out using the Biacore X SPR system

Experiment	Sensor Chip	Type of analysis	Ligand	Analyte	Volume of analyte injected (µL)	Flow rate (µL/min)	Temperature (°C)	Running buffer	Regeneration solution
SPR1	SA	Single-channel	Streptavidin	Biotinylated-DNA (32 $\mu g \cdot mL^{-1}$)	30	10	25	HBS-EP	-
SPR2	Modified SA (SPR1)	Multiple-channel	DNA immobilised on the SA sensor chip	5a-AuNPs	30	50	25	HBS-EP	-
SPR3	Modified SA (SPR1)	Multiple-channel	DNA immobilised on the SA sensor chip	SIGMA gold colloidal solution (5-10nm particle size)	30	50	25	HBS-EP	-
SPR4	SA	Single-channel	Streptavidin-dextran matrix	5a-AuNPs	30	50	25	HBS-EP	-
SPR5	Modified SA (SPR4)	Multiple-channel	3C-AuNP immobilised on the SA sensor chip	RNA (96$\mu g \cdot mL^{-1}$)	30	10	25	HBS-EP	-
SPR6	CM5	Single-channel	Carboxy-methylated dextran matrix	5a-AuNPs	30	10	25	HBS-EP	-
SPR7	CM5	Single-channel	Carboxy-methylated dextran matrix	5b-AuNPs	30	10	25	HBS-EP	-
SPR8	Modified CM5 (SPR6)	Multiple-channel	3C-AuNP immobilised on the CM5 sensor chip	cDNA (54$\mu g \cdot mL^{-1}$)	30	10	25	HBS-EP	15% formic acid solution
SPR9	Regenerated CM5 (SPR8)	Single-channel	Carboxy-methylated dextran matrix	5a-AuNPs	30	10	25	HBS-EP	-

purification column (Sigma, UK) previous utilisation. This method yielded a cDNA sample (54 $\mu g \cdot mL^{-1}$) of 100 base pair double-stranded DNA sequence.

The protocol for the biotinylated DNA immobilisation on SA sensor chip followed in experiment SPR1 (Table 9), was the method reported by Bailly and co-workers.[198] They immobilised 5'-biotinylated DNA (25nM, samples in HBS-EP buffer) on the flow cell surface of an SA sensor chip by noncovalent capture. The protocol and the experimental conditions used in their work were the followings:

- The chip was prepared for use by conditioning with three to five consecutive 1 minute injections of 1 M NaCl in 50mM NaOH followed by extensive washing with running buffer (HBS-EP, pH 7.4).
- One flow cell of the SA chip was used to immobilise DNA oligomer sample and the other one was left blank as a control.
- The flow rate used was 7 to 10 $\mu L \cdot min^{-1}$ and the sample injection volume was 30 µL.
- And the SPR experiments were performed at 25 °C.

Bailly and co-workers reported that the amount of DNA immobilised was approximately 350 RUs.[198]

The gold nanoparticles used in experiments SPR2, SPR4, SPR6 and SPR9, and SPR7 (Table 9) were the freeze-dried phosphonium-functionalised gold nanoparticles obtained from the synthesis using 3-triphenylphosphoniopropylthiosulfate (**5a-AuNPs**) and 6-triphenylphosphoniohexylthiosulfate (**5c-AuNPs**) zwitterions, respectively.

Colloidal suspensions of each of these gold nanoparticles were prepared in deionised water and in running buffer ($1 mg \cdot mL^{-1}$) to perform the SPR experiments. Commercially available citrate-functionalised gold nanoparticles (SIGMA gold colloid solution, absorbance 0.754, particle size range 5-10 nm) were used to carry out experiment SPR3 (Table 9). SA and CM5 sensor chip, running buffer HBS-EP (pH 7.4), and BIAmaintenance Kit were purchased from Biacore, Uppsala, Sweden.

7.3 Results and Discussion

Experiment SPR1: immobilisation of biotinylated DNA on the SA sensor chip

In order to study the interaction of phosphonium gold nanoparticles with DNA, biotinylated DNA was immobilised on a streptavidin SA sensor chip as first step. However, before the modification of the streptavidin SA sensor chip (Experiment SPR1), five injections of a solution of 50 mM NaOH and 1M NaCl, called regeneration solution, were carried out in order to remove all the possible impurities present on the surface of the sensor chip, as suggested in the BIACORE user guide. The flow rate of 20 $\mu l \cdot min^{-1}$ and multiple-channel analysis mode were used for this cleaning process. The injection volume of the regeneration solution was 30 µl for each injection.

The results of this cleaning process are shown in Figure 68. In this figure, three sensorgrams can be observed. FC1 and FC2 correspond to the association-dissociation curves resulting of the interaction between ions present in the cleaning solution and the streptavidin-dextran matrix of the sensor chip. FC1-FC2 represents the subtraction between FC1 and FC2 sensorgrams. After this process, the SA sensor chip should be free of non-specific species that could interfere with the ligation of the biotinylated DNA with the streptavidin.

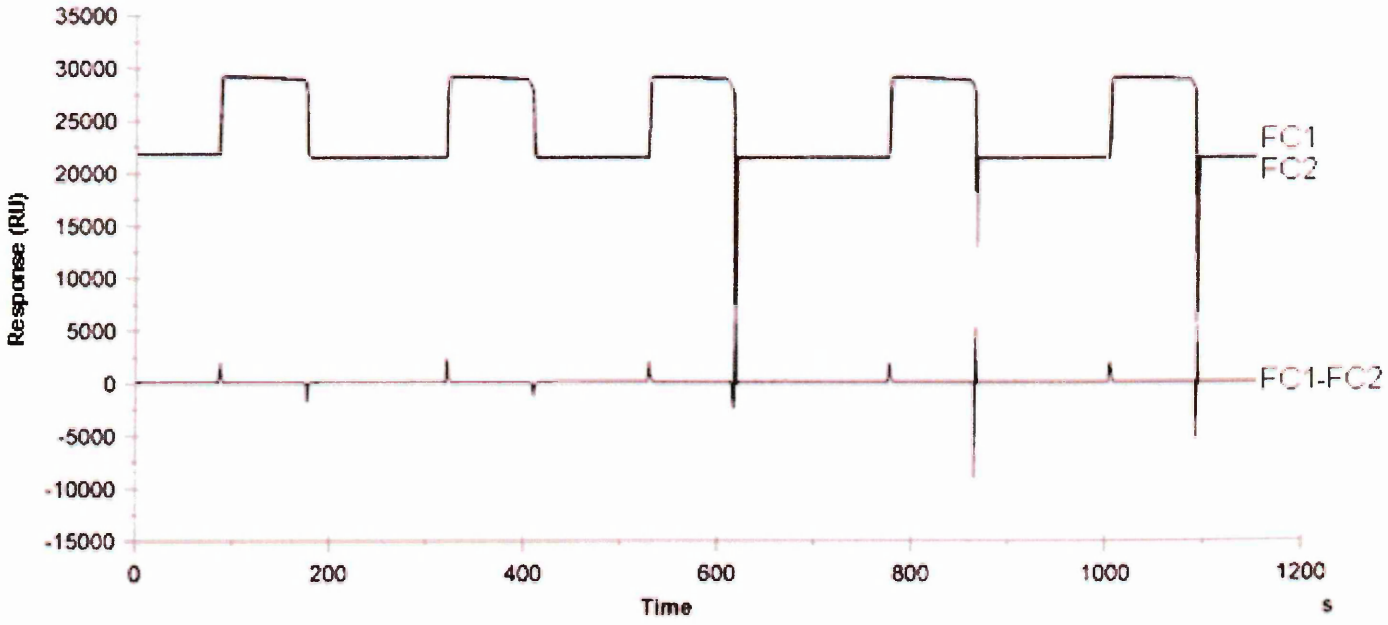

Figure 68. Sensorgrams resulting of the cleaning process of the SA sensor chip with a solution of 50 mM NaOH and 1M NaCl (FC1, FC2 and FC1-FC2)

Once the SA sensor chip was fully cleaned, one of the flow cells was modified with the biotinylated DNA (experiment SPR1), leaving the other one as a reference channel. The Biacore X instrument was set to run a sensorgram at 10 $\mu l \cdot min^{-1}$. The biotinylated DNA (analyte) was immobilised on the streptavidin (ligand) SA sensor chip following the protocol suggested by Bailly and co-workers[198] (method described in Section 7.2, Chapter 7). The instrument was set to run the analyte in single-channel analysis mode in order to leave one of the flow cell channels free of DNA and use it as a control surface for further analysis.

The result of the ligation is shown in Figure 69. The injection of the sample containing biotinylated DNA starts at 70 seconds and finishes at 180 seconds. An association curve can be observed in the sensorgram (event showed by the red circle in Figure 69). The signal of this curve did not recede even after the injection finished. The starting response value is 22,000 RU and the finishing value is 24,000 RU. This event showed that the biotinylated DNA has been bound to the streptavidin present on the surface of the SA sensor chip. The sharp peaks which can be observed between 110 and 135 seconds on the sensorgram, could be due to other species present in the biotinylated DNA sample, such as, templates, enzymes and buffers. These species did not interfere with the rest of the experiment due to their dissociation at 135 seconds.

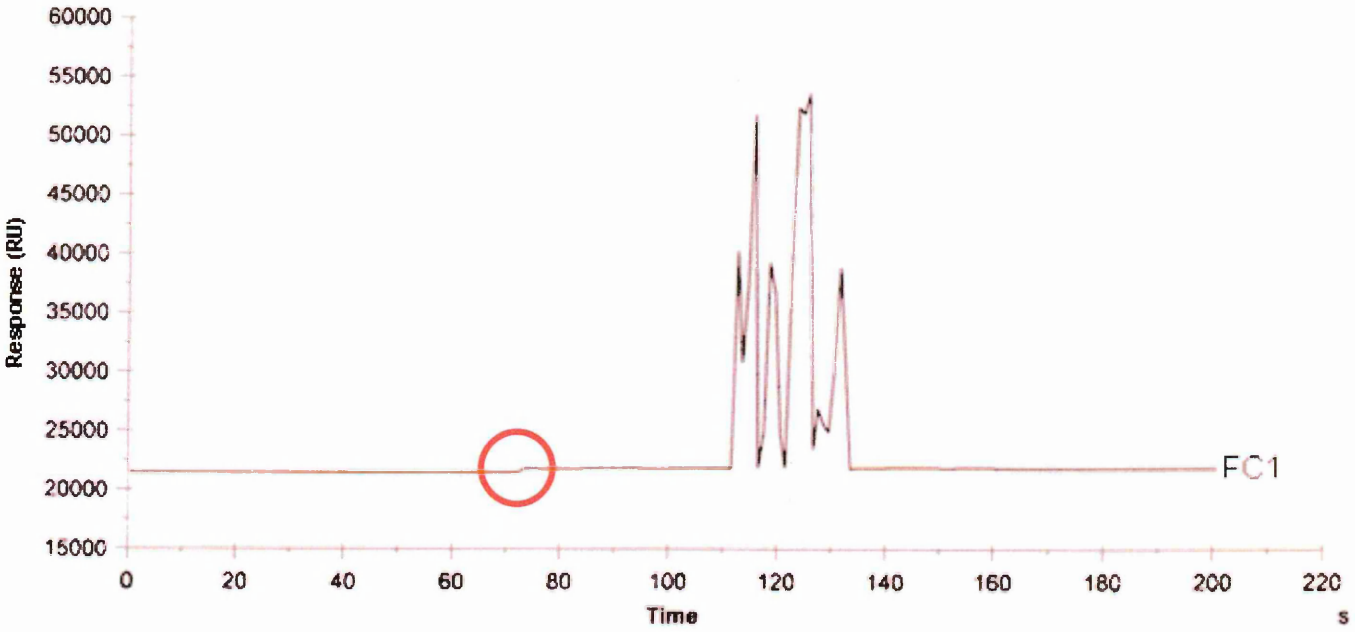

Figure 69. Sensorgram resulting of the ligation of the biotinylated DNA to the streptavidin of the SA sensor chip (FC1)

Experiment SPR2: interaction between the phosphonium gold nanoparticles and the SA sensor chip modified with DNA

Studies of the interaction between the DNA (ligand) immobilised on the SA sensor chip and the phosphonium gold nanoparticles (analyte) were carried out by passing a gold colloid solution through both flow cell channels of the SA chip. The gold nanoparticles used in this experiment (experiment SPR2) were the freeze-dried particles obtained from the synthesis using 3-triphenylphosphoniopropylthiosulfate zwitterion (**5a-AuNPs**) as protecting ligand. The colloidal solution was made by re-suspending the dried nanoparticles in deionised water ($1 mg \cdot mL^{-1}$). A flow rate of 50 $\mu L \cdot min^{-1}$ was used.

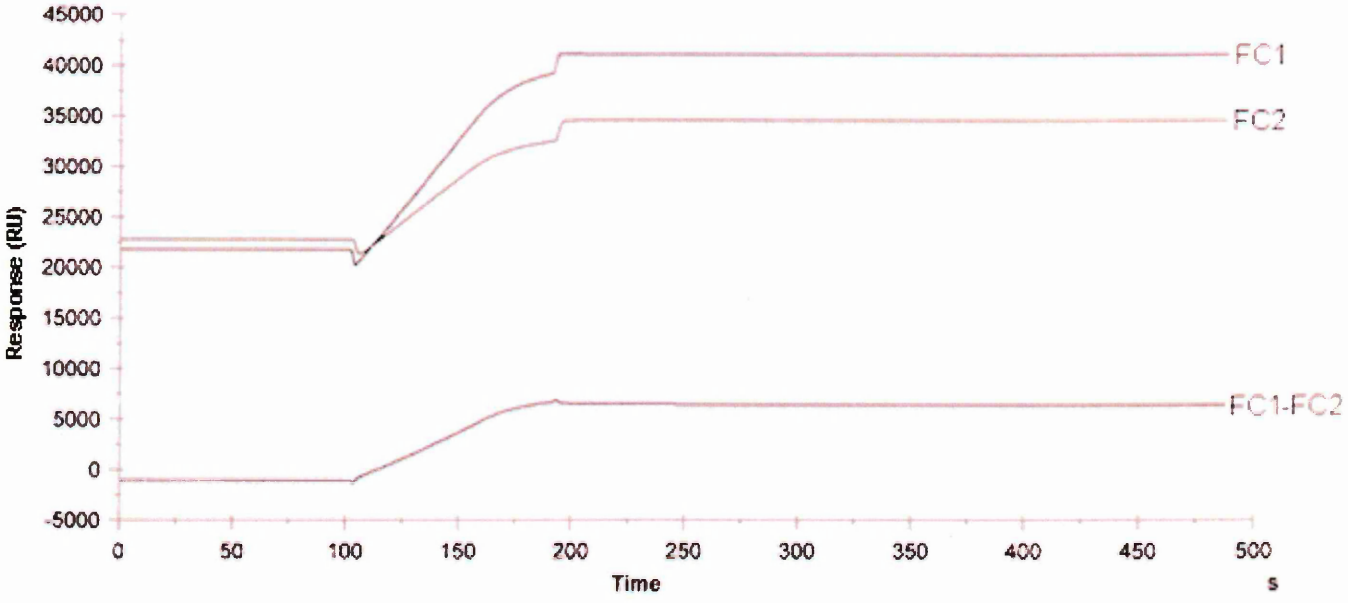

Figure 70. Sensorgrams of interaction curves between **5a-AuNPs** (analyte) and DNA modified SA sensor chip in real time (FC1, FC2, FC1-FC2)

The results of this analysis are shown in Figure 70. Three sensorgrams can be observed in this figure. The injection of the sample containing the functionalised gold nanoparticles starts at 100 seconds and finishes at 200 seconds. In Figure 70, FC1 sensorgram corresponds to the interaction between the **5a-AuNPs** and the DNA immobilised on the stretptavidin-dextran matrix, FC2 sensorgram corresponds to the interaction between these gold nanoparticles and the streptavidin-dextran matrix (reference cell), and FC1-FC2 sensorgram corresponds to the specific interaction that occurred during the injection of the gold nanoparticles. Both FC1 and FC2 sensorgrams showed association curves. Changes in response at 200 seconds can be observed in FC1 and FC2. At this time, the injection was finished and the running buffer was started to flow through the flow cells. The observed changes in response are due to the difference in refractive index between the sample solution and the running buffer.

According to Löfås and co-workers,[199] the carboxy-methylated dextran matrix covalently attached to a gold substrate is negatively charged at pHs around 7. They suggested that this negatively charged hydrogel-covered surface can be used to immobilise positively charged proteins by electrostatic attraction forces and also for covalent coupling of various other ligands. The FC2 sensorgram showed the association event between the particles and the dextran matrix of the reference channel (non-modified channel). Therefore, it would appear that the cationic **5a-AuNPs** are not only interacting with the negatively charged DNA (immobilised on the SA chip), as showed in the FC1-FC2 sensorgram but also with the negatively charged dextran matrix. No evidence of dissociation can be observed in either case, FC1 and FC2, indicating that

the gold nanoparticles are bound to the negatively charged carboxy-methylated matrix of the SA chip through ionic interactions.

Several attempts to remove the gold nanoparticles from the dextran matrix were carried out by injecting the same running buffer (HPB-S buffer pH 7.4) and the regeneration solution (50 mM NaOH and 1M NaCl). However, the use of these solutions did not remove the gold nanoparticles. Therefore, the interaction studies between DNA and the phosphonium gold nanoparticles could not be continued using the DNA modified SA sensor chip because the regeneration of the sensor chip was unsuccessful. Consequently, it was decided to try an alternative strategy and the interaction of polyanionic DNA with functionalised gold nanoparticles was investigated.

Experiment SPR3: interaction study between the commercially available citrate-functionalised gold nanoparticles and the SA sensor chip modified with DNA

Immobilisation experiments have been performed using commercially available citrate-functionalised gold nanoparticles (SIGMA gold colloid solution, absorbance 0.754, size range: 5-10 nm), which has a similar particle size range to the 3-carbon chain phosphonium gold nanoparticles. This experiment (SPR3, Table 9) was done using the DNA-modified SA sensor chip and it was hoped that the experiment would show whether the immobilisation of the gold nanoparticles is by physical trapping or through electrostatic interaction between the positively charged phosphonium head

groups of the coating ligands and the negatively charged dextran matrix of the SA senor chip under slightly basic conditions (pH 7.4).

The experimental conditions in this test were the same used in Experiment SPR2 (Table 9). The Biacore X instrument was set to run a sensorgram at 50 $\mu l \cdot min^{-1}$. The instrument was set to the multiple-channel analysis mode in order to study the interaction between the citrate-functionalised gold nanoparticles with the DNA modified and the reference flow cell channels (FC1 and FC2). The injection volume of the SIGMA gold colloid solution was 30 µl.

The result of this experiment is shown in Figure 71. The injection started at 80 seconds and finished at 180 seconds. During this period of time, no significant changes in response were observed either FC1 or FC2 sensorgrams. All the events recorded for both flow cells are the same, indicating that the citrate-stabilised gold nanoparticles do not bind to the dextran matrix and the DNA immobilised on the sensor chip. This result is the opposite of that observed for the **5a-AuNPs** in the experiment SPR2. With this result, it can be concluded that the binding event observed in the experiment SPR2 is not due to physical trapping and the cationic phosphonium gold nanoparticles bind to the negatively charged carboxy-methylated dextran matrix through electrostatic interactions.

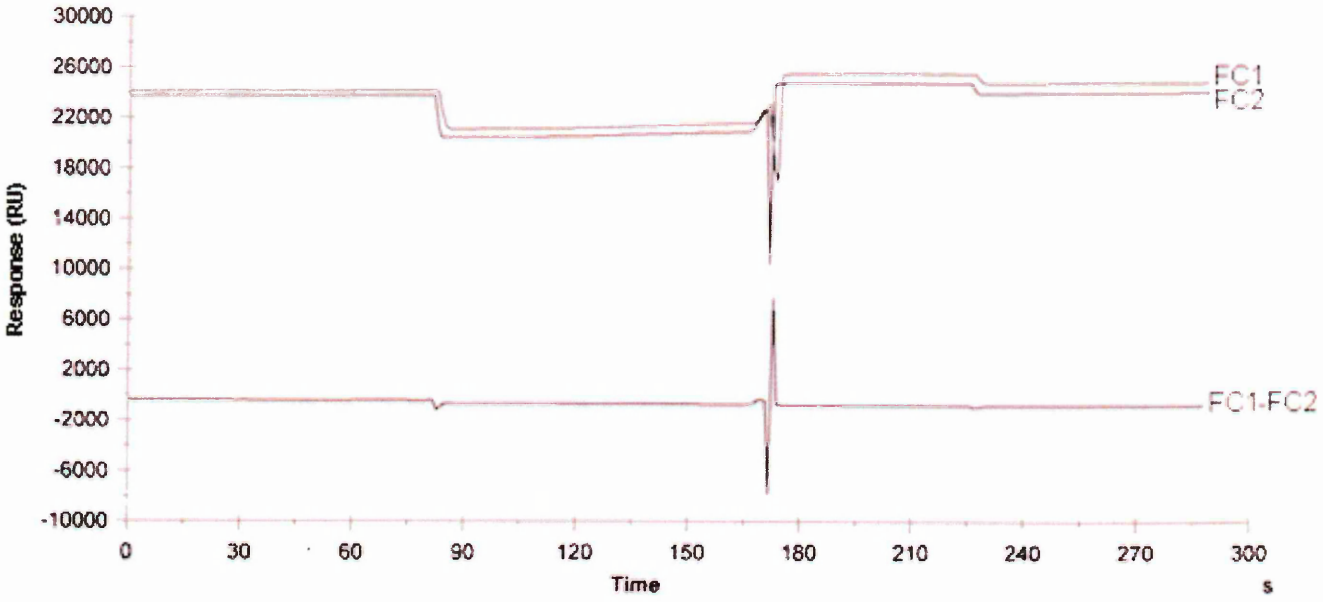

Figure 71. Sensorgrams of interaction curves between SIGMA gold nanoparticles (analyte) and DNA modified SA sensor chip in real time (FC1, FC2, FC1-FC2)

Experiment SPR4: immobilisation of phosphonium gold nanoparticles on SA sensor chip

The aim of this experiment (SPR4, Table 9) was to immobilise the phosphonium gold nanoparticles on a SA sensor chip. A freeze-dried sample of **5a-AuNPs** was used to prepare the colloidal solution (3mg of **5a-AuNPs** in 3mL of running buffer, 1mg/mL) to be injected. The flow rate was set to 50 $\mu L \cdot min^{-1}$ and 50 µL (instrument set volume : 30 µL) of this suspension were placed in the sample loop, and then the instrument was instructed to run in single-channel analysis mode, leaving one of the flow cell channels as reference. The result of this experiment is shown in Figure 72.

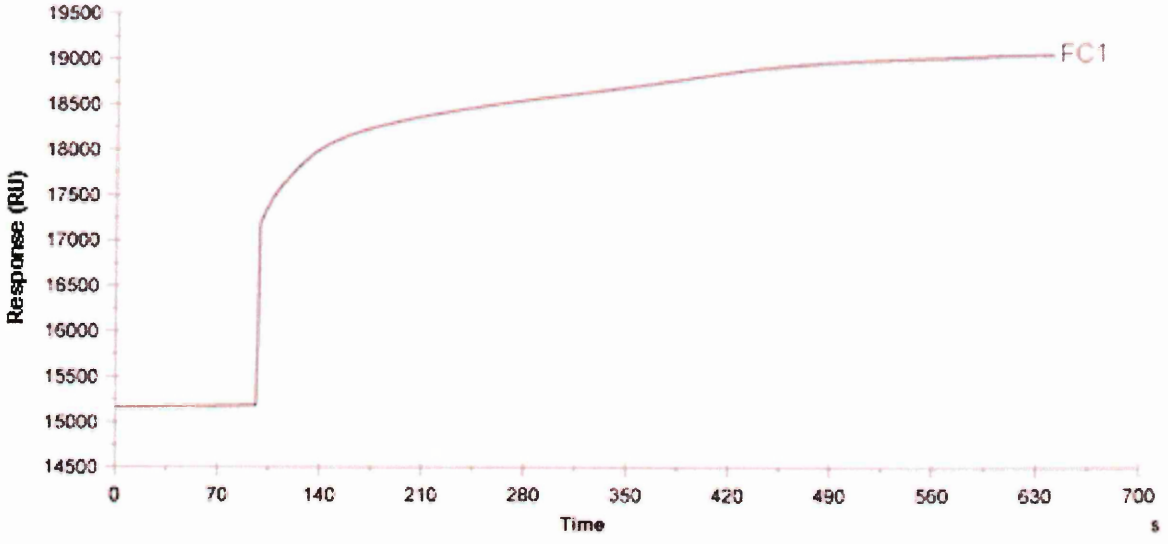

Figure 72. Sensorgram of interaction curve between **5a-AuNPs** (analyte) and SA sensor chip in real time (FC1)

In the sensorgram FC1, only an association curve was observed indicating that the particles are embedded on the streptavidin-dextran matrix on the surface of the sensor chip. This specific binding event is likely due to the electrostatic interaction between the positive charges on the functionalised gold nanoparticles and the negative charges of the carboxy-methylated dextran at pH 7.4. No evidence of dissociation was observed during or after the injection of the nanoparticle sample when the modified flow cell channel (FC1) was eluted with the running buffer. Two additional injections of **5a-AuNPs** were carried out using the same modified SA sensor chip. With these injections, an increase in response from around 20,000 to 46,000 RU was observed. Saturation was reached with the last injection. No increase in response was observed.

Differences in background signal could be observed between the sensograms obtained in experiments SPR1, SPR3 and SPR4. These variations in response (RU) can be intrinsic to the manufaturing process of the sensor chips.

Experiment SPR5: interaction study between the phosphonium-functionalised gold nanoparticles immobilised on the SA sensor chip and RNA (as binding analyte)

Experiment SPR 5 was carried out in order to show that the phosphonium-functionalised gold nanoparticles embedded on the SA sensor chip can interact with negatively charged biomolecules, such as RNA. The phosphonium gold nanoparticle-modified SA sensor chip used for this experiment was the one obtained in experiment SPR4. The experimental details of experiment SPR5 are shown in Table 9. The flow rate was set to 50 $\mu L \cdot min^{-1}$ and 30 μL of a solution containing RNA (96 $ng \cdot \mu L^{-1}$) was injected. The instrument was run in multiple-channel analysis mode. The result of this experiment is shown in Figures 73, 74, 75, and 76. Figure 73 shows the sensorgrams of the binding events which occurred in both flow cells (FC1 and FC2) during the RNA sample injection and the sensorgram resulting of the subtraction of FC1 and FC2 which represents the specific interaction.

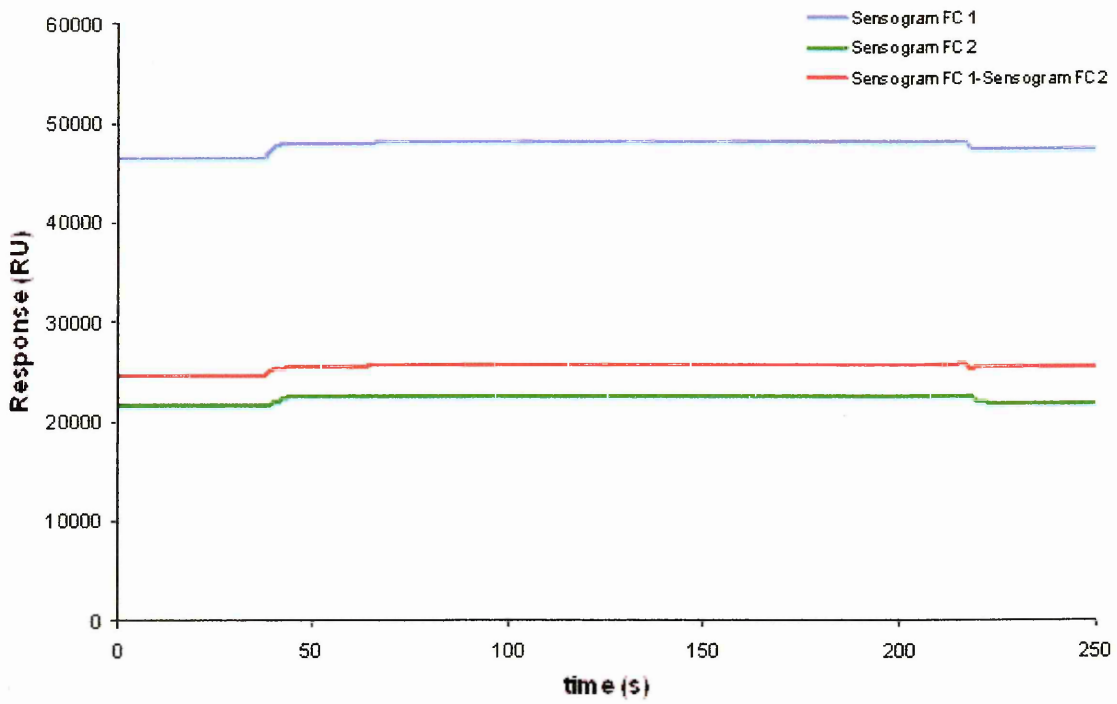

Figure 73. Sensorgrams of interaction curves between RNA (analyte) and **5a-AuNP** modified SA sensor chip in real time (FC1, FC2, FC1-FC2)

The sensorgram corresponding to FC1 (Figure 74), shows an association and dissociation event between the RNA (analyte) and the flow cell channel modified with phosphonium gold nanoparticles. It can be observed in sensorgram FC1 that the dissociation was not complete. The signal (47,500RU) did not reach the initial value (46,500 RU) in response when the injection was finalised at the time of 210 seconds. This indicates that the concentration of the RNA sample was too high for this trial, and some of the RNA was dissociated from the modified surface (FC1), while the rest of the injected RNA remained attached to the modified SA sensor chip. This observed dissociation is due to the saturation of RNA.

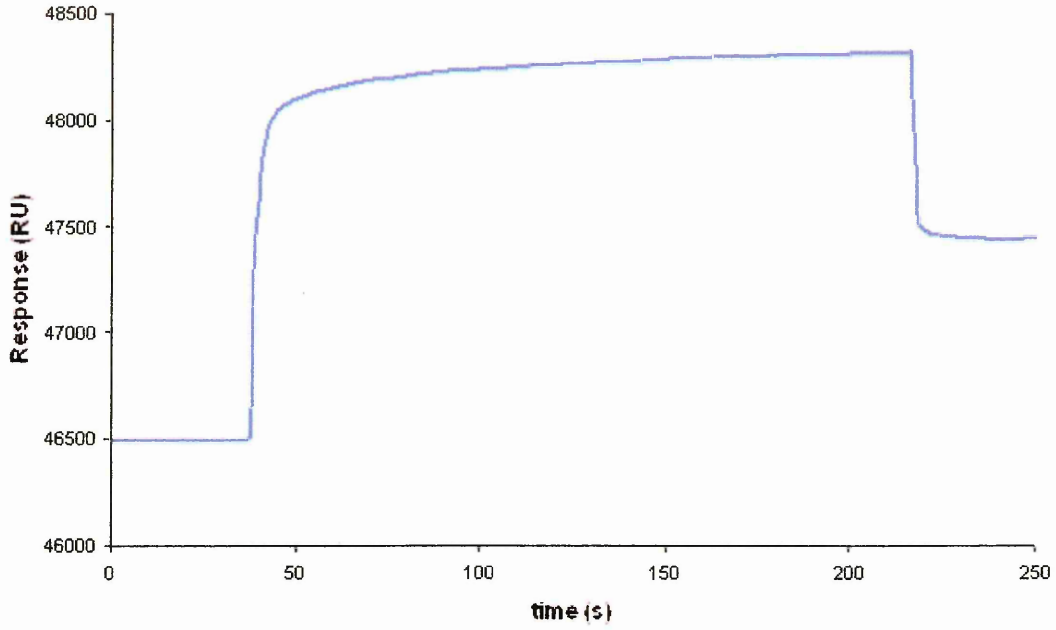

Figure 74. Sensorgram of an association curve resulting of the interaction between RNA and the **5a-AuNPs** immobilised on one of the channels of the SA sensor chip (FC1)

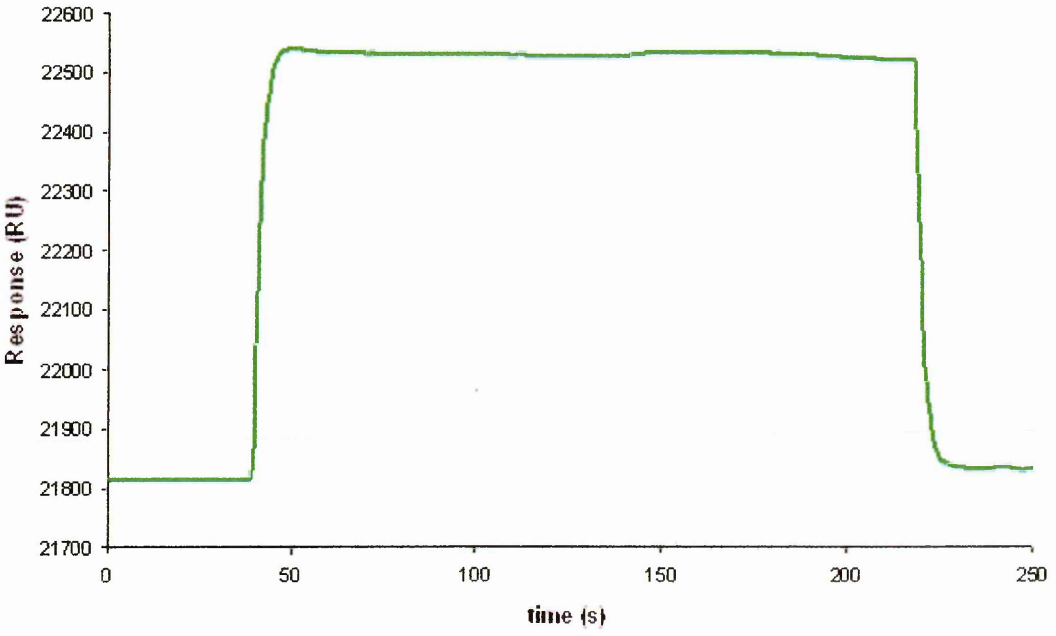

Figure 75. Sensorgram of an association-dissociation curve resulting of the interaction between RNA and the reference channel of the SA sensor chip (FC2)

The sensorgram for to the interaction of the RNA and the non-modified matrix of the reference flow cell channel (FC2) is shown in Figure 75. As with FC1, an association-dissociation curve can be observed. When the injection is finished, after the binding event, the signal returns to the initial value in response (21,800 RU). The dissociation event is complete, indicating that the RNA is not bound to the streptavidin-dextran matrix. The specific interaction between the RNA and the cationic phosphonium gold nanoparticles FC1-FC2, is shown in Figure 76, and shows that the RNA is binding to the phosphonium gold nanoparticles embedded in the streptavidin-dextran matrix of the SA sensor chip.

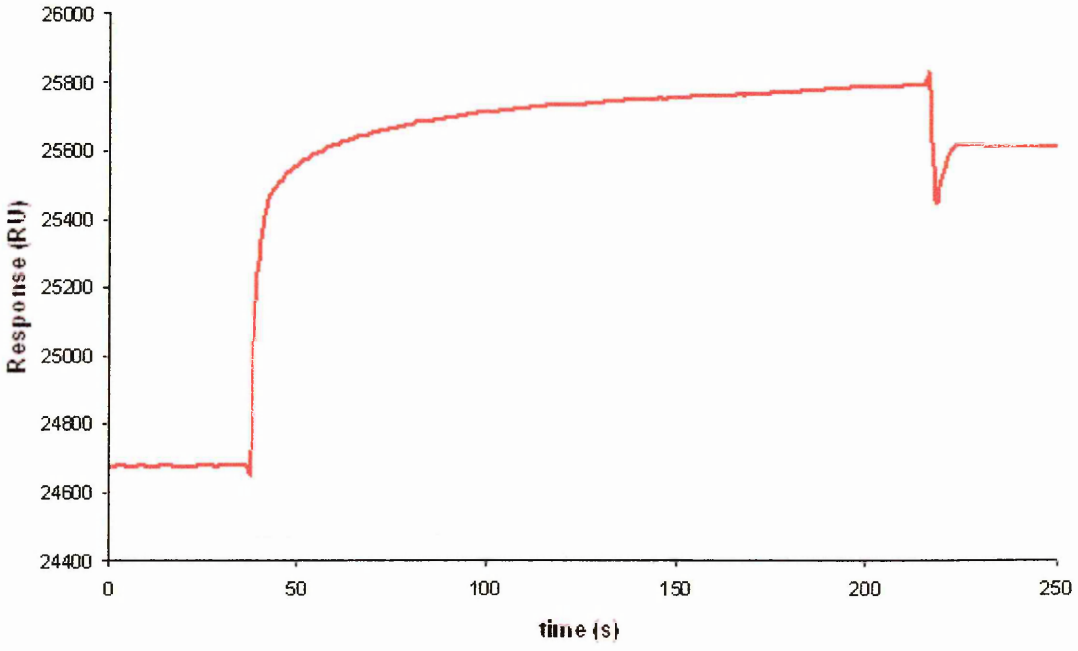

Figure 76. Specific binding curve resulting of the subtraction of sensorgrams FC1 and FC2 (FC1-FC2). Results obtained of the interaction study between RNA (analyte) and **5a-AuNP** modified SA sensor chip in real time.

Experiment SPR6: immobilisation of 5a-AuNPs on CM5 sensor chip

Due to the results obtained in previous experiments, it was decided to use a carboxy-methylated dextran matrix sensor chip (CM5) instead of the SA chip. According to the Biacore SA sensor chip data sheet, this sensor chip is based on the same carboxy-methylated dextran matrix derivatised with tetrameric protein molecules, so-called streptavidin, which is used to anchor biotinylated molecules. Therefore, the presence of the streptavidin in the dextran matrix appeared to be unnecessary in this case and the CM5 sensor chip can represent an advantage over the use of the SA chip.

In principle, the phosphonium gold nanoparticles could be embedded in SA and CM5 sensor chips. However, the use of CM5 chip would help to avoid any possible non-specific interactions between the streptavidin molecules and polyanionic biomolecules such as, RNA and DNA, which can appear with the use of the SA sensor chip. Consequently, the following interaction studies between the gold nanoparticles embedded on the sensor chip and biomolecules were carried out using CM5 sensor chips and DNA as the binding partner. The DNA immobilisation strategy planned to be used in this project is shown in Figure 77. However, this experiment (SPR6) shows the results of the first step of this presented strategy which is the immobilisation of the phosphonium gold nanoparticles on the negatively charged carboxy-methylated dextran matrix of the CM5 sensor chip.

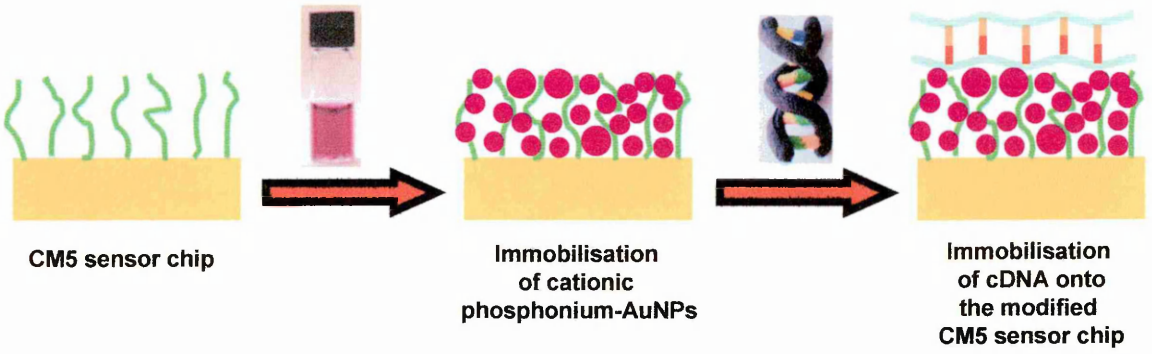

Figure 77. Illustration of the strategy used to immobilise cDNA onto the CM5 sensor chip

The particles immobilised on the CM5 sensor chip were the **5a-AuNPs**. In this experiment, the freeze-dried particles were re-suspended in the same running buffer (HSB-EP, pH 7.4) instead of deionised water. The flow rate was set to 10 $\mu L \cdot min^{-1}$. To prepare the modified CM5 sensor chip, 30 µL of a re-suspended gold nanoparticle solution (1 $mg \cdot mL^{-1}$) were set to be injected in a single-channel analysis mode. After the injection of the colloidal solution, HBS-EP buffer pH 7.4 was run overnight at 20 $\mu L \cdot min^{-1}$ through the modified flow cell channel (FC1) in order to remove the excess and unbound gold nanoparticles.

The result of this experiment is shown in Figure 78. An increase from 28,000 to 74,000 RU in response was observed when the sample injection started. This association event indicated that the cationic gold nanoparticles were interacting with the negatively charged dextran matrix during the sample injection. No evidence of dissociation was observed indicating that the nanoparticles are bound permanently on the surface of the CM5 sensor chip.

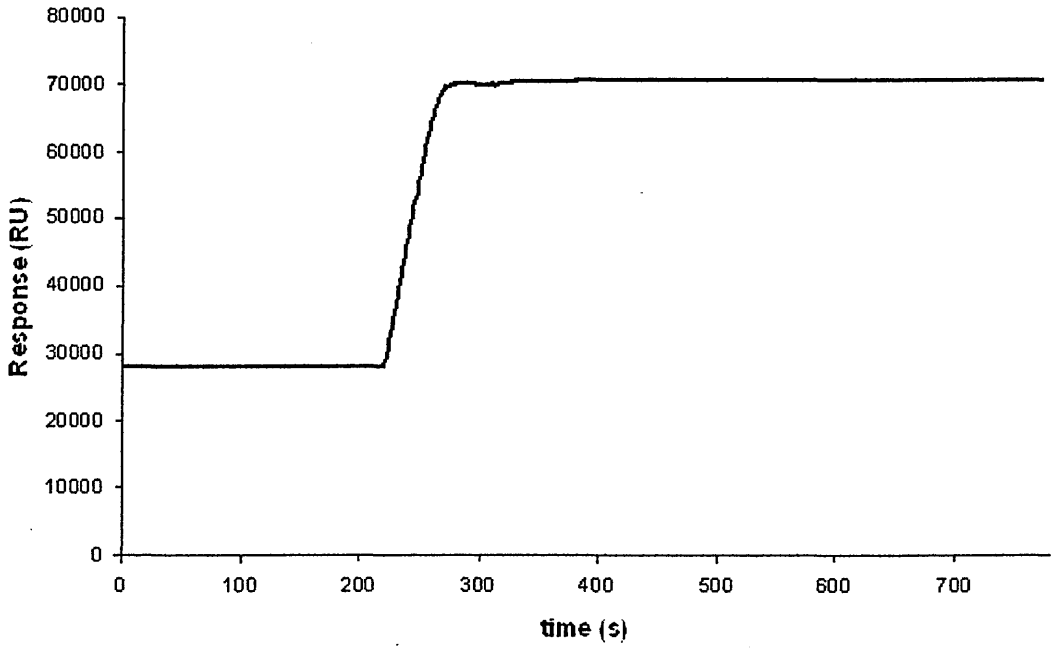

Figure 78. Sensorgram of an association curve resulting of the interaction between **5a-AuNPs** (analyte) on one of the channels of the CM5 sensor chip (FC1)

Experiment SPR7: immobilisation of 6C-phosphonium gold nanoparticles on CM5 sensor chip

In this experiment, phosphonium gold nanoparticles with longer carbon chain coating ligands were immobilised on the carboxy-methylated dextran matrix of the CM5 sensor chip. Gold nanoparticles functionalised using 6-triphenylphosphoniohexylthiosulfate zwitterion (**5c-AuNPs**) as precursors of the protecting ligand, were used in this test. A colloidal solution of **5c-AuNPs** (1 $mg \cdot mL^{-1}$) was prepared by re-suspending the particles in the running buffer (HSB-EP, pH 7.4). 30 µL of this solution were injected in single-channel analysis mode. The flow rate used in this experiment was 10 $\mu L \cdot min^{-1}$.

Similar results to those found in the previous experiment (SPR6) were obtained when a same concentration solution (1 $mg \cdot mL^{-1}$) of **5c-AuNPs** was injected to interact with the dextran matrix of the CM5 sensor chip (Figure 79). No evidence of dissociation was observed indicating that the phosphonium gold nanoparticles stabilised with longer carbon chain ligands can also bind permanently on the surface of the CM5 sensor chip.

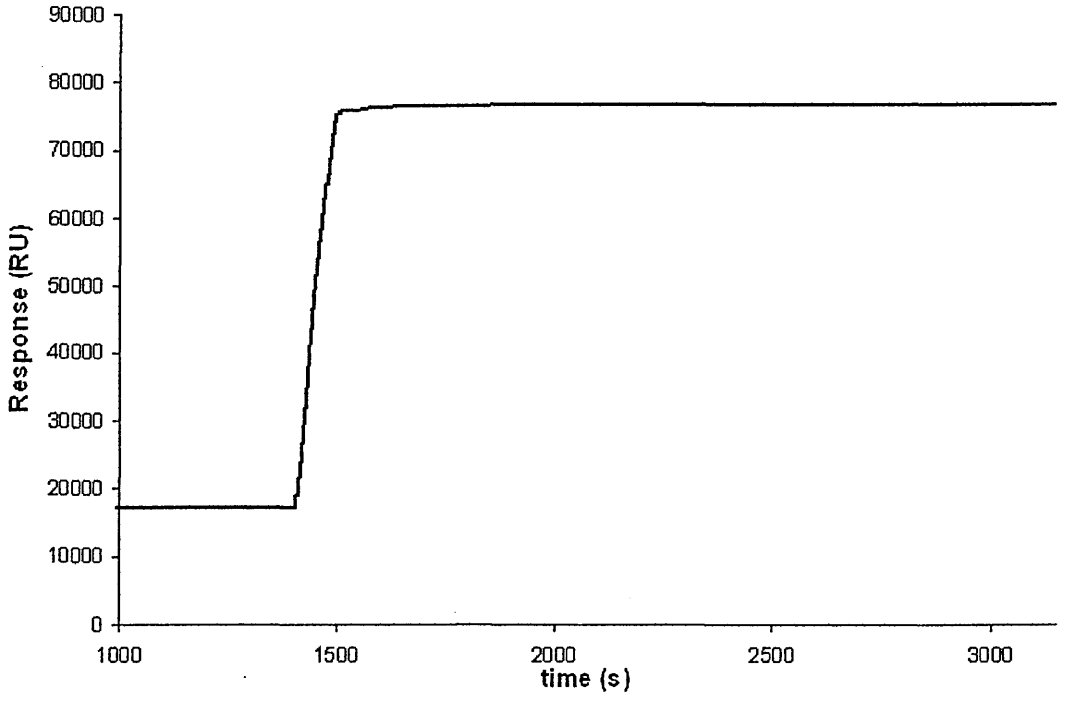

Figure 79. Sensorgram of an association curve resulting of the interaction between **5c-AuNPs** (analyte) on one of the channels of the CM5 sensor chip (FC1)

Experiment SPR8: interaction study between the 5a-AuNPs immobilised on the CM5 sensor chip and DNA (as binding analyte)

Once the phosphonium gold nanoparticles were immobilised on CM5 sensor chip, this modified chip was used to carry out qualitative studies of the capacity of these nanoparticles to interact with DNA. The modified CM5 chip used in this experiment was the sensor chip customized with **5a-AuNPs** obtained in experiment SPR6. cDNA (54 $\mu g \cdot mL^{-1}$, 100 base-pair double-stranded DNA molecule) was the polyanionic biomolecule used as the binding partner (analyte). The same experimental conditions (SPR8, Table 9), sample volume and flow rate used in the previous interaction studies with the RNA and the modified SA sensor chip (experiment SPR5), were used in this experiment.

The results are shown in Figures 80, 81 and 82. Figure 80 shows the sensorgrams of the binding events that occurred in both flow cells (FC1 and FC2) during the cDNA sample injection and the sensorgram resulting from the subtraction of FC1 and FC2 which represents the specific interaction.

Figure 81 shows the sensorgram (FC1) corresponding to the interaction between the cDNA and the cationic gold nanoparticles embedded on the surface of the sensor chip. An association curve and an increase in response from 74,800 to 76,400 RU were observed. Once the injection finished, when the running buffer started to flush, the signal in response was the same (around 76,400 RU), and stable, indicating that the cDNA molecules were permanently bound on the modified CM5 sensor chip. This evidence indicates that the cationic phosphonium gold nanoparticles are interacting electrostatically with the negatively charged double stranded cDNA, and also indicates

that this interaction is strong enough to keep the DNA linked to the positive charges corresponding to the gold nanoparticles on the surface of the CM5 sensor chip (Figure 77).

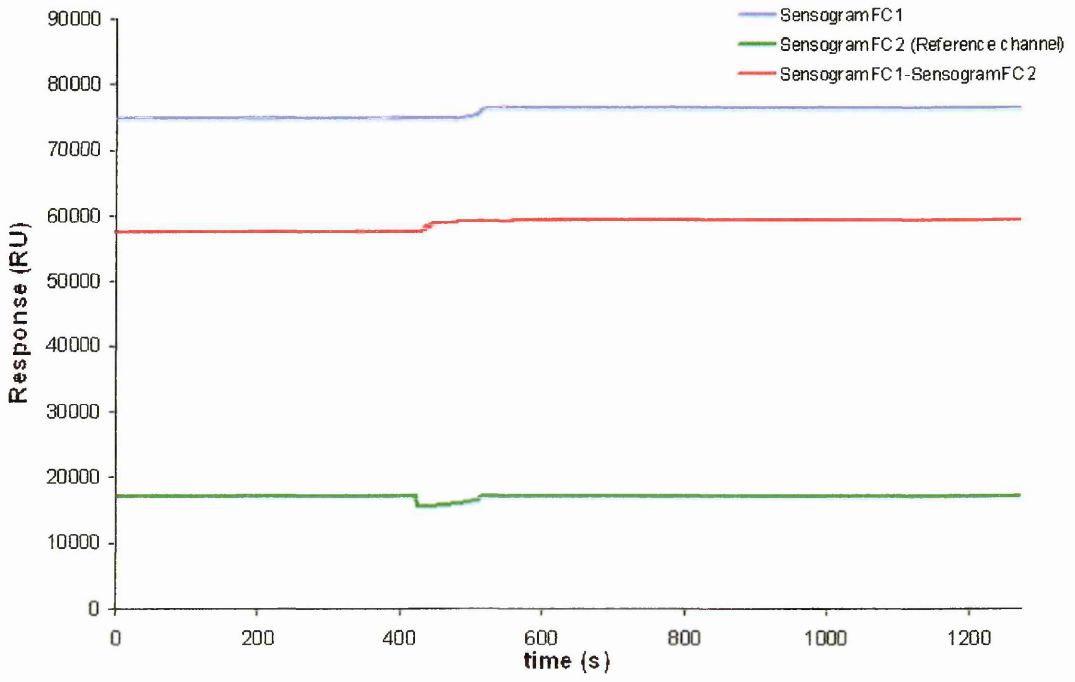

Figure 80. Sensorgrams of interaction curves between cDNA (analyte) and **5a-AuNP** modified CM5 sensor chip in real time (FC1, FC2, FC1-FC2)

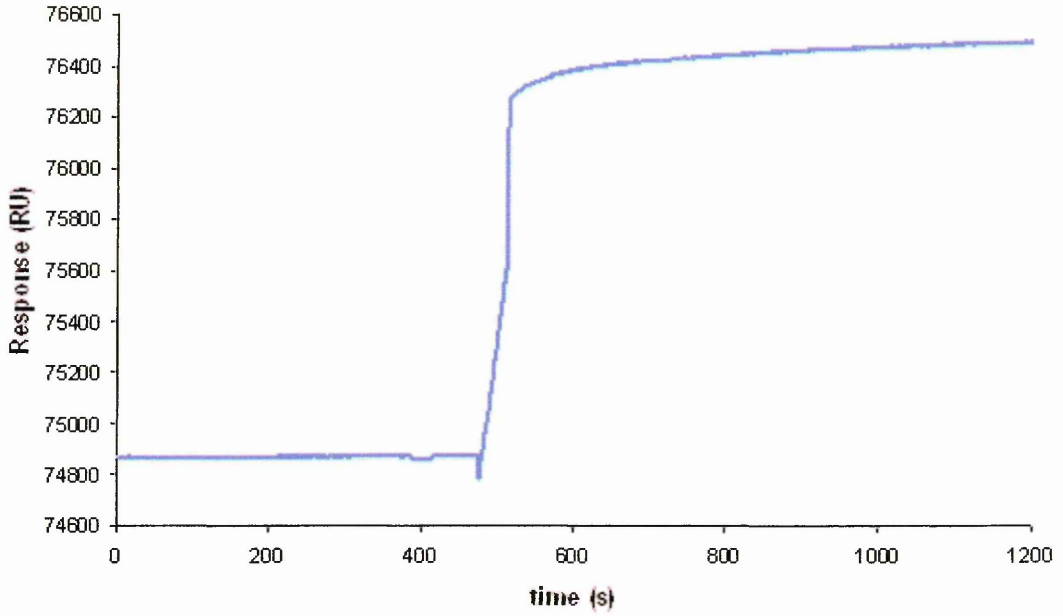

Figure 81. Sensorgram of an association curve resulting of the interaction between cDNA and the **5a-AuNPs** immobilised on one of the channels of the CM5 sensor chip (FC1)

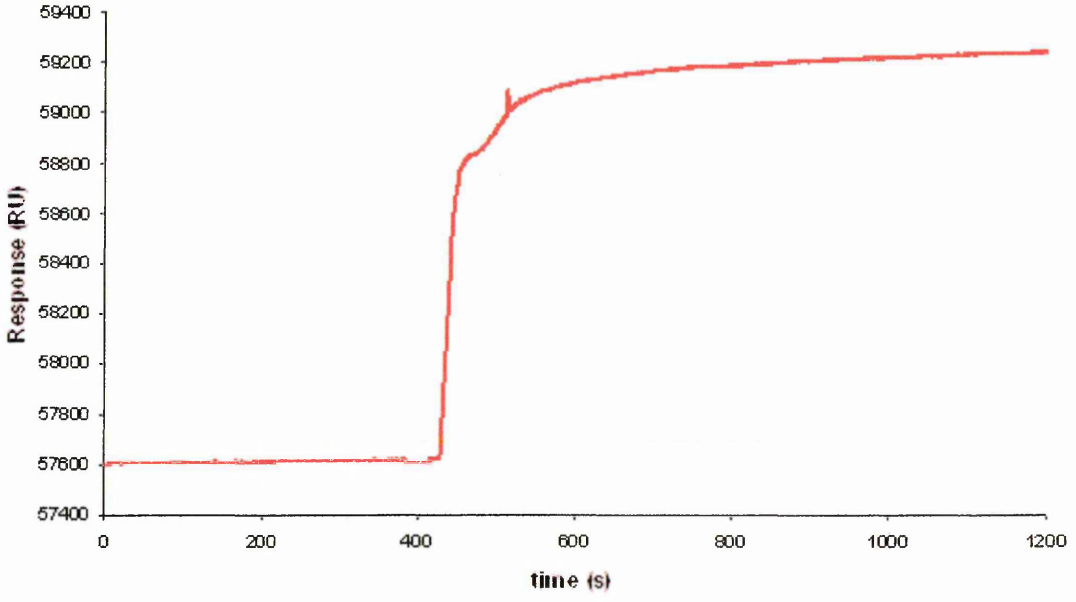

Figure 82. Specific binding curve resulting of the subtraction of sensorgrams FC1 and FC2 (FC1-FC2). Results obtained of the interaction study between cDNA (analyte) and **5a-AuNP** modified CM5 sensor chip in real time.

A sensorgram corresponding to the interaction of the cDNA and the non-modified matrix of the reference cell (FC2) is shown in Figure 80. No considerable change in response was observed during the injection time indicating that the cDNA did not bind to the dextran matrix and its interaction with the nanoparticles on the surface was almost non-detectable. Figure 82 shows the specific interaction between the cDNA and the cationic gold nanoparticles resulting from the subtraction of FC1 and FC2. This experiment confirms the ability of the phosphonium gold nanoparticles to interact and bind negatively charged DNA.

Experiment SPR9: regeneration of modified CM5 sensor chip (obtained in experiment SPR8) and immobilisation of 5a-AuNPs on regenerated CM5 sensor chip

The cDNA immobilised on the CM5 sensor chip modified with 5a-AuNPs (sensor chip obtained in experiment SPR8), was regenerated using 15 % of formic acid aqueous solution, as recommended in the CM5 chip data sheet.[200] 100 μL of this regenerating solution were set to be injected in single-channel analysis mode (flow cell channel modified with **5a-AuNPs** and cDNA, FC1) and run at a flow rate of 20 $\mu L \cdot min^{-1}$. This regeneration process was carried out in order to remove the cDNA attached to the modified CM5 chip and re-use it for additional DNA immobilisation.

The result of this regeneration process is shown in Figure 83. The response before the injection of the formic acid solution was 58,000 RU. However, once the

injection started at a time of 100 seconds, the signal continuously decreased until the injection finalised (29,000 RU). This decrease in response could due to the change in ionic conditions of the dextran matrix which might release part of the gold nanoparticles and cDNA from the matrix.

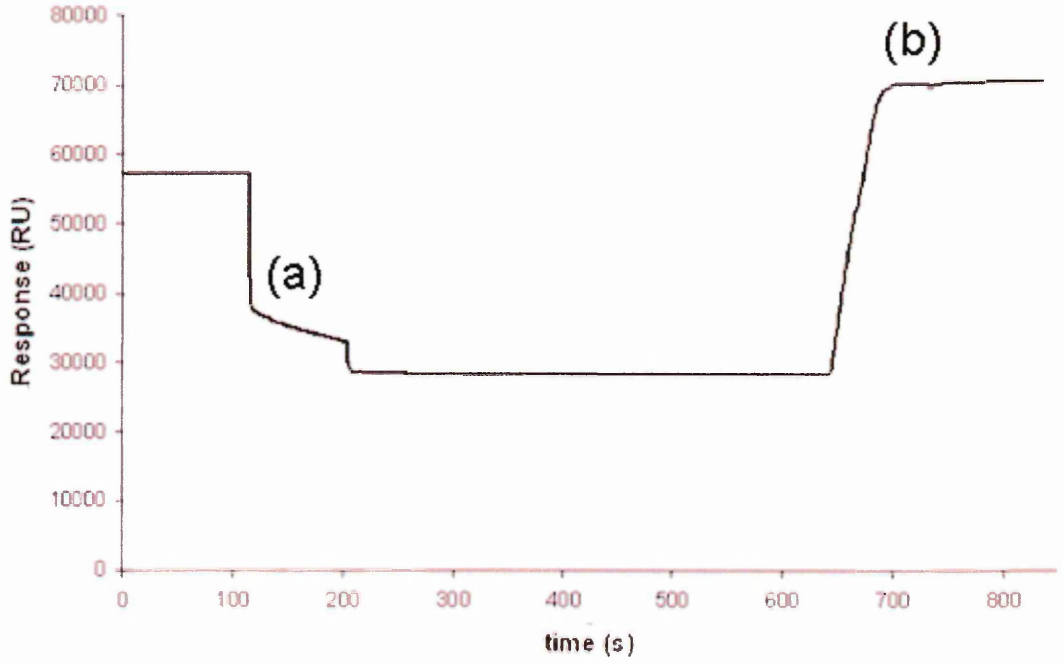

Figure 83. Sensorgrams resulting of the modified CM5 sensor chip regeneration process (using a solution of 15% formic acid, **a**) and the injection of a **5a-AuNP** solution to the regenerated CM5 sensor chip (**b**)

With the previous evidence, the regenerated CM5 sensor chip was re-used to immobilise more cationic gold nanoparticles. This injection was carried out under the same experimental conditions (SPR9, Table 9) used for the immobilisation of phosphonium gold nanoparticles on the CM5 sensor chip (experiment SPR6) Once the injection of the regeneration solution finished, a fresh gold colloid solution was injected

to the regenerated CM5 sensor chip. The result of this experiment is shown in the same Figure 83. The injection started at the time of 650 seconds and at this point an increase in response from 29,000 to 75,000 was observed, indicating that regenerated CM5 sensor chip could be re-used to immobilise more cationic phosphonium gold nanoparticles and, therefore, more DNA molecules.

Further evidence for the immobilisation of the phosphonium gold nanoparticles onto the CM5 sensor chip can be observed in the image obtained using an optical microscope (Figure 84). In a non-modified CM5 sensor chip, two flow cell channels of white colour can be observed with the naked eye. After the gold nanoparticle immobilisation process in one of the channels of the sensor chip, a different colour can be observed. This experimental observation was confirmed by the optical microscope. The image was obtained by analysing of one of the CM5 sensor chips with **5a-AuNPs**. In this image, a dark blue stain is observed on the right hand side (A) of the insert sensor chip. Therefore, this colour might correspond to the aggregated gold nanoparticles, which are known to have blue colour,[19] immobilised on one of the channels of the chip. The left hand side (B) of the metal substrate is the section of the sensor chip which corresponds to the reference channel. Further studies, e.g. by AFM or XPS are necessary to confirm this visual observation. These techniques would provide a detailed topography of the modified and reference channels of the sensor chip.

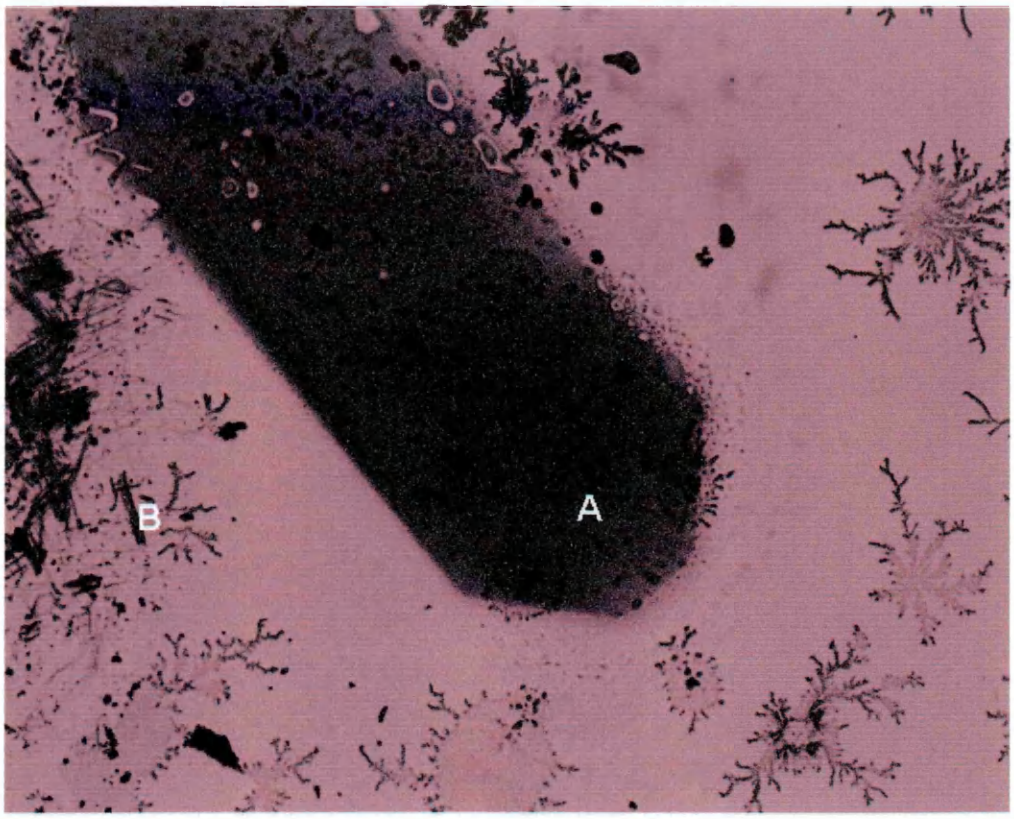

Figure 84. Image of the two channels (A and B) of the **5a-AuNP** modified CM5 sensor chip using and Optical Microscope

With this group of experiments based on the interactions studies using the Biacore X system, it has been shown that phosphonium-functionalised gold nanoparticles can be used as biomolecule anchoring systems, which augurs well for their future use as biorecognition systems. With the SPR system, it was possible to immobilise phosphonium gold nanoparticles on the CM5 sensor chip and observe the interaction between these cationic nanoparticles and negatively charged biomolecules, such as, RNA and DNA, in real time. The immobilisation events between nanoparticles and the negatively charged dextran matrix of the CM5 sensor chip, and between

biomolecules and nanoparticles embedded on the sensor chip surface, were known to be a success due to the presence of association curves. It has also been shown that the modified CM5 sensor chips can be regenerated for further nanoparticle and DNA immobilisation. With all the evidences obtained in this part of the study, it is possible that this strategy can be used to develop an analytical technique to detect specific DNA sequences and possible mutations in their structure.

CHAPTER 8

Conclusions and Future Work

8.1 Conclusions

The results described in this thesis have clearly shown that the family of phosphonium-containing ligands synthesised in this study act as protecting ligands in the synthesis of monolayer protected-gold clusters. Phosphonium gold nanoparticles, of *ca* 5 nm in particle size, were obtained by the reduction of tetrachloroaurate salts in presence of the protecting ligands in a two-phase DCM:H_2O system. Phosphonium-gold nanoparticles were shown to possess affinity for the aqueous phase. Their stability for up to 6 months was proved by UV-visible spectroscopy and TEM. These functionalised gold colloid solutions were freeze-dried in order to remove the water. The latter represents an advantage and provides the possibility to store the materials as stable solids for longer periods of time and enables their re-dispersal in suitable solvents for additional analyses. X-ray photoelectron spectroscopy determined the ligand-substrate bond characteristics for the gold nanoparticles functionalised with phosphonioalkylthiolate ligands, and binding energies corresponding to S-Au bond were observed.

In this study, the ability of the cationic phosphonium gold nanoparticles to interact with negatively charged biomolecules such as RNA and cDNA, by using the Biacore Surface Plasmon Resonance technique has also been demonstrated. The immobilisation of phosphonium-functionalised gold nanoparticles on commercially available dextran matrix-containing chips has been achieved. Using these modified sensor chips, RNA and cDNA were also successfully immobilised on this cationic phosphonium gold nanoparticle containing surface.

8.2 Suggestions for future work

With all the evidence obtained from the qualitative studies carried out using the Biacore SPR technique, it would be interesting developing an analytical technique to detect specific DNA sequences and possible mutations in the chemical structure of these biomacromolecules. The first step in achieving this goal could be the immobilisation a single-stranded DNA on sensor chips modified with cationic phosphonium gold nanoparticles and then to study the interaction with a complementary strand (Figure 85).

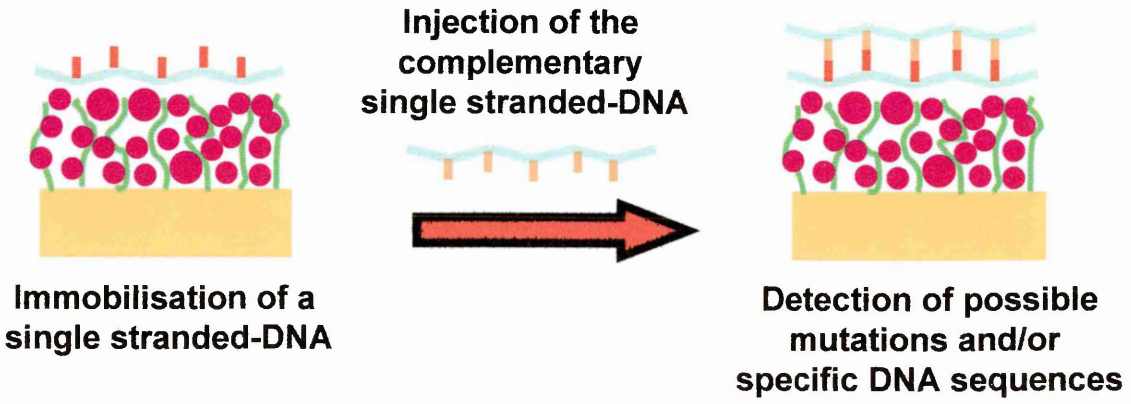

Figure 85. Strategy for specific DNA sequences and mutations

Other workers have demonstrated the utility of phosphonium-containing molecules as transfection vectors and probes in mitochondrial medicine, [125] it would be interesting to study the interaction of these phosphonium-functionalised gold nanoparticles synthesised here, and the parent phosphonium-thioacetate and thiosulfate ligands with cells, with a view to their potential use in diagnostics and targeted drug delivery.

References

1. NIEMEYER, C.M. *Angew. Chem. Int. Ed.*, **2001**, *40*, 4128-4158.

2. LANGER, R. and TIRRELL, D. A. *Nature*, **2004**, *428*, 487-492.

3. DREXLER, K. E. *Nanosystems, Molecular Machinery. Manufacturing and Computation.* Ed. Wiley, New York, **1992.**

4. BRADLEY, D. *Science*, **1993**, *259*, 890-892.

5. MIRKIN, C. A. and STORHOFF, J. J. *Chem. Rev.*, **1999**, *99*, 1849-1862.

6. ROSI, N. L. and MIRKIN, C. A. *Chem. Rev.*, **2005**, *105*, 1547-1562.

7. SCHIMD, G. *Chem. Rev.*, **1992**, *92*, 1709-1727.

8. SHIPWAY, A. N., KATZ, E. and WILLNER, I. *Chem. Phys. Chem.*, **2000**, *1*, 18-52.

9. PENN, S. G., HE, L. and NATAN, M. J. *Current Opinion in Chemical Biology*, **2003**, *7*, 609-615.

10. PELLEGRINO, T., KUDERA, S., LIEDL, T., MUNOZ, H. A., MANNA, L. and PARAK, W. J. *Small*, **2005**, *1*, 48-63.

11. PARAK, W. J., GERION, D., PELLEGRINO, T., ZANCHET, D., MICHEEL, C., WILLIAMS, S. C., BOUDREAU, R., LEGROS, M. A., LARABELL, C. A., and ALIVISATOS, A. P. *Nanotechnology*, **2003**, *14*, R15-R27.

12. KAYSER, O., LEMKE, A., and HERNANDEZ-TREJO, N. *Curr. Pharm. Biotechnol.*, **2005**, *6*, 3-5.

13. ALIVISATOS, A. P. *Nat. Biotechnol.*, **2004**, *22*, 47-52.

14. POOLE, C. P., and OWENS, F. J. *Introduction to Nanotechnology*. Wiley-Interscience, Hoboken, **2003.**

15. PARAK, W. T., GERION, D., ZANCHET, D., WOERZ, A. S., PELLEGRINO, T., MICHEEL, C., WILLIAMS, S. C., SEITZ, M., BRUEHL, R. E., BRYANT, Z., BUSTAMANTE, C., BERTOZZI, C. R., and ALIVISATOS, A. P. *Chem. Mat.*, **2002**, *14*, 2113-2119.

16. WANG, J. *Small*, **2005**, *1*(11), 1036-1043.

17. HIRSCH, L. R., JACKSON, J. B., LEE, A., HALAS, N. J., and WEST, J. L. *Anal. Chem.*, **2003**, *75*, 2377-2381.

18. TKACHENKO, A.G., XIE, H., COLEMAN, D., GLOMM, W., RYAN, J., ANDERSON, M. F., FRANZEN, S., and FELDHEIM, D. L. *J. Am. Chem. Soc.*, **2003**, *125*(16), 4700-4701.

19. DANIEL, M. C., and ASTRUC, D. *Chem. Rev.*, **2004**, *104*, 293-346.

20. THOMAS, K. G., and KAMAT P. V. Acc. *Chem. Res.*, **2003**, *36*, 888-898.

21. SCHMID, G., and CORAIN, B. *Eur. J. Inorg. Chem.*, **2003**, 3081-3098.

22. BRUST, M., and KIELY, C. J. *Colloids and Surfaces A: Physicochemical and Engineering Aspects*, **2002**, *202*, 175-186.

23. MALLICK, K., WANG, Z. L., and PAL, T. *J. Photochem. Photobiol.*, **2001**, *140*, 75-80.

24. ZHOU, Y., WANG, C. Y., ZHU, Y. R., and CHEN Z. Y. *Chem. Mater.*, **1999**, *11*, 2310-2312.

25. REED, J. A., COOK, A., HALAAS, D. J., PARAZOLLI, P., ROBINSON, A., MATULA, T. J., and GRIEZER, F. *Ultrason. Sonochem.*, **2003**, *10*, 285-289.

26. KHOMUTOV, G. B. *Colloids Surf.*, **2002**, 243-267.

27. NAKAMOTO, M., YAMAMOTO, M., and FUKUSUMI, M. *Chem. Commun.* **2002**, 1622-1623.

28. CHI, L. F., HARTING, M., DRESCHLER, T., SCHWAACK, T. H., SEIDEL, C., FUCHS, H., and SCHMID, G. *Appl. Phys. A*, **1998**, *66*, S187-S190.

29. SHIPWAY, A. N., LAHAV, M., and WILLNER, I. *Advanced Materials*, **2000**, *12*(13), 993-998.

30. SHIPWAY, A. N., LAHAV, M., GABAI, R., and WILLNER, I. *Langmuir*, **2000**, *16*, 8789-8795.

31. TURKEVITCH, J., STEVENSON, P. C., and HILLIER, J. *Discuss. Faraday Soc.*, **1995**, *11*, 55-75.

32. FRENS, G. *Nature: Phys. Sci.*, **1973**, *241*, 20-22.

33. GRABAR, K. C., GRIFFITH, R., HOMMER, M. B., and NATAN, M. *Anal. Chem.* **1995**, *67*, 735-743.

34. BROWN, K. R., and NATAN, M. J. *Langmuir*, **1998**, *14*, 726-728.

35. WATSON, K. J., ZHU, J., NGUYEN, S. B. T., and MIRKIN, C. A. *J. Am. Chem. Soc.*, **1999**, *121*, 462-463.

36. TEMPLETON, A. C., WUELFING, W. P., and MURRAY, R. W. *Acc. Chem. Res.*, **2000**, *33*, 27-36.

37. SCHMID, G., PFEIL, R., BOESE, R., BANDERMANN, F., MEYER, S., CALIS, G. H.M., and VANDER VELDEN, J. W. *A. Chem. Ber.*, **1981**, *114*, 3634-3642.

38. SCHMID, G., and LEHNERT, A. *Angew. Chem. Int. Ed. Engl.*, **1989**, *28*, 780-781.

39. GIERSIG, M., and MULVANEY, P. *Langmuir*, **1993**, *9*, 3408-3413.

40. BROWN, L. O., and HUTCHISON, J. E. *J. Am. Soc., Chem.*, **1997**, *119*, 12384-12385.

41. BRUST, M., WALKER, M., BETHELL, D., SCHIFFRIM, D. J., and WHYMAN, R. J. *J. Chem. Soc. Chem. Commun.*, **1994**, 801-802.

42. BRUST, M., FRINK, J., BETHELL, D., SCHIFFRIN, D. J., and KIELY, C. J. *J. Chem. Soc. Chem. Commun.*, **1995**, 1655-1656.

43. JANA, N. R., GEARHEART, L., and MURPHY, C. J. *Langmuir*, **2001**, *17*, 6782-6786.

44. VERMA, A., and ROTELLO, V. M., *Chem. Commun.*, **2005**, 303-312.

45. IPE, B. I., THOMAS, K. G., BARAZZOUK, S., HOTCHANDANI, S., and KAMAT, P. V. *J. Phys. Chem. B*, **2002**, *106*, 18-21.

46. WANG, T. X., ZHANG, D. Q., XU, W., YANG, J. L. HAN, R., and ZHU, D. B. *Langmuir*, **2002**, *18*, 1840-1848.

47. LUKKARI, J., MERETOJA, M., and KARTIO, I. *Langmuir*, **1999**, *15*, 3529-3537.

48. SHON, Y-S., GROSS, S. M., DAWSON, B., PORTER, M., and MURRAY, R.W., *Langmuir*, **2000**, *16*, 6555-6561.

49. YEE, C. K., ULMAN, A., RUIZ, J. D., PARIKH, A., WHITE, H., and RAFAILOVICH, M. *Langmuir*, **2003**, *19*, 9450-9458.

50. ZELAKIEWICZ, B. S., YONEZAWA, T., and TONG, YY. *J. Am. Chem. Soc.*, **2004**, *126*, 8112-8113.

51. CHEN, S., and KIMURA, K. *Langmuir*, **1999**, *15*, 1075-1082.

52. AKAMATSU, K., HASEGAWA, J., NAWAFUNE, H., KATAYAMA, H., and OZAWA, F., *J. Mater. Chem.*, **2002**, *12*, 2862-2865.

53. HASAN, M., BETHELL, D., and BRUST, M. *J. Am. Chem. Soc.*, **2003**, *125*, 1132-1133.

54. GRABAR, K. D., BROWN, K. R., KEATING, C. D., STRANICK, S. J., TANG, S-L., and NATAN, M. J. *Anal. Chem.*, **1997**, *69*, 471-477.

55. JUNNO, T., CARLSSON, S. B., XU, H., MONTELIUS, L., and SAMUELSON, L. *Appl. Phys. Lett.*, **1998**, *72*, 548-550.

56. LI, Q., ZHENG, J., and LIU, Z. *Langmuir*, **2003**, *19*, 166-171.

57. NAKAMURA, K., KAWABATA, T., and MORI, Y. *Powder Technol.* **2003**, *131*, 120-128.

58. VEFF, D. V., OHARA, P. C., HEATH, J. R., and GELBART, W. M. *J. Phys. Chem.*, **1995**, *99*, 7036-7041.

59. BATTISTONI, C., MATTOGNO, G., ZANONI, R., and NALDINI, L. *J. Electron Spec.*, **1982**, *28*, 23-31.

60. TEMPLETON, A. C., HOSTETLER, M. J., KRAFT, C. T., and MURRAY, R. W. *J. Am. Chem. Soc.*, **1998**, *120*, 1906-1911.

61. BADIA, A., CUCCIA, L., DEMERS, L., MORIN, F., and LENNOX, R. B. *J. Am. Chem. Soc.*, **1997**, *119*, 2682-2692.

62. BADIA, A., DEMERS, L., DICKINSON, L., MORIN, F. G., LENNOX, R. B., and REVEN, L. *J. Am. Chem. Soc.*, **1997**, *119*, 11104-11105.

63. SCHNABEL, U., FISCHER, C. H., and KENNDLER, E., *J. Microcolumn Sep.*, **1997**, *9*, 529-534.

64. ALIVISATOS, A. P. *Science*, **1996**, *271*, 933-937.

65. FELDHEIM, D. L., and COLBY, A. F. *Metal Nanoparticles-Synthesis, Characterization and Applications*, Jr., Eds., Marcel Dekker, New York, **2002**.

66. LOGUNOV, S. L., AHMADI, T. S., EL-SAYED, M. A., KHOURY, J. T., and WHETTEN, R. L. *J. Phys. Chem. B*, **1997**, *101*, 3713-3719.

67. ZAITOUN, M. A.; MASON, W. R.; and LIN, C. T. *J. Phys. Chem. B*, **2001**, *105*, 6780-6784.

68. SCHAFF, T. G., SHAFIGULLEN, M. N., KHOURY, J. T., VEZMAR, I., WHETTEN, R. L., CULLEN, W. G., FIRST, P. N., GUTIERREZ-WING, C., ASCENCIO, J., and JOSE-YACAMUN, M. J. *J. Phys. Chem. B*, **1997**, *101*, 7885-7891.

69. MELINGER, J. S., KLEINMAN, V. D., McMORROW, D., GROHN, F., BAUER, B. J., and AMIS, E. *J. Phys. Chem. A*, **2003**, *107*, 3424-3431.

70. LINK, S., and EL-SAYED, M. A. *J. Phys. Chem. B*, **1999**, *103*, 4212-4217.

71. SU, K. H., WEI, Q. H., ZHANG, X., MOCK, J. J., SMITH, D., and SCHULZ, S. *Nano Lett.*, **2003**, *3*, 1087-1090.

72. LINK, S., MOHAMED, M. B., and EL-SAYED, M. A. *J. Phys. Chem. B*, **1999**, *13*, 3073-3077.

73. YAN, B., YANG, Y., and WANG, Y. *J. Phys. Chem. B*, **2003**, *107*, 9159-9159.

74. TEMPLETON, A. C., PIETRON, J. J., MURRAY, R. W., and MULVANEY, P. *J. Phys. Chem. B*, **2000**, *104*, 564-570.

75. CHEN, M. M. Y., KATZ, A. *Langmuir*, **2002**, *18*, 2413-2420.

76. HU, J., ZHANG, J., LIU, F., KITTREDGE, K., WHITESELL, J. K., and FOX, M. A., *J. Am. Chem. Soc.*, **2001**, *123*, 1464-1470.

77. POL, V. C., GEDANKEN, A., and CALDERRO-MORENO, *J. Chem. Mater.*, **2003**, *15*, 1111-1118.

78. XU, P., and YANAGI, H. *Chem. Mater.*, **1999**, *11*, 2626-2628.

79. DUBERTRET, B., CALAME, M., and LIBCHABER, A. *J. Nat. Biotechnol.*, **2001**, *19*, 365-370.

80. SARATHY, V. K., NARAYAN, K. S., KIM, J., and WHITE, J. O. *Chem. Phys. Lett.*, **2000**, *318*, 543-548.

81. IMAHORI, H., and FUKUZUMI, S. *Adv. Mater.* **2001**, *13*, 1197-1199.

82. IMADORI, H., ARIMURA, M., HANADA, T., NISHIMURA, Y., YAMAZAKI, I., SAKATA, Y., and FUKUZUMI, S. *J. Am. Chem. Soc.*, **2001**, *123*, 335-336.

83. HOSTETLER, M. J., TEMPLETON, A. C., and MURRAY, R. W. *Langmuir*, **1999**, *15*, 3782-3789.

84. MONTALTI, M., PRODI, L., ZACCHENRONI, N., BAXTER, R., TEOBALDI, G., and ZERBETTO, F. *Langmuir*, **2003**, *19*, 5172-5174.

85. SONG, Y., and MURRAY, R. W. *J. Am. Chem. Soc.*, **2002**, *124*, 7096-7102.

86. SIMARD, J., BRIGGS, C., BOAL, A. K., and ROTELLO V. M. *Chem. Commun.*, **2000**, 1943-1944.

87. CHEN, S., PEI, R., and DYER, D. J., *J. Phys. Chem. B*, **2002**, *106*, 1903-1908.

88. MILES, D. T., and MURRAY, R. W. *Anal. Chem.*, **2001**, *73*, 921-929.

89. SUDEEP, P. K., IPE, B. I., THOMAS, K. G., GEORGE, M. V., BARAZZOUK, S., HOTCHANDANI, S., and KAMAT, P. V. *Nano Lett.*, **202**, *2*, 29-35.

90. LI, H., LUK, Y. Y., and MRKISICH, M. *Langmuir*, **1999**, *15*, 4957-4959.

91. WARNER, M. G., REED, S. M., and HUTCHINSON, J. F. *Chem. Mater.*, **2000**, *12*, 3316-3320.

92. TSHIKHUDO, T. R., WANG, Z., and BRUST, M. *Mater. Sci. Tech.*, **2004**, *20*, 980-984.

93. BARON, R., WILLNER, B., and WILLNER, I. *Chem. Commun.*, **2007**, 323-332.

94. LEHN, J. M. *Supramolecular Chemistry: Concepts and Perspectives*; VCH: Weinheim, **1995**.

95. BOAL, A., ILHAN, F., DEROUCHEY, J. E., THURN-ALBRECHT, T., RUSSELL, T. P., and ROTELLO, V. *Nature*, **2000**, *404*, 746-748.

96. JIN, J., IYODA, T., CAO, C., SONG, Y., JIANG, L., LI, T. J., and ZHU, D. B. *Angew. Chem. Int. Ed.*, **2001**, *40*, 2135-2138.

97. LIU, J., MENDOZA, S., ROMAN, E., LYNN, M. J., XU, R., and KAIFER, A. E. *J. Am. Chem. Soc.*, **1999**, *121*, 4304-4305.

98. PATIL, V., MAYYA, K. S., PRADHAN, S. D., SASTRY, M. *J. Am. Chem. Soc.*, **1997**, *119*, 9281-9282.

99. CARUSO, F., CARUSO, R. A., MOHWALD, H. *Science*, **1998**, *282*, 1111-1114.

100. SHENTON, W., DAVIES, S. A., MANN, S. *Adv. Mater.*, **1999**, *11*, 449-452.

101. WATANABE, S., SONOBE, M., ARAI, M., TAZUME, Y., MATSUO, T., NAKAMURA, T., YOSHIDA, K. *Chem. Commun.*, **2002**, 2866-2867.

102. KIM, Y., JOHNSON, R. C., HUPP, J. T. *Nano Lett.*, **2001**, *1*, 165-167.

103. XU, H., KÄLL, M. *Sens. Actuators B*, **2002**, *87*, 244-249.

104. WEST, J. L., and HALAS, N. J. *Current Opinion in Biotechnology*, **2000**, *11*, 215-217.

105. SALATA, O. V. *Journal of Nanobiotechnology*, **2004**, 2-3.

106. MIRKIN, C. A., LETSINGER, R. L., MUCIC, R. C., STORNOFF, J. J. *Nature*, **1996**, *382*, 607-609.

107. ALIVISATOS, A. P., JOHNSON, K. P., PENG, X., WILSON, T. E., LOWETH, C. J., BRUCHEZ, M. P., Jr., SCHULTZ, P. G. *Nature*. **1996**, *382*, 609-611.

108. NIEMEYER, C. M., BURGER, W., PEPLIES, J. *Angew. Chem., Int. Ed. Engl.*, **1998**, *37*, 2265-2268.

109. STORNOFF, J. J., ELGHANIAN, R., MUCIC, R. C., MIRKIN, C. A., LETSINGER, R. L. *J. Am. Chem. Soc.*, **1998**, *120*, 1959-1964.

110. ELGHANIAN, R., STORNOFF, J. J., MUCIC, R. C., LETSINGER, R. L., MIRKIN, C. A. *Science*, **1997**, *277*, 1078-1081.

111. WANG, Z., LEE, J., COSSINS, A. R., BRUST, M. *Anal. Chem.*, **2005**, *77*, 5770-5774.

112. DAVIES, S. P., REDDY, H., CAIVANO, M., COHEN, P. *Biochem. J.*, **2000**, *351*, 95-105.

113. SUN, H., LOW, K. E., NOBLE, R. L., GRAHAM, R. J., CONNAUGHTON, S. S., GEE, M. A., LEE, L. G. *Anal. Chem.*, **2005**, *77*, 2043-2049.

114. WANG, Z., LEVY, R., FERNIG, D. G., BRUST, M. *J. Am. Chem. Soc.*, **2006**, *128*, 2214-2215.

115. KUMAR, A., PATTARKINE, M., BHADBHADE, M., MANDALE, A. B., GANESH, K. N., DATAR, S. S., DHARMADHIKARI, C. V., SASTRY, M. *Adv. Mater.*, **2001**, *13*, 341-344.

116. PETTY, J. T., ZHENG, J., HUD, N. V., DICKSON, R. M., *J. Am. Chem. Soc.*, **2004**, *126*, 5207-5212.

117. HOSTETLER, J. E., WINGATE, J. E., ZHONG, C. J., HARRIS, J. E., VACHET, R. W., CLARK, M. R., LONDONO, J. D., GREEN, S. J., STOKES, J. J., WIGNALL, G. D., GLISH, G. L., PORTER, M. D., EVANS, N. D., MURRAY, R. W. *Langmuir*, **1998**, *14*, 17-30.

118. BOAL, A. K., and ROTELLO, V. M. *J. Am. Chem. Soc.*, **2000**, *122*, 734-735.

119. VERMA, A., NAKADE, H., SIMARD, J. M., ROTELLO, V. M. *J. Am. Chem. Soc.*, **2004**, *126*, 10806-10807.

120. KUZMINE, I., MARTIN, C. T. *J. Mol. Biol.*, **2001**, *305*, 559-566.

121. McINTOSH, C. M., ESPOSITO, E. A., BOAL, A. K., SIMARD, J. M., MARTIN, C. T., ROTELLO, V. M. *J. Am. Chem. Soc.*, **2005**, *123*, 7626-7629.

122. NIIDOME, T., NAKASHIMA, K., TAKAHASHI, H., NIIDOME, Y. *Chem. Commun.*, **2004**, 1978-1979.

123. SANDHU, K. K., McINTOSH, C. M., SIMARD, J. M., SMITHAND, S. W., ROTELLO, V. M. *Bioconjugate Chem.*, **2002**, *13*, 3-6.

124. WANG, G., ZHANG, J., MURRAY, R. W., *Anal. Chem.*, **2002**, *74*, 4320-4327.

125. ROSS, M. F., DA ROS, T., BLAIKIE, F. H., PRIME, T. A., PORTEOUS, C. M., SEVERINA, I. I., SKULACHEV, V. P., KJAERGAARD, H. G., SMITH R. A. J., and MURPHY, M. P. *Biochem. J.*, **2006**, **400**, 199-208.

126. MURPHY, M. P. *Trends Biotechnol.*, **1997**, *15*, 326-330.

127. McKEAGE, M. J., MAHARAJ, L., and BERNERS-PRICE, S. J. *Coordination Chem. Revs.*, 2002, **232**, 127-135.

128. ROSS, M. F., KELSO, G. F., BLAIKIE, F. H., JAMES, A. M., COCHEME, H. M., FILIPOVSKA, A., DA ROS, T., HURD, T. R., SMITH R. A. J., and MURPHY, M. P. *Biochemistry*, **2005**, *70*, 222-230.

129. D'SOUZA, G. G. M., BODDAPATI, S.V., and WEISSIG, V. *Pharmaceutical Res.*, **2007**, *24*, 228-238.

130. CHRZANOWSKA-LIGHTOWLERS, Z. M. *Gene*, **1999**, *230*, 241-247.

131. NAGLEY, P., and DEVENISH, R. J. *Trends Biochem. Sci.*, **1989**, *14*, 31-35.

132. ZULLO, S. *J. Neurol.*, **2001**, *21*, 327-335.

133. WEISSIG, V., and TORCHILIN, V. P. *J. Drug Target*, **2001**, *9*, 1-13.

134. D'SOUZA, and WEISSIG, V. *Curr. Gene Ther.*, **2004**, *4*, 317-328.

135. WEISSIG, V. Crit. Rev. *Ther. Drug Carrier Syst.*, **2003**, *20*, 1-62.

136. WEISSIG, V., and TORCHILIN, V. P. *Curr. Pharm. Biotechnol.*, **2000**, *1*, 325-346.

137. WEISSIG, V., and TORCHILIN, V. P. *Adv. Drug Delivery Rev.*, **2001**, *49*, 127-149.

138. BODDAPATI, S. V., and WEISSIG, V. *J. Liposome Res.*, **2005**, *15*, 49-58.

139. MURPHY, M. P., and SMITH R. A. J. *Adv. Drug Delivery Rev.*, **2000**, *41*, 235-250.

140. KELSO, G. F., PORTEOUS, C. M., COULTER, C. V., HUGHES, G., PORTEOUS, W. K., LEDGERWOOD, E. C., SMITH R. A. J., and MURPHY, M. P. *J. Biol. Chem.*, **2001**, *276*, 4588-4596.

141. FILIPOVSKA, A., KELSO, G. F., BROWN, S. E., BEER, S. M., SMITH R. A. J., and MURPHY, M. P. *J. Biol. Chem.*, **2005**, *280*, 24113-24126.

142. RIDEOUT, D., CALOGEROPOULOU, T., JAWORSKI, J. S., DAGNINO, R., and McCARTHY, M. R. *Anti-Cancer Drug Design*, **1989**, *4*, 265-280.

143. BURNS, R. J., SMITH, R. A. J., and MURPHY, M. P. *Arch. Biochem. Biophys.*, 1995, **322**, 60-68.

144. BURNS, R. J., and MURPHY, M. P. *Arch. Biochem. Biophys.*, 1997, **339**, 33-39.

145. LE FLOCH, P. *Coor. Chem. Rev.*, **2006**, *250*, 627-681.

146. WALKER, B. J. *Organophosphorus chemistry*, Penguin Books Ltd., Middlesex, England, **1972**.

147. ONAKA, S., KATSUKAWA, Y., SHIOTSUKA, M., KANEGAWA, O., and YAMASHITA, M. *Inorganic Chimica Acta*, **2001**, *312*, 100-110.

148. WARNER, M. G., REED, S. M., and HUTCHISON, J. E. *Chem. Mater.*, **2000**, *12*, 3316-3320.

149. SEOUNG, U. S., YOUNG, J. J., KI, Y. Y., EURNAE, K., and HYEON, T. *Nano Lett.*, **2004**, *4*, 1147-1151.

150. NARAYANAN, R., and EL-SAYED, M. A. *J. Phys. Chem. B*, **2005**, *109*, 4357-4360.

151. GOETTMANN, F., MOORES, A., BOISSIERE, C., LE FLOCH, P., and SANCHEZ, C. *Thin Solid Films*, **2006**, *495*, 280-285.

152. STEFANESCU, D. M., GLUECK, D. S., SIEGEL, R., and WASYLISHEN, R. E. *Langmuir*, **2004**, *20*, 10379-10381.

153. MOORES, A., GOETTMANN, F., SANCHEZ, C, and LE FLOCH, P. *Chem. Commun.*, **2004**, 2842-2843.

154. ZHU, H., TAO, C., ZHENG, S., and LI, J. *Colloids and Surfaces A: Physicochem. Eng. Aspects*, **2005**, *257-258*, 411-414.

155. HE, P., and URBAN, M. W. *Biomacromolecules*, **2005**, *6*, 1224-1225.

156. GACOIN, T. *Nanoparticles: Functionalization and Elaboration of Materials*, Springer, Netherlands, **2005**.

157. GREEN, M., RAHMAN, P., and SMYTH-BOYLE, D. *Chem. Commun.*, **2007**, 574-576.

158. STEFANSKA, J. Z., STAROSCIAK, B. J., ORZESZKO, A., and KAZIMIERCZUK, Z. *Pharmazie*, **1998**, *53*, 190-192.

159. DISTLER, H. *Angew. Chem. Internat. Edit.*, **1967**, *6*, 544-553.

160. CZERWIŃSKI, A., ORZESZKO, A., KAZIMIERCZUK, Z., MARASSI, R., ZAMPONI, S. *Anal. Lett.*, **1997**, *30*, 2391-2408.

161. CRAFT, D. T., ARCELLA, S. M., McDOWELL, S. M., STORHOFF, B. N., GAY, A. E., DEIBEL, M. A., OGREN, P. J., FANWICK, P. E., *Phosphorus, Sulfur, and Silicon*; **2004**, *179*, 1365-1377.

162. SCUDDER, M., and DANCE, I. *J. Chem. Soc., Dalton Trans.*, **2000**, 2909-2915.

163. SAMANT, M. G., BROWN, C. A., and GORDON, J. G. II. *Langmuir*, **1992**, *8* 1615-1618.

164. HAN, S. W. and KIM, K. *Journal of Colloid and Interface Science*, **2001**, *240*, 492-497.

165. SHAPORENKO, A., CYGANIK, P., BUCK, M., TERFORT, A., and ZHARNIKOV, M.. *J. Phys. Chem. B*, **2005**, *109*, 13630-13638.

166. DICKSON, P. M., McGOWAN, M. A. D., YEARWOOD, B., HEEG, M-J., and OLIVER, J. P. *J. Organomet. Chem.*, **1999**, *588*, 42-50.

167. BACK, T. G. and CODDING, P. W. *Can. J. Chem.*, **1983**, ***61***, 2749-2752.

168. KRIEF, A., DUMONT, W. and ROBERT, M., *Chem. Commun.*, **2005**, 2167-2168.

169. OSCARSSON, S. *Eur. J. Org. Chem.* **2006**, 1193-1199.

170. ASHWELL, G. J., CHWIALKOWSKA, A., and HERMANN HIGH, L. R. *J. Mater. Chem.*, **2004**, *14*, 2389-2394.

171. MAYA, F., FLATT, A. K., STEWART, M. P., SHEN, D. E., and TOUR, J. M. *Chem. Mater.*, **2004**, *16*, 2987-2997.

172. ASHWELL, G. J., TYRRELL, W. D., and WHITTAM, A. J. *J. Mater. Chem.*, **2003**, *13*, 2855-2857.

173. VORFALT, T., and PLENIO, H. *Synthesis*, **2007**, *4*, 565-571

174. FIURASEK, P., and REVEN, L. *Langmuir*, **2003**, *23*, 2857-2866.

175. YAMAMOTO, S-I., OKUMA, K., and OHTA, H. *Bull. Chem. Soc. Jpn.*, **1988**, *61*, 4476-4478.

176. WESTCOTT, S. L., OLDENBERG, S. J., LEE, T. R, and HALAS, N. *J. Chem. Phys. Lett.*, **1999**, *300*, 651-655.

177. QUINTEN, M., and KREIBIG, U. *Surf. Sci.*, **1986**, *172*, 557-577.

178. SKOOG, D. A., and LEARY, J. J. *Principles of Instrumental Analysis*; Saunder College: Philadelphia, **1992**.

179. LEFF, D. V., BRANDT, L., and HEATH, J. R. *Langmuir*, **1996**, *12*, 4723-4730.

180. McNEILLIE, A., BROWN, D. H., SMITH, W. E., GIBSON, M., and WATSON, L. *J. Chem. Soc., Dalton Trans.*, **1980**, 767-769.

181. FORNASIERO, D., FENGSHENG, L., RALSTON, and J., SMART, R. St. C. *J. Colloid Interface Sci.*, **1994**, *164*, 333-337.

182. BAIN, C. D., BLEBUYCK, H. A., and WBITESIDES, G. M. *Langmuir*, **1989**, *5*, 723-729.

183. FABIANOWSKI, W., COYLE, L. C., WEBER, B. A., GRANATA, R. D., CASTNER, D. G., SADOWNIK, A., and REGEN, S. L. *Langmuir*, **1989**, *5*, 35-42.

184. KRIEF, A., DUMONT, W. and ROBERT, M. *Chem. Commun.*, **2005**, 2167-2168.

185. GREENWOOD, N. N., and EARNSHAW, A. *Chemistry of the Elements,* Pergamon Press, Oxford, **1984**.

186. SCHNEIDER, D., NOGAI, S., SCHIER, A., and SCHMIDBAUR, H. *Inorg. Chim. Acta*, **2003**, *352*, 179-187.

187. WANG, T., ZHANG, D., XU, W., YANG, J., HAN, R., and ZHU, D. *Langmuir*, **2002**, *18*, 1840-1848.

188. AGUILA, A., and MURRAY, R. W. *Langmuir*, **2000**, *16*, 5949-5954.

189. KNOLL, W. *Annu. Rev. Phys. Chem.*, **1998**, *49*, 569-638.

190. JONSSON, U., FAGERSTAM, L., IVARSSON, B., JOHNSSON, B., KARLSSON, R., LUNDH, K., LOFAS, S., PERSSON, B., ROOS, H., RONNBERG, I., SJOLANDER, S., STENBERG, E., STAHLBERG, R., URBANICZKY, OSTLIN, H., and MALQVIST, M. *Biotechniques*, **1991**, *11*, 620-627.

191. LEE, S., and PEREZ-LUNA, V. H. *Anal. Chem.* **2005**, *77*, 7204-7211.

192. KARLSSON, R. *Anal. Biochem.* **1994**, *221*, 142-151.

193. LYON, L. A., MUSICK, M. D., and NATAN, M. J. *J. Anal. Chem.*, **1998**, *70*, 5177-5178.

194. GHOSH, P. S., VERMA, A., and ROTELLO, V. M. *Chem. Commun.*, **2007**, 2796-2798.

195. *Biacore X Instrument Handbook*, edition January **2001** (version AB), Uppsala, Sweden.

196. NATH, N., and CHILKOTI, A. *Anal. Chem.*, **2002**, *74*, 504-509.

197. MATSUI, J., AKAMATSU, K., HARA, N., MIYOSHI, D., NAWAFUNE, H., TAMAKI, K., and SUGIMOTO, N. *Anal. Chem.*, **2005**, *77*, 4282-4285.

198. TANIOUS, F. A., HAMELBERG, D., BAILLY, C., CZARNY, A., BOYKIN, D. W., and WILSON, D. *J. Am. Chem. Soc.*, **2004**, *126*, 143-153.

199. LÖFÅS, S., and JOHNSSON, B. *J. Chem. Soc., Chem. Commun.*, **1990**, 1526-1528.

200. www.biacore.com

Appendix

Appendix A

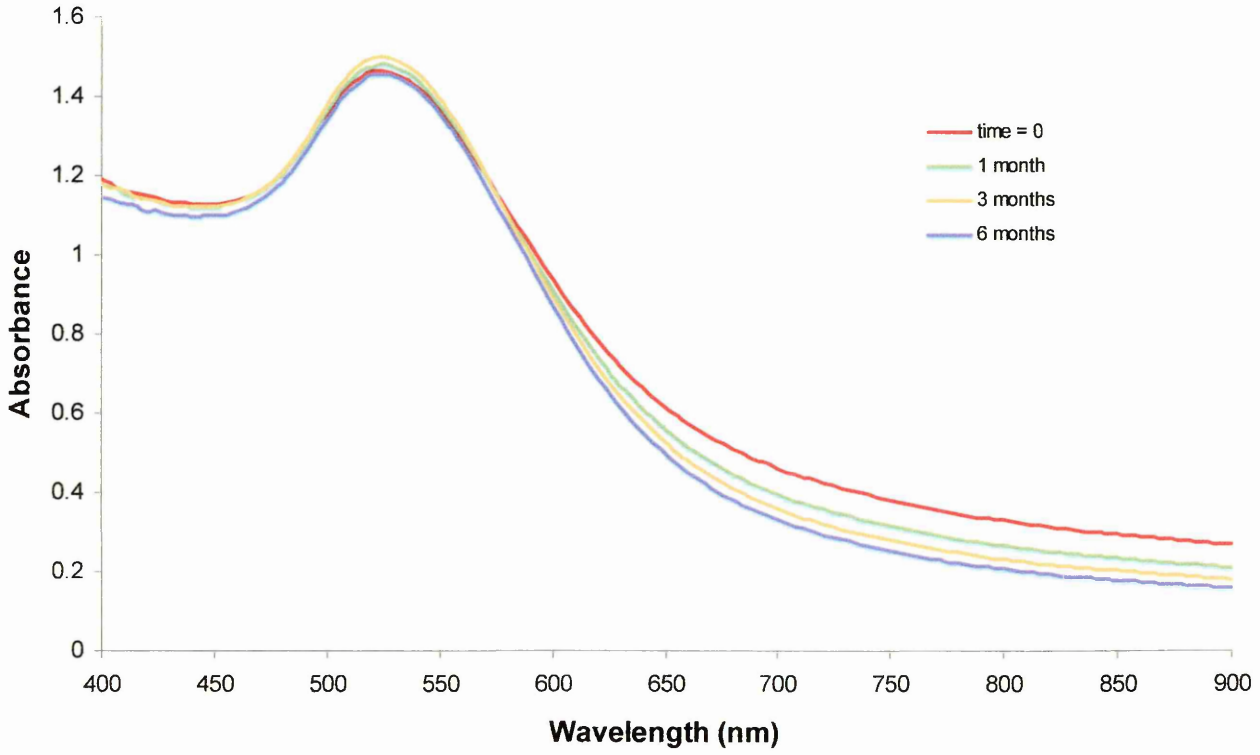

Figure 86. UV-visible spectra of a solution of AuNPs functionalised with triphenyl(3-thioacetylpropyl)phosphonium bromide (**17a**), after 1, 3, and 6 months

Appendix B

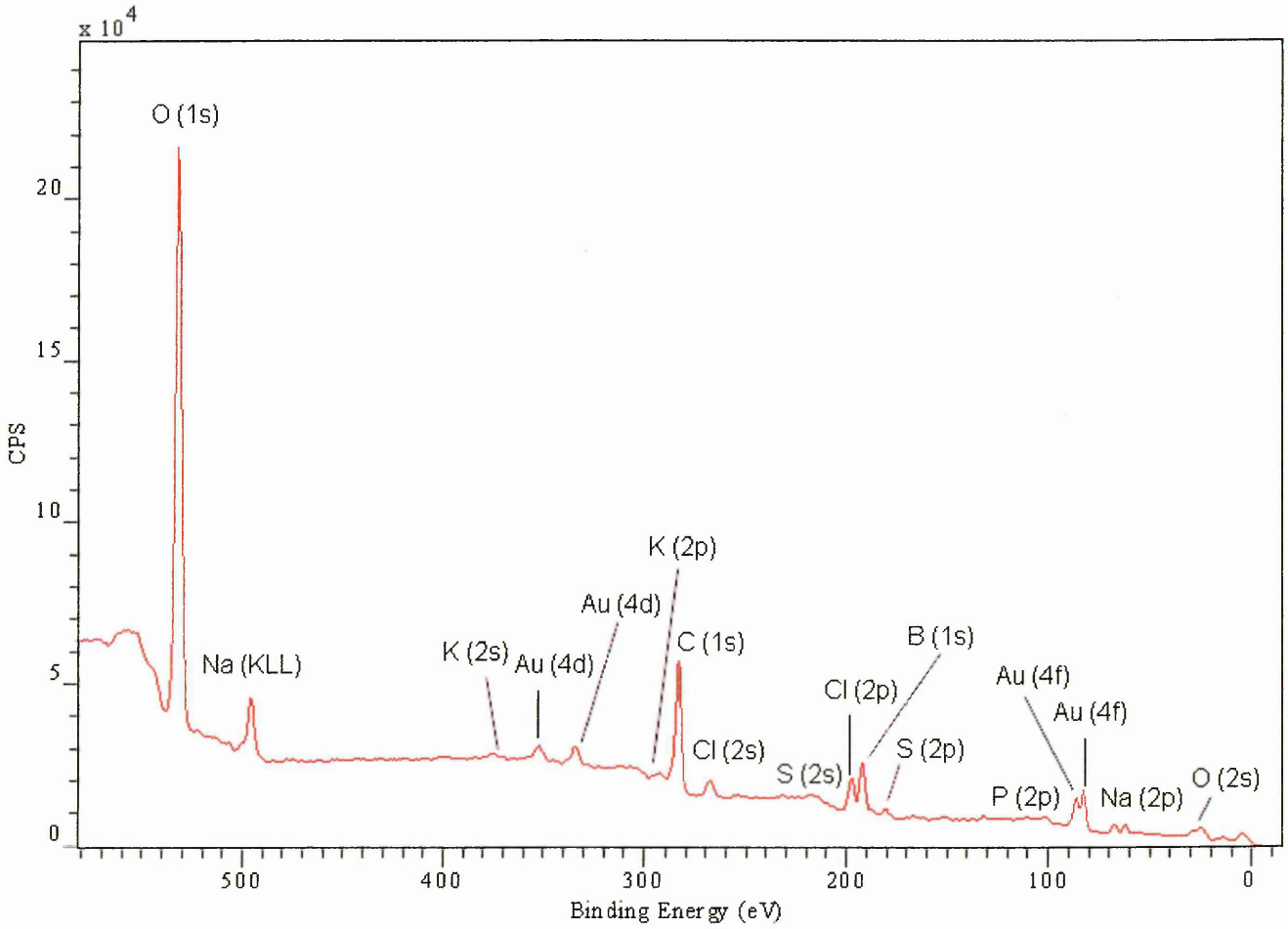

Figure 87. XPS wide scan spectrum corresponding to the freeze-dried sample of gold nanoparticles functionalised with the triphenyl(3-thioacetylpropyl)phosphonium bromide (**17a-AuNPs**)